Implications of Nanoparticle-Polymer Composites as Probes and Therapeutic Agents

A Thesis

Submitted in Partial Fulfillment of the
Requirements for the Degree of

DOCTOR OF PHILOSOPHY

by

PALLAB SANPUI

Centre for Nanotechnology
Indian Institute of Technology Guwahati
Assam, India

August 2010

Acknowledgement

I would like to express my foremost acknowledgement to my thesis supervisors, Dr. Siddhartha Sankar Ghosh and Prof. Arun Chattopadhyay for their continuous support and encouragement throughout my research work. I am obliged for the ample freedom they allowed me in conducting my research. Any sort of appreciation or acknowledgement will, in fact, only demean their deeds towards my thesis work. Appreciation is expressed to the members of my doctoral committee, Dr. A. Ramesh, Dr. A. Paul and Dr. G. Das for their constructive criticism and precious suggestions in completing this work. I owe my gratitude to the Centre for Nanotechnology, Dept. of Biotechnology and CIF, IIT Guwahati for providing me all the supports and necessary facilities and thanks to all staff members in the Centre for their help during my PhD studies. I sincerely acknowledge the financial support from MHRD and CSIR.

I owe my gratitude to the Heads of the Dept. of Biotechnology, Prof. R. Swaminathan and Prof. P. Goswami for allowing me to use the departmental facilities in their respective tenures. My sincere thanks to all the senior scholars and technical assistants (Mr. Sharan, Mr. Nurul, Mrs. Anita, Mrs. Prathana) of the Dept. of Biotechnology, who always helped me in my research work and never let me feel that I was from a different department. I must acknowledge Dr. P. Gopinath, Mr. Sonit K. Gogoi and Dr. A. Murugadoss for their helpful guidance at the initial stages of my research work. I take this opportunity to express my sincere gratitude to some of my close friends, Jaambu, Atul Paaji, Panditji, Amit, Abhijit Da and Bedo; who, apart from their active help in my thesis work, always encouraged me in my academic and non-academic endeavors. I am fortunate to have group members like Dr. M. Banerjee, Vinod, Kohila, Shilpa, Choks, Subhamay, Nidhi and Amaresh who provided me a healthy and enjoyable environment for the research. I cherish my close association with friends, Bise Da, Deba Da, Subham Da, Bitta Da, Pradip Da, Mehbub Da, Apruban Da, Anirban Da, Avijit Da, Mohanty Da, Shampa Di, Sanjay, Mota, Achlesh, Koushik Da, Hari, Bachha ……… and other friendly faces always abound in my memories.

I would like to express my deep sense of gratitude to my best friend Aditi, who is and has been, perhaps, the strongest support for me since my B.Tech days. It is her friendship, care, love, sacrifices and encouragement that made it possible for me to come so far. Lastly, and also most importantly, I would like to thank my parents and my brother for their endless love and affection. I appreciate the courage, understanding and dedicated support shown by all of them despite many testing times at their end. Without them, none of my achievements would have been possible.

CONTENTS

ABSTRACT

The size and shape dependent properties of the nanomaterials, as a consequence of the recent progress in the understanding of the physico-chemical and optoelectronic properties of materials at nanoscale, have successfully been harnessed in diverse field of science and technology. The potential of nanobiotechnology in addressing health related issues has also been demonstrated by the researchers in various laboratories around the world. In this regard, fundamental understanding of the interactions between novel nanomaterials and biological systems merits further investigation in order to develop novel materials with potential therapeutic implications. In the present study, newer 'green' methods of synthesizing metal nanoparticles (NPs) – especially Ag NPs – have been developed and the effects of these NPs on proteins, bacterial or mammalian cells have been investigated in order to evaluate their possible therapeutic significance. Chitosan, in addition to being used as the reducing and stabilizing agent, has been combined with the NPs in order to either potentiate the bactericidal efficacy of metal NPs in bacterial system or serve as novel biodegradable nanocarriers for NPs in mammalian cells.

In order to investigate the interaction of metal NPs with protein, a single-step synthesis of gold nanoparticles (Au NPs) with extraordinary size specificity in aqueous medium by purified green fluorescent protein (GFP) expressed in recombinant *E. coli* has been developed. The fluorescence of GFP offered a probe for concomitant changes in the protein during the course of synthesis, while the time-dependent formation of Au NPs was monitored by its surface plasmon resonance (SPR). GFP, in presence of trace amount of silver nitrate ($AgNO_3$, 10^{-5} M), produced uniform spherical Au NPs with particle diameter of 2.2 nm by cysteine–mediated reduction of $AuCl_4^-$. Fluorescence spectroscopic measurements indicated that during synthesis of Au NPs in absence of $AgNO_3$, partial denaturation of the protein occurred resulting in the lowering of fluorescence intensity. However, formation of Au NP in the presence of $AgNO_3$ led to complete denaturation of GFP with concomitant loss of fluorescence. This was further confirmed by native- and denaturing polyacrylamide gel electrophoresis (PAGE). However, use of $AgNO_3$ only neither resulted in the formation of NPs nor had any significant effect on the fluorescence of GFP.

The antibacterial potential of a novel chitosan-Ag-nanoparticle composite has been evaluated against *E. coli* expressing GFP. The composite was found to have significantly higher bactericidal activity than its components at their respective concentrations. The one-pot synthesis method led to the formation of small Ag NPs attached to chitosan. The presence of a small amount (2.15%, w/w) of Ag NPs in the composite was enough to significantly enhance the inactivation of *E. coli* as compared to unaltered chitosan. Fluorescence spectroscopy indicated that bacterial growth stopped immediately (in 2 hours) after exposure of *E. coli* to the composite, with release of cellular GFP into the medium at a faster rate than with chitosan. Fluorescence confocal laser scanning microscopy and scanning electron microscopy (SEM) results showed attachment of the bacteria to the composite and their subsequent fragmentation. Native PAGE indicated no effect of the composite on bacterial proteins.

In the next part of my thesis work, I developed a completely 'green' method of preparing a novel biodegradable chitosan based nanocarrier (NC) system for Ag NPs. The method takes advantage of conversion of bulk polymer–Ag NP composite into nanoscale particles. Electron microscopy revealed that the polymer NCs were about 172.6 nm in size with homogenously embedded Ag NPs of diameter ca. 4.9 nm. The SPR band of Ag NPs in the NCs confirmed that the shape and size of the metal NPs were unaffected during the preparation of the NCs, indicating excellent applicability of the present method to develop NCs for metal NPs. The functional activity of the Ag NPs impregnated in the chitosan NCs were evaluated by studying the catalytic activity of the Ag NP–containing NC system in $NaBH_4$ mediated reduction of p-nitro phenol. Turn over frequency (TOF) of the nanocarriers was calculated and found to be much higher than that of the bulk polymer-Ag NP composite.

The potential of these chitosan based NC of Ag NPs (Ag-CS NCs) in inducing apoptosis in mammalian cells at very low concentrations of the Ag NPs was investigated. Cell viability assay demonstrated that the concentration of Ag NPs required to reduce the viability of HT 29 cells by 50% was 0.33 μg mL^{-1}, much less than previously reported data. The nuclear and morphological changes characteristic of apoptotic cell death were investigated by fluorescence microscopy and SEM, respectively. The efficient induction of apoptosis by Ag-CS NCs was confirmed and subsequently quantified by flow cytometry. The involvement of mitochondrial pathway of cell death in the Ag-CS NC induced apoptosis was evident from the depolarization of mitochondrial membrane potential (MMP, $\Delta\Psi_m$). Real time quantitative RT-PCR analysis demonstrated the up-regulation of caspase 3 expression, which was further reflected in the formation of oligo-nucleosomal DNA 'ladders' in Ag-CS NC treated cells, indicating the important role of caspases in the present apoptotic process. The increased production of intracellular reactive oxygen species (ROS) due to Ag-CS NC treatment indicated that the oxidative stress could augment the induction of apoptosis in HT 29 cells in addition to classical caspase signaling pathway.

Finally, I developed a self–trackable chitosan nanocomposite with potential implication as drug delivery system. As a preliminary step to achieve this goal, chitosan stabilized and water dispersible ZnS:Mn^{2+} quantum dots (QDs) of ca. 3.6 nm, having strong orange fluorescence, were synthesized in an environment friendly method. Binding of plasmid DNA containing bifunctional cytosine deaminase-uracilphosphoribosyltransferase (pCD-UPRT) gene, with immense therapeutic importance in suicide gene therapy, has been investigated and shown to follow the Langmuir reversible adsorption model. The biocompatibility of the composite on HT29 cells was confirmed by viability assay. The chitosan stabilized ZnS:Mn^{2+} QDs synthesized in the present study could be a promising alternative to conventional organic fluorophore-tagged gene delivery systems for real-time monitoring in gene therapy applications.

In summary, the present study demonstrated the effect of metal NPs on biological systems, which can further facilitate their application in therapeutics. Furthermore, the potential of chitosan–Ag NP composite material as therapeutic agent and chitosan–ZnS:Mn^{2+} as biomedical probe has been established. Finally, the chitosan based NCs of Ag NPs developed in the present study, after appropriate in vivo experiments, could lead to alternative strategies of cancer therapy.

Keywords: gold nanoparticle, silver nanoparticle, quantum dots, chitosan, nanocomposite, nanocarrier, catalysis, protein denaturation, antibacterial, colon cancer, apoptosis, gene delivery.

ABBREVIATIONS

Ag NP(s)	Silver Nanoparticle(s)
Ag-CS NC	Silver nanoparticle containing chitosan nanocarrier
AO	Acridine Orange
Au NP(s)	Gold Nanoparticle(s)
a.u.	Arbitrary Unit
BHK 21	Baby Hamster Kidney cells
CD-UPRT	Cytosine deaminase-uracilphosphoribosyltransferase
cFDA	5-Carboxyfluorescein Diacetate
CLSM	Confocal Laser Scanning Microscopy
CS	Chitosan
DTG	Differential thermogravimatric analysis
EB	Ethidium bromide
FITC	Fluorescein Isothiocyanate
GFP	Green Fluorescent Protein
HT 29	Human adenocarcinoma cells
IC_{50}	Concentration of any toxic material to inhibit cell proliferation by 50%
LDH	Lactate dehydrogenase
MMP	Mitochondrial Membrane Potential
MTS	3-(4,5-dimethylthiazol-2yl)-5-(3carboxymethoxyphenyl)-2-(4-sulfophenyl)-2H-tetrazolium
NP(s)	Nanoparticle(s)
4-NP	4-Nitrophenol
PAGE	Polyacrylamide Gel Electrophoresis
PCR	Polymerase Chain Reaction
PI	Propidium Iodide
QD(s)	Quantum Dot(s)
ROS	Reactive Oxygen Species
SDS	Sodium Dodecyl Sulfate
SEM	Scanning Electron Microscopy
(L)SPR	(Localized) Surface Plasmon Resonance
TEM	Transmission Electron Microscopy
TGA	Thermogravimetric Analysis
TOF	Turn Over Frequency
TPP	Sodium Tri-Polyphosphate

LIST OF TABLES

LIST OF FIGURES

FIGURE PAGE

CHAPTER 1

Introduction and Literature Review

This chapter gives a brief introduction on the potential of nanotechnology in biodiagnostics and therapeutics. The therapeutic applications of metal and semiconductor nanoparticles have been discussed in detail. The chapter also presents the importance of the polymeric nanoparticles in biomedical applications with a particular emphasis on the naturally abundant biopolymer, chitosan.

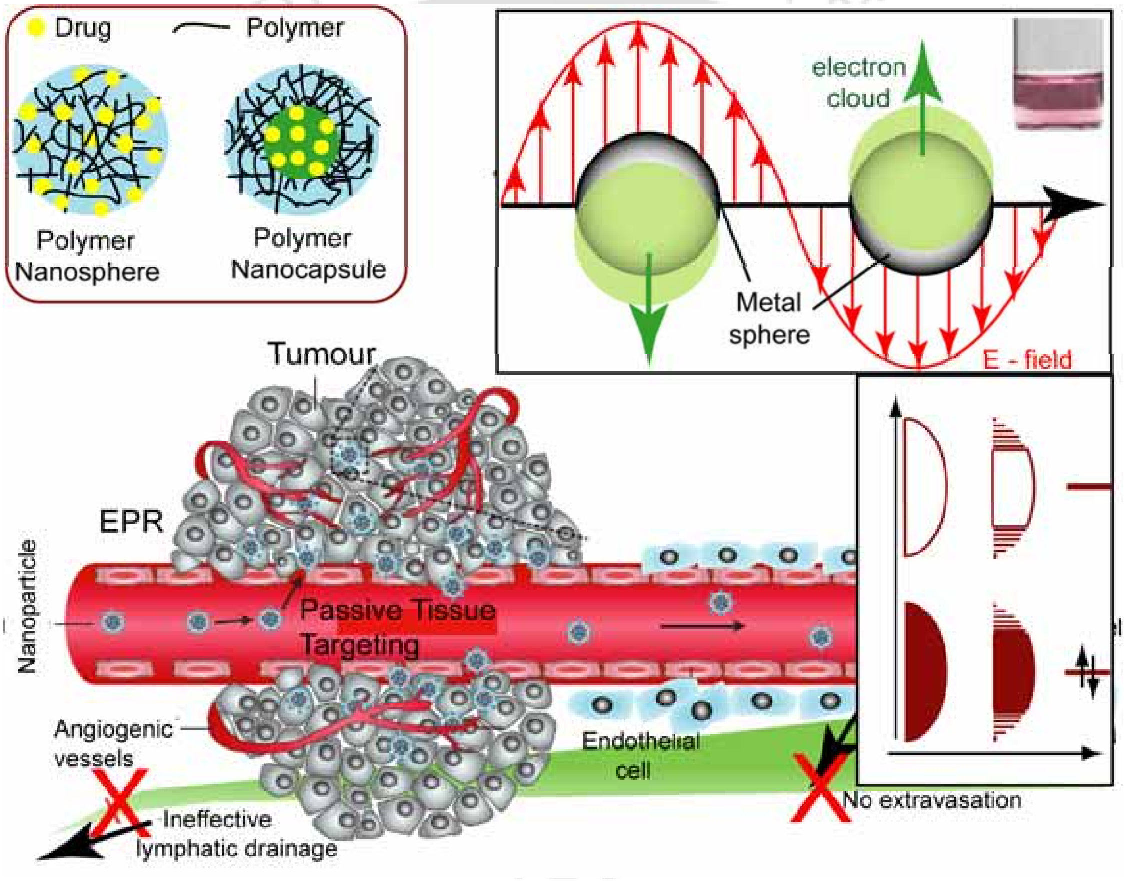

Chapter 1

INTRODUCTION AND LITERATURE REVIEW

1.1. Introduction

The recent advancement in the understanding of the physico-chemical and optoelectronic properties of materials at the nanoscale has revolutionized the present day science and technology by opening a whole new spectrum of possibilities. The phenomenal progress in nano- science and technology, in fact, reverberate the vision of Prof. Richard Richard Feynman that *'There's Plenty of Room at the Bottom'*. Manipulating the building blocks of materials at nanoscale has enabled us to exploit the size and shape dependent properties of these nanomaterials in addressing problems in diverse fields of science and technology.

There are a limited number of basic building blocks such as amino acids, lipids and nucleic acids in nature. However, the chemical diversity of these biomolecules provides the innumerable ways of combining or assembling them to produce an endless set of possible structures. In this regard, the rapid progresses in synthetic chemistry and biotechnology have propelled the possibility of producing newer functional and structural materials with unique application as well as enhanced efficacy. Biomolecules are highly promising for nanotechnology applications because of their dimensional comparability and functional specificity. For example, proteins fold only into predefined three-dimensional structures whereas nucleic acids bind themselves according to specific complimentarity. The enzymes and antibodies are highly specific in recognizing and binding their substrates or ligands as well. The researchers in various laboratories around the world have already shown the promising aspect of nano-biotechnology to encounter health related problems. In this respect, fundamental understanding of the interaction between novel nanoscale materials and biological systems is required to construct novel materials with potential biological values.

1.2. Nanomaterials in Biology

Recent developments in biological application of nanomaterials range from biodiagnostic to therapeutic aspect of nanomaterials (Niemeyer, 2001; Rosi and Mirkin, 2005). From therapeutic point of view, current research mainly centers around the application of various polymeric nanoparticles as delivery vehicles of either nucleic acids or pre-existing drugs against different diseases (Peer et al., 2007). On the other hand, metal as well as semiconductor nanoparticles (NPs) have been successfully applied as biosensors, due to their exciting optoelectronic and physico-chemical properties, for the detection of DNA or proteins of therapeutic importance (Rosi and Mirkin, 2005). Conversely, the researchers have also been able to assemble metal nanoparticles in a patterned way exploiting the striking specificity of bio-molecules such as DNA or proteins in order to construct functional nano-structures in a bottom-up approach (Niemeyer, 2000).

1.2.1. Metal Nanoparticles

Metal NPs, especially Au and Ag NPs, have been the focus of research for many decades owing to their fascinating optical properties (El-Sayed, 2001). The metal NPs, when dispersed in liquid media, display very intense colors due to the localized surface plasmon resonance (LSPR). According to the Mie theory (Mie, 1908), an electromagnetic frequency induces a resonant coherent oscillation of the free electrons, called the LSPR, at the surface of a spherical NP if it is much smaller than the light wavelength (**Figure 1.1**). This absorption lies in the visible region for Au, Ag and Cu. The LSPR frequency of metal NPs has been shown to strongly depend on their size, shape, aggregation, and structure (solid vs. hollow), as well as the dielectric properties of surrounding media (Kelly et al., 2003; Sun and Xia, 2002; Perez-Juste et al., 2005; Novak and Feldheim, 2000). This extraordinary size and shape dependent optoelectronic properties of metal NPs have been successfully exploited in various biodiagnostics and therapeutic applications in recent times.

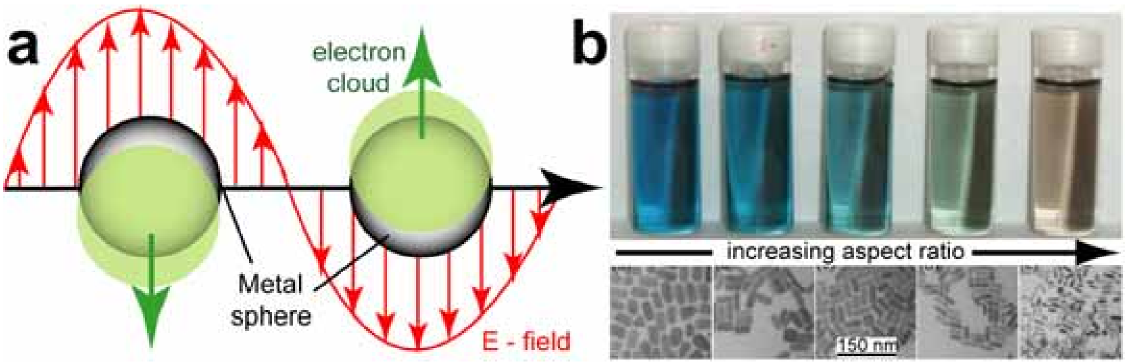

Figure 1.1. (a) Schematic of plasmon oscillation for a sphere, showing the displacement of the conduction electron charge cloud relative to the nuclei. **(b)** The color of Au nanorods change for very small variation in mean aspect ratio (ratio of length to width). Bottom panel shows the respective TEM micrographs (Courtesy: Perez-Juste et al., 2005).

1.2.1.1. Gold Nanoparticles

In 1857, Faraday reported, for the first time, the preparation of colloidal gold by reducing gold chloride with phosphors and attributed the red color to the colloidal nature of Au NPs. Mie, in 1908, explained visible absorption of Au NPs using Maxwell's electromagnetic equations. In 1951, Turkevich et al. simplified the synthesis method by using sodium citrate as reducing agents. Since then, Au NPs have been investigated as well as exploited in several applications in optics, catalysis, materials science and nanotechnology including biology and nanomedicine (Daniel and Astruc, 2004). It is well established that Au NPs usually show very little toxicity. Finally, Au NPs are redox active and, therefore, reduce the production of reactive oxygen and nitrite species, which is of great importance with respect to therapeutic implications (Shukla et al., 2005). The corresponding non-cytotoxicity, non-immunogenicity and biocompatibility make Au NP potential candidate in the field of nanomedicine.

Photodynamic Therapy (PDT)

The singlet oxygen generated from a photosensitizer has been shown to have potential application in photodynamic therapy (PDT) of cancer (Weishaupt et al., 1976). In this regard, Au NPs have been successfully used by Russell et al. as a delivery system of phthalocyanines to generate singlet oxygen in PDT of HeLa cells (a cervical cancer cell line) (Hone et al., 2002; Wiederet al., 2006). Cheng et al. (2008) has recently shown that silicon phthalocyanine 4 (Pc 4), a hydrophobic PDT drug currently under phase I clinical trials (Oleinick et al., 1993; Detty et al., 2004) accumulated to the target tumor *in vivo* within only <2 h when conjugated with PEGylated Au NPs. Au NPs were used as a vehicle to deliver 5-aminolevulinic (5-ALA) acid for selective and efficient PDT of fibrosarcoma tumor cells (Oo et al., 2008). Protoporphyrin IX accumulated preferentially in fibrosarcoma tumor cells treated with 5-ALA conjugated Au NPs yielding significantly higher reactive oxygen species that resulted in 50% more cytotoxicity to tumor cells than that of 5-ALA alone.

Photothermal therapy (PPT)

In photothermal therapy (PTT), photothermal agents get excited by absorbing light and subsequently relax through nonradiative decay channels which results in increase in the kinetic energy leading to the overheating of the local environment around the PPT species (Jori, 1990; Soncin et al., 1999; Camerin et al., 2005). The heat produced can be employed for local cell or tissue destruction (Sturersson and Andersson-Engels, 1995; He and Bischof, 2003). In this regard, the potential of gold nanostructures such as gold nanospheres (El-Sayed et al., 2006; Huang et al., 2006; Khlebtsov et al., 2006), gold nanorods (Takahashi et al., 2006a; Huff, 2007), gold nanoshells (O'Neal et al., 2004; Loo et al., 2005) and gold nanocages (Chen et al., 2005; Hu et al., 2006) in PPT have been successfully demonstrated due to their strongly enhanced absorption in the visible and NIR regions on account of their LSPR oscillations. Furthermore, these nanostructures are especially promising in PPT because of their ease of preparation, ready multi-functionalization, and tunable optical properties.

Nitric Oxide Release

The release of nitric oxide (NO) in a controlled way could lead to effective therapy for hypoxic respiratory failure associated with pulmonary hypertension as several cellular events such as angiogenesis, vasodilation, neurotransmission and the immune response are regulated by NO (Paciotti et al., 2006; Ignarro, 2000; Radomski et al., 1992; Williams, 2003). NO, in a recent study, was efficiently stored in polyamines-tabilized Au NPs by covalent linking via formation of acid labile N-diazeniumdiolate (Rothrock et al., 2005; Polizzi et al, 2007). The effective release of NO from these water-soluble nanocontainers in acidic condition merits important therapeutic implications due to presence of mild acidic environment inside inflammatory and tumor tissues (pH ~ 6.8), or cellular vesicles (endosomes, pH ~ 5.5–6 and lysozomes, pH ~ 4.5–5.0) (Mellman et al., 1986; Engin et al., 1995).

Delivery Applications

Au NPs are particularly attractive candidates for gene delivery because of their high surface-to-volume ratio which maximize the payload/carrier ratio. The most important advantage is that the charge and hydrophobicity of Au NPs can easily be tuned to enhance the transfection efficiency keeping the toxicity at minimum. Au NPs functionalized with cationic quaternary ammonium groups have been shown to bind plasmid DNA through electrostatic interactions, protect DNA from enzymatic digestion and subsequently release the bound DNA on addition of GSH *in vitro* (McIntosh et al., 2001; Han et al., 2006b; 2005). Furthermore, these DNA–Au NPs conjugates demonstrated efficient gene delivery in mammalian 293T cells with transfection efficiency 8-fold more than polyethyleneimine (PEI) (Sandhu et al., 2002). Thomas et al. (2003) reported the synthesis of AuNP-PEI transfection vectors and demonstrated that the transfection efficiency of the hybrid vectors in Cos-7 cells were ~12- fold more than the polymer itself. Han et al., (2006a) in an elegant study, loaded DNA on surface of the photolabile Au NPs tailored with a photocleavable o-nitrobenzyl ester linker and a quaternary ammonium salt as end-groups. *In vitro* studies showed that the complexed DNA was released, upon near-UV irradiation which cleaved the nitrobenzyl linkage creating an anionic carboxylate group, and DNA transcription was restored in T7 RNA polymerase assay. On the other hand, nucleic acids have been covalently attached to Au NPs via thiol (–SH) modification for grafting onto NPs. Au NPs conjugated thiolated siRNA have been used as a smart delivery system for effective gene silencing in HuH-7 cells (Oishi et al., 2006). Au NPs have also been demonstrated as efficient transporters of peptides and proteins of interest. Verma et al. (2004) have reported that cationic tetra-alkyl ammonium functionalized Au NPs recognize the surface of β-galactosidase through complementary electrostatic interaction and inhibit its activity, which can be further restored upon addition of free glutathione releasing the protein. Recently, chitosan stabilized Au NPs have been demonstrated to adsorb insulin on their surface and, thus, are effective for transmucosal delivery of insulin (Bhumkar et al., 2007).

Au NPs have been successfully used for targeted delivery of therapeutic drugs, via both ‘active’ and ‘passive’ targeting. Folic acid conjugated Au NPs (FA-Au NPs) have been demonstrated to be efficiently taken up by folate receptor-positive KB cells whereas little cellular uptake was detected in WI cells that do not overexpress folate receptor (Dixit et al., 2006). Chen et al. (2007) have demonstrated that methotrexate functionalized Au NPs (MTX–Au NPs) inhibits tumor growth in a mouse ascites model of Lewis lung carcinoma (LL2). Fuente et al. (2005) functionalized Au NPs with TAT peptides (a nuclear localization signal) and demonstrated enhanced localization of TAT-Au NPs in the nucleus. Paciotti et al. (2004) reported that the PEGylated Au NPs with adsorbed tumor necrosis factor, after intravenous injection into mice, accumulated in MC-38 colon carcinoma tumors compared to liver, spleen, or other healthy organs.

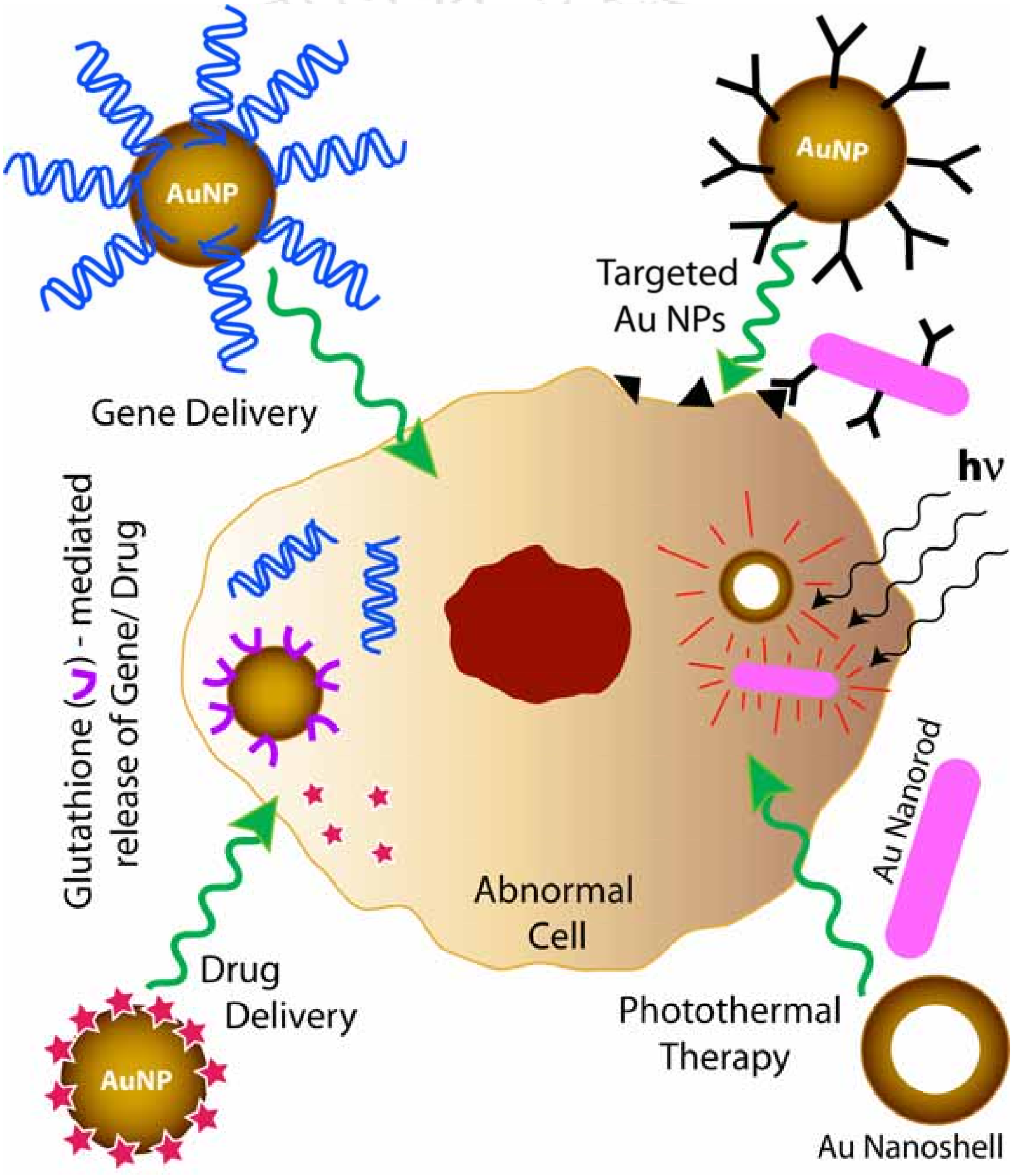

Figure 1.2. Schematic representation of various therapeutic applications of Au NPs.

1.2.1.2. Silver Nanoparticle

For centuries, silver and silver ions have been used for their excellent bactericidal properties. The history of using silver as an antimicrobial agent dates back to the ancient Romans who used to treat their water with silver coins to make it potable. Although the use of colloidal silver for wound treatment was approved by the US Food and Drug Administration as early as 1920s, the arrival of antibiotics in the 1940s halted the research on therapeutic application of silver (Jain et al., 2009). In 1960s, use of 0.5% silver nitrate solution and 1% silver sulfadiazine (SSD) cream in burn wounds by Moyer et al. (1965) and Fox et al. (1968) respectively revived the research interest in silver once again. Furthermore, the recent development in nano-science and technology coupled with the emergence of antibiotic resistance has propelled the research in antimicrobial efficacy of silver nanoparticles (Ag NPs).

Mechanism and Antimicrobial activities

In 2004, Sondi et al. first reported the antimicrobial activity of Ag NPs against *E. coli* as a model gram-negative bacterium. They observed that the Ag NPs caused damage to the cell wall which was evident from the formation of pits on the cell surface. Baker et al. (2005) showed the antibacterial efficiency of Ag NPs synthesized by inert gas condensation and co-condensation techniques on *E. coli* in liquid and solid medium. The mechanism behind the antibacterial activity of Ag NPs was considered to be due to the surface area to volume ratio of NPs; with smaller Ag NPs having larger surface area to volume ratio and hence, higher bactericidal efficacy. The in-depth study of antibacterial activity of commercially available Ag NPs in the size range of 1–100 nm on *E. coli* by Morones et al. (2005), using scanning transmission electron microscopy (STEM), confirmed the presence of Ag NPs in the cell membrane and inside the bacteria. The turbidometric study indicated that a concentration of 75 μg mL^{-1} of Ag NPs inhibited the bacterial growth. The high angled annular dark field (HAADF) images revealed that the smaller sized (~5 nm) NPs depicted efficient antibacterial activity, thus relating the activity of Ag NPs to the NP size.

In this regard, the research from our laboratory (Gogoi et al., 2006) also demonstrated the efficient bactericidal effect of Ag NPs on GFP expressing *E. coli*. The results revealed that Ag NPs of less than 10 nm diameter make pores on the bacterial cells walls, as evident from the TEM investigation, and subsequently releasing the cytoplasmic materials to the medium leading to cell death without affecting the intracellular proteins and nucleic acids. Ag NPs synthesized in one step by Panacek et al. (2006) showed high bactericidal activity against Gram-positive and Gram-negative bacteria including multi-resistant strains such as methicillin resistant *S. aureus*. The bactericidal efficacy of these Ag NPs was found to be size dependent showing the toxic effect at concentrations of 1.69 µg mL^{-1} Ag NPs. The combined effect of Ag NPs synthesized using *Klebsiella pneumonia,* with antibiotics was studied by Shahverdi et al. (2007) against *S. aureus* and *E. coli*. It was reported that the antibacterial activity of antibiotics like penicillin G, amoxicillin, erythromycin, clindamycin and vancomycin increased in the presence of Ag NPs against *E. coli* and *S. aureus*. In 2007, Pal et al. demonstrated the shape dependency of the antibacterial efficacy of Ag NPs by preparing spherical, rod shaped and truncated triangular Ag NPs via seeded growth method. Gong et al. (2007) synthesized Fe_3O_4@Ag core–shell nanoparticles having super paramagnetic as well as antibacterial properties. These bifunctional NPs showed excellent bactericidal activity against *E. coli*, *S. epidermis*, and *Bacillus subtilis* with the minimum inhibitory concentration (MIC) determined to be >70 µg/ml for *E. coli* and *B. subtilis* and >60 µg/ml for *S. epidermis*. According to the authors, these Fe3O4@Ag NPs could be used as recyclable antibacterial agents having broad antibacterial activity. The interaction of Ag NPs in NH_2–terminated hyperbranched poly(amidoamine) (HPAMAM-NH_2)/Ag nanocomposites with bacteria has also been revealed in a recent study (Zhang et al., 2008), in which the antibacterial activity of 4–15 nm Ag NPs was tested against *S. typhus*, *E. coli*, *B. subtilis*, and *Klebsiella mobilis*. The interaction between negatively charged bacterial cell wall and HPAMAM-NH_2 macromolecules (Ye et al., 2005; Sambhy et al., 2006; Lenoir et al., 2006) could possibly lead to strong interaction of Ag NPs with bacteria, which could further facilitate the release of active Ag into the bacteria resulting in a synergistic antibacterial effect of the HPAMAM-NH_2/Ag nanocomposites.

Biomedical Applications

In 2004, Furno et al. reported the successful impregnation of Ag NPs in polymeric biomaterials in order to produce improved medical devices having better antimicrobial efficacy. They used silicon discs of 0.45 mm thickness as a model biomaterial and *Staphylococcus epidermis* as the test bacterium. The bactericidal efficacy of Ag NPs–impregnated discs were evaluated in solid phase using tryptone soya agar (TSA) plates as well as in liquid medium using suspension culture of *S. epidermis* by means of plate count and chemiluminescence. The impregnation of Ag NPs in medical devices, in fact, also ensures the continuous release of silver ions providing antimicrobial activity (Wilcox et al., 1998; Darouiche et al., 1999).

Recently, the development of newly designed wound dressings based on Ag NPs has been proved to be a major breakthrough against the emerging problem of multi-drug resistant strains of pathogens. These Ag NP–based wound dressings act like the delivery systems which can maintain the sustained release of silver in different concentrations. Kim et al. (2007) demonstrated the ability of Ag NPs to control the infections occurring due to microorganisms such as the yeast isolated from bovine mastitis, *E. coli* and *S. aureus* using the modified agar disc diffusion method of the National Committee for Clinical and Laboratory Standards Institute, CLSI, 2000. Detailed electron spin resonance (ESR) studies revealed the presence of free radicals from Ag NPs which may be responsible for the antimicrobial effect. Poly(vinyl alcohol) (PVA) nanofibres impregnated with Ag NPs were shown to have efficient antibacterial property against *E. coli* (ATCC25922) and *S. aureus* (ATCC6538) by Jun et al. (2007) and were proposed to be used for the preparation of wound dressings. Moreover, the antimicrobial activity of commercially available Ag NP– based dressings such as Acticoat, Acticoat7, Acticoat Moisture control, Aquagel Ag, Urgotul SSD, ACTISORB, Contreet foam and Silvercel was demonstrated by Castellano et al. (2007) against *E. coli*, *S. aureus, Streptococcus faecalis* and *P. aeruginosa*. Recently, Maneerung et al. (2008) proposed a novel technique for preparing wound dressing based on bacterial cellulose and impregnated Ag NPs which demonstrated efficient antimicrobial activity against *E. coli* and *S. aureus*.

Applied Toxicology and its Therapeutic Implication

Although the Ag NPs have been emerged as potential antimicrobial and anticancer agents, the cytotoxicity and possible genotoxicity associated with Ag NPs remain critical for their successful therapeutic applications (Asharani et al., 2008, 2009). In 2005, Hussain et al. first reported the cytotoxic effect of Ag NPs *in vitro* using the rat liver derived cell line, BRL 3A. The authors demonstrated that exposure to Ag NPs caused depletion of GSH level, reduction in mitochondrial membrane potential and increase in ROS levels in BRL 3A cells, which suggested that the cytotoxicity of Ag NPs in liver cells was possibly due to oxidative stress. In a systematic study, Arora et al. (2008) investigated the interactions of 7–20 nm spherical Ag NPs with HT-1080 and

A431 cells *in vitro*. They also demonstrated involvement of oxidative stress in Ag NP–mediated cytotoxicity, which was apparent from decreased GSH (~2.5-folds in HT-1080, ~2-folds in A431) and SOD (~1.6-folds in HT-1080, 3-folds in A431) as well as increased lipid peroxidation (~2.5-folds in HT-1080, ~2-folds in A431). The threshold concentrations of Ag NPs for inducing apoptotic cell death (0.78 µg mL^{-1} in HT-1080, 1.56 µg mL^{-1} in A431) as determined by caspase-3 assay, were found to be much lower than the necrotic concentration (12.5 µg mL^{-1} in both cell types). The results led the authors to propose a safe range of Ag NPs in which they can be used therapeutically, still avoiding the necrotic effects. Hsin et al. (2008) further demonstrated the cytotoxicity of Ag NPs including the induction of mitochondria-dependent apoptosis in NIH3T3 fibroblast cells. Their results provided a molecular mechanism of Ag NP cytotoxicity, showing that Ag NPs acts through ROS and JNK to induce apoptosis via the mitochondrial pathway.

However, the possibility of using Ag NPs, by themselves or in combination with gene therapy, in order to induce apoptosis in mammalian cells has been explored recently (Gopinath et al., 2008 and 2010) by our group. In a recent study, the activity of Ag NPs towards HIV-1 infected Hut/CCR5 cells was investigated and the potential cytoprotective activities of Ag NPs were revealed (Sun et al., 2005). Elechiguerra et al. (2005) demonstrated the interaction of Ag NPs with HIV-1 virus and found that it preferentially binds to gp120 glycoprotein knobs of HIV-1, which caused the virus not to bind with the host cell.

1.2.1.3. Other Metal Nanoparticles

There are very few reports of potential therapeutic application of metal NPs other than Au and Ag. Platinum based yolk–shell nanocrystals of FePt@CoS_2 have been found to be more potent in killing HeLa cells compared to cis-platin (Gao et al., 2007). Recently, Caruso et al. (2007) reported the synthesis of carboxy-terminated water soluble platinum nanoparticles that can act as NO under the control of visible light stimuli. Kim et al. (2006) has recently demonstrated the efficient antibacterial efficacy of Cu NPs formed on the surface of SiO_2 NPs against *Staphylococcus aureus* and *E. coli*.

1.2.2. Quantum Dots

Semiconductor NPs or popularly known as quantum dots (QDs) represent a intriguing class of nanomaterials that possess unique size-dependent opto-electronic properties arising from quantum confinement of the electronic motion otherwise unavailable in either discrete atoms or bulk materials (Alivisatos, 1996) (Figure 1.3). QDs have several advantages over the conventional organic fluorophores being used for biological tagging and imaging due to their excellent resistance to photobleaching, broad absorption with narrow emission spectra and tunable optical properties according to size and material composition (Bruchez et al., 1998; Chan et al., 1998). Due to their novel optical and electronic properties, QDs have drawn intense research interest as a new class of nanoparticle probe for molecular, cellular, and *in vivo* imaging (Fan et al., 2004; Chan et al. 2002).

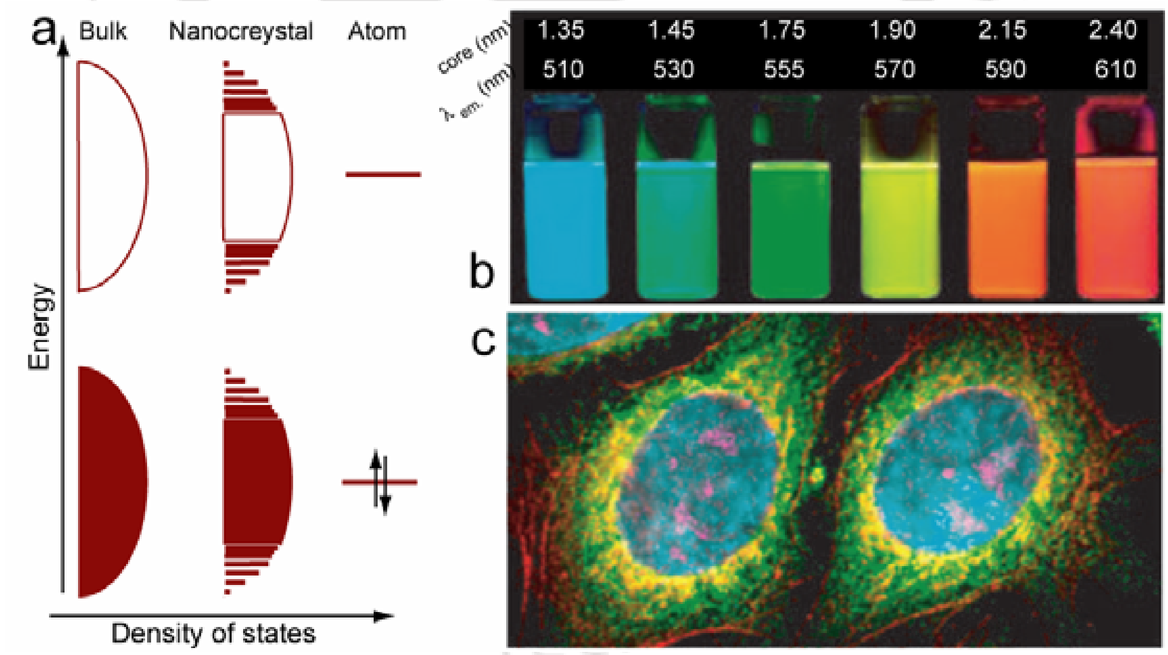

Figure 1.3. (a) Schematic representation of density of states in semiconductor nanocrystals. (Redrawn from Alivisatos, 1996); **(b)** the size-tunable fluorescence properties of CdSe QDs (corresponding core size and emission maxima indicated on the top, $\lambda_{excitation}$ = 365 nm) (Courtesy: Medintz et al., 2005); **(c)** five-colour QD staining of fixed human epithelial cells: cyan – 655-nm QDs labelling the nucleus, magenta – 605 nm QDs labelling Ki-67 protein, orange – 525 nm QDs labelling mitochondria, green – 565 nm QDs labelling microtubules and red – 705 nm QDs labelling actin filaments (Courtesy of Quantum Dot Corp.).

QDs as Fluorescent Labels to Biomolecules

QD-bioconjugates have emerged as potential imaging agents for simultaneous recognition and tracking of specific plasma membrane receptors in living cells. Diffusion dynamics of glycine receptors on the membranes of living neurons was revealed by single-QD tracking of the QDs conjugated to an antibody fragment specific for glycine receptors (Dahan et al. 2003). In an elegant study, Lidke et al. (2004) successfully demonstrated that CdSe-ZnS core-shell QDs coupled with epidermal growth factor could be identified at the single-molecule level on the membranes of cultured human cancer cells. The continuous observation of protein diffusion on the cellular membrane and even after internalization was only possible due to the bright and stable QD fluorescence. Moreover, the application of QDs for monitoring other plasma membrane proteins such as tyrosine kinases (Echarte et al., 2007; Rajan and Vu 2006), integrins (Chen et al., 2007; Lieleg et al., 2007), G-protein coupled receptors (Young and Rozengurt 2006), and membrane lipids associated with apoptosis (Gac et al., 2006; Koeppel et al., 2007) have also been reported.

There are many reports where QDs have been successfully delivered and tracked taking the advantage of the inherent capacity of uptaking extracellular space through endocytosis by many cell types (Hanaki et al., 2003; Jaiswal et al., 2003; Parak et al., 2002). Furthermore, conjugation of membrane receptors to the QDs could augment this process (Lidke et al., 2004; Jaiswal et al., 2003; Derfus et al, 2004). Recently, cell-penetrating peptides such as polyarginine and HIV-1 derived Tat have emerged as promising transfecting agent because of high transfection efficiency and low toxicity. In this regard, QDs have also been successfully delivered by conjugating cell-penetrating peptides (Lagerholm et al., 2004; Nan et al., 2005; Delehanty et al., 2006). Duan and Nie (2007) designed a fascinating class of cell-penetrating as well as ‘endosome-disrupting’ (endosomolytic) QDs by coating the surface of these QDs with hyperbranched copolymer ligands such as PEG-grafted polyethylenimine (PEI-g-PEG). The QDs could penetrate cell membranes and subsequently disrupt endosomal organelles in living cells due to the cationic charges and the “proton sponge effect” (Neu et al., 2005; Boussif et al., 1995; Pack et al., 2005) stemmed from the polyvalent amine groups.

In vivo imaging

The poor transmission of visible light through biological tissues due to the absorption of the majority of the signals has left the optical imaging, especially fluorescence imaging, with limited success in living animal models. The key to overcome this problem is to use a 'near-infrared optical window' which has been suggested as a region where most chromophores of mammals show local minima in absorption (Weissleder 2001). The QDs, in this regard, have the potential for imaging in living tissue as their emission properties can be tuned by simply adjusting their composition and size.

One of the most successful demonstrations of using QDs *in vivo* imaging has been their application for imaging of the cardiovascular system and the lymphatic system. Green-light emitting CdSe-ZnS QDs, after intravenous injection in a living mouse, were shown to retain their fluorescence and remain detectable in capillaries of adipose tissue and skin of the mouse by Larson et al. (2003). In a similar study, Lim et al. imaged the coronary vasculature of a rat heart using near-infrared QDs (Lim et al., 2003). In 2004, Kim et al. successfully showed the possibility of using QDs for imaging of the lymphatic system by intradermally injecting near-infrared CdTe(CdSe) core(shell) QDs in mice and pigs, where the QDs translocated to lymph nodes. The technique has successfully been exploited to recognize lymph nodes originating from the lungs (Soltesz et al., 2005; Parungo et al., 2005), esophagus (Parungo et al., 2005), and from subcutaneous tumors (Ballou et al., 2007). The multiplexing potential of QDs has been recently applied for mapping lymphatic drainage networks (Hama et al., 2007; Kobayashi et al., 2007). One of the first studies on *in vivo* imaging of tumors with QDs was reported by Akerman et al. in 2002. They demonstrated that the ZnS-capped CdSe QDs, conjugated to peptides with affinity for different tumor cells, specifically accumulated into the tumor vasculature following intravenous administration of the QDs into tumor-bearing mice. Later on Gao et al. (2004) reported that the tumor contrast on the scale of whole-animal imaging could be achieved by active tumor targeting of the QDs with the antibody against the prostate-specific membrane antigen (PSMA) followed by intravenous injection of these probes into mice bearing subcutaneous human prostate cancers. Similarly, active targeting and imaging of mouse models of human liver cancer by ZnS-capped CdSe QDs conjugated to an antibody against alpha-fetoprotein (Yu et al., 2007) have also been reported.

Toxicity Issues

In spite of the promising potential of QDs in biomedical applications, the cytotoxicity of QDs remains critical to human health and the environment. QD toxicity depends on multiple factors namely QD size, charge, concentration, capping material (functional groups), and oxidative, photolytic, and mechanical stability. In this regard, first and most important is the composition of QDs (Braydich-Stolle et. al, 2005; Oberdorster et.al, 2005). Cd, Se and Te, the most frequently used constituent metals in QD core, are known to cause acute and chronic toxicities in vertebrates (Hamilton 2004; Kondoh et al. 2002; Poliandri et al. 2003).

Another important aspect of QD toxicity is their stability *in vivo* and during prolonged storage. Under oxidative and photolytic conditions, QD shell coatings become labile and degradable, exposing potentially toxic "capping" material or resulting in dissolution of the core complex to QD core metals (e.g., Cd, Se). Several studies have demonstrated the correlation of free Cd^{2+} ions released from QDs with cytotoxic manifestations (Derfus et al., 2004; Cho et al., 2007; Chang et al., 2006). By facilitating oxidative release of Cd^{2+} ions from the surface of CdSe QDs by exposure to air or ultraviolet irradiation, Derfus et al. (2004) showed that the cell death in primary rat hepatocytes exposed to CdSe QDs exhibited was due to photo-lysis and oxidation of the QD coating. However, adding one or two monolayers of ZnS to the QDs virtually eliminated cytotoxicity due to oxidation. BSA-coated ZnS capped QDs also showed reduced cytotoxicity compared with non-BSA-coated ZnS-capped QDs.

Doped Semiconductor Nanocrystals: Overcoming QD Toxicity

To alleviate the toxicity of QDs, a variety of synthesis, storage, and coating strategies have been proposed. The decrease in QD cytotoxicity of CdSe QDs with the overgrowth of a ZnS shell has been verified in several reports (Kirchner et al., 2005; Maysinger et al., 2007). Surface coatings such as ZnS, bovine serum albumin (BSA) and Vitamin E (Warren et. al, 2000) were shown to reduce cytotoxicity. With different surface modifications including mercaptopropionic acid, silanization, and polymer coating, there were always quantitative concentration limits of QDs for the onset of cytotoxic effects to occur (Kirchner et al., 2005; Guo et. al, 2007). As Cd^{2+} release is a major hindrance for the use of QDs in cells and in animals, several new types of QDs having no heavy metal atoms may be useful for advancing this field.

Doped semiconductor nanocrystals (d-dots), containing no heavy metals, have the potential to compete with the mainstream emissive materials. Pradhan et al. (2005) recently demonstrated that Mn- and Cu-doped ZnSe d-dots can cover an emission window similar to that of the widely used CdSe QDs (Murray et al., 1993; Hines and Guyot-Sionnest, 1996). The d-dots markedly differ from undoped QDs in terms of mechanisms. When an undoped QD is excited by photons with energy higher than its band gap, an exciton (an electron-hole pair) is generated. The quantum confinement of the direct recombination of electron-hole pair in case of QDs (Brus, 1983) gives the well-known band edge or exciton emission. However, the energy of a photogenerated electrn-hole pair in a d-dot, after the absorption of the host semiconductor nanocrystal, is transferred into the electronic levels of the dopant ions. The recombination in a dopant ion center leads to the characteristic dopant emission, such as the $^4T_1$ to $^6A_1$ transition in case of Mn^{2+} ion in Mn doped ZnSe (or ZnS) d-dots (Pradhan et al., 2005) as shown in Figure 1.4. In addition to low cytotoxicity, d-dots can also overcome the intrinsic disadvantages of strong self-quenching in undoped QDs caused by small ensemble Stokes shift (Kagan et al., 1996; Achermann et al., 2003). Moreover, the d-dots are also advantageous over the conventional QDs in terms of sensitivity to thermal, chemical, and photochemical disturbances (Pradhan et al., 2005; Empedocles et al., 1996; Li et al., 2003).

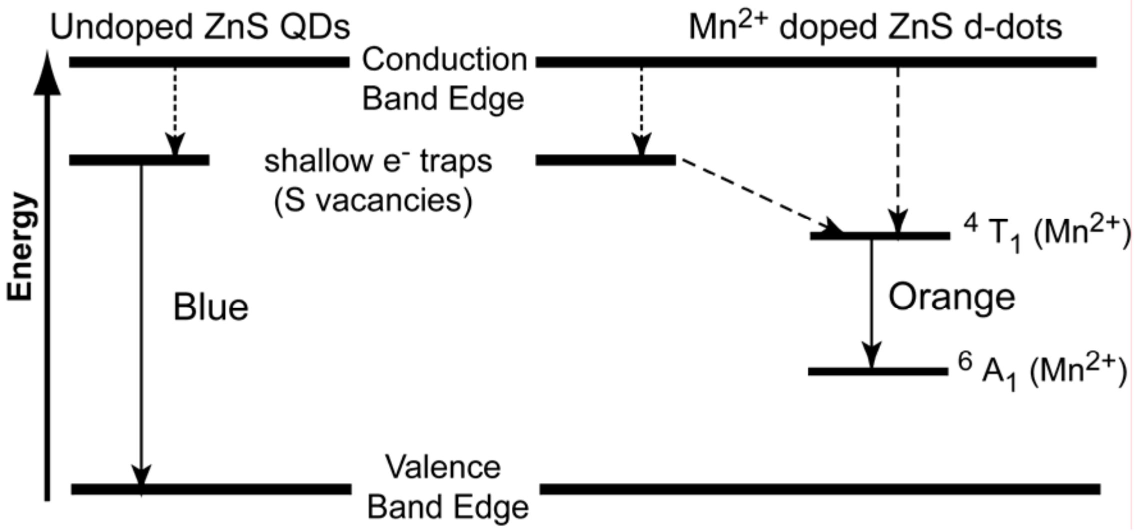

Figure 1.4. Schematic of emission mechanisms in undoped and Mn^{2+} doped ZnS QDs.

1.2.3. Polymeric Nanoparticles

The development of polymer–based particulate (micro and nano) material has revolutionized the pharmaceutical research and was one of the most broadly investigated strategies for drug delivery during the last decades. Polymeric NPs are solid, colloidal particles made of synthetic or natural polymeric substances and vary in size from 1 nm to 1000 nm (Hans and Lowman, 2002). The polymer materials used for the preparation of for nanoparticulate drug delivery systems can be classified into two broad categories:

I) Synthetic polymers

In recent years, novel polymers are being designed primarily for medical applications and have entered the arena of controlled release of bioactive agents. They are polyesters [poly(lactic acid), poly(glycolic acid), poly(lactic-co-glycolic acid), poly(hydroxy butyrate), poly(ε-caprolactone)], polyanhydrides [poly(sebacic acid), poly(adipic acid), etc], polyamides [poly(amino acids], acrylic polymers [polymethacrylates, poly(methyl methacrylate)], phosphorous based polymers and others like poly(cyanoacrylates), polyurethanes, polyortho esters, polydihydropyrans, polyacetals, polyvinyl pyrrolidone, ethyl vinyl acetate, poloxamers, poloxamine, etc. (Guerin, 2006; Gill and Ballesteros, 1983). As these polymers are synthesized in laboratory with controlled environment, they can be tailored to achieve required functionalities which can improve the efficacy of the drug used (Uhrich et al., 1999). A potential problem with synthetic polymers is the presence of unwanted monomers which can be toxic for *in vivo* applications (Pillai and Panchagnula, 2001).

II) Natural polymers

In spite of development of various synthetic and semi synthetic polymers, natural polymers hold promising prospect in drug delivery due to their biodegradability and easy availability. The important natural polymers, in this regard, include mainly polysaccharides (alginate, chitosan, dextran, etc) polypeptides (albumin, collagen, gelatin, casein, whey, etc) and nucleic acids (single and double stranded DNA, oligonucelotides etc). The major problems associated with the natural polymers are the immunogenecity and wide variability in their composition and therefore physicochemical properties, which may result in poor reproducibility in delivery characteristics.

Generally, in drug delivery applications, the drug of interest is dissolved, entrapped, adsorbed, attached and/or encapsulated into or onto the nano-matrix for effective delivery. Depending on the preparation methodology, two types of nanoparticles can be constructed i.e. nanospheres and nanocapsules, in order to achieve optimum particle properties and release characteristics for specific therapeutic application. Nanospheres are matrix systems in which the drug is physically and uniformly dispersed whereas nanocapsules are vesicular systems in which a drug is confined to a cavity surrounded by the polymer (Hans and Lowman, 2002; Soppimath et al., 2001; Panyam and Labhasetwar, 2003). Oral administration of peptides or proteins has been performed effectively by encapsulation in polymer nanospheres which provides improved stability, less degradation and greater absorption in gastro-intestinal tract (Vila et al., 2002). Nanoencapsulation enhanced the transfer of drugs across the blood brain barrier (BBB) for delivery into the brain through intravenous administration. Drugs that have successfully been transported into the brain using polymeric nanocarriers include hexa-peptide dalargin, di-peptide kytorphin, loperamide, tubocurarine, the NMDA receptor antagonist MRZ 2/576 and doxorubicin. (Kreuter, 2001).

Polymeric nanoparticles have also been used extensively against cancer (Pridgen et al., 2007). Furthermore, the surface of polymer nanoparticles can be modified easily to target cancer cells by conjugating ligands such as antibody, folate, transferrin, peptides and aptamers (Byrne et al., 2008). The successful delivery of anticancer drugs via polymeric NPs exploits the unique biological architecture inherent to cancerous tissue. The blood vessels in tumors, formed during angiogenesis, have irregular constructions and wide endothelial pores large enough to allow the extravasations of particles up to ~ 400 nm in size, which can accumulate in the tumor micro-environment due to a lack of effective lymphatic drainage (Jain 1999; Maeda et al., 2000; Matsumura and Maeda 1986). This "enhanced permeability and retention (EPR)" effect constitute the basis of 'passive targeting', in addition to the 'active targeting' of cancer antigens, for *in vivo* delivery of drugs encapsulated in polymeric nanocarriers (Figure 1.5).

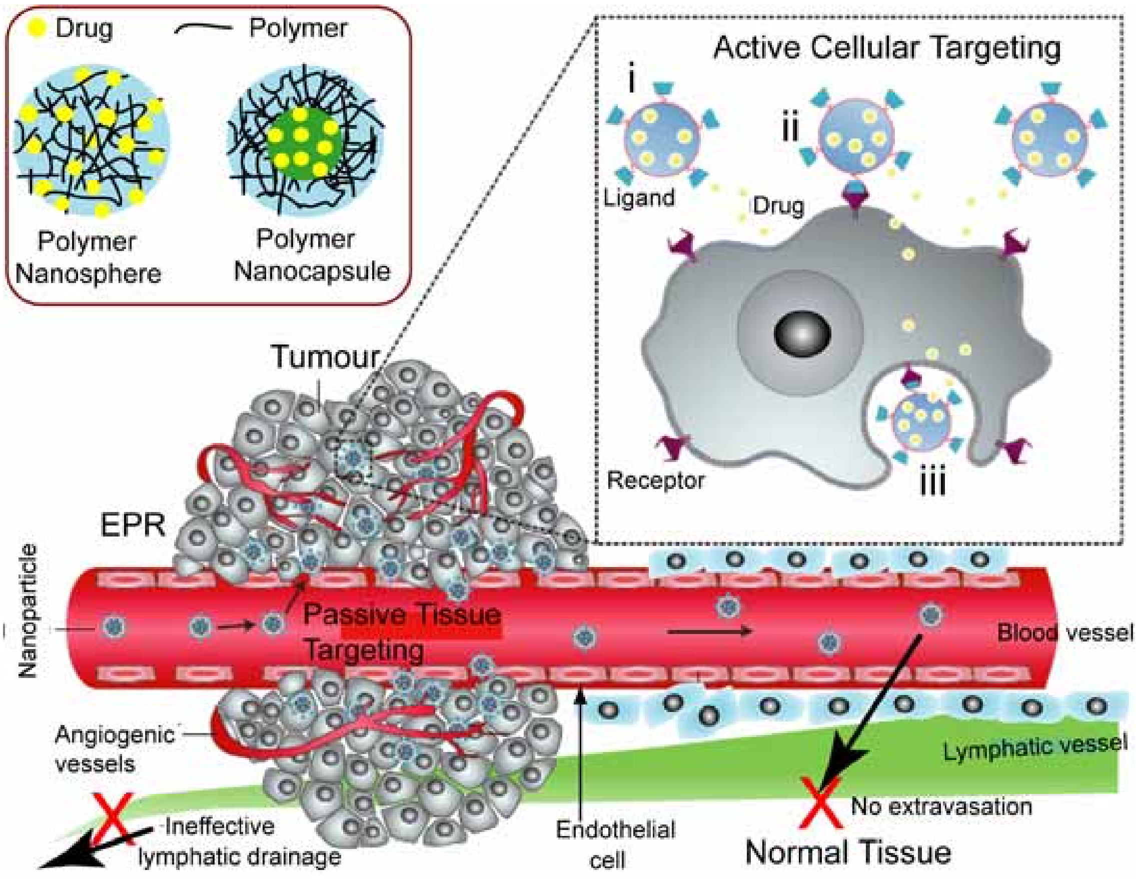

Figure 1.5. Schematic representation of different mechanisms of polymeric nanoparticle-mediated delivery of anticancer drugs: Passive tissue targeting is achieved through the EPR effect. Active cellular targeting can be achieved through the surface functionalization of nanoparticles with cancer cell-specific ligands. The polymeric nanoparticles can (i) release their contents in close proximity to the target cells; (ii) attach to the membrane of the cell and act as an extracellular sustained-release drug depot; or (iii) internalize into the cell (Courtesy: Peer et al., 2007). Two different approaches of encapsulating drug into polymeric nanoparticle, namely polymer nanosphere and polymer nanocapsule, are also shown schematically (inset).

1.3. Chitosan

Chitosan is a naturally abundant poly-cationic biopolymer composed of polymeric 1→ 4-linked 2-amino-2-deoxy-β-D-glucose. It is commonly found in shells of marine crustaceans such as shrimp, crab, etc. as well as cell wall of fungi. Commercially, chitosan is prepared by alkaline (NaOH, 40-50%) deacetylation of chitin (Wu et al., 2002; Rabea et al., 2003). However, the process of deacetylation is almost never complete and, thus making the distinction between chitin and chitosan on the basis of the degree of N-deacetylation, subjective. Native chitosan is insoluble in water, alkaline medium and organic solvents, but soluble in organic acids when the pH is < 6.

Recently, successful efforts have been made to prepare functional derivatives of chitosan by chemical modifications to increase the solubility in water (Muzzarelli, 1992; Heras et al., 2001; Jia et al, 2001; Ding et al, 2003; Kurita et al., 2002; Ramos et al., 2003; Ronghua et al., 2003).

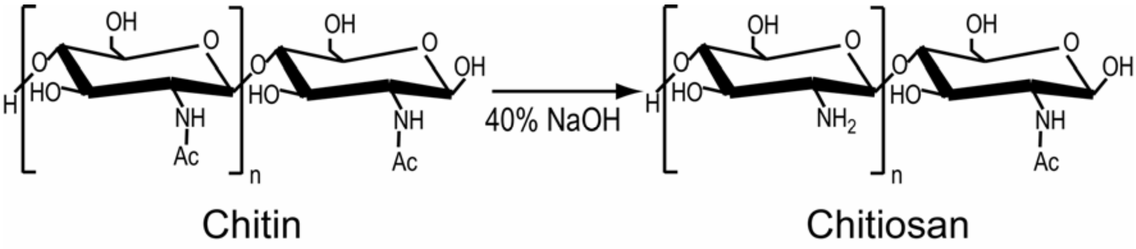

Figure 1.6. Preparation of chitosan by alkaline deacetylation of chitin.

Chitosan has drawn potential research interest in diverse areas such as agriculture, food industry, cosmetics, pharmaceutics and various biomedical applications (Martino et al., 2005; Sashiwa and Aiba, 2004; Majeti, 2000; Roy et al., 1999; Shi et al., 2006) because of ease of processing due to unique molecular structure, broad spectrum of antimicrobial activity (Rabea et al., 2003), inherent biodegradability (Sashiwa et al., 1990; Shigemasa et al.,1994) and biocompatibility (Khor et al., 2003). The physico-chemical properties of chitosan such as the degree of deacetylation and the molecular weight can be varied as required with respect to a specific application.

1.3.1. Antimicrobial Applications of Chitosan and Its Derivatives

The antimicrobial potential of chitosan has been well studied against a wide range of microorganisms such as fungi, algae and some bacteria, and observed to be influenced by inherent factors including the type of chitosan, the degree of chitosan polymerization, the host, the chemical or nutrient composition of the substrates or both, and the environmental conditions (e.g., substrate water activity or moisture or both).

Fungicidal activity

The fungicidal activity of chitosan against several fungi has been demonstrated with reported MICs (Table 1) for specific target organisms ranging from 0.0018% to 1.0%

(Liu et al, 2001). The inhibitory effect of chitosan against soilborne phytopathogenic fungi was shown by Stossel and Leuba (1984). Laflamme et al. (1999) demonstrated that chitosan successfully inhibited *F. acuminatum*, *Cylindrocladium floridanum*, and other pathogens of forest nurseries *in vitro*. Similarly, *Aspergillus flavus* was completely inhibited in field-growing corn and peanut (El Ghaouth and Asselin, 1992). Roller and Covill (1999) demonstrated that, 15 yeasts and molds in apple juice associated with food spoilage including *Mucor racemosus* and *Byssoclamys spp.* were efficiently inactivated by chitosan at various concentrations, pH values, and temperatures. Being a safe biopolymer for oral administration, chitosan has emerged as promising fungicidal in the food industry. Chitosan has been successfully used as food wraps (Muzzarelli, 1986) and the use of N,O-carboxymethyl chitin films to preserve fruits for long periods has already been approved in both Canada and the U.S.A (Davies et al., 1989).

Bactericidal activity

Chitosan has been shown to inhibit the bacterial growth in a wide range of bacteria (Table 2). Furthermore, bactericidal effect of chitosan derivatives containing quaternary ammonium salts, such as N,N,N-trimethyl chitosan, N-propyl-N,Ndimethyl chitosan and N-furfuryl-N,N-dimethyl chitosan against *E. coli* has been demonstrated by Jia et al. (2001). The authors found that the antibacterial activity of quaternary chitosan in acetic acid medium is stronger than that in water as well as stronger than that of chitosan itself. Sudarshan et al. (1992) investigated the antimicrobial efficacy of water-soluble chitosans derivatives including chitosan lactate and chitosan hydroglutamate on different bacterial cultures and found the derivatives showing excellent bactericidal effect against both gram-positive and gram-negative bacteria with 1-5 log cycle reductions within 1 h. They also reported that chitosan was no longer bactericidal at pH 7 due to the absence of a significant proportion of charged amino groups and the poor solubility of chitosan. A similar study by Papineau et al. (1991) also showed that chitosan lactate (0.2 mg/mL) was most effective against *E. coli* with a population reduction of 2 and 4 log cycles within 2 min and 1 h exposure, respectively. The authors also reported the effectiveness of chitosan glutamate and chitosan lactate in inhibiting growth of yeast cultures such as *Saccharomyces cerevisiae* and *Rhodotorula glutensis*.

Table 1.1. MIC of Native Chitosan against Fungi and Bacteria (Rabea et al., 2003)

Fungi	MIC [a]	Bacteria	MIC [a]
Botrytis cinerea	10	*Agrobacterium tumefaciens*	100
Fusarium oxysporum	100	*Bacillus cereus*	1000
Drechstera sorokiana	10	*Corinebacterium michiganence*	10
Micronectriella nivalis	10	*Erwinia sp.*	500
Piricularia oryzae	5000	*Erwinia carotovora subsp.*	200
Rhizoctonia solani	1000	*Escherichia coli*	20
Trichophyton equinum	2500	*Klebsiella pneumoniae*	700
		Micrococcus luteus	20
		Pseudomonas fluorescens	500
		Staphylococcus aureus	20
		Xanthomonas campestris	500

[a] Minimum inhibitory concentration in ppm

1.3.2. Biomedical Applications of Chitosan and Chitosan-Based Composite Materials

A number of methods have been developed to fabricate chitosan-based micro or nanoscale particles, fibers, hydrogels, membranes, and three dimensional scaffolds, which can be used in various applications such as biosensors, drug delivery systems, and non-viral vectors for gene transfection, tissue reconstruction and wound healing. Several studies have already demonstrated the significant promise of chitosan, alone or in combination with other polymers, in various fields of biomedical applications.

In 2001, Ma et al. demonstrated the utility of chitosan scaffolds to support cell growth and proliferation. In this regard, the combination of chitosan with another material to produce ‘composite’ material has been well investigated. The interaction of chitosan–gelatin hydrogels with cells was studied by Risbud et al. (2001b). On the other hand, chitosan–PVP hydrogels have been found not to have significant interactions with endothelial cells and therefore might be used as immunoisolation materials (Risbud et al., 2001a). Chitosan has also been shown to exert a strong influence on nerve cell attachment and proliferation (Haipeng et al., 2000). By combining with alginate, Cho et al. prepared chitosan-based scaffolds with galactosylated chitosan (Chung et al., 2002). The efficient attachment of hepatocytes to the alginate-galactosylated chitosan scaffolds was demonstrated by the authors. Zhu et al. (2002) reported improved cell attachment to photochemically attached chitosan onto polylactic acid (PLA) film surfaces. The authors also demonstrated the possibility of inhibiting platelet adhesion and activation by modifying the chitosan with heparin. Zhu et al. (2002) showed that the amino acid–chitosan–PLA membranes are cyto-compatibile to chondrocytes mimicking the characteristics of glycosaminoglycans (GAGs) found in tissue. In a recent study, chitosan grafted with cell adhesive peptides has been shown to promote the proliferation of human endothelial cells compared to neat chitosan (Chung et al., 2002). In summary, chitosan can be combined with a variety of delivery materials such as alginate, hydroxyapatite, hyaluronic acid, calcium phosphate, PMMA, poly-L-lactic acid (PLLA) and growth factors for potential therapeutic application. Furthermore, chitosan, which provide the feasibility of preparing a whole spectrum of matrices as shown in Figure 1.7, could efficiently be exploited in cell-based tissue engineering (Hu et al., 2004).

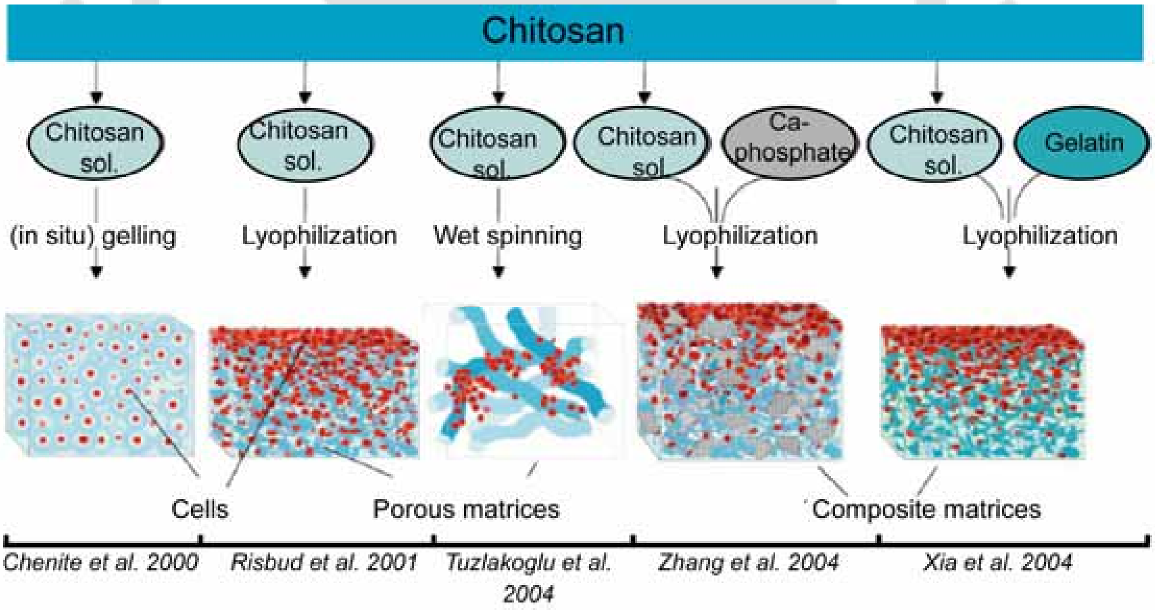

Figure 1.7. Schematic of chitosan processing for the application in tissue engineering (Courtesy: Martino et al., 2005).

The application of chitosan based materials in wound healing has been another important area of biomedical research. It has been proposed that chitin and chitosan could have potential implications in wound healing due the presence of monomeric N-acetylglucosamine which also occurs in hyaluronic acid, an important extracellular macromolecule in wound repair. In this regard, polyelectrolyte complex (PEC) films have been prepared by combining chitosan with alginate and investigated as potential wound dressing materials (Yan et al., 2001). The PEC membranes were found to promote accelerated healing of incisional wounds in a rat model (Wang et al., 2001). Lee et al. (2000) prepared a silver sulfadiazine–containing gel based on β-chitin combined with PEG and subsequently freeze dried to produce the dressing material. The *in vivo* study of this dressing material indicated infection controlled wound healing. The excellent wound dressing potential of a novel bilayered membrane made of a thin layer of chitosan as the antibacterial and moisture control barrier attached to a sponge layer augmenting the absorption of wound exudates was demonstrated by Mi et al. (2001). Recently, chitosan fibers combined with acidic GAGs was found to release the GAGs, which could lead to an alternative wound healing approach (Hirano et al., 2001).

1.3.3. Chitosan Nanoparticles in Drug Delivery

Several methods such as emulsion crosslinking, coacervation, spray drying, emulsion droplet coalescence, ionic gelation, and reverse micellar micro-emulsuion method have been developed to prepare chitosan NPs (Agnihotri et al., 2004; Bodnar et al., 2005). The size of these NPs can vary depending on the molecular weight of chitosan, its concentration and its surface charge (Lopez-Leon et al., 2005). Since chitosan becomes positively charged in aqueous acidic solutions due to the protonation of the free amine groups below its pKa ($pH<6.2$) (Kumar et. al, 2004), it can form a variety of complexes with natural or synthetic polyanions of various characteristics by the oppositely charged electrostatic interactions. Bodmeier reported the technique of preparing micro or nano-particulate drug delivery systems using chitosan/TPP complexes (Bodomier et al., 1989).

A wide variety of drugs ranging from small organic molecules to proteins and nucleic acids have been successfully delivered using chitosan NPs. Chitosan NPs when used as anticancer drug carrier have shown potent cytotoxic effects on various tumor cell lines *in vitro* and *in vivo*. The water-soluble drugs can easily be incorporated into chitosan NPs without any modification of chitosan. The cationic anthracycline drug doxorubicin hydrochloride forms complex with anionic chitosan, showed anti-proliferative activity against human melanoma A375 cells, C26 murine colorectal carcinoma cells *in vitro* and potential *in vivo* therapeutic efficacy against J774A.1 macrophage tumor cells implanted in Balb/c mice (Janes et al., 2001; Mitra et al., 2001). Zhang et al. (2008) demonstrated the usefulness of the nucleotide analogue 5-fluorouracil, when capsulated in chitosan NPs prepared by ionic gelation, for the treatment of human gastric carcinoma model *in vivo*.

Chitosan NPs, prepared through modification with hydrophobic moieties such as cholic acid, 5β-cholanic acid and cholesterol, have been used to encapsulate hydrophobic anticancer drugs (Lee et al., 1998; Wang et al., 2007). These modified chitosan NPs were used for the delivery of poorly soluble anticancer drugs such as paclitaxel, cisplatin, docetaxel, etc (Kim et al., 2006; Min et al., 2008). A recent study showed that hydrophobically modified chitosan NPs can also be used for the delivery of small peptide drugs in cancer therapy (Kim et al., 2008). Moreover, the conjugates of anticancer agents with chitosan and its derivatives display good anticancer effects with a decrease in the adverse effects of the original drug due to a predominant distribution into the cancer and a gradual release of free drug from the conjugates (Kato et al., 2005).

1.4. Delivery of Suicide Genes

Suicide gene therapy, a promising approach for cancer treatment, involves the transfer of suicide genes in cancer cells resulting in the conversion of non-toxic prodrug into toxic drug, which kill the cancer cell as well as neighboring damaged cells (Figure1.8). Suicide gene therapy has gained much importance due to its selective approach to eliminate tumor cells by the local production of toxic agents, which exhibits strong bystander effects and reduces systemic toxicity (Springer and Duvaz, 2000). However, the successful implication of suicide gene therapy has been limited by the inefficient gene delivery systems (Yazawa et al., 2002).

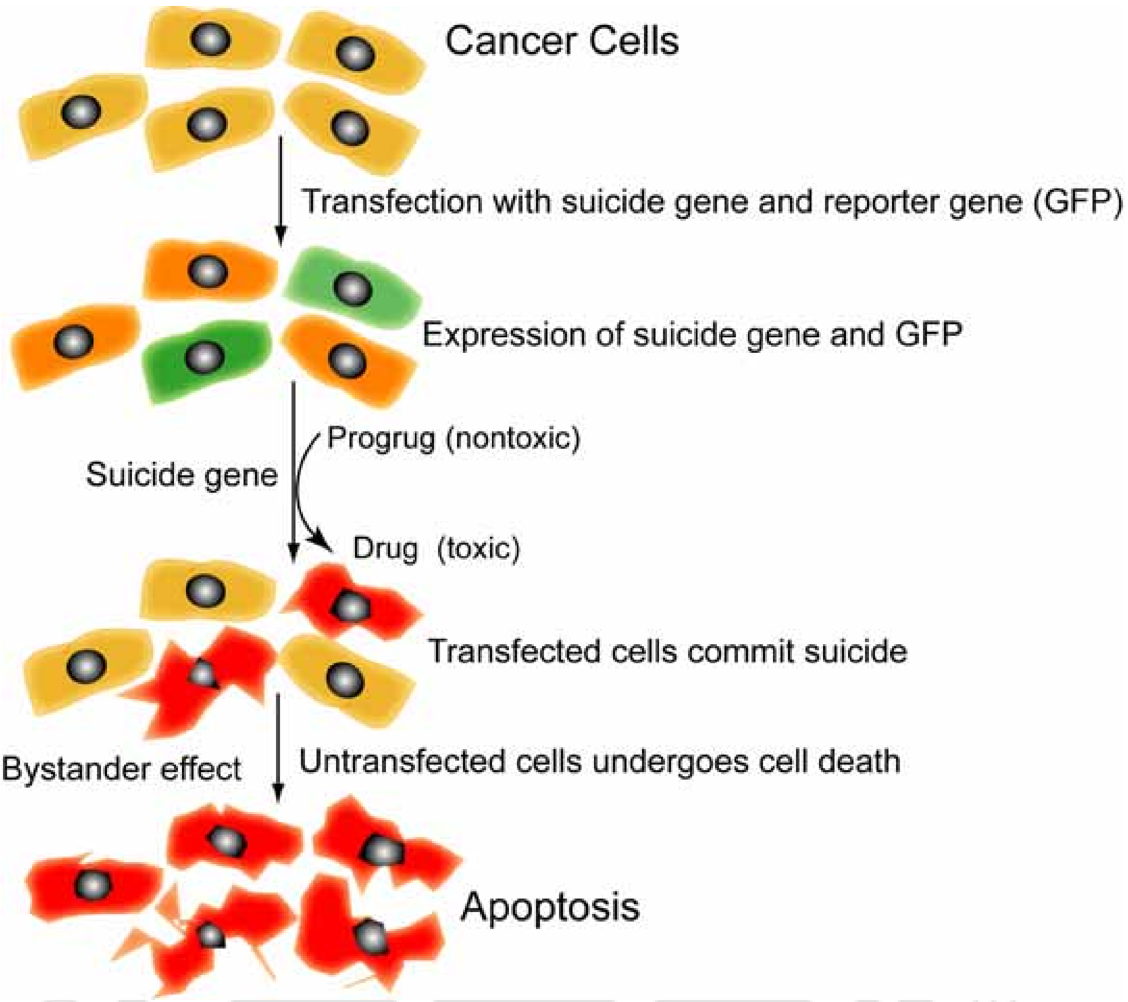

Figure 1.8. Schematic representation of suicide gene therapy.

One of the most intensely studied suicide genes is the bacterial cytosine deaminase (CD). CD converts the prodrug antifungal agent 5-fluorocytosine (5-FC) into anticancer agent 5-fluorouracil (5-FU), which can diffuse across the cell membrane and kill adjacent neighboring cells (Rowley et al. 1996). However, certain cancer cells are resistant to 5-FC treatment, where the CD enzyme exhibits poor efficiency in converting 5-FC into its toxic metabolites. This problem can be addressed by using a bifunctional cytosine deaminase -uracil phosphoribosyltransferase (CD-UPRT) gene (Gopinath and Ghosh, 2008), where UPRT, a pyrimidine salvage enzyme, converts 5-FU into more cytotoxic metabolites as shown in Figure 1.9.

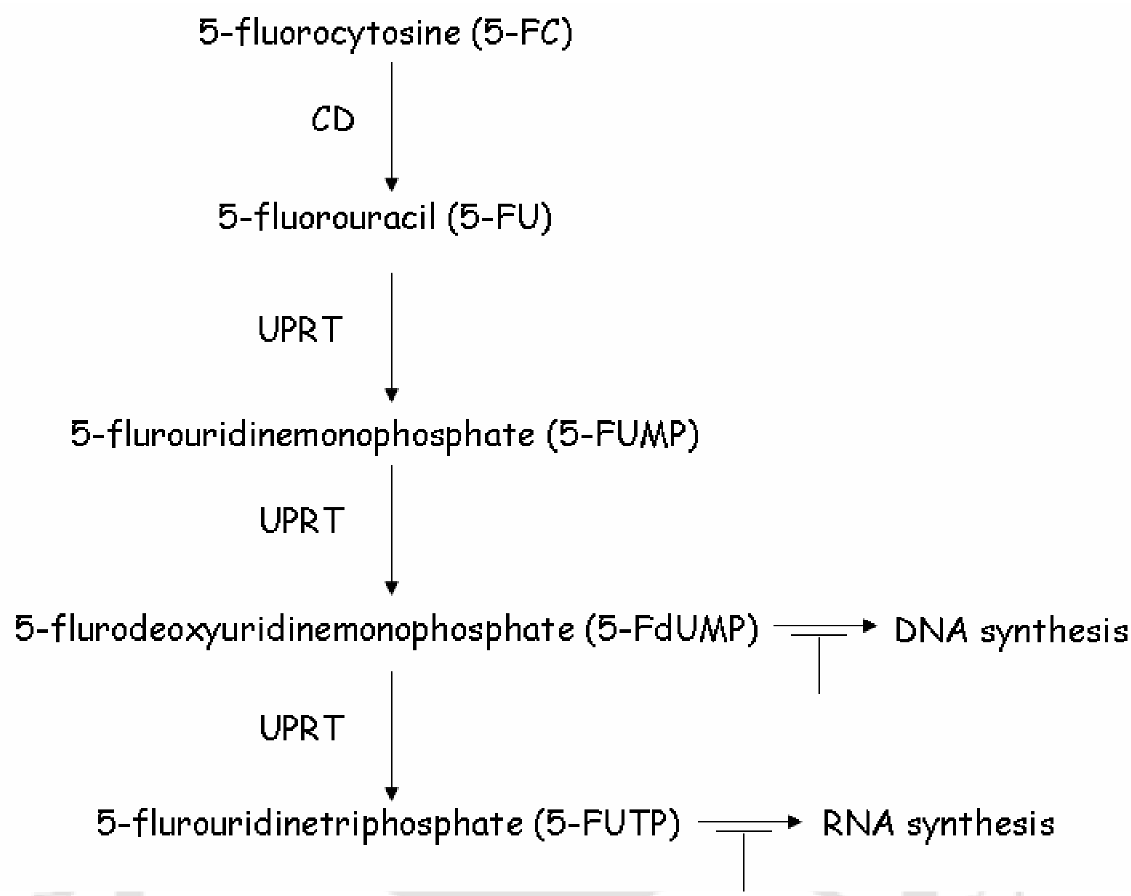

Figure 1.9. Schematic representation of 5-FC metabolism by CD and UPRT enzymes

1.5. Key Areas and Scopes

Based on the literature review in the field of therapeutic implication of nanomaterials, the research areas with potential scope are summarized below,

- Development of newer "green" synthesis methods of nanomaterials.
- Biocompatible polymer based composite nanomaterials.
- Investigating the interaction of nanomaterials and their composites with bacterial and mammalian cells.
- Understanding molecular mechanism of interaction.
- Development of traceable delivery materials.

1.6. The Present Work

1.6.1. Objectives

The main objectives of the present work are as follows:

- To develop a ‘green’ method of synthesizing small and highly uniform Au NPs by purified GFP and monitor the protein denaturation during the synthesis.
- To evaluate the antibacterial efficacy of a ‘novel’ chitosan–Ag NP nanocomposite on GFP expressing *E. coli*.
- To develop a ‘novel’ chitosan–based biodegradable nanocarrier system for Ag NPs and investigate the potential of these nanocarriers in catalytic applications.
- To investigate the potential of chitosan–based nanocarriers for successful delivery of Ag NPs in cancer cells in order to induce apoptotic cell death.
- To develop biocompatible gene delivery system based on chitosan–QDs nanocomposite using ZnS:Mn^{2+} QDs as non-toxic fluorescent probes.

1.6.2. Significance and Salient Features of the Present Study

The significance and salient features of the present study are summarized below

- GFP, expressed in recombinant *E. coli* bacteria, was purified and used for single-step synthesis of uniform spherical Au NPs with particle diameter of 2.2 nm.
- The denaturation of the protein during synthesis of Au NPs was demonstrated and the feasibility of probing the fluorescence of GFP to study the protein denaturation was also established.
- Efficient antibacterial activity of chitosan-Ag NPs composite on GFP expressing *E. coli* was demonstrated.
- The chitosan-Ag NP composite was shown to exert enhanced antibacterial activity compared to either chitosan or Ag NPs, due to the synergistic effect of chitosan and Ag NPs.
- A completely ‘green’ method of preparing a novel chitosan-based nanocarrier system for Ag NPs was developed.
- The Ag NPs in the nanocarrier were demonstrated to have significantly higher catalytic efficiency than those in bulk composite and can be applied as efficient catalyst.
- Novel chitosan based nanocarrier were employed to deliver Ag NPs in human colon cancer cells in order to induce Ag NP–mediated apoptosis.

- Successful induction of apoptosis by Ag NPs in cancer cells with minimization of NP-toxicity was demonstrated.
- Involvement of reactive oxygen species (ROS), in addition to the mitochondria dependent caspase pathway, in the Ag NP induced apoptosis was established.
- A novel chitosan stabilized Mn^{2+} doped ZnS QDs having excellent water solubility was synthesized.
- The efficient binding of pCD-UPRT, an important plasmid in suicide gene therapy, with these QDs indicating the potential of the composite material in gene delivery application was demonstrated.

CHAPTER 2

Green Fluorescent Protein Mediated Synthesis of Highly Uniform Gold Nanoparticles

In this chapter, a single-step 'green' synthesis of gold nanoparticles (Au NPs) with extraordinary size specificity (2.2 ± 0.5 nm) in aqueous medium by purified green fluorescent protein (GFP) expressed in recombinant E. coli has been reported. The concomitant changes in GFP structure during the synthesis of Au NPs was also investigated using fluorescence spectroscopy and polyacrylamide gel electrophoresis (PAGE).

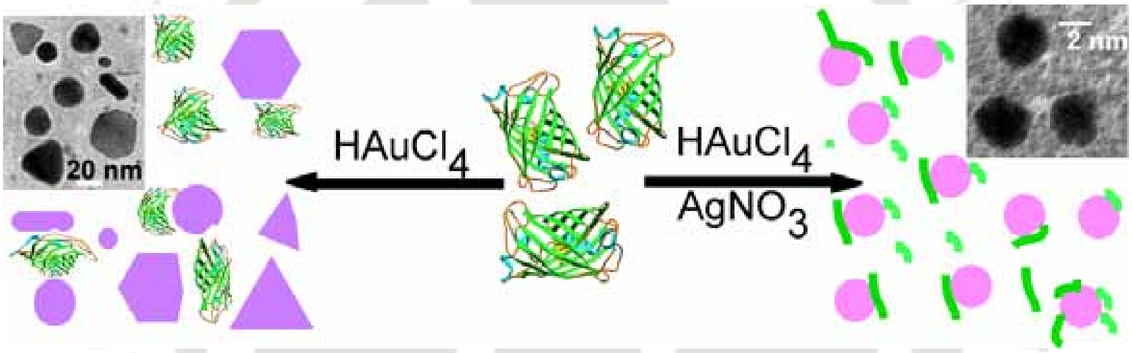

Chapter 2

GREEN FLUORESCENT PROTEIN MEDIATED SYNTHESIS OF HIGHLY UNIFORM GOLD NANOPARTICLES

2.1. Introduction

At present, a vast array of different semiconductor and metal nanoparticles can be synthesized by wet chemical methods – aqueous-phase as well as organic-phase synthesis – with fair control on the size and shape of the synthesized nanoparticles (Masala and Seshadri, 2004). However, use of stringent reaction conditions and hazardous chemicals in the syntheses of these NPs by chemical methods not only pose problems for large-scale synthesis but also make them less attractive for biological applications. On the other hand, "greener" methods to synthesize NPs employing biological systems have mainly centered on the microbial syntheses of nanoscale materials (Klaus et al., 1999; Mukherjee et al., 2001; Nair and Pradeep, 2002; Dameron et al., 1989; Kowshik et al., 2002; Shankar et al., 2004). The microbial syntheses, however, offer less flexibility over the control of particle sizes and shapes. Although there are some reports of synthesizing metal NPs using biological macromolecules (Naik et al., 2002; Rangnekar et al., 2007; Zhou et al., 2001; Raveendran et al., 2003; Tomczak et al., 2007), synthesis of uniform and well defined metal NPs of less than 5 nm, suitable for biological applications, by biomolecules such as purified protein still remains a challenge. It is important to know that while synthesis of small NPs using biomolecules is of great value, understanding the mechanism involved and the fate of the NPs as well as that of the biomolecules following synthesis are equally important. This assumes greater significance especially for the development of hierarchically assembled functional nano-structured devices and in the evaluation of the biocompatibility associated with these materials (Roach et al., 2005).

The changes in structural as well as functional stability of specific proteins adsorbed on macroscopic surface have already been reported (Hlady and Buijs, 1996). However, the effects of the physicochemical properties of the surface at the nanoscale on protein integrity has been investigated only recently (Vertegel et al., 2004; Lundqvist et al., 2004; Asuri et al., 2006; Karajanagi et al., 2004; Shang et al., 2007) and is far from being exhaustive. On the other hand, the primary focus in the biosynthesis of nanoparticles (NPs) has been on the product NPs, their properties and occasionally the properties of the composite system. There is no report on the accompanying changes in the bio-precursor, as the synthesis of NPs takes place.

2.2. Outline of the Research Work

1) Green fluorescent protein (GFP) expressed in recombinant *E. coli* bacteria was purified and used for single-step synthesis of gold nanoparticles (Au NPs) with extraordinary size specificity in aqueous medium.
2) Incubation of GFP with $AuCl_4^-$ produced spherical Au NPs having diameters ranging from 5 nm – 70 nm. Remarkably, addition of trace amount (1.0×10^{-5} M) of $AgNO_3$ in the medium produced uniform spherical Au NPs with particle diameter of 2.2 ± 0.5 nm.
3) The fluorescence of GFP offered an easy probe for concomitant changes in the protein during the course of synthesis, in addition to the monitoring of the time-dependent formation of Au NPs by the surface plasmon resonance (SPR). Additionally, the fate of GFP was also investigated by native- and denaturing polyacrylamide gel electrophoresis (PAGE)
4) Experimental results revealed that the partial denaturation of the protein occurred during synthesis of Au NPs in absence of $AgNO_3$, resulting in the lowering of fluorescence intensity. On the other hand, when the NPs were synthesized in the presence of $AgNO_3$ complete denaturation of the protein was observed.
5) Incubation of GFP in presence of $AgNO_3$ only neither formed NPs nor had any significant effect on the fluorescence of GFP.

2.3. Experimental Section

2.3.1. Growth media and chemicals

Silver nitrate ($AgNO_3$), sodium chloride (NaCl) and dimethyl sulfoxide (DMSO) were purchased from Merck India Ltd. $HAuCl_4$ solution (17% w/v in dilute HCl), 2,2'-dithiobis (5-nitropyridine) (DTNP) and other high purity molecular biology grade chemicals and reagents for native- and SDS-PAGE were obtained from Sigma-Aldrich

Chemical Corporation. *E. coli* growth medium Luria-Bertani (LB) was purchased from HiMedia, India. Milli-Q grade water (Millipore, USA) was used in all the experiments.

2.3.2. Isolation and purification of GFP

GFP (wild type) was isolated and subsequently purified from overnight grown culture of GFP expressing *E. coli*. This was based on the modification of methods reported by other workers (Jain et al., 2004; McRae et al., 2005). The procedure related to the generation of recombinant green fluorescent protein (GFP) expressing *E. coli* (DH5α) cell has been previously described by Gogoi et al. (2006). After purification of GFP, excess salts from the protein sample were removed by dialysis. The dialyzed sample was subsequently lyophilized and the resulting purified GFP in powder form was stored at -20^{0}C for further use.

2.3.3. Synthesis of Au NPs by GFP

The stock solution of GFP was prepared in 0.02 M Tris-HCl, pH 8.0, buffer containing 0.15 M NaCl and 5 mM EDTA. In a typical reaction, 14 μg mL^{-1} GFP was added to 5 mL reaction medium containing 1.0×10^{-4} M $HAuCl_4$ and incubated at 37^{0}C for 4 days. The same buffer, used for making the GFP stock solution, was also used as the reaction medium. Additional reactions were also carried out in the presence of different concentration of $AgNO_3$, keeping all other conditions the same as above. Appropriate control samples, namely sample containing only $HAuCl_4$ in reaction buffer and sample containing only GFP in reaction buffer, were also incubated in same conditions. A complementary set of experiments was also carried out where GFP were incubated with different concentrations of $AgNO_3$ in the same reaction conditions (in absence of $HAuCl_4$) as above to check the formation of Ag NPs by GFP.

2.3.4. Characterization of Au NPs

The formation of Au NPs was followed by monitoring the UV-vis spectra of the samples taken at regular time intervals in a Cary 100 UV-visible spectrophotometer (Varian Inc.). The fluorescence of GFP in all the samples were also measured at regular intervals by recording the fluorescence emission spectra of GFP ($\lambda_{emission}$ =509 nm) using excitation at 395 nm with a FluoroMax-3 (HORIBA Jobin Yvon) fluorescence spectrophotometer. The fluorescence emission spectra of GFP with $\lambda_{emission}$ = 505 nm and $\lambda_{excitation}$ = 475 nm for each sample were also recorded. The measurements were carried out under ambient conditions. For XRD measurements, as prepared solution of Au NPs was spread on glass slide and subsequently air-dried under ambient conditions. The measurements were performed using a Bruker D8 ADVANCE (Bruker AXS Inc.) X-ray powder diffractometer using Cu-Kα (λ=1.54 Å) source. In order to observe Au NPs under transmission electron microscope (TEM), 5 μL of as prepared Au NPs solutions from different samples were drop cast on carbon coated copper TEM grids followed by air-drying. The grids were then analyzed by a JEOL 2100 UHR- TEM instrument operating at an accelerating voltage of 120 KeV.

2.3.5. Protein gel electrophoresis

After incubation of GFP with $HAuCl_4$, both in presence and in absence of $AgNO_3$, aliquots of the different samples were taken at 90 h and subjected to native as well as SDS-PAGE. Protein profiles were visualized by staining the gel using silver staining method as well as under UV trans-illuminator before silver staining in case of native PAGE only.

2.3.6. Blocking of free thiol groups of GFP

The free thiol groups of cysteine residues of GFP were modified by previously described method (Rangnekar et al., 2007). Briefly, 10.3 μL of 5 mM DTNP in DMSO was added to 35 μL of 2 mg mL^{-1} GFP. The final reaction volume was made up to 5 mL with 0.02 M Tris-HCl (pH 8.0), 0.15 M NaCl and 5 mM EDTA so as to give a final GFP concentration of 14 μg mL^{-1}. After overnight incubation at 37 ^{0}C with gentle stirring, the reaction mixture turned to a pale yellow colored solution. The modification of free thiol groups was followed spectrophotometrically with a Cary 100 UV-visible spectrophotometer (Varian Inc.). The solution was then incubated with $HAuCl_4$ (final concentration of 1.0×10^{-4} M), both in presence and absence of 1.0×10^{-5} M $AgNO_3$. Appropriate control experiments were also carried out with unmodified GFP in presence of DMSO.

2.4. Results and Discussion

2.4.1. Synthesis of Au NPs

Following incubation of GFP in pH 8.0 buffer solution along with $HAuCl_4$ (1.0×10^{-4} M) at 37 ^{0}C, the color of the solution became purple by 8 h indicating the formation of Au NPs. UV-visible spectra of the solution (**Figure 2.1a**), comprised of gradually increasing absorption peak at ca. 532 nm with an additional absorption band at ca. 680 nm. The maximum absorption was reached by 90 h of incubation. The peak at 532 nm is characteristic of transverse plasmon resonance of Au NPs, whereas the peak at 680 nm is characteristic of longitudinal plasmon resonance of either Au nanorods or triangular or hexagonal shaped Au NPs (Shankar et al., 2004; Daniel and Astruc, 2004). When the same reaction was carried out in presence of 1.0×10^{-5} M $AgNO_3$, the solution became light pink in 10 h, which further turned to intense pink color after 48 h of incubation. The time dependent UV-visible spectra of the solution (**Figure 2.1b**) showed consistent increase in the absorbance at 532 nm till 90 h of incubation. There was no second peak at higher wavelength as was observed with the sample prepared from $HAuCl_4$ and in absence of $AgNO_3$. In both cases, the resulting colloidal Au NPs were stable for more than a week without any detectable sign of aggregation or change in UV-visible spectrum. Interestingly, when GFP was incubated with $AgNO_3$ (in absence of $HAuCl_4$) there was no change in the absorption spectra of the solution and appearance of any peak characteristic of Ag NPs was also not observed. Further, **Figure 2.1c** depicts the XRD pattern obtained from evaporation of samples of GFP incubated with $HAuCl_4$ only and $HAuCl_4$ in presence $AgNO_3$ (1.0×10^{-5} M). As is clear from the figure, both the patterns consisted of peaks at 38^0, 44^0, 64^0 and 77^0. The peaks are assigned to the principal Bragg reflections corresponding to the (111), (200), (220) and (311) lattice planes, respectively of Au with indexing based on the face-centered cubic (fcc) structure of Au crystal (Mukherjee et al., 2001; Zhang and Sham, 2003). The broadening of the peaks implied the formation of NPs of Au in the samples. Thus, the present observations suggest that in the presence of GFP, Au NPs were produced from $HAuCl_4$ as well as from $HAuCl_4$ mixed with $AgNO_3$. However, Ag NPs were not formed when $AgNO_3$ alone was incubated with GFP under the same conditions.

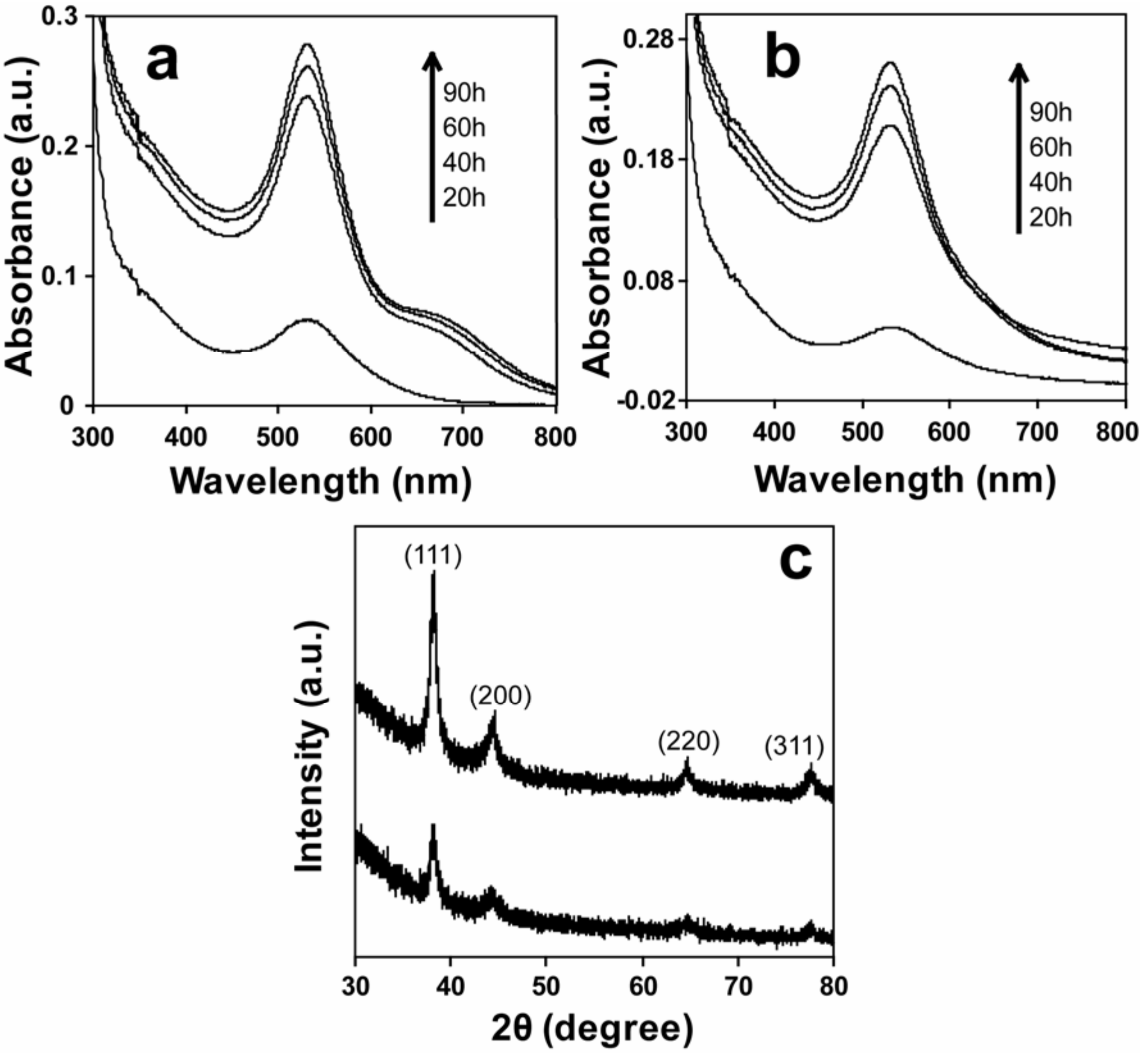

Figure 2.1. UV-visible spectra of Au NP solution synthesized by GFP in presence of **(a)** $HAuCl_4$ only and **(b)** $HAuCl_4$ and 1.0×10^{-5} M $AgNO_3$. **(c)** XRD spectra of Au NPs synthesized by GFP in presence of $HAuCl_4$ only (upper) and $HAuCl_4$ and 1.0×10^{-5} M $AgNO_3$ (lower).

In order to study the size and the shape of the Au NPs synthesized in present method, NPs were investigated under TEM (**Figure 2.2**). From **Figure 2.2a**, it can be clearly seen that Au NPs, synthesized by GFP in the presence of $HAuCl_4$ only, were polydisperse in nature with a wide size distribution (**Figure 2.2b**). The average particle size was calculated to be 18.0 ± 16.0 nm. The particles were mainly spherical in shape with a considerable fraction being triangular, polygonal or rod-shaped. It may be mentioned here that the anisotropy in the shape of the Au NPs can well be correlated with the observation of the absorption band at ca. 680 nm in the corresponding UV-visible spectrum during the synthesis process (Jin et al., 2001; Shankar et al., 2004; Daniel and Astruc, 2004). The selected area electron diffraction (SAED) pattern of these Au NPs (**Figure 2.2c**) indicated that the NPs were polycrystalline and of face-centered cubic (fcc) type in structure. In order to gain insight into the structural details, the Au NPs were further investigated under high resolution transmission electron microscope (HRTEM). The HRTEM image of a typical polygonal Au NP is shown in **Figure 2.2d**, where the individual lattice fringes can easily be observed. Furthermore, it was interesting to find out that, under HRTEM, some of the Au NPs actually produced Moiré pattern consisting of a periodic array of dots (**Figure 2.2e**). The occurrence of Moiré pattern could possibly be due to different orientations of two sets of lattices, as a result of the polycrystalline nature of these Au NPs (Sun et al., 2003). Interestingly, the SAED image of an individual triangular Au NP (**Figure 2.2f**) showed characteristic hexagonal pattern of spots indicating the presence of a single crystal of fcc Au oriented in the [111] direction with top surface of the nano-triangle parallel to the TEM grid (Jin et al., 2001; Shankar et al., 2004; Sun et al., 2003). In addition to the allowed {220} and {422} reflection for the fcc lattice, the presence of weak spots due to the forbidden 1/2{422} reflection (**Figure 2.2f**) implied that the top and bottom faces of these nano-triangles were atomically flat.

On the other hand, Au NPs synthesized by GFP in the presence of a mixture of $HAuCl_4$ and 1.0×10^{-5} M $AgNO_3$ were well dispersed and uniform in size without the presence of any detectable agglomeration (**Figure 2.3a**). The particles were mostly spherical (~ 95%) in shape and exhibited a narrow size distribution with an average diameter of 2.2 ± 0.5 nm (**Figure 2.3b**). The SAED image (**Figure 2.3c**) of these NPs showed typical pattern characteristic of polycrystalline Au NPs in fcc structure. A typical HRTEM image (**Figure 2.3d**) of one of these Au NPs clearly showed the well separated individual lattice fringes.

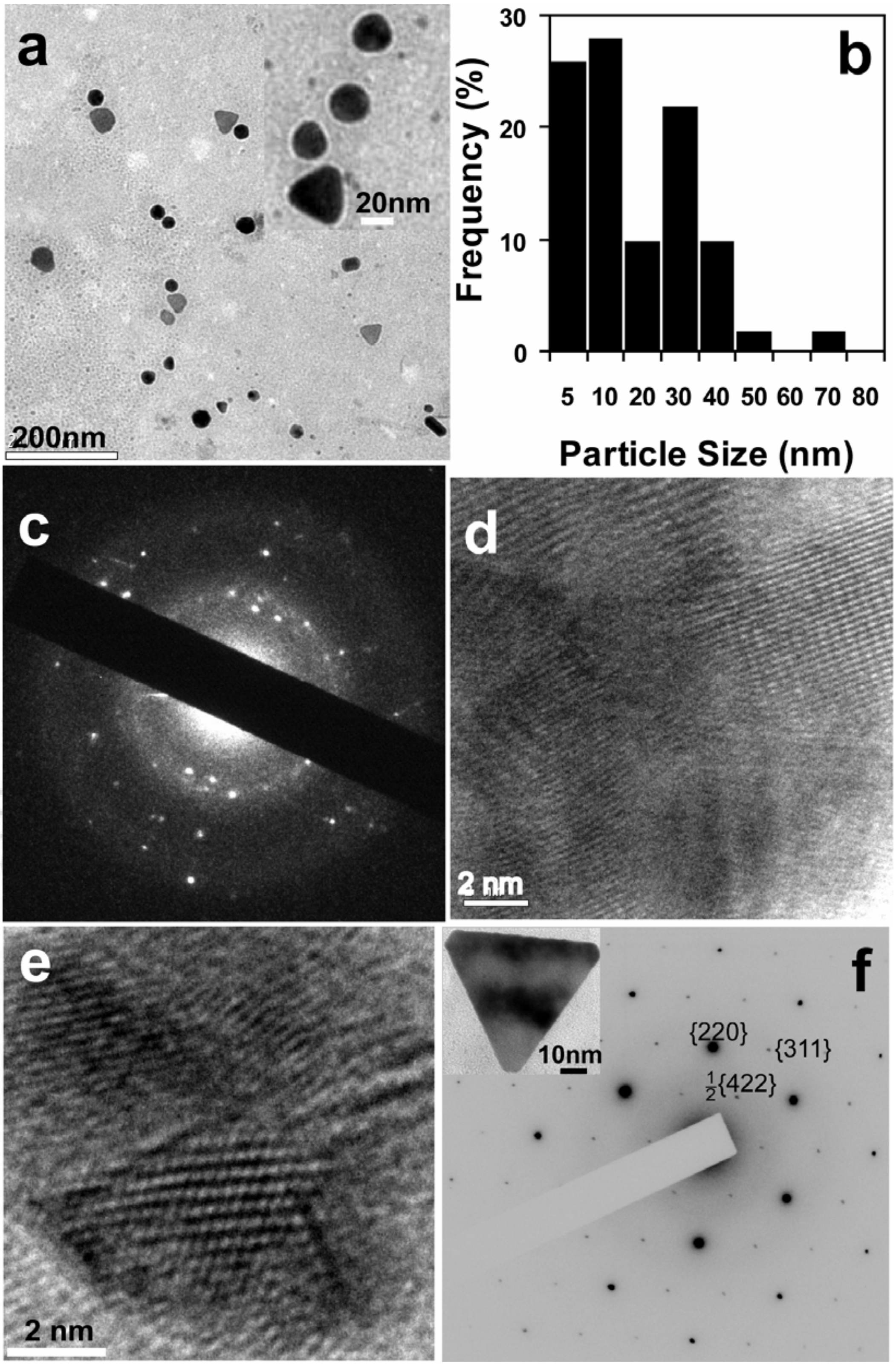

Figure 2.2. (a) TEM micrographs of Au NPs synthesized by GFP in presence of $HAuCl_4$ with corresponding size distribution **(b)** and SAED image of polygonal Au NPs **(c)**. **(d)** HRTEM image of one of these Au NPs showing well-separated lattice fringes. **(e)** HRTEM image of a polygonal Au NP showing Moiré pattern. **(f)** SAED image of an individual triangular Au NP (shown in inset); the original image was inverted for clarity.

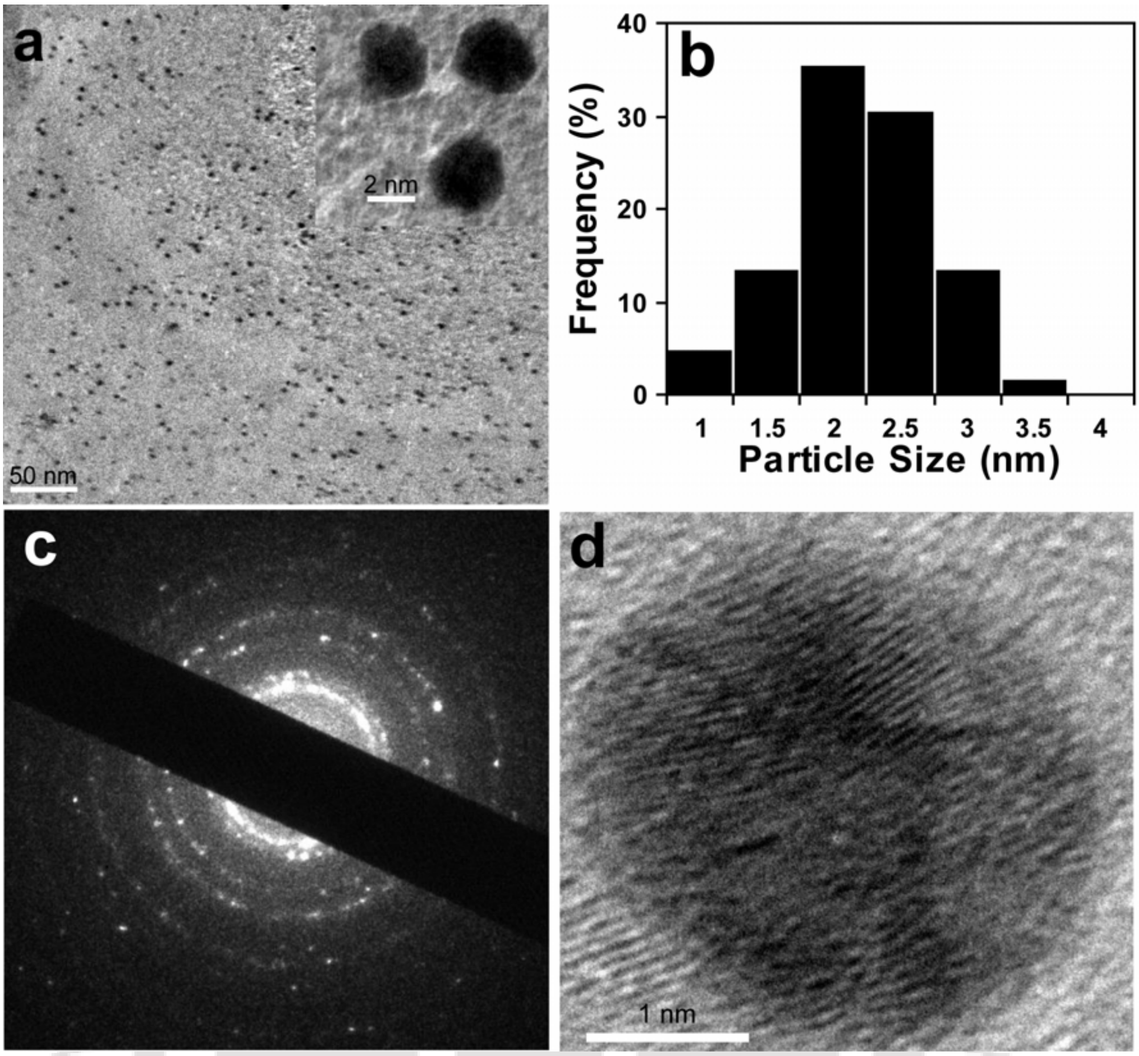

Figure 2.3. (a) TEM micrographs of Au NPs synthesized by GFP in presence of $HAuCl_4$ and 1.0×10^{-5} M $AgNO_3$ with corresponding size distribution **(b)** and SAED pattern of Au NPs **(c)**. **(d)** HRTEM image of individual Au NP showing well-separated lattice fringes.

From the TEM observation of the Au NPs synthesized by GFP, it was evident that addition of $AgNO_3$ to the reaction medium led to the formation of rather small (~2.2 nm) and uniform Au NPs, which had otherwise generated larger particles having different kind of shapes in absence of $AgNO_3$. In order to investigate the effect of $AgNO_3$ concentration on the size and shape of the synthesized Au NPs, further TEM studies were carried out with Au NPs prepared in presence of 1.0×10^{-4} M and 1.0×10^{-3} M $AgNO_3$. The particle sizes were found out to be 23.3 ± 4.3 nm and 30.6 ± 7.6 nm for 1.0×10^{-4} M and 1.0×10^{-3} M $AgNO_3$ respectively (**Figure 2.4**). Furthermore, under TEM these Au NPs were found to be mostly spherical in shape with a small fraction being triangular or rod-shaped, which were also evident from the corresponding UV-visible spectra showing weak peak at longer wavelengths (ca. 680 nm) (Figure 2.4c, 2.4f). In the present study, the average Au NP size increased by ~21 nm from 1.0 × 10^{-5} M to 1.0 × 10^{-4} M of $AgNO_3$ whereas the same was found to be ~7 nm from 1.0 × 10^{-4} M to 1.0 × 10^{-3} M of $AgNO_3$.

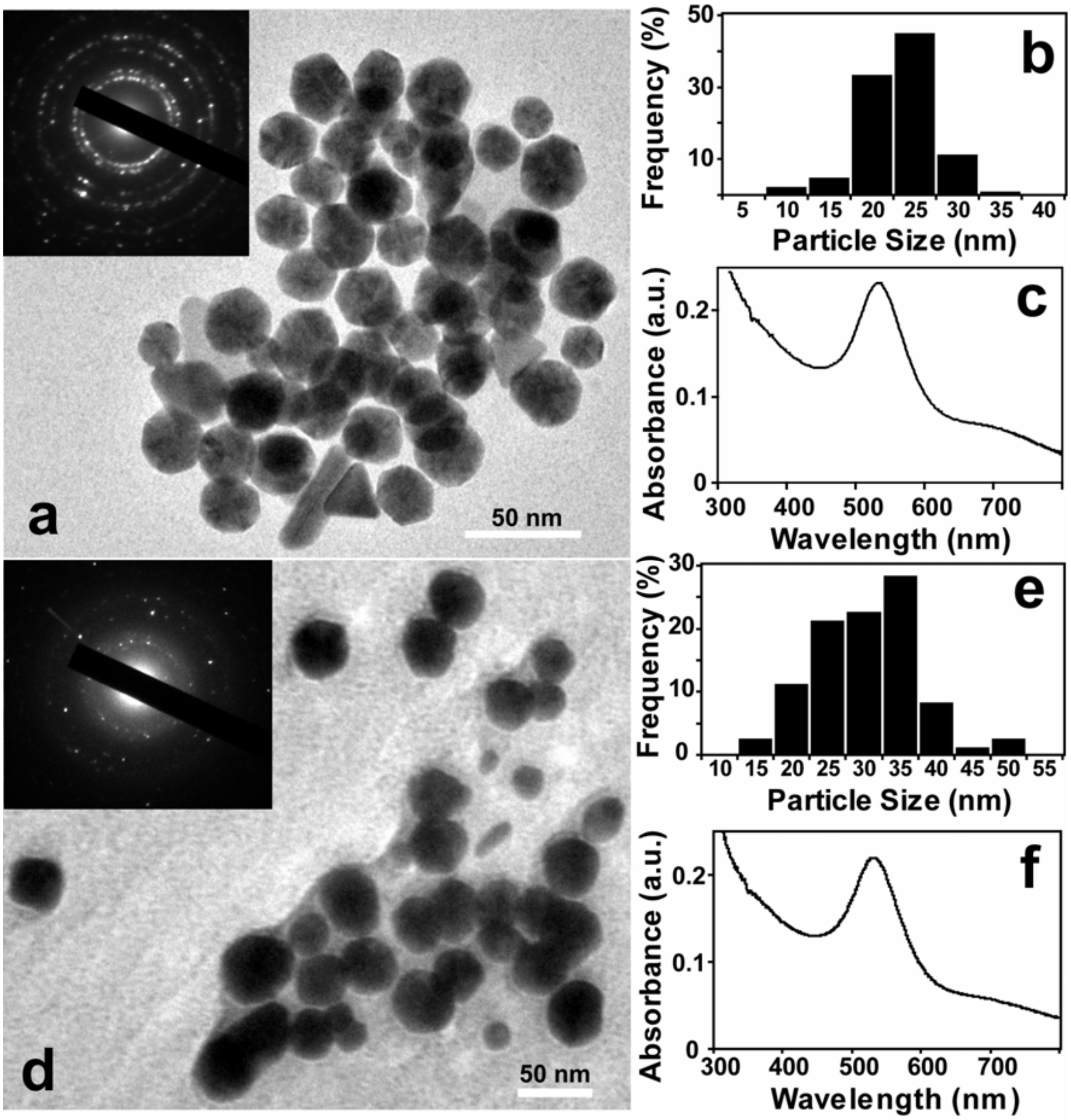

Figure 2.4. (a) TEM micrographs and SAED image (inset) of Au NPs synthesized by GFP in presence of $HAuCl_4$ and 1.0 × 10^{-4} M $AgNO_3$; **(b)** particle size distribution and **(c)** UV-visible spectrum corresponding to these particles. **(d)** TEM micrographs and SAED image (inset) of Au NPs synthesized by GFP in presence of $HAuCl_4$ and 1.0 × 10^{-3} M $AgNO_3$; **(e)** particle size distribution and **(f)** UV-visible spectrum corresponding to these particles.

2.4.2. Changes in GFP fluorescence

In order to study the structural integrity of GFP in the course of synthesis of Au NPs, the time dependent fluorescence spectroscopy of GFP was pursued (Zimmer, 2002). The changes in fluorescence characteristic of GFP due to the synthesis of Au NPs are shown in Figure 2.5. At the initial stages, all the samples showed comparable amount of fluorescence which decreased only marginally in case of control sample (only GFP in buffered solution) and the sample where only $AgNO_3$ was incubated with GFP solution (Figure 2.5a and 2.5b). On the other hand, the fluorescence of the GFP solution treated with $HAuCl_4$ only (Figure 2.5c) progressively decreased up to 56 h, without further decrease in fluorescence in later hours. However, in case of the GFP solution incubated with $HAuCl_4$ in presence of $AgNO_3$ (Figure 2.5d), the fluorescence reduced drastically with time resulting in the loss of detectable fluorescence after 24 h only.

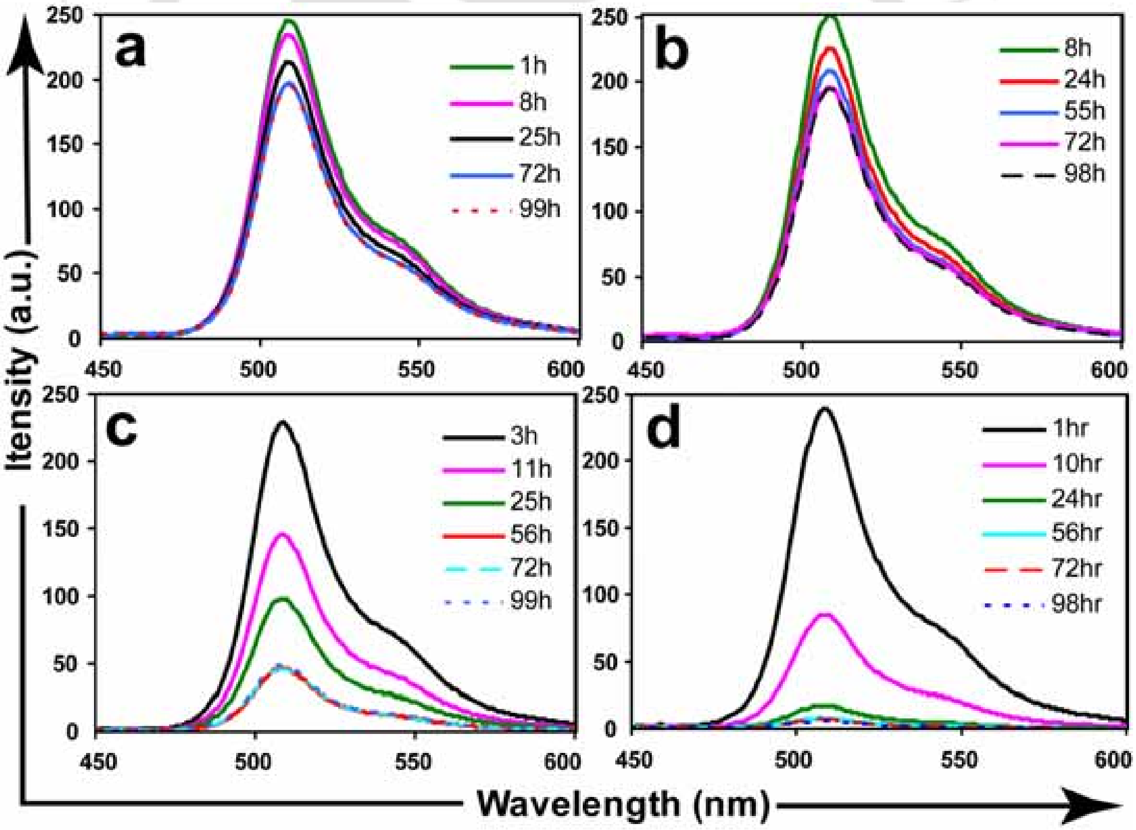

Figure 2.5. Fluorescence emission spectra of GFP during the synthesis of Au NPs in **(a)** control sample (only GFP), **(b)** GFP in presence of $AgNO_3$ (1.0×10^{-4} M) only, **(c)** GFP in presence of $HAuCl_4$ only and **(d)** GFP in presence of $HAuCl_4$ and $AgNO_3$ (1.0×10^{-5} M).

Figure 2.6 shows the fluorescence decay of GFP, expressed in terms of relative fluorescence intensity at different time intervals. The results essentially reveal that the fluorescence intensities of the samples containing $HAuCl_4$ alone or $AgNO_3$ (at different concentrations) along with $HAuCl_4$ decreased compared to control sample or sample incubated with $AgNO_3$ only, which in turn implied the loss of tertiary structure of GFP in those samples. Further, it was interesting to observe complete loss of fluorescence in samples containing GFP incubated with $HAuCl_4$ in the presence of $AgNO_3$ in 24 h, whereas GFP treated with $HAuCl_4$ only retained 40% of fluorescence in that period. On the other hand, only $AgNO_3$ had apparently no effect on the GFP structure by this time. Finally the relative fluorescence of the GFP treated with $HAuCl_4$ only, attained a minimum value of approximately 20% in later hours, which did not decrease further. Additionally, a difference in the rate of loss of fluorescence in the presence of various amount of $AgNO_3$ was observed. For example, when the concentrations were at 1.0×10^{-3} M as well as 1.0×10^{-4} M, the intensity was down to about 15% in 10 h and near-complete loss was observed at 24 h. On the other hand, when the concentration of $AgNO_3$ was at 1.0×10^{-5} M the intensity went down to 35% in 10 h and to about 5% at 24 h.

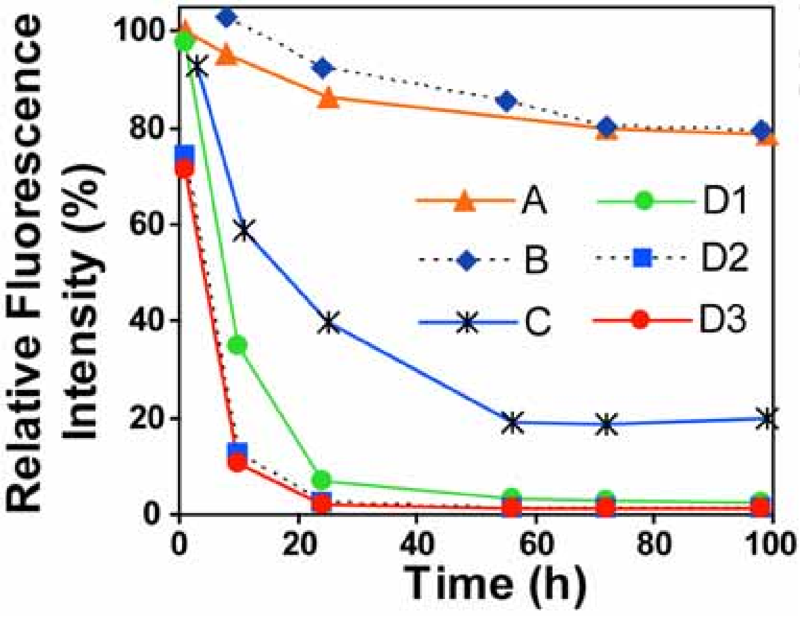

Figure 2.6. Kinetics of GFP fluorescence decay expressed (relative fluorescence intensity) in GFP only (A); GFP and 10^{-4} M $AgNO_3$ only (B); GFP and $HAuCl_4$ only (C); GFP and $HAuCl_4$ in presence of 10^{-5} M (D1), 10^{-4} M (D2), 10^{-3} M $AgNO_3$ (D3).

2.4.3. Structural changes in GFP

In order to further investigate the structural changes of GFP, the samples were analyzed by native PAGE (**Figure 2.7**). **Figure 2.7a** depicts the electrophoretic migration pattern of the native GFP in the control sample as well as in other treated samples, when the gel was observed on the UV- transilluminator. The fluorescent bands of GFP in lanes 6, 7, 8, 9 implied the retention of tertiary structure of GFP, and hence the detectable fluorescence, in the samples incubated with $HAuCl_4$ only as well as the samples treated with different concentrations of $AgNO_3$ only. On the other hand, absence of any detectable fluorescent band in lanes 2, 3, 4 or 5 could be due to the total disruption of the GFP native structure in the samples containing $AgNO_3$ in addition to $HAuCl_4$. These observations could be well correlated with the results in **Figure 2.6**. Interesting results were found after staining the gel with silver stain (**Figure 2.7b**), where the band intensity in lane 6 corresponding to the sample treated with $HAuCl_4$ only was apparently comparable to that of the control or only $AgNO_3$ treated samples. However, no bands were observed in lanes 2, 3, 4, 5. This could be due to extensive protein adsorption on the surface of Au NPs synthesized in presence of $AgNO_3$ resulting in the complete disappearance of the protein from the medium. Furthermore, the fact that the protein stabilizes the Au NPs by being attached to NP surface through cysteine thiol groups or by adsorption also supports the above possibility.

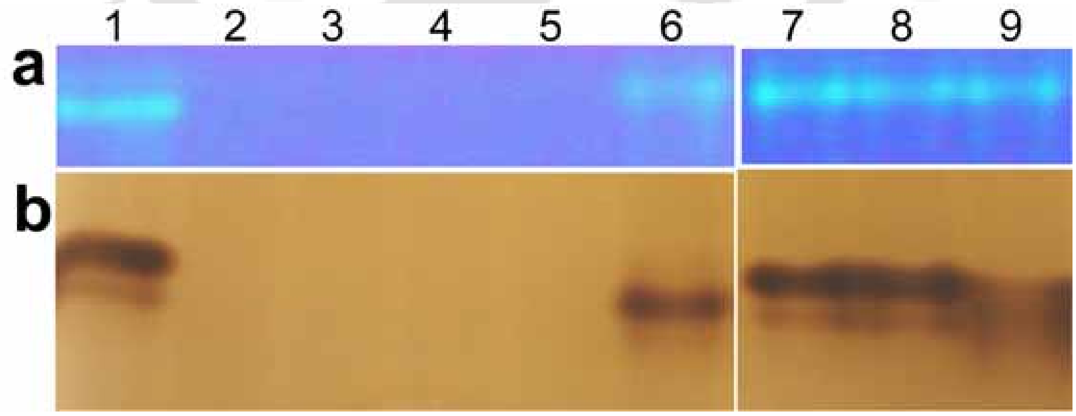

Figure 2.7. Structural integrity of GFP after the synthesis of Au NPs as followed by native PAGE: **(a)** under UV-transilluminator and **(b)** subsequent silver staining of the gel. Lanes: control (lane 1); GFP in $HAuCl_4$ with 10^{-5} M (lane 2), 10^{-4} M (lane 3), 5.0×10^{-4} M (lane 4) and 10^{-3} M (lane 5) $AgNO_3$; GFP in 10^{-4} M $HAuCl_4$ only (lane 6) and GFP in presence of 10^{-5} M (lane 7), 10^{-4} M (lane 8), and 10^{-3} M (lane 9) $AgNO_3$ only.

In order to have further insight on the adsorbed protein, samples were investigated in SDS-PAGE. The gel (**Figure 2.8**) clearly shows the GFP bands in the samples of Au NPs synthesized in presence of $AgNO_3$ (lane 6 and 7), along with the control (lane 2) and the only $HAuCl_4$ treated sample (lane 4). These results confirmed the complete attachment of GFP to the Au NPs synthesized in presence of Ag^+. This can be explained by considering the fact that Au NPs synthesized in presence of $AgNO_3$ are more uniformly small and spherical than in its absence and hence more surface area is available for protein attachment. Further, Ag^+ could play a role in this differential protein attachment by increasing positive charges on the protein. This could explain the excellent colloidal stability shown by the Au NPs synthesized in presence of $AgNO_3$ at high salt (e.g. 0.5 M NaCl) concentration compared to those in absence of $AgNO_3$, as probed by their UV-visible spectra (**Figure 2.9**). These findings essentially led to the revelation that, when GFP was incubated with $HAuCl_4$, the protein was not completely denatured although most of the tertiary structure was lost; whereas the GFP was completely attached to the Au NP surface and eventually denatured in case of the sample containing $AgNO_3$ in addition to $HAuCl_4$.

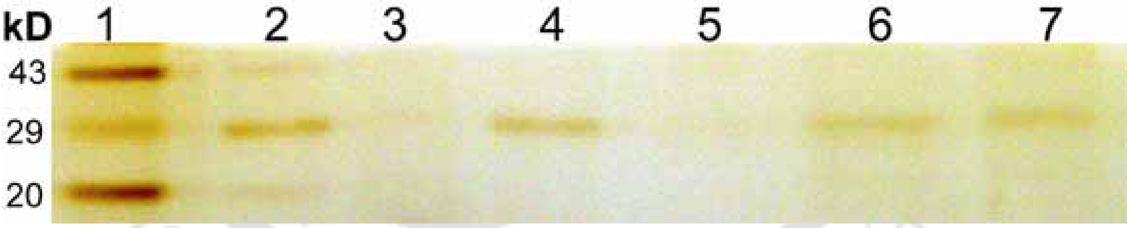

Figure 2.8. Electrophoresis profile of GFP in a denaturing gel after the synthesis of Au NPs as followed by SDS-PAGE and subsequent silver staining. Lanes: molecular weight marker (lane 1), control (lane 2), GFP in 10^{-4} M $HAuCl_4$ only (lane 4) and GFP in $HAuCl_4$ with 10^{-5} M (lane 6), 10^{-4} M (lane 7) $AgNO_3$. Lane 3 and lane 5 were left blank.

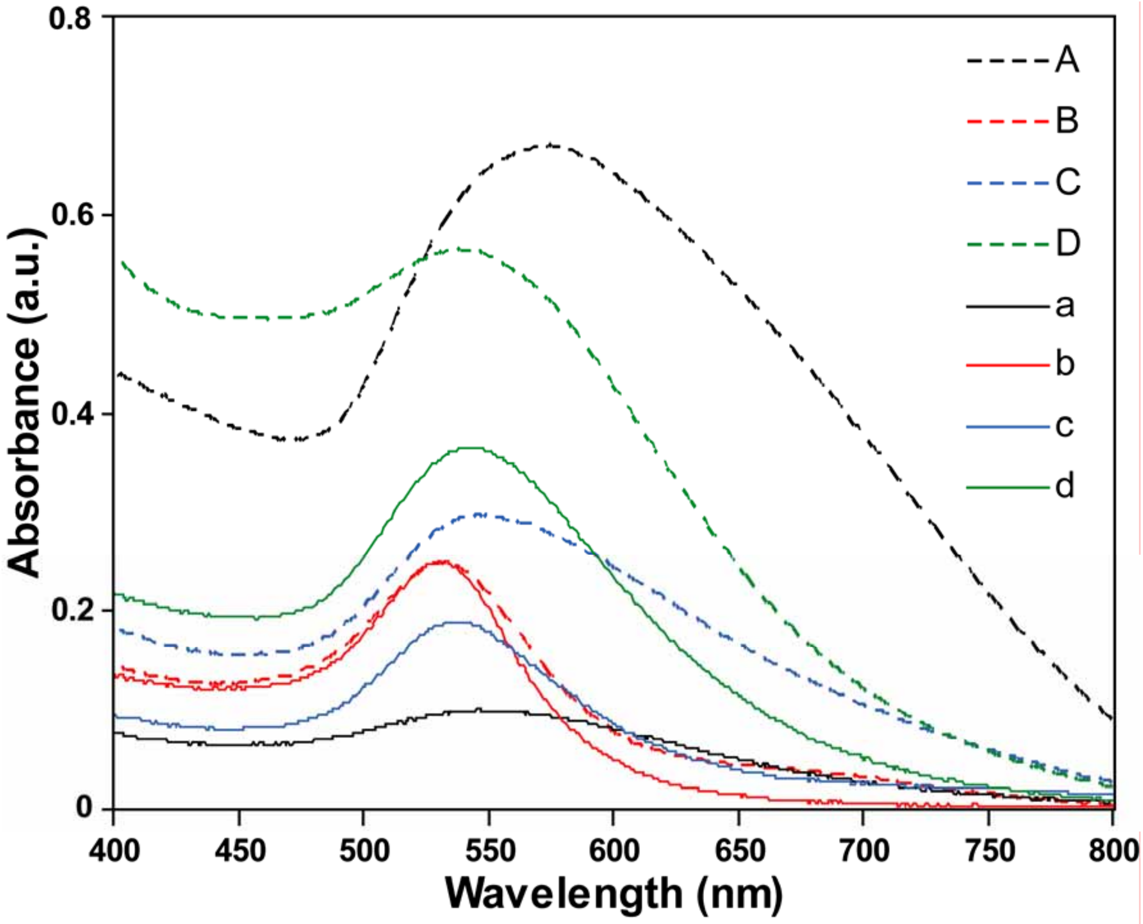

Figure 2.9. Effect of NaCl concentration on the colloidal stability of the Au NPs synthesized by GFP. UV-visible spectra of Au NPs synthesized by GFP with $HAuCl_4$ only (A. 0 M and a. 0.5 M NaCl) and $HAuCl_4$ in presence of 10^{-5} M (B. 0 M and b. 0.5 M NaCl), 10^{-4} M (C. 0 M and c. 0.5 M NaCl), 10^{-3} M (D. 0 M and d. 0.5 M NaCl) of $AgNO_3$.

In order to investigate whether the loss of GFP fluorescence was due to the denaturation of protein or the quenching of fluorescence by Au NPs, samples were further analyzed by the standard SDS-PAGE without boiling the samples before loading (partial denaturation condition) (**Figure 2.10**). Under UV-transillumination (**Figure 2.10a**), fluorescent bands were seen in control and Au NPs sample synthesized in absence of $AgNO_3$; whereas no fluorescent bands were present in the $AgNO_3$ supplemented Au NPs samples. The same gel when silver-stained (**Figure 2.10b)**, revealed protein bands in $AgNO_3$ supplemented Au NPs samples along with other samples namely control and Au NPs synthesized in absence of $AgNO_3$. Interestingly, additional non-fluorescent protein band can be observed in case of Au NPs synthesized in absence of $AgNO_3$ (**Figure 2.10b**, lane 3), which could be attributed to the denatured

GFP population present in the sample supporting fluorescence spectroscopic results (**Figure 2.5(c) and 2.6**). Finally, the absence of any fluorescent band in the $AgNO_3$ supplemented Au NPs samples and the presence of additional non-fluorescent band in non-$AgNO_3$ supplemented Au NP sample demonstrates that the loss of fluorescence of GFP adsorbed on the Au NPs is due to the denaturation of the protein structure rather than quenching of fluorescence by Au NPs.

.

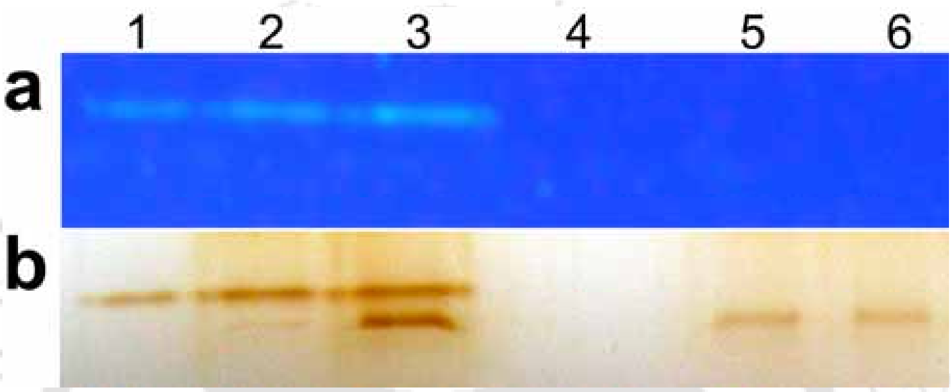

Figure 2.10. Electrophoresis profile of GFP in a partially denaturing gel after synthesis of Au NPs: **(a)** under UV-transillumination and **(b)** subsequent silver staining of the gel. Lanes: Control (lane 2), GFP in 10^{-4} M $HAuCl_4$ only (lane 3) and GFP in $HAuCl_4$ with 10^{-5} M (lane 5), 10^{-4} M (lane 6) $AgNO_3$; purified GFP reconstituted in SDS-free sample loading buffer was loaded in lane 1 as a reference. Lane 4 was left blank.

2.4.4. Mechanism of Au NP synthesis

Synthesis of Au NPs from $HAuCl_4$ by GFP essentially involves the reduction of Au^{3+} (in $AuCl_4^-$) to metallic gold (Au^0). Now the potential of a protein to be used as a reducing agent for the synthesis of metal NPs has not been widely studied despite the fact that there are different functional groups in the side chain of the constituting amino acids in a protein. Out of these various functional groups, thiol (-SH) associated with cysteine residue is of principal interest as it can readily react with gold to form Au-S bond as well as reduce Au^{3+} to Au^0. Recently, Rangnekar et al. (2007) have reported the enzymatic synthesis of Au NPs by α-amylase and proposed that free and exposed thiol groups of the enzyme were responsible for the reduction of Au^{3+} to metallic Au NPs. The structural analyses revealed that GFP (**Figure 2.11a**) has two free cysteine thiol groups – one of which is exposed on the surface of the protein while the other one is buried in the three dimensional structure (Yang at al., 1996). On the other hand, the fundamental role of tyrosine in the reduction of Au^{3+} to Au^0 has recently been identified by others (Zhou et al., 2001; Tomczak et al., 2007). There are ten tyrosine residues in a GFP molecule among which five are surface exposed. Because of their strong electron donating properties, the tyrosine residues of GFP could also be the potential candidates for Au^{3+} reduction in the present study.

In order to ascertain the mechanism of Au NP synthesis involved in the present study, the free cysteine thiol groups of GFP were modified with DTNP as described previously (Rangnekar et al., 2007). The UV-visible spectrum of the reaction mixture initially showed the characteristic DTNP peak at 317 nm (**Figure 2.11b**). The DTNP peak completely disappeared after overnight incubation with the concomitant appearance of a pale yellow coloured solution which indicated the modification of the free thiol groups as mentioned previously (Rangnekar et al., 2007). This was further confirmed by examining the UV-visible spectrum of the yellow colored solution (**Figure 2.11b**), which consisted of a single peak at 390 nm characteristic of 5-nitropyridine-2-thione formed as a product of the reaction between DTNP and thiols. We also observed that DTNP-treated GFP retained its fluorescence property. Incubation of thiol-modified GFP with $HAuCl_4$ did not produce Au NPs either in presence or in absence of $AgNO_3$ (1.0×10^{-4} M), whereas control experiments with unmodified GFP resulted in the formation of Au NPs under identical conditions (**Figure 2.11c**). **Figure 2.11c** clearly shows that $HAuCl_4$ incubated with unmodified GFP exhibited the characteristic Au NP absorption band around 550 nm and 528 nm in absence and presence of $AgNO_3$, respectively. On the other hand, thiol-modified GFP did not produce any visible absorption band upon $HAuCl_4$ treatment either in presence or in absence of $AgNO_3$. Furthermore, it has already been demonstrated that 5-nitropyridine-2-thione, product of the reaction between DTNP and thiols, does not affect the Au NP formation (Rangnekar et al., 2007). These results clearly demonstrate that the free thiol groups of cysteine residues in GFP are responsible for the reductive synthesis of Au NPs and also eliminate the possibility of the involvement of tyrosine residues in the Au^{3+} reduction process.

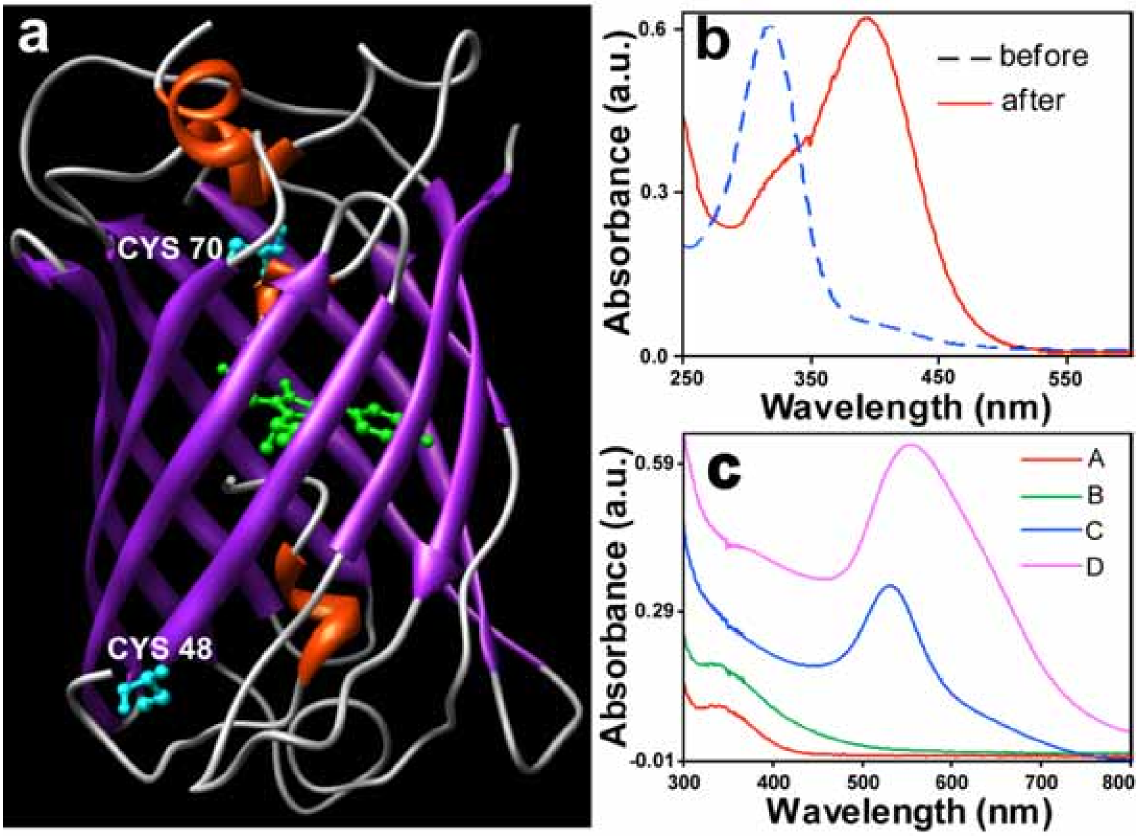

Figure 2.11. **(a)** Three dimensional structure of GFP (PDB ID: 1EMA) showing buried Cys 70 and exposed Cys 48 residue bearing free thiol group; **(b)** UV-visible spectra of GFP plus DTNP before and after overnight incubation at 37^{0}C. **(c)** UV-visible spectra of GFP incubated with $HAuCl_4$ only (A. DTNP treated and D. unmodified GFP) and GFP incubated with $HAuCl_4$ in presence of 10^{-5} M $AgNO_3$ (B. DTNP treated and C. unmodified GFP).

The three dimensional structure of GFP is a β-can structure consisting of 11 β-sheets, forming a barrel like structure, and a α-helix running diagonally through the barrel with the chromophore attached to this α-helix at the centre (Yang at al., 1996; Zimmer, 2002). The stability of the chromophore and hence the fluorescence of the GFP is strongly dependent on the tertiary structure which covers almost all of the primary sequence of GFP. The plot of time-dependent changes in fluorescence of the protein as well as the increase in absorbance due to the formation of NPs as shown in **Figure 2.12** indicates that the process of protein destabilization and the synthesis of Au NPs occur separately. As is clear from the figure, the addition of $AuCl_4^-$ to GFP, both in the presence and absence of $AgNO_3$, possibly leads to the destabilization of the native structure of the protein and hence the loss of fluorescence at the early hours. This is followed by the thiol-mediated reduction of the metal salt leading to the formation of

NPs and hence increases in the absorbance at 532 nm, which takes place at a much slower pace compared to the rate of loss of fluorescence. It may be mentioned here that it is plausible that the destabilization of GFP makes the Cys 70 thiol group also exposed, which is otherwise buried in the three dimensional structure of native protein. The free thiol groups of Cys 70 along with the surface exposed Cys 48 help both in the formation and concurrent stabilization of the Au NPs, as established above. In brief, the loss of fluorescence due to the denaturation of the protein occurs much earlier than the formation and stabilization of the NPs.

Furthermore, synthesis of Au NPs by heat-denatured GFP was investigated in order to understand the importance of native structure of the protein for NP synthesis (**Figure 2.13**). Although Au NPs were synthesized by the denatured protein in presence as well as in absence of $AgNO_3$, the particle sizes were not commensurate with those formed starting with native protein under the same experimental condition. Also, the particles formed with the heat-denatured proteins tend to agglomerate into lumps of structures indicating random agglomeration following the synthesis of particles. It is interesting to observe the formation of Au NPs by heat denatured protein in the presence of $AuCl_4^-$ alone resulted in a red-shift of the absorbance maxima in comparison to those synthesized by native protein. This indicates formation of larger particles as a result of agglomeration which can also be seen in the TEM micrographs. On the other hand, the UV-visible spectra of the NPs synthesized by heat-denatured protein in the presence of $AgNO_3$ consisted of peak at the same wavelength as those formed without heat-denaturation. This indicates that although the particles appeared to have lumped together in the TEM micrograph they might actually be separated by the denatured protein thus exhibiting absorption spectra of those produced with the native protein. Essentially, the process of NP formation by the heat-denatured proteins and native proteins are different, although the proteins in the end get denatured even in the case of starting with native proteins. The denaturation of protein by $AuCl_4^-$ and $AgNO_3$ involved a process leading to well-separated and uniform NPs, which is very different from those produced through heat-mediated denaturation of the protein.

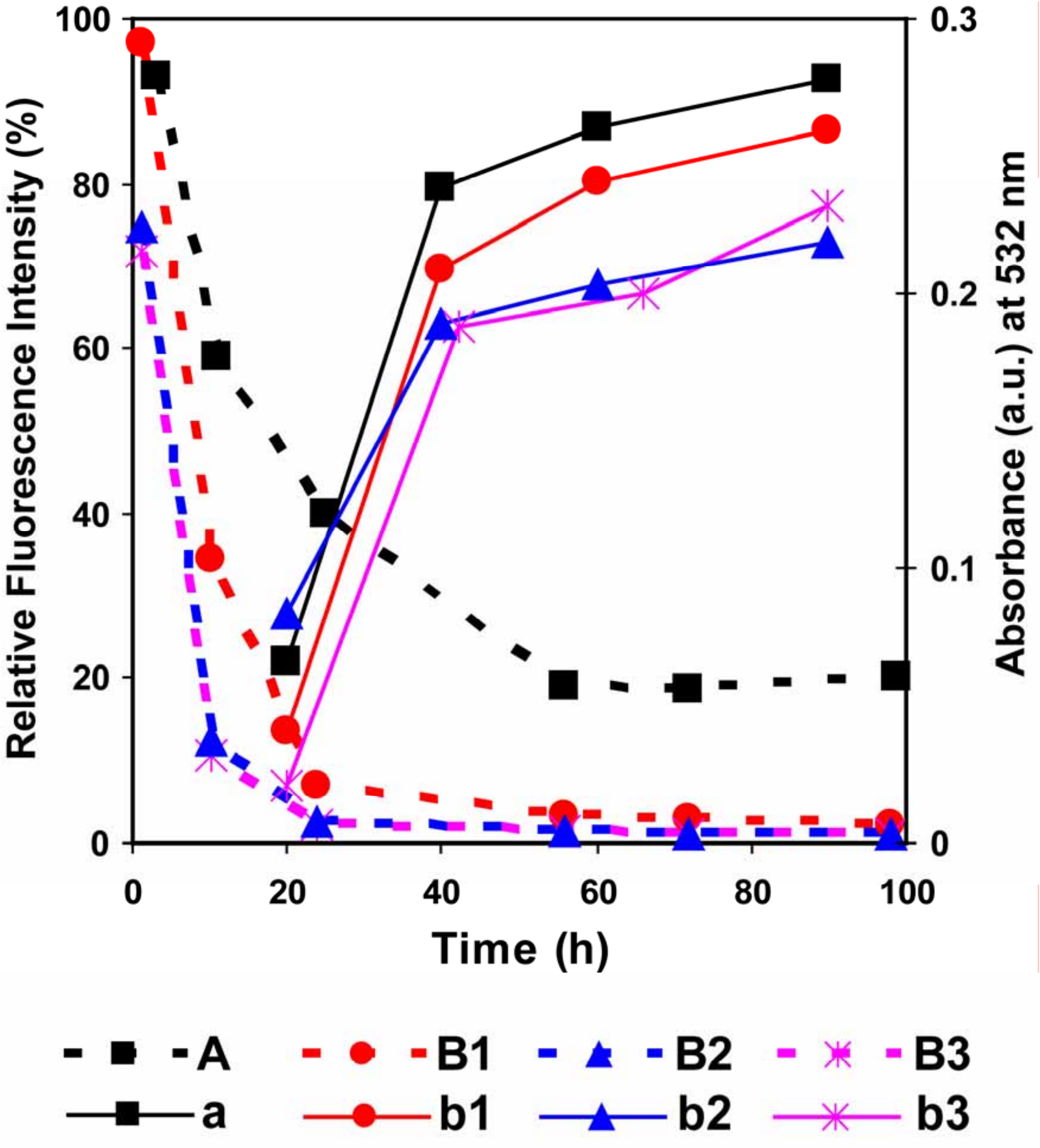

Figure 2.12. Concomitant changes in GFP fluorescence intensity (expressed in terms of relative fluorescence intensity calculated based on initial fluorescence intensity at λ $_{emission}$ = 509 nm) and surface plasmon resonance of Au NPs (expressed in terms of absorbance at 532 nm) in sample containing GFP and $HAuCl_4$ only (**A-** fluorescence profile and **a-** absorbance profile); sample containing GFP and $HAuCl_4$ in presence of 1.0 × 10^{-5} M (**B1-** fluorescence profile and **b1-** absorbance profile), 1.0 × 10^{-4} M (**B2-** fluorescence profile and **b2-** absorbance profile), 1.0 × 10^{-3} M $AgNO_3$ (**B3-** fluorescence profile and **b3-** absorbance profile).

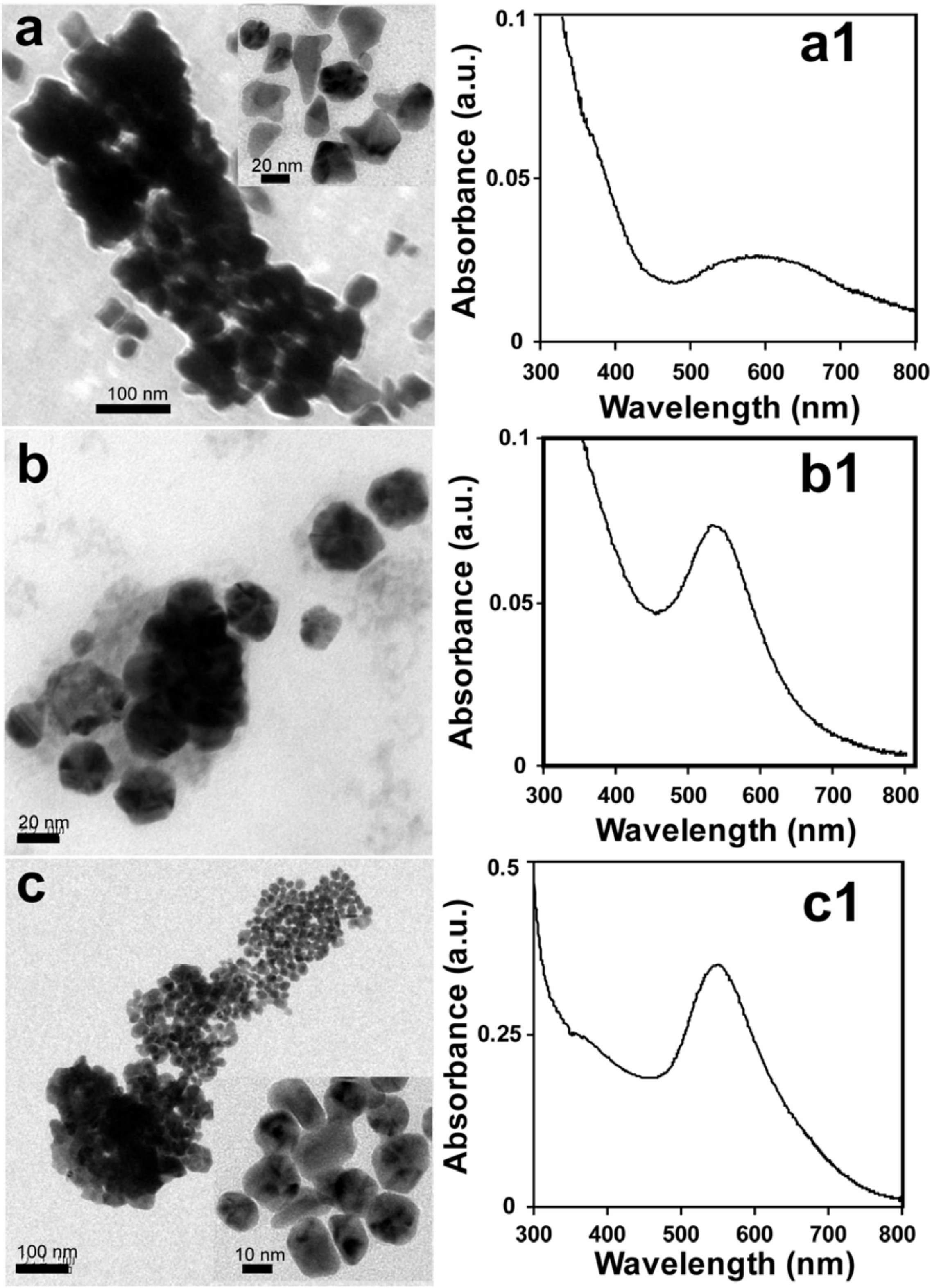

Figure 2.13. TEM micrographs Au NPs synthesized by heat-denatured GFP in presence of $HAuCl_4$ only **(a)**; $HAuCl_4$ and 10^{-5} M $AgNO_3$ **(b)**; $HAuCl_4$ and 10^{-4} M $AgNO_3$ **(c)**. The UV-visible spectra of corresponding Au NPs are shown in **a1**, **b1** and **c1**, respectively.

2.5. Conclusion

In brief, a novel one-step method of synthesizing monodisperse Au NPs of ca. 2.2 nm using purified recombinant GFP as the reducing agent have been developed. For the synthesis of these sub-5 nm Au NPs, the role of $AgNO_3$ as well as the native structure of GFP have been found to be critical. Using GFP as the model system for the reductive synthesis of Au NPs, it was also possible to study the fate of the protein during the synthesis of NPs by simply probing the fluorescence of GFP. Also, the Au NPs synthesized in presence of $AgNO_3$ exhibited complete adsorption and subsequent denaturation of the protein. The insight gained in the present study about the synthesis of the Au NPs and concurrent interaction with GFP would be critical in developing functional nanobio-devices intended to be applied in biological systems as delivery vehicle or even as probes. It will be interesting, in this regard, to further investigate the effect of biocompatible metal NPs on the prokaryotic as well as eukaryotic cells in search of potential therapeutic implications.

CHAPTER 3

Antibacterial Properties of a Novel Chitosan– Silver Nanoparticle Composite

Chapter 3 describes the antibacterial potential of a newly synthesized chitosan-Ag-nanoparticle composite against E. coli expressing green fluorescent protein (GFP). The composite was found to have significantly higher bactericidal activity than its components at their respective concentrations.

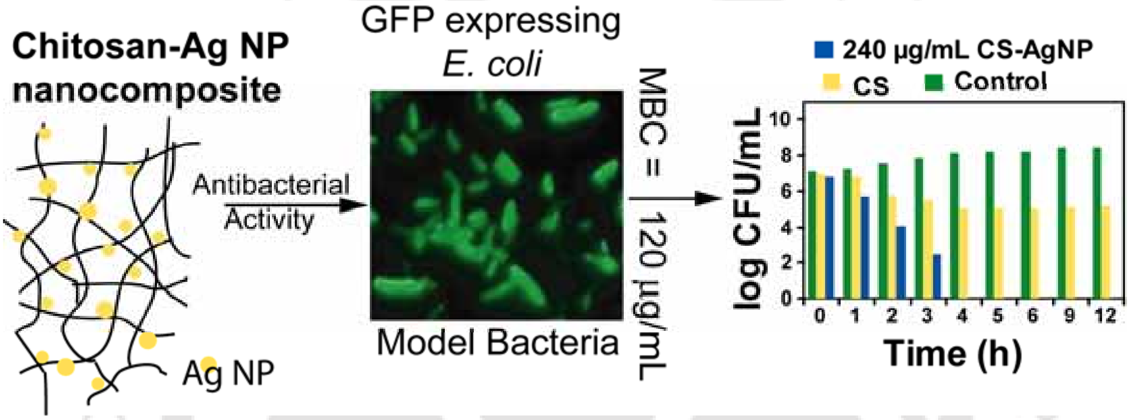

Chapter 3

ANTIBACTERIAL PROPERTIES OF A NOVEL CHITOSAN–SILVER NANOPARTICLE COMPOSITE

3.1. Introduction

Chitosan is an important poly-cationic biopolymer having high antimicrobial activity (Rabea et al., 2003). Chitosan has been used in diverse areas such as agriculture, food industry, cosmetics, pharmaceutics and various biomedical applications because of ease of processing due to unique molecular structure, broad spectrum of antimicrobial activity, inherent biodegradability and biocompatibility (Martino et al., 2005; Sashiwa et al., 1990; Shigemasa et al., 1994 and 2004; Majeti and Kumar, 2000; Roy et al., 1999; Shi et al., 2006; Khor and Lim, 2003). The antibacterial activity of chitosan and its derivatives has been extensively studied with proposed mechanism being the binding of cationic chitosan with negatively charged bacterial cell wall and subsequent destabilization of the cell envelope, which leads to altered permeability followed by possible attachment of chitosan with DNA inhibiting DNA replication (Rabea et al., 2003; Helander et al., 2001; Yi et al., 2003; Wang et al., 2004).

On the other hand, the possible potential of Ag NPs as antibacterial agent has been revealed recently as a consequence of the emergence of bacterial resistance to the conventional bactericides and antibiotics (Sondi and Salopek-Sondi, 2004; Morones et al., 2005; Gogoi et al., 2006; Jain and Pradeep, 2005; Lee et al., 2005). The proposed mode of bactericidal action of Ag NPs is that Ag NPs attach to the bacterial cell wall via thiol containing proteins and possibly bind to DNA by penetrating the cell membrane with compromised permeability. Recent results from our laboratories (Gogoi et al., 2006), however, suggest that Ag NPs do not have any direct effect either on the bacterial DNA or on intracellular protein structures. Despite the potential of Ag NP-based chitosan nanocomposite as effective bactericides, there are only a few reports (Rhim et al., 2006) on the antimicrobial activity of Ag NP-chitosan nanocomposite. Therefore, further investigations on the interactions between Ag NP-chitosan composite and microorganisms accompanied by mechanistic details are needed in order to provide biomedical and food-industrial applications with biocompatible nanocomposite having enhanced antimicrobial activity.

3.2. Outline of the Research Work

1) A novel and ‘green’ method of synthesizing chitosan-Ag NPs composite using chitosan as the reducing as well as stabilizing agent has been developed.
2) The antibacterial effect of chitosan-Ag NPs composite was investigated on GFP expressing recombinant *Escherichia coli* (*E. coli*) as a model system, using GFP as an easy probe to understand the bactericidal mechanism by spectroscopic and microscopic tools.
3) Modern analytical tools such as, fluorescence microscopy, scanning electron microscopy (SEM), transmission electron microscopy (TEM) and confocal laser scanning microscopy (CLSM) were used to monitor morphological changes in bacterial cells, while biochemical changes were studied by viability tests, fluorescence spectroscopy and electrophoretic analysis of proteins.
4) The chitosan-Ag NP composite showed elevated antibacterial activity compared to either chitosan or Ag NPs, due to their synergistic effect of chitosan and Ag NPs. Furthermore, the bactericidal properties of the composite did not have any direct effect on cellular proteins.

3.3. Experimental Section

3.3.1. Growth media, chemicals and GFP expressing E. coli

E. coli growth media Luria-Bertani (LB) and agar powder (bacteriological grade) were purchased from HiMedia, India. Silver nitrate ($AgNO_3$) and acetic acid (glacial, 99-100%) were purchased from Merck India Ltd. Chitosan (high MW, >75% deacetylated) and other high purity molecular biology grade chemicals and reagents for native-PAGE were obtained from Sigma-Aldrich Chemical Corporation. The procedure related to the generation of GFP expressing recombinant *E. coli* cells has been described previously from our laboratory (Gogoi et al., 2006).

3.3.2. Synthesis of chitosan-Ag NPs composite

Chitosan-Ag NPs composite was prepared by adding freshly prepared $AgNO_3$ solution (4×10^{-4} M) followed by 100 µL of 0.3 M NaOH solution, to 50mL of 0.2 % chitosan solution in a beaker under constant stirring at 95^0C. The appearance of yellow color within 1 min of NaOH solution addition indicated formation of Ag NPs. The reaction was stopped after 10 min and the resultant yellow color precipitate was filtered and washed with water. The filtrate was dried and finally a 0.2 % solution of chitosan-Ag NPs composite was made in 0.1 % acetic acid solution. Appropriate amount of this solution were added to the bacterial medium for bactericidal study as described below.

3.3.3. Characterization of chitosan-Ag NPs composite

UV-visible spectra of the nanocomposite samples (in 0.1 % acetic acid) were recorded using a Perkin-Elmer Lambda-25 spectrophotometer. The dynamic light scattering measurements of the samples were performed with an ALV 400 (Peters) particle size analyzer. The composite was dissolved in 0.1 % acetic acid and then kept in the sample compartment of the equipment. The above measurements were performed at room temperature. For transmission TEM analysis, 5 µL of appropriate sample of the chitosan-Ag NPs composite in LB media was drop coated on carbon coated copper TEM grids followed by air-drying. The grid was then analyzed by a JEOL 2100 UHR-TEM instrument operating at an accelerating voltage of 200 KeV.

3.3.4. Antibacterial activity of the nanocomposite

GFP expressing *E. coli* cells (10^6 CFU) were grown overnight in 150 mL LB medium (pH 6.3) supplemented with 100 µg mL^{-1} ampicillin. The cells were then harvested by centrifugation and resuspended in 300 µL LB medium. 100 µL of the cell suspension was separately inoculated into 50 mL fresh LB – ampicillin media (pH 6.3) with two different chitosan-Ag NPs concentrations (240 and 360 µg mL^{-l}) and incubated aerobically at 37°C. Appropriate control was kept by growing bacteria in absence of chitosan-Ag NP. Bacterial growth was monitored by observing the turbidity of periodically withdrawn culture by a UV-visible spectrophotometer (SPEKOL 1200, Analytikjena, Germany) at 595 nm. Simultaneously, the GFP fluorescence of each sample was measured by a fluorescence spectrophotometer (Varian Cary Eclipse) with an excitation wavelength of 400 nm. The cell viability was also quantified by plating serially diluted bacterial culture on LB-agar ampicillin plates.

The minimum inhibitory concentration (MIC) is the minimum concentration of an antimicrobial substance below which the test compound fails to inhibit the microbial growth. The minimum killing concentration (MKC) is, on the other hand, the minimum concentration of the test compound required to kill the microbes. The minimum concentration of the nanocomposite, at which no visual turbidity could be observed, represented the MIC of chitosan-AgNP nanocomposite. The cultures lacking turbidity were re-inoculated into fresh LB media containing ampicillin to check their viability. Similarly, MKC of the nanocomposite was the concentration that prevented growth of the bacterial cells following re-inoculation. Appropriate control experiments were performed with acetic acid only.

3.3.5. Fluorescence and confocal laser scanning microscopy (CLSM)

Antibacterial effects of chitosan-Ag NPs composite on GFP expressing *E. coli* cells were monitored under epifluorescence microscope (Axioskop2 MAT, Carl Zeiss) as well as confocal microscope (Axiovert 200 M, LSM 510 META, Carl Zeiss) at different time intervals. Aliquots of 5μL bacterial culture withdrawn from the control and treated samples were placed over microscope slides, air-dried and observed under microscopes. The excitation wavelengths were 445-495 nm and 488 nm for epifluorescence microscope and confocal microscope, respectively, while the observation filters had long-pass filter wavelength above 515 nm for both.

3.3.6. Scanning electron microscopic (SEM) Analysis

The interaction of chitosan-Ag NPs composite with bacterial cells at different time points of study were examined in LEO1430VO SEM by depositing 10 μL of each sample on glass slides followed by air drying. The slides were then coated with gold film for investigations under SEM.

3.3.7. Poly-acrylamide gel electrophoresis (PAGE)

For protein analysis by native PAGE, cells from 2 ml portions of control and treated samples were harvested by centrifugation, washed and resuspended in 500 μl of phosphate buffer saline (PBS). The samples were sonicated using an ultra-sonicator

(VibraCell, Sonics, Newtown, CT, USA) to disrupt the cells, then centrifuged to remove the cell debris. An 8 µl portion of supernatant from each sample was mixed with 2 µl of 5× sample loading buffer [310 mM Tris–HCl, pH 6.8, 50% (v/v) glycerol, and 0.05% (w/v) bromophenol blue] and loaded onto a 12% (w/v) polyacrylamide gel prepared in 1.5 M Tris–HCl buffer, pH 8.8. Electrophoresis was performed at 20 mA for 3 h using Tris/glycine electrophoresis buffer, pH 8.3 (Tris base, 3 g/l and glycine,14.4 g/l). Proteins were visualized by staining with Coomasie Brilliant Blue R-250 solution. GFP bands were visualized by UV trans-illumination of the gel.

3.4. Results and Discussion

3.4.1. Characterization of chitosan-Ag NPs composite

Chitosan has strong affinity towards metal ions due to extensive presence of amine and hydroxyl groups which can absorb metal ions either by chelation or by ion exchange mechanism (Varma et al., 2004; Vold et al., 2003). These properties have been exploited by Huang and Yang (2004) to synthesize Au NP-chitosan composite. It has recently been found in our laboratory that chitosan can also reduce Ag^+ ions to Ag atoms under alkaline condition (Murugadoss and Chattopadhyay, 2008). This observation was used to synthesize Ag NPs using chitosan as the reducing agent in the present study.

The UV-visible absorption spectrum of chitosan-Ag NPs composite (**Figure 3.1a**) showed a single and narrow peak at ca. 410 nm, characteristic of surface plasmon resonance (SPR) of Ag NPs. The resultant NPs get anchored to the polymer once produced in the reaction and thus proving a single-step synthesis and stabilization of Ag NPs. In order to find the sizes and shapes of the Ag NPs synthesized using the present method, the composite was further investigated by TEM **(Figure 3.1b)**. **Figure 3.1b** indicated that the Ag NPs produced were small and spherical in nature. The selected area electron diffraction pattern (SAED) in **Figure 3.1c** confirmed the presence of single crystalline Ag NPs. A typical particle size distribution determined by DLS (**Figure 3.1d**) indicates that more than 90% of the particles produced in this method have diameters between 2 nm - 4 nm. This is important as it is well established that the Ag NPs must necessarily be less than 10 nm in diameters to be effective bactericidal. It is also evident from the TEM image that the small Ag NPs were uniformly distributed over the flakes of chitosan, which is critical for effectiveness of the composite as more uniformly distributed NPs in the composite have better antimicrobial activities than those distributed less homogeneously.

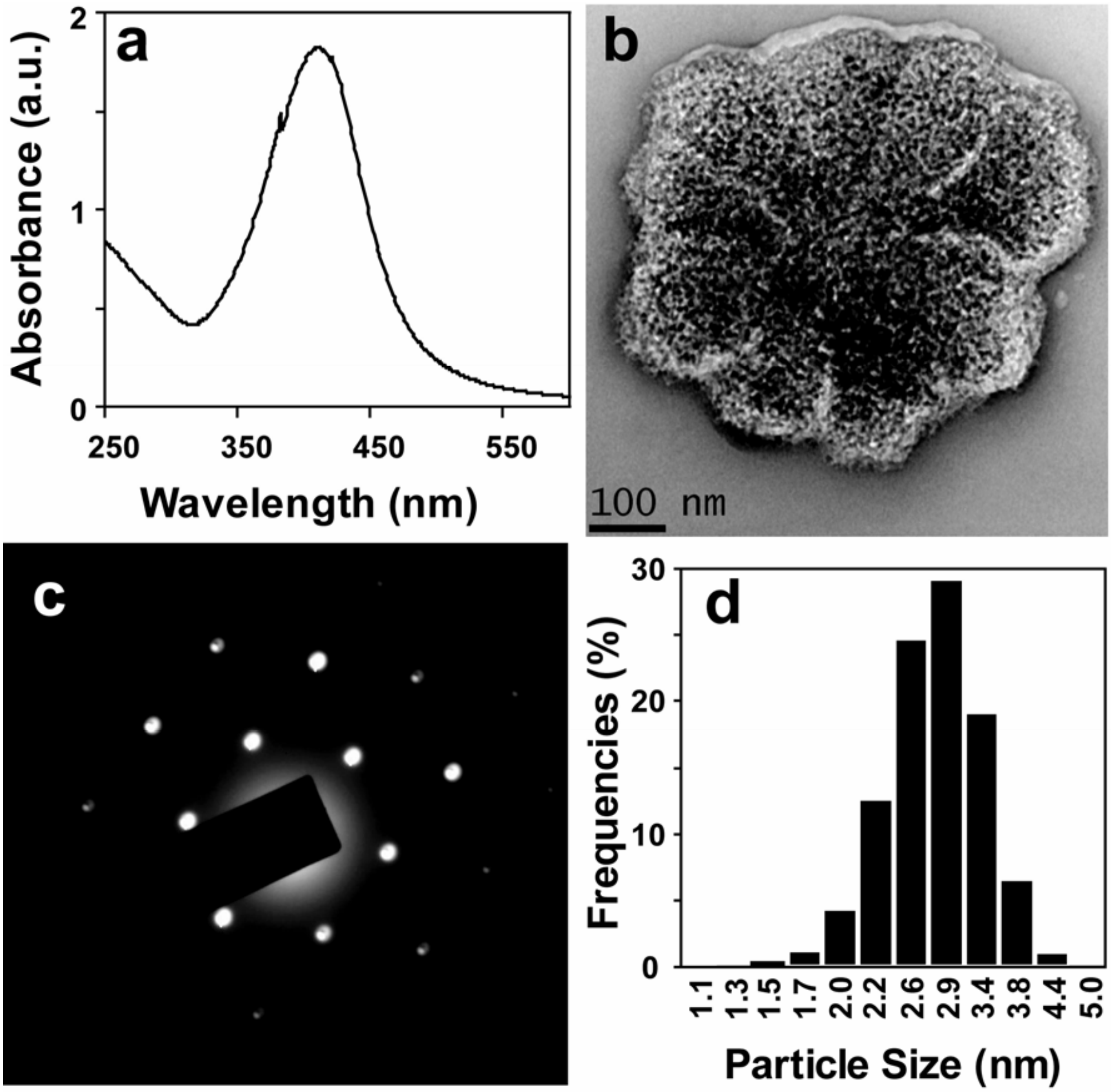

Figure 3.1. **(a)** UV-visible absorption spectrum of the chitosan-Ag NP composite. **(b)** TEM micrograph of chitosan-Ag NP with corresponding SAED pattern **(c)**. **(d)** Particle size distribution of chitosan-Ag NP composite as determined by DLS.

3.4.2. Antibacterial activity

The primary challenge in determining the efficacy of the nanocomposite as bactericide and bacteriostatic is to be able to have the aqueous solution of the composite near physiological pH conditions so that the NPs would be working under micro-heterogeneous conditions. This would also allow the testing of the composite near to ideal conditions in contrast to the conventional tests for chitosan carried out at low pH conditions or under heterogeneous conditions (Fujimoto et al., 2006). In order to achieve this, the composite was dispersed in the bacterial medium at pH 6.3 in the presence of acetic acid. It was observed that this was an optimal condition for the intended studies without affecting the bacteria due to harsh experimental conditions as well as for obtaining stable composite dispersion in water.

The effect of the chitosan-Ag NPs composite on the growth of GFP expressing *E. coli* was investigated through a time-dependent turbidity measurement study by monitoring OD_{595}. As evident from **Figure 3.2**, the bacterial growth was completely inactivated at chitosan-Ag NPs composite concentration of 100 µg mL^{-1} or more, whereas a concentration of 10 µg mL^{-1} caused a retarded growth. On the other hand, the negligible growth inhibition in the sample treated with 300 ppm acetic acid (acetic acid control) indicated that using acetic acid at low concentration (60 ppm), for the dispersion of chitosan-Ag NP composite in the present system, did not show any adverse effect on the bacterial growth. The MBC and MIC in the present study were found to be 100 µg mL^{-1} and 120 µg mL^{-1}, respectively. The literature reference for MBC of chitosan on *E. coli* ranges from 0.0075 % - 1.0 % (w %) (Rabea et al., 2003). The variations in bactericidal efficiency of chitosan can be ascribed to the fact that antimicrobial activity of chitosan depends on a number of parameters such as its molecular weight, degree of deacetylation, viscosity, ionic strength, pH and presence of metallic ions in the media and the temperature (Liu et al., 2006; No et al., 2002; Chung et al., 2003). Due to variation of the parameters mentioned above, it is difficult to get an unambiguous comparison among individual studies. However, it was observed that 0.012 % is the concentration of chitosan (in the composite) needed for inhibiting the growth of the bacteria in the medium. This value is comparable to other reports as the conditions of the present study were much milder (such as pH) in comparison to other reports. The concentration of Ag NPs at MIC and MBC values of the chitosan-Ag NPs composite are 2.2 µg mL^{-1} and 2.6 µg mL^{-1} respectively, which are much less than earlier reports for Ag NPs only (Gogoi et al., 2006). In other words, the amount of Ag NPs needed for antimicrobial activities are much less in the composite than the NPs alone.

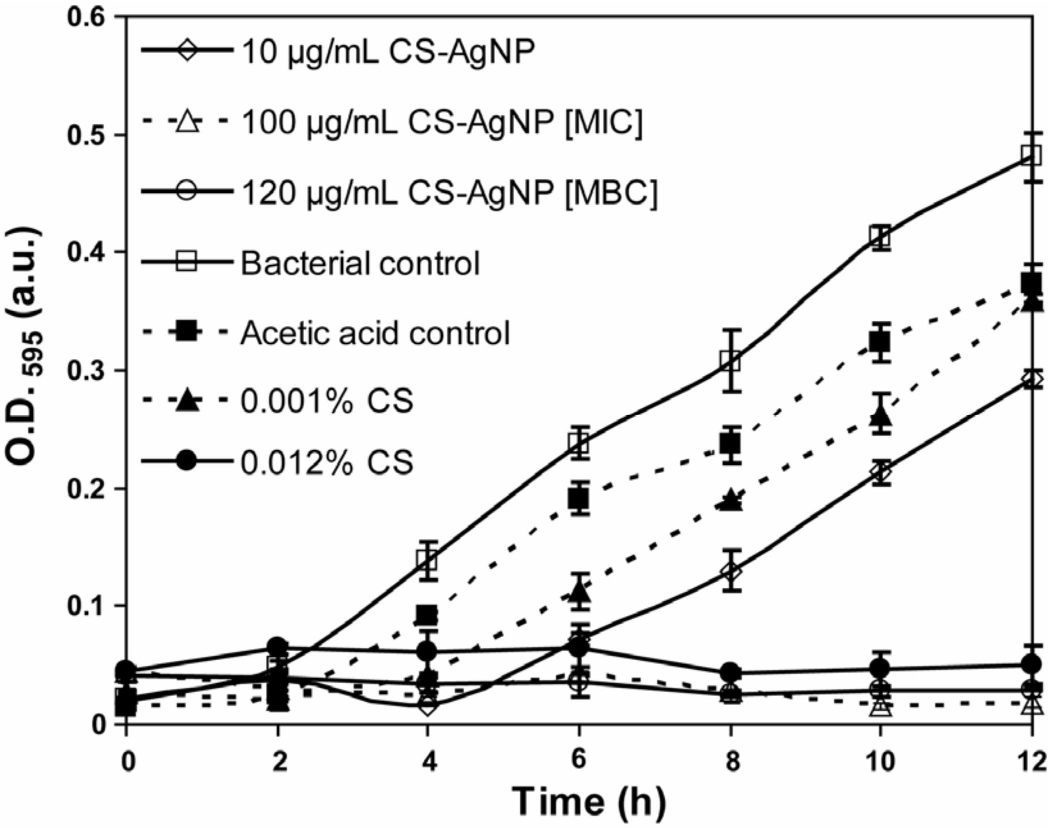

Figure 3.2. Effect of different concentrations of chitosan-Ag NP composite on the growth of recombinant *E. coli*. CS in the figure represents chitosan.

Also clear from **Figure 3.2**, only chitosan is less efficient than chitosan-Ag NPs composite in inhibiting the bacterial growth. There could be several factors contributing to this efficiency. As discussed before, the NPs synthesized herein were less than 5 nm in diameters whereas previous studies have reported with particles around or less than 10 nm in diameters. Smaller NPs are known to be more reactive and hence could be more efficient in their antimicrobial activities. Also, it has to be considered that chitosan itself is known for having strong antibacterial properties. The present investigation, therefore, indicates that chitosan-Ag NPs composite is more efficient than either Ag NPs or chitosan alone in killing bacteria.

A more quantitative understanding of the antibacterial activities was pursued by standard viability test of the bacteria in the presence of the composite. **Figure 3.3a** shows the comparative effect of chitosan-Ag NPs composite (at 2× MBC) and only chitosan on the bacterial growth. Also, it is evident from **Figure 3.3a**; chitosan-Ag NP composite killed all the bacteria within 4h, whereas chitosan was found to be bacteriostatic only at the test concentration. Furthermore, it was important to investigate the killing rate of bacteria as a function of concentration of the composite. This was pursued by following the time-dependent viability of composite-treated bacteria, at the concentration of twice and thrice of the MKC. The results, shown in **Figure 3.3b**, demonstrated that the rate of bacterial inactivation by the composite varied proportionally with the composite concentration.

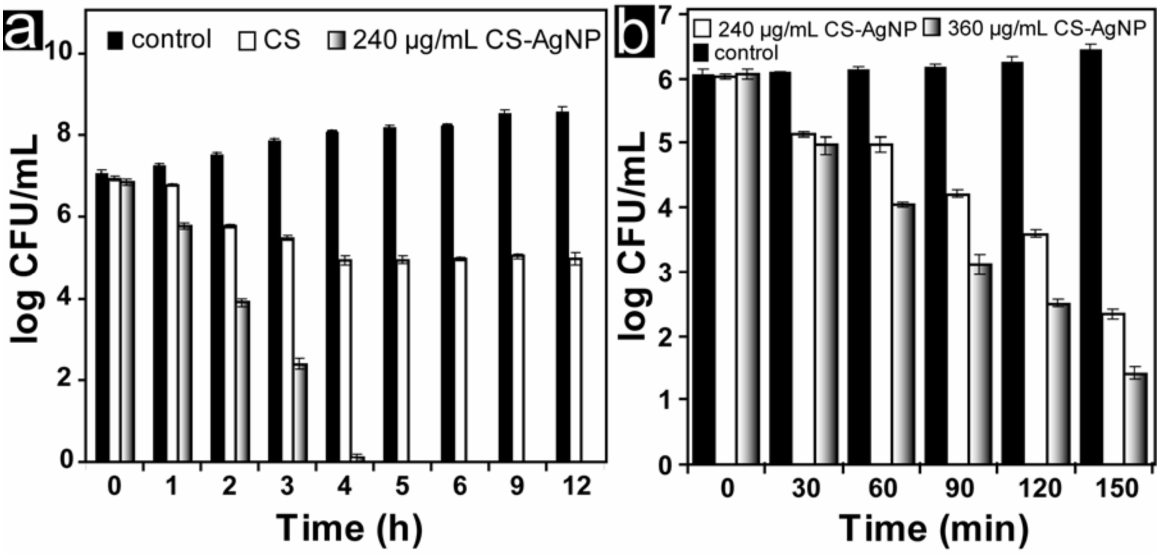

Figure 3.3. (a) Comparative effect of chitosan-Ag NPs and chitosan only on recombinant *E. coli* viability. **(b)** Effect of chitosan-Ag NPs composite of higher concentration (2× and 3× MBC) on the viability of recombinant *E. coli*. CS represents chitosan.

3.4.3. Fluorescence microscopy

Time-dependent fluorescence micrographs of control and chitosan-Ag NPs composite treated GFP expressing *E. coli* are shown in **Figure 3.4**. At 0 h, the bacterial populations in all the three samples were proportionate. The little variation in **Figures 3.4A1**, **3.4B1** and **3.4C1** are due to exact distributions of bacteria present on the spot as observed under microscope, after evaporation of the droplets containing bacterial solution. However, important observation is that while the population increased with time in the control sample, the number of bacteria as well as the fluorescence intensity decreased in the treated samples with time. The results indicate that the nanocomposite is efficient in terms of antimicrobial activities. Further, it is important to note that the antimicrobial activities of the composite could easily be probed by fluorescence microscopy under milder conditions.

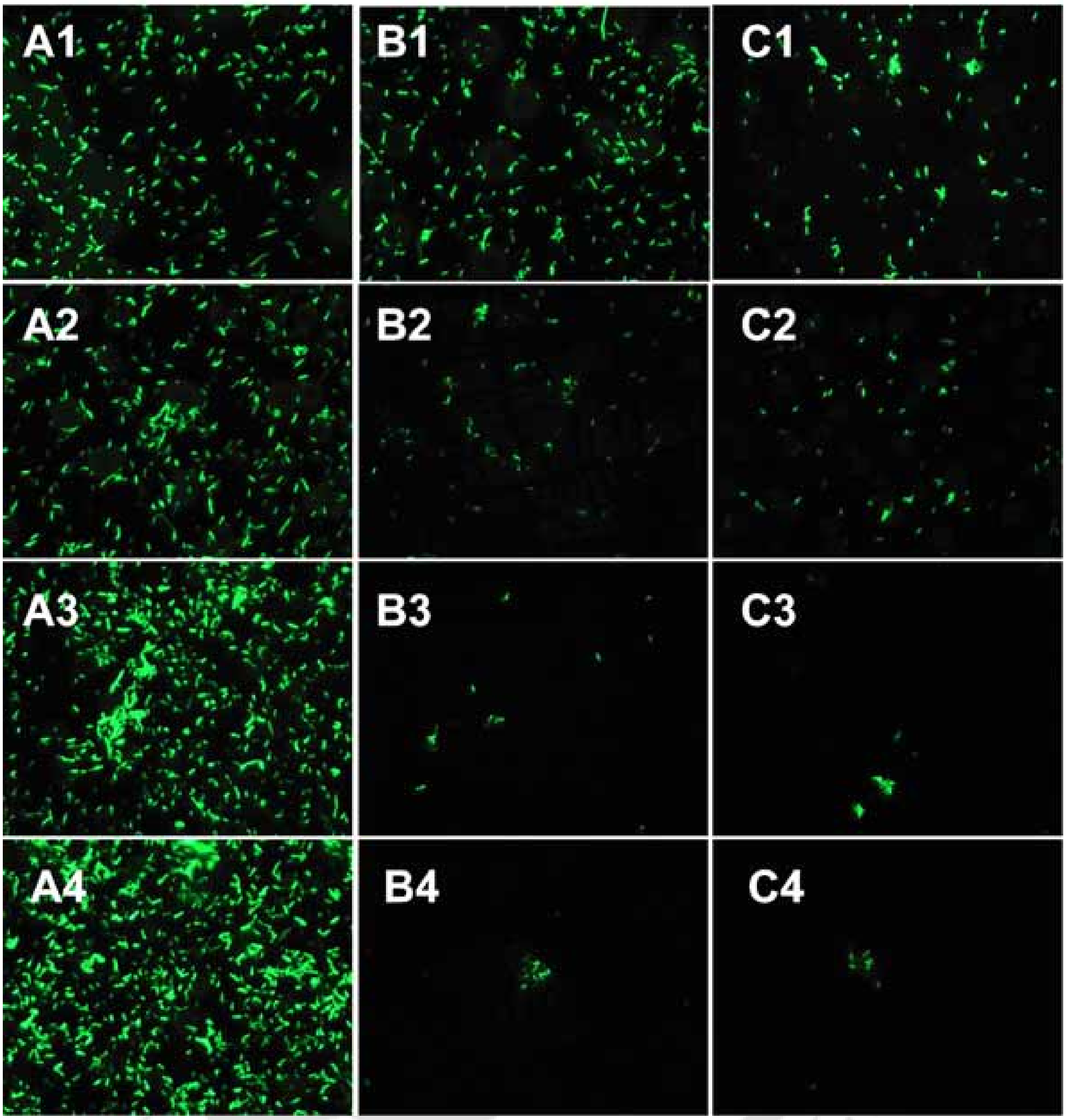

Figure 3.4. Time dependent fluorescence micrograph of GFP expressing *E. coli*. Columns **A**, **B** and **C** represent control, 240 µg mL^{-1} of chitosan-Ag NPs and 360 µg mL^{-1} of chitosan-Ag NPs composite treated samples, respectively. Rows **1**, **2**, **3**, and **4** stand for samples at 0, 3, 6 and 12 h time interval, respectively.

3.4.4. Mechanism of antibacterial activity

There are several studies regarding the antibacterial activity of chitosan and also about its effect specifically on *E. coli*. Although different hypotheses have been proposed, the exact mechanism behind the bactericidal activity of chitosan has still not been fully understood (Rabea et al., 2003). On the other hand, the antibacterial effect of Ag NPs has also been reported with different mechanisms proposed by different groups (Sondi and Salopek-Sondi, 2004; Morones et al., 2005; Gogoi et al., 2006). In order to investigate the mechanism of bactericidal action of chitosan-Ag NP composite in the present study, the chitosan as well as composite-treated *E. coli* bacteria were observed under SEM (**Figure 3.5**). Under SEM, the composite treated bacteria were seen to be attached to the composite immediately after the treatment (**Figure 3.5a**). By 60 min, fragmentation of the attached bacteria was apparent (**Figure 3.5b**). Within 90 min most of the bacteria appeared to be fragmented and deformed (**Figure 3.5c**). In contrast, with chitosan alone the numbers of bacteria attached to the polymer appeared to be less than the numbers attached to the composite (**Figure 3.5d**). That the attachment of bacteria to the polymer leads to the killing of the bacteria can be understood in terms of immobilization of the bacteria and thereby preventing any further activity. The outer membrane (OM) of gram negative bacteria (*E. coli*) consists of lipopolysachharides (LPS) containing phosphate and pyrophosphate groups which render the cell surface negatively charged (Prescott et al., 2002). On the other hand, chitosan is a cationic polymer and can, therefore, attach with *E. coli* cell wall easily by electrostatic interaction.

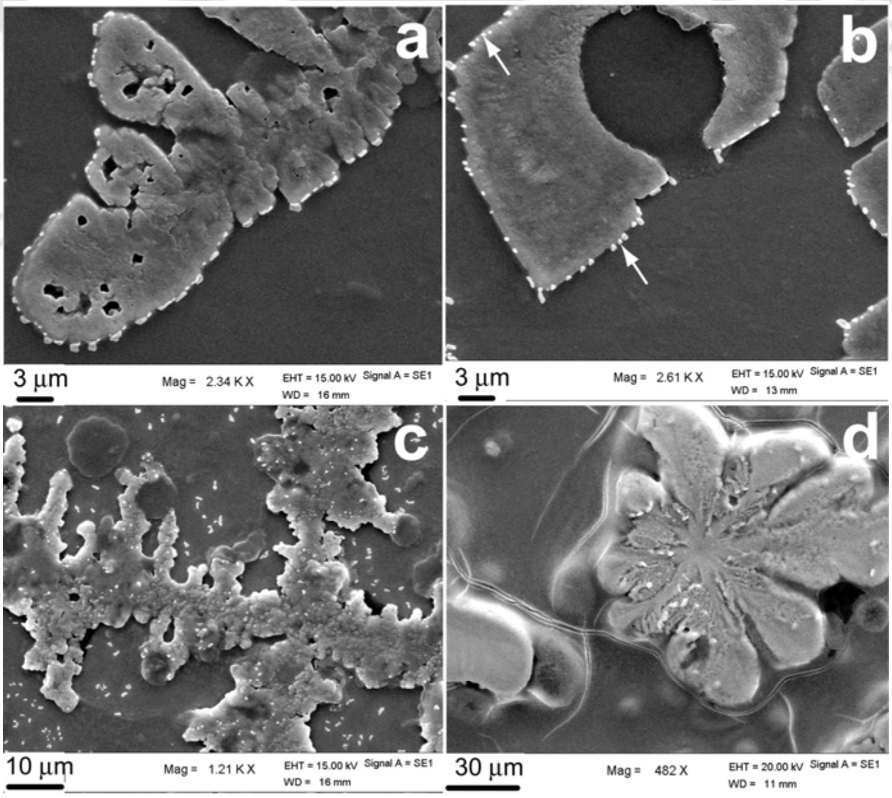

Figure 3.5. SEM micrograph of *E. coli* cells after **(a)** 30 min, **(b)** 60 min, **(c)** 90 min treatment with chitosan-Ag NPs composite material and **(d)** after 90 min treatment with chitosan only.

Under careful observation of **Figures 3.5**, it is clear that most of the bacteria appeared to be attached on the boundary and/or the crevices in the chitosan structures, whereas the bacterial cells should ideally be found all over the chitosan structure due to the electrostatic interaction. It may be mentioned here that, chitosan is known to form gel by interaction with phosphates and sulphates (Sinha et al., 2004) present in both LB medium and LPS of bacterial cell itself. The formation of gel could interfere with the clear view of the bacterial distribution over the chitosan structures under SEM (Walker et al., 2003). To overcome this problem, chitosan-Ag NP treated recombinant bacterial cells were further examined under CLSM. **Figure 3.6** clearly shows that the GFP expressing recombinant *E. coli* bacteria were attached all over the chitosan structure. Thus it is clear that the bacteria get attached to the chitosan and subsequently die. The use of GFP expressing recombinant *E. coli* bacteria as a model system in the present study was crucial in this respect as the fluorescence of GFP enabled the visualization of the effect of interaction of bacteria with chitosan-Ag NP composite.

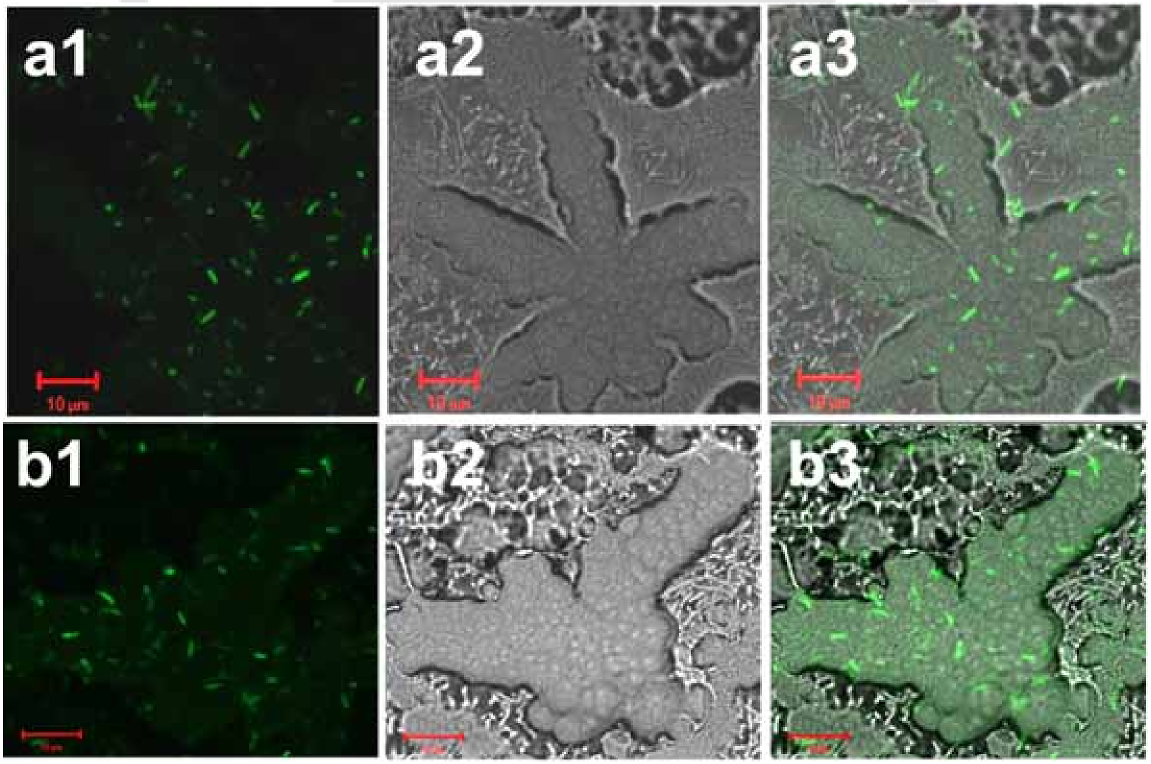

Figure 3.6. Confocal laser scanning micrographs of GFP expressing *E. coli* treated with **(a)** chitosan-Ag NP composite and **(b)** chitosan only. Series 1 and 2 correspond to images in fluorescence and DIC mode respectively while series 3 represents the combined image.

Further analysis of the CLSM micrograph of *E. coli* cells treated with chitosan-Ag NP for 1 h (**Figure 3.7a**) showed considerable number of lyzed bacteria with some extracellular fluorescence. The destabilization of the cell wall by chitosan in chitosan-Ag NPs composite treated bacteria may be enhanced by the binding of Ag NPs to the thiol containing proteins present in the cell wall. At the same time, some of the Ag NPs could actually penetrate the barrier of the cell wall resulting into compromised permeability (Morones et al., 2005; Gogoi et al., 2006; Feng et al., 2000). This can lead to leakage of proteins and other intracellular constituents (Rabea et al., 2003; Helander et al., 2001), followed by bacterial death. This was substantiated by fluorescence spectroscopic studies for the presence of GFP in the cell free supernatant. The fluorescence intensities of the GFP released into the medium by untreated, chitosan treated and composite treated bacterial cultures are shown in **Figure 3.7b**. The fluorescence spectroscopic studies showed that the amount of GFP released into the medium was much higher for both the composite and chitosan treated *E. coli* cells compared to the amount released by untreated cells. Also, the release of GFP into the medium, which indicated the degree of membrane destabilization, was faster in the composite treated sample than in the chitosan treated sample.

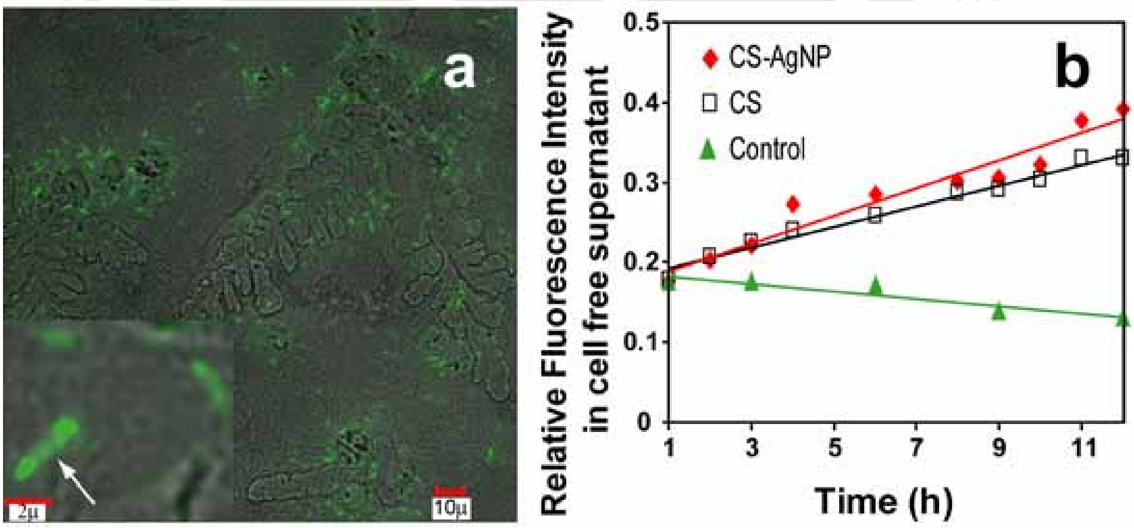

Figure 3.7. **(a)** CLSM micrograph of GFP expressing *E. coli* after 1 h incubation with chitosan-Ag NPs composite; the fragmentation of bacteria is evident (inset). **(b)** Ratio of GFP fluorescence intensity in cell free supernatant to that of the total bacterial culture for 360 µg ml^{-1} of chitosan-Ag NPs treated, 0.036 % chitosan treated and control sample.

3.4.5. Effect on bacterial proteins

In order to investigate the effect of the composite on the bacterial proteins, whole cell proteins from the control and treated samples were analyzed by PAGE in non-denaturing condition. **Figure 3.8** shows the quantitative difference in protein profile for control and treated samples. The growth of *E. coli* was responsible for the progressive increase in the band intensities in untreated samples. The band positions in the composite treated samples were similar to those in untreated samples at different times. In contrast, the band intensities in treated samples were less than those in untreated samples. Under UV trans-illumination the differences between untreated and treated samples with respect to GFP fluorescence were again apparent.

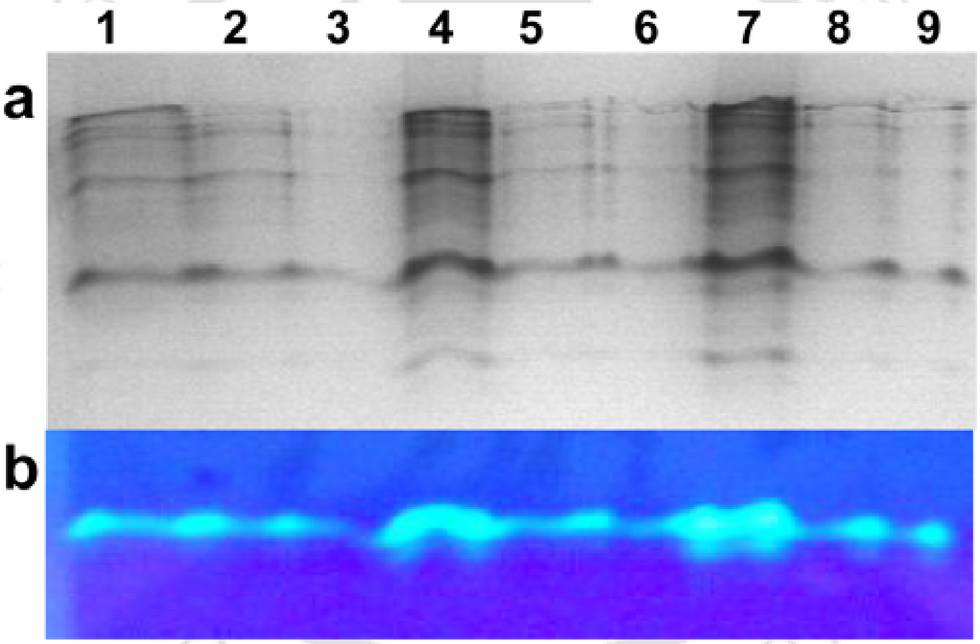

Figure 3.8. **(a)** Whole cell protein profile of chitosan-Ag NPs composite treated *E. coli* in native PAGE, **(b)** Fluorescence profile of GFP in whole cell lysate observed by keeping the same gel under UV-transilluminator Lanes 1, 4 and 7 show protein isolated from control, lanes 2, 5 and 8 show protein isolated from 240 µg mL^{-1} composite treated, and lanes 3, 6, 9 show protein isolated from 360 µg mL^{-1} composite treated *E. coli* cells all at 3 h, 6 h and 12 h respectively.

It has been proposed by Liau et al (1997) that the interaction of Ag^{+} with thiol groups of the proteins had important role in the bactericidal activity of silver. It has also been proposed that Ag NPs could interact with the sulfur containing intracellular proteins in the bacterial cells (Morones et al., 2005; 2006; Feng et al., 2000). However, recent study from our laboratory has indicated that Ag NPs have no observable effect on the proteins of *E. coli* bacteria (Gogoi et al., 2006). The present study also indicates that the chitosan-Ag NP composite does not have any discernible effect on the cellular proteins of the *E. coli* bacteria.

4. Conclusion

In the present study, it has been shown that a newly synthesized chitosan-Ag NPs composite material is more effective in antibacterial activity compared to those of either Ag NPs or chitosan alone. The synthesis of chitosan-Ag NPs composite by a novel method using chitosan as the reducing as well as capping agent provides a 'green' approach to study the antimicrobial characteristics of nanomaterials. Moreover, the inherent stability and uniformity of the fluorescence property and nominal photo-bleaching of GFP allowed us to use GFP expressing *E. coli* as the model system to understand the antibacterial effects more efficiently compared to previous reports (Newman, 2006) involving use of commercial dye which are known not to stain uniformly because of physiological and morphological differences. The results primarily indicate that the composite not only kills the bacteria more efficiently in comparison to the polymer alone, it also induces faster release of cellular GPF into the medium by rupturing the cell wall at a shorter time. Finally, the present work shows the promise combining nanotechnology and biotechnology in deciphering the role of an antimicrobial agent with consequential potential biomedical applications. In this regard, it is important to develop an effective biodergradable nanocarrier system embedding Ag NPs and study its interaction with the mammalian cells.

CHAPTER 4

Chitosan-Based Nanocarrier for Silver Nanoparticles with Enhanced Catalytic Activity

Development of a completely 'green' method of preparing a chitosan based biodegradable nanocarrier system for silver nanoparticles (Ag NPs) is reported in this chapter. The polymer nanocarriers were about 172.6 nm in size with homogenously embedded Ag NPs of diameter ca. 4.9 nm. The catalytic activity of the nanocarrier system was investigated by following the $NaBH_4$ mediated reduction of 4-nitrophenol and found to be much superior to the bulk polymer-Ag NP composite.

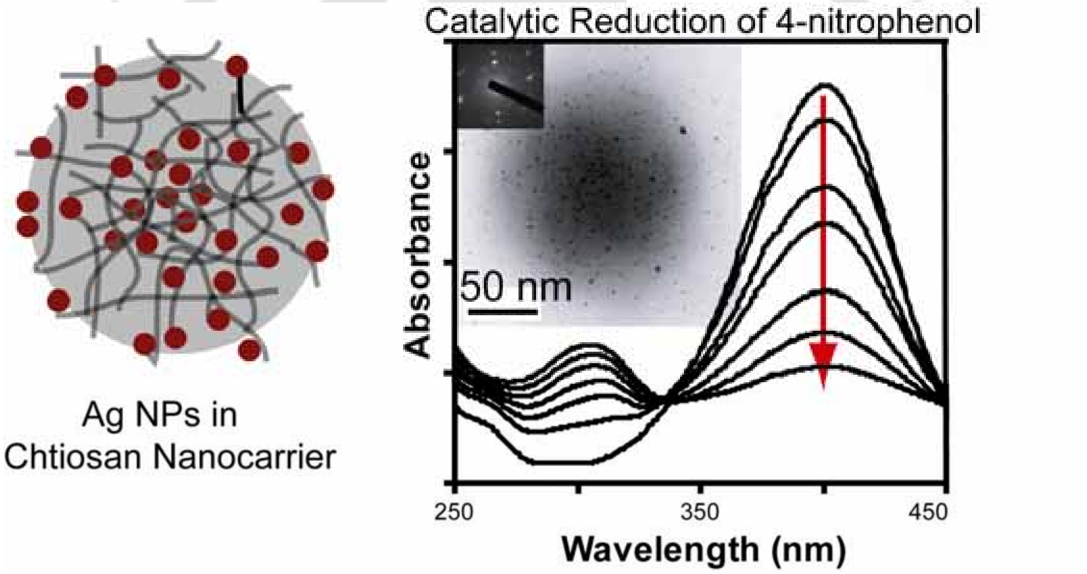

Chapter 4

CHITOSAN – BASED NANOCARRIER FOR SILVER NANOPARTICLES WITH ENHANCED CATALYTIC ACTIVITY

4.1. Introduction

Metal nanoparticles (MNPs) are particularly promising candidates for catalysis and other surface-associated applications because a large fraction of metal atoms in MNPs, due to high surface-to-volume ratio, are exposed to substrate molecules. However, the nanoscopic size and their susceptibility towards aggregation mainly due to van der Waals forces (Chen et al., 2002) have made direct application of MNPs in industrial field a challenging issue. In order to facilitate their application in practical field, MNPs have been synthesized in presence of various stabilizing agent namely surfactants (Masala and Seshadri, 2004; Daniel and Astruc, 2004), polymers (Laudenslager et al., 2008; Cai et al., 2009) and dendrimers (Manna et al., 2001; Esumi et al., 2000). Another promising strategy, in this regard, is to develop polymer based carrier system, such as microgel (Lu et al., 2009; Budhlall et al., 2008; Palioura et al., 2007), micro- or nanoparticles (Wen et al., 2008; Tamai et al., 2008; Lu et al., 2006a). MNPs loaded into polymeric nanocarriers can easily be separated by centrifugation and subsequently reused. Moreover, excellent dispersion of these carrier systems, in fact, enhance the extent of surface associated phenomena, such as catalysis by allowing substrate molecules to easily access the active sites on the surface of MNPs.

Although the synthesis of polymeric micro- or nanoparticle with immobilized MNPs has been well-studied, it is far from being exhaustive. In particular reference to silver nanoparticles (Ag NPs), Ballauf and coworkers have successfully immobilized Ag NPs onto various core-shell polymeric nanoparticles showing excellent catalytic activity (Lu et al., 2006a, 2007). Wen et al. (2008) immobilized Ag NPs selectively in the outer shell layer of the poly (styrene-co-4-vinylpyridine) core-shell microspheres. The formation of Ag NPs by UV irradiation on the surface of polystyrene particles incorporating poly (methylphenylsilane) has been reported by Tamai et al. (2008).

Although the strategy of immobilizing Ag NPs onto the surface of polymeric particles employed in these systems leads to easy access of NP surface to substrates, it also increases the possibility of leaching of Ag NPs from the carrier system compromising the reusability issue.

4.2. Outline of the Research Work

1) A completely 'green' method of preparing a novel biodegradable polymer based nanocarrier system for Ag NPs has been developed.
2) Chitosan based nanocarriers for Ag NPs were prepared by synthesizing Ag NPs using the biopolymer itself as the reducing as well as the stabilizing agent, followed by ionic gelation of the Ag NP-impregnated bulk polymer with tri-polyphosphate.
3) Electron microscopy revealed that the polymer nanocarriers were about 172.6 nm in size with homogenously embedded Ag NPs of diameter ca. 4.9 nm. The surface plasmon resonance (SPR) band of Ag NPs in the nanocarrier confirmed that the shape and size of the MNPs were unaffected during the preparation of the nanocarriers indicating excellent applicability of the present method to develop nanocarriers for MNPs.
4) The catalytic activity of the nanocarriers was investigated by $NaBH_4$-mediated reduction of 4-nitrophenol (4-NP), a refractory pollutant in industrial wastewater (Pradhan et al., 2002; Lu et al., 2006a). The results indicate that Ag NPs in the nanocarrier have significantly higher catalytic efficiency than those in bulk composite and can be applied as efficient catalyst.

4.3. Experimental Section

4.3.1. Synthesis of chitosan nanoparticle (CS NP) and Ag NP-chitosan nanocarrier (Ag-CS NC)

Stock solution (2 mg mL^{-1}) of chitosan was prepared in 0.1% (v/v) glacial acetic acid and used in subsequent reactions. CS NPs were prepared according to the process developed by Calvo et al. (1997) based on the ionotropic gelation of chitosan by tri-polyphosphates (TPP). Briefly, NPs were formed upon addition of 2.5 mL of aqueous TPP solution (1.6 mg mL^{-1}) to 7.5 mL chitosan solution under magnetic stirring at room temperature. The optimum ratio of chitosan to TPP was standardized based on preliminary experiments.

Chitosan stabilized Ag NPs were synthesized as described previously (Murugadoss and Chattopadhyay, 2008). In brief, freshly prepared $AgNO_3$ solution (4×10^{-4} M) was added to 50 mL of 2 mg mL^{-1} chitosan solution under constant stirring at 95^0C. The appearance of yellow color after the addition of 100μL of 0.3 M NaOH to the reaction mixture indicated formation of Ag NPs. The yellow color precipitate was filtered and washed five times with water to remove NaOH completely. The filtrate was dried in vacuum and 2 mg mL^{-1} solution of chitosan-Ag NPs composite was prepared in 0.1 % acetic acid for synthesizing Ag-CS NCs. Ag-CS NCs were prepared by following the same procedure described above for blank CS NPs.

4.3.2. Characterization of CS NPs and Ag-CS NCs

SEM was performed in a LEO1430VO SEM by depositing 10 μL of nanoparticle sample on glass slides followed by air drying. The slides were coated with gold film with a Polaron Sputter Coater before analyzing under SEM. For TEM, 5 μL different liquid nanoparticle samples were drop cast on carbon coated copper TEM grids and subsequently air dried at room temperature. The grids were then analyzed by a JEOL 2100 UHR-TEM instrument operating at an accelerating voltage of 200 KeV. The histograms for particle size distribution were constructed analyzing several frames of similar images.

The formation of Ag NPs was followed by monitoring the UV–visible spectra of the samples in a Perkin-Elmer Lambda-45 spectrophotometer at room temperature. Fourier transform infrared (FTIR) spectra of chitosan, CS NPs and Ag-CS NCs were measured using a Perkin-Elmer Spectrum one spectrometer. The nanoparticle samples were lyophilized and resulting powders were mixed with KBr to make pellets for the FTIR studies. The amount of Ag NPs present in the Ag-CS NCs was determined by atomic absorption spectroscopy in a Varian AA240 atomic absorption spectrophotometer.

4.3.3. X-Ray diffraction (XRD) and thermogravimetric analysis (TGA)

CS NPs and Ag-CS NCs were lyophilized and subsequently used for XRD and thermogravimetric analysis. For XRD measurements, samples were analyzed by a Bruker D8 ADVANCE (Bruker AXS Inc.) X-ray powder diffractometer using Cu-Kα (λ=1.54 Å) source at ambient temperature. TGA analysis was carried out using a

Mettler Toledo Thermogravimetric Analyzer (TGA/SDTA851e/LF/1100) with a heating rate of 10 ^{0}C min^{-1} under Ar.

4.3.4. Catalytic study

In order to study the catalytic activity of Ag-CS NCs, first 0.3 mL of freshly prepared aqueous solution of $NaBH_4$ (100 mM) was added to 2.7 mL of 4-NP (final conc. 0.1 mM). To this solution different amount of Ag-CS NCs (4.9 – 19.6 mgL^{-1}) were added and the catalytic reaction was followed by recording the UV- visible spectra of the reaction mixture every 30 s, immediately after the addition of the nanocarrier. The spectra were recorded with a UV-visible spectrometer (Perkin-Elmer Lambda-45 spectrophotometer) in the range 250–500 nm at room temperature. The rate constant of the reaction was calculated by recording the change in absorbance at λ = 400 nm with time.

4.4. Results and Discussion

4.4.1. Synthesis of Ag-CS NCs

Chitosan, the second most abundant biopolymer after cellulose, is a linear polysaccharide composed of glucosamine and N-acetyl glucosamine monomers linked in a $\beta(1\rightarrow4)$ fashion. Chitosan acts as an excellent adsorbent of metal ions due to its high content of primary amine and hydroxyl groups which help in adsorbing metal ions by chelation or complexation (Varma et al., 2004). Exploiting this property, an environment-friendly method of synthesizing chitosan stabilized Ag NPs has been recently developed in our laboratory using chitosan as a reducing as well as stabilizing agent (Murugadoss and Chattopadhyay, 2008). On the other hand, preparation of chitosan nanoparticle (CS NP) by TPP via ionic gelation method has already been well-established by Calvo et al. (1997) and others. In principle, chitosan based ‘nanocarrier’ of MNPs can be prepared by synthesizing chitosan stabilized MNPs followed by ionic gelation of the MNP-chitosan composite by TPP. In the present study, a novel Ag-CS NC has been developed following the scheme shown in **Figure 4.1**.

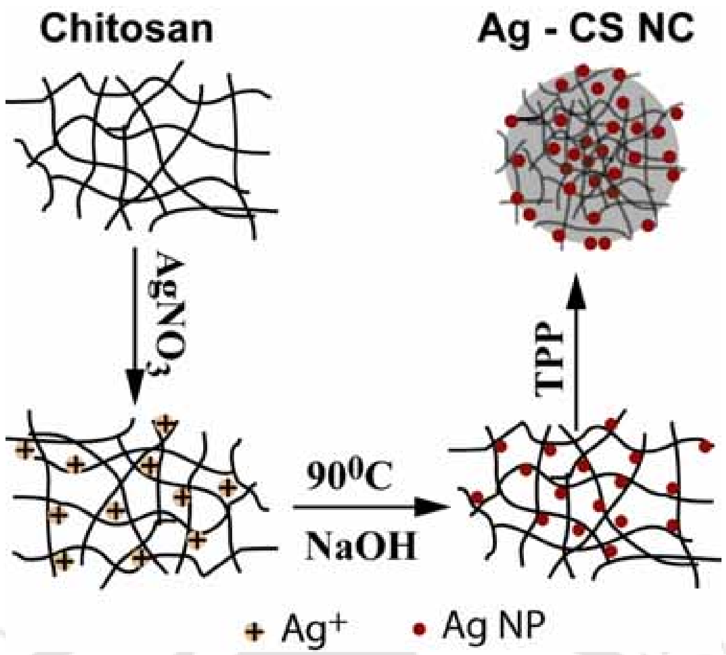

Figure 4.1. Schematic representation of preparing Ag-CS NCs.

4.4.2. Characterization of Ag-CS NCs

The SEM images of as prepared CS NPs and Ag-CS NCs are shown in Figure 2, which shows that CS NPs as well as Ag-CS NCs were spherical in shape. Absence of considerable number of aggregated particles in SEM images (**Figures 4.2a and 4.2b**) indicated formation of well dispersed CS and Ag-CS NCs in the present method. Particle size distribution (**Figure 4.2c, 4.2d**) revealed the average particle size of CS NPs and Ag-CS NCs to be 136.9 nm (±28.5 nm) and 172.6 nm (±27.1 nm), respectively. The larger size of Ag-CS NCs compared to CS NPs could be due to the impregnation of polymer NPs with Ag NPs. However, it was difficult to identify individual Ag NPs in Ag-CS NCs using SEM. In order to examine the Ag NPs immobilized into the chitosan nanoparticle, Ag-CS NCs were further investigated under TEM. **Figure 4.2e** displays the TEM image of an Ag-CS NC. It is evident from the TEM image that the Ag NPs immobilized in the Ag-CS NCs were spherical in shape and homogenously incorporated into the chitosan NPs. The selected area electron diffraction (SAED) pattern (**Figure 4.2e**) confirmed the presence of crystalline Ag NPs in the composite. The size distribution of Ag NPs in Ag-CS NCs, estimated from the TEM image, is shown in **Figure 4.2f**. Figure 2f demonstrates that Ag NPs were 4.9 ± 1.6 nm in size with narrow size-dispersion.

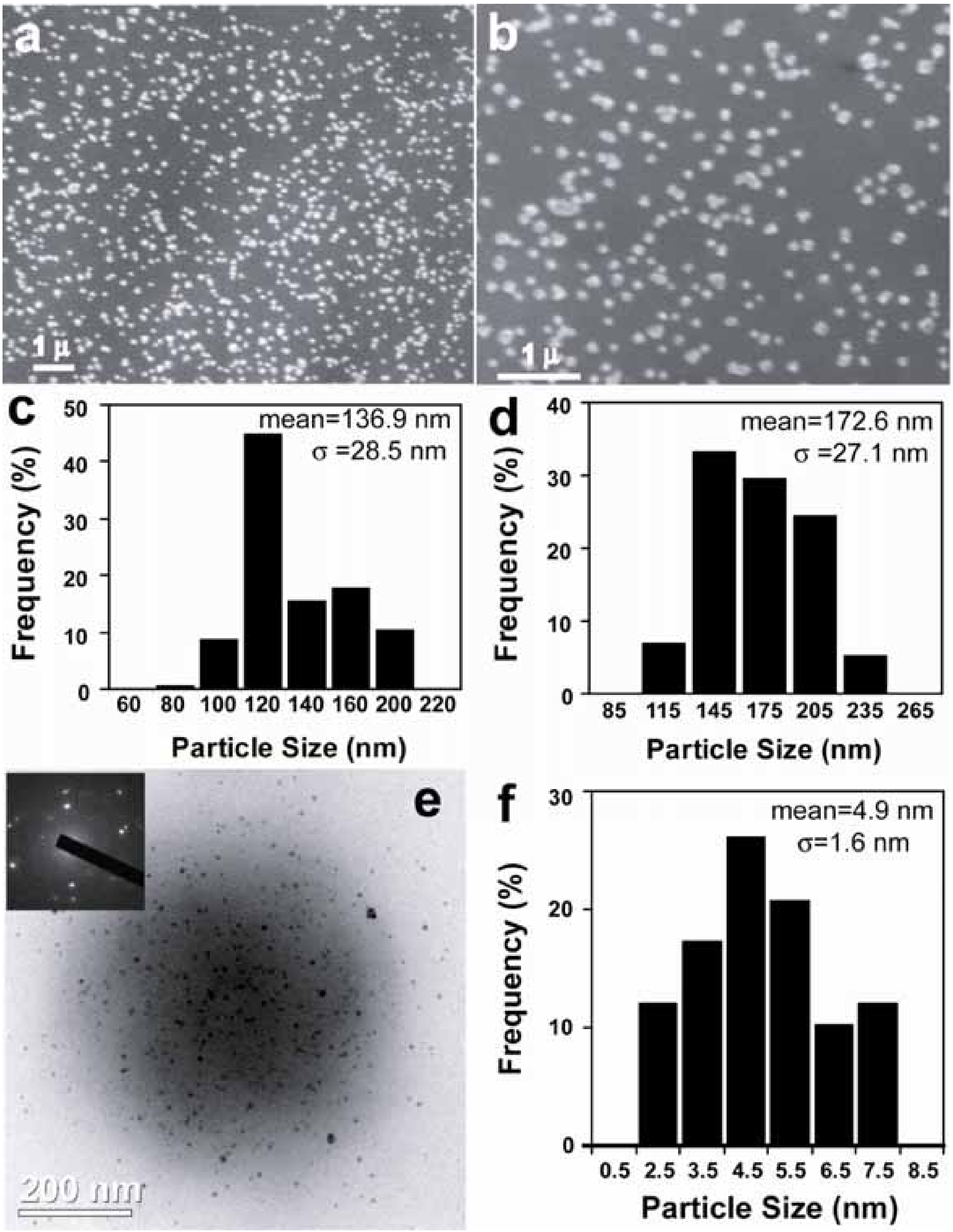

Figure 4.2. SEM images of **(a)** CS NPs and **(b)** Ag-CS NCs with particle size distributions shown in **(c)** and **(d)**, respectively. **(e)** TEM image of an Ag-CS NC with SAED pattern (inset) and corresponding particle size distribution for Ag NPs **(f)**.

Figure 4.3a shows the UV-visible spectra of colloidal solution of CS NPs and Ag-CS NCs. The UV-visible spectra of Ag-CS NCs exhibited a strong absorption band at ca. 409 nm corresponding to characteristic SPR of metallic Ag NPs. The position of SPR band of Ag NPs in Ag-CS NCs remained almost unaltered compared to that of Ag NP-chitosan bulk composite, used as the starting material for preparing Ag-CS NCs in the present study. This implied that the size and shape of Ag NPs were unaffected during the encapsulation of Ag NPs in chitosan nanoparticle by TPP-mediated ionic gelation method, which was also evident from the TEM image of bulk Ag NPs-CS composite (**Figure 4.3b**). Moreover, the sharp Ag NP SPR band in UV-visible spectrum of Ag-CS NCs indicated the presence of well separated Ag NPs with narrow size distribution in Ag-CS NCs, which is in good agreement with TEM observation. The results clearly demonstrated the excellent applicability of the present method for immobilizing Ag NPs in chitosan particle at the micronscale and the nanoscale.

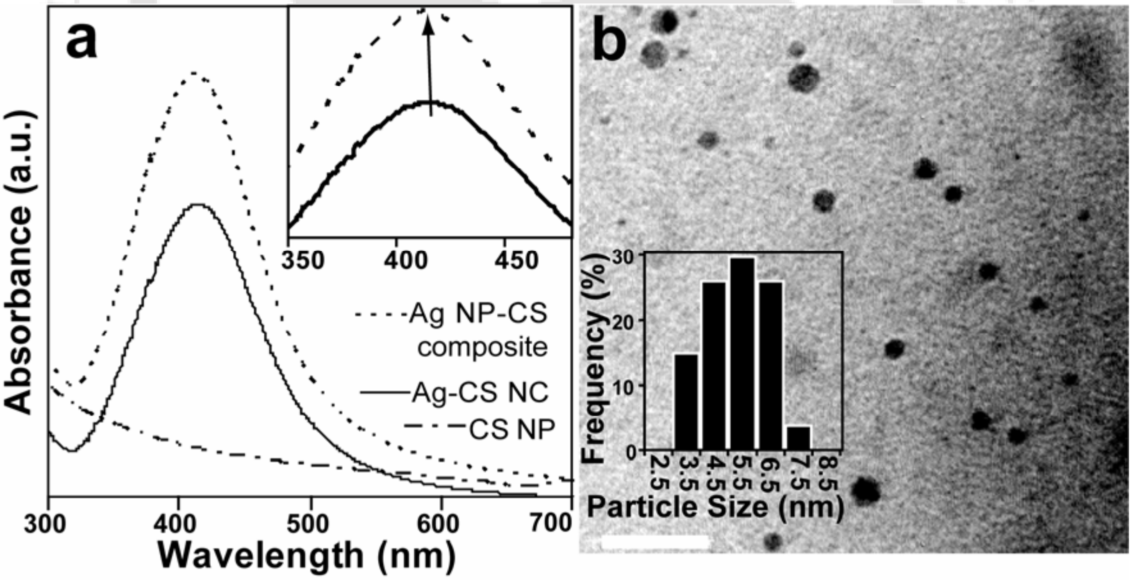

Figure 4.3. (a) UV-visible spectra of colloidal solutions of CS NPs, Ag-CS NCs and Ag NP-chitosan composite. The spectra of Ag-CS NCs were recorded with respect to blank CS NPs as the reference in order to compare the SPR band of Ag NPs. **(b)** TEM images of bulk Ag NPs-chitosan composite with corresponding particle size distribution (Scale bar: 10 nm).

4.4.3. XRD analysis

In order to examine the crystallinity of Ag-CS NCs, XRD analysis of the powdered samples were carried out. **Figure 4.4** shows the powder XRD pattern of chitosan powder, CS NPs and Ag-CS NCs. The XRD pattern of pure chitosan powder showed characteristic peaks around $2\theta = 9.6^0$ and 20^0, corresponding to the hydrated crystalline structure and amorphous structure of chitosan, respectively (Rhim et al., 2006; Wang et al., 2005). On the other hand, CS NPs exhibited characteristic peaks around $2\theta = 8.1^0$, 11.2^0, 18^0 and 22.8^0. The former two peaks were due to hydrated crystallinity of chitosan, while latter two peaks indicated amorphous structure of chitosan (Rhim et al., 2006; Wang et al., 2005). In Ag-CS NCs, the XRD pattern consisted of two peaks around 20^0 and 38.5^0. The peak at 20^0 indicated the amorphous nature of chitosan in Ag-CS NCs which, in turn, indicated the loss of crystallinity of chitosan matrix in Ag-CS NCs. The other peak at 38.5^0 was due to Bragg reflection corresponding to (111) planes of fcc structure of silver and confirmed the presence of Ag NPs in Ag-CS NCs. The broadening of diffraction peaks confirmed the presence of nano-sized Ag NPs. The average particle size of Ag NPs was estimated to be 3.4 nm from Scherrer equation (Cullity, 1978),

$$d = \frac{0.9\lambda}{\beta \cos\theta} \qquad (1)$$

where λ is the X-ray wavelength, β is the full width at half maxima (FWHM) of the diffraction peak and θ is the diffraction angle.

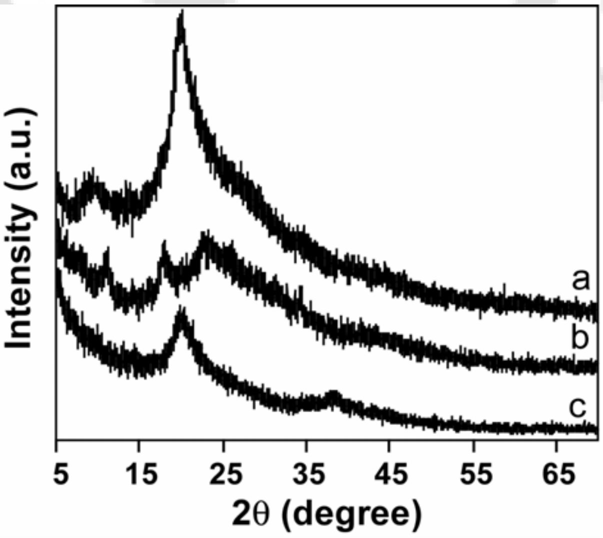

Figure 4.4. XRD patterns of (a) chitosan, (b) CS NPs and (c) Ag-CS NCs.

4.4.4. FTIR analysis

FTIR analysis of chitosan (**Figure 4.5**) revealed characteristic peaks of primary and secondary alcohols at 1026 cm^{-1}, 1067 cm^{-1} and 1133 cm^{-1} (Laudenslager et al., 2008). On the other hand, the sharp peaks at 1533 cm^{-1} and 1627 cm^{-1} were due to amines and amides. In CS NPs, the alcohol peak at 1067 cm^{-1} shifted to 1643 cm^{-1} while amine/amide peak of 1533 cm^{-1} appeared at 1549 cm^{-1}. This subtle change could be due to the ionic incorporation of polyphosphates into chitosan matrix in CS NPs. Interestingly the peak at 1533 cm^{-1} of the amine and amide region drastically shifted in Ag-CS NCs while the peaks in alcohol region remained almost unaffected. This confirmed the amine groups of chitosan to be involved in the ionic complexation of Ag^{+} followed by subsequent formation of Ag NPs *in situ*. Similar results were also observed by Laudenslager et al. (2008) for MNPs in chitosan matrix.

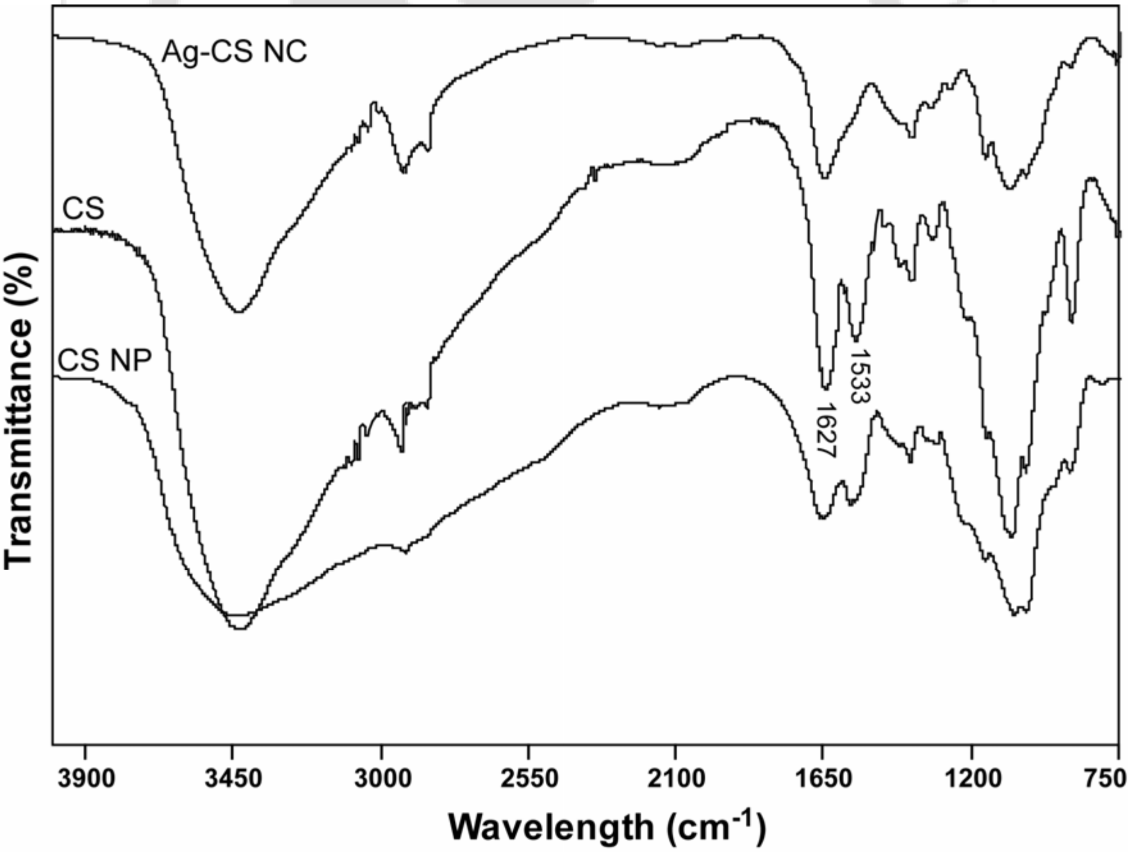

Figure 4.5. FTIR spectra of chitosan (CS), chitosan nanoparticle (CS NP) and Ag-CS NCs.

4.4.5. TGA analysis

In order to investigate the thermal stability, the thermal properties of Ag-CS NCs were studied by TGA. The thermogravimetric (TG) and differential thermogravimetric (DTG) analysis curves of pure chitosan powder, blank CS NPs and Ag-CS NCs are shown in **Figure 4.6a** and **4.6b**, respectively. The major thermal events with corresponding temperature range as well as mass losses are summarized in **Table 4.1**.

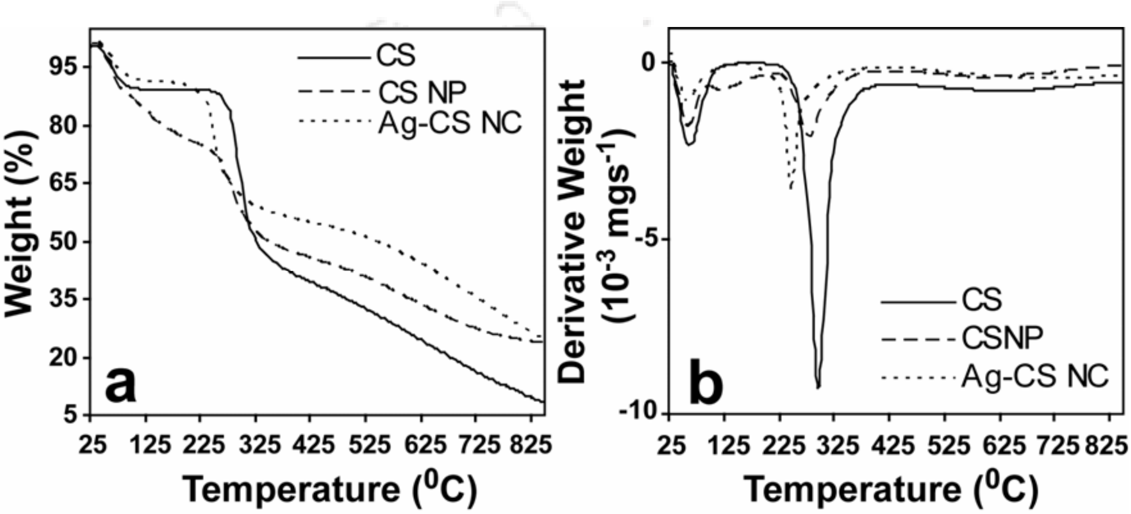

Figure 4.6. (a) TG and **(b)** DTG curve of chitosan, CS NPs and Ag-CS NCs.

Table 4.1: Major Thermal Events in TGA

	Temperature (^{0}C) [a]		T_m (^{0}C) [b]	Weight loss (%) [a]
	Range	Midpoint		
First stage				
Chitosan	33-98	65.5	64	12
CS NPs	33-93	63.0	61	13
Ag-CS NCs	33-105	69.0	60	10
Second stage				
Chitosan	227-375	301.0	299	46
CS NPs	221-377	299.0	281	27
Ag-CS NCs	173-326	249.5	247	32

[a] Calculated from TG curve. [b] Temperature of maximal thermal degradation rate (T_m) were calculated from DTG curve.

It is clear from **Figure 4.6a** that the thermal degradation of chitosan occurred in two stages. The first stage of weight loss due to loss of water (Wan et al., 2009; Neto et al., 2005) started at ca. 60^{0}C with maximum loss being at 64 ^{0}C and accounted for 12% weight loss. On the other hand, the weight losses in blank CS NPs and Ag-CS NCs at this stage were 13% and 10%, respectively. DTG data in **Figure 4.6b** showed that the temperature of maximal thermal degradation rate (T_m) decreased to 61 ^{0}C and 60 ^{0}C in CS NPs and Ag-CS NCs, respectively. Being a polysaccharide, chitosan has a strong affinity for water. The hydroxyl and amino groups of chitosan play important role in its hydrated properties by strongly interacting with water molecules (Neto et al., 2005). The decrease in T_m observed in CS NPs and Ag-CS NCs could be attributed to the fact that the ionic complexation of polyphosphates and/or Ag^+ with hydroxyl and amino groups in chitosan during the formation of NPs reduce the number of hydroxyl and amino groups available for interacting with water molecules.

The second stage of thermal degradation of pure chitosan powder, starting from 227 ^{0}C to 375 ^{0}C with a weight loss of ca. 46%, indicated the thermal decomposition of chitosan resulting in vaporization as well as elimination of volatile products (Neto et al., 2005). Similarly the thermal decomposition of chitosan in CS NPs and Ag-CS NCs took place in the temperature range of 221 ^{0}C- 377 ^{0}C and 173 ^{0}C- 326 ^{0}C, respectively. The DTG (**Figure 4.6b**) curves clearly showed that the T_m of the thermal decomposition of chitosan moiety decreased to 281 ^{0}C and 247 ^{0}C in CS NPs and Ag-CS NCs, respectively compared to 299 ^{0}C in pure chitosan. Interestingly, Ag NPs and polyphosphates incorporated into the chitosan matrix during the formation of Ag-CS NCs had an effect on the decomposition temperature of chitosan by decreasing it by ca. 52 ^{0}C. Similar results were also observed for PDLLA matrix by Blaker et al. (2005) when they used Bioglass® as filler in the PDLLA matrix. The decrease in thermal stability of Ag-CS NCs compared to pure chitosan could be due to significant loss of crystallinity of chitosan in Ag-CS NCs as a result of incorporation of Ag NPs and polyphosphates through ionic interaction with hydroxyl and amino groups.

4.4.6. Catalytic Study

In order to investigate the catalytic activity of Ag NPs in Ag-CS NCs, the reduction of 4-NP by an excess of $NaBH_4$ was studied as the model reaction (Pradhan et al., 2002; Lu et al., 2006a, 2007; Murugadoss and Chattopadhyay, 2008). The kinetics of the reaction in presence of Ag NPs can be followed simply by recording the absorption spectra of 4-NP having a characteristic absorbance maxima at 400 nm. The peak at 400 nm is due to the 4-nitrophenate ions formed immediately after the addition of $NaBH_4$ in the system. The absorption spectra for the reduction of 4-NP in presence of Ag-CS NCs were recorded at different time intervals and are shown in **Figure 4.7a**. It is clearly evident from **Figure 4.7a** that the peak intensity at 400 nm decreased gradually while a new peak around 290 nm due to the reduced product, 4-aminophenol (Lu et al., 2006a), appeared and continued to increase in intensity with time. It may be mentioned here that the SPR band of Ag NPs in Ag-CS NCs did not interfere with the absorption spectra of 4-NP in the present study as the amount of Ag-CS NCs in the reaction media was very low (**Figure 7b**).

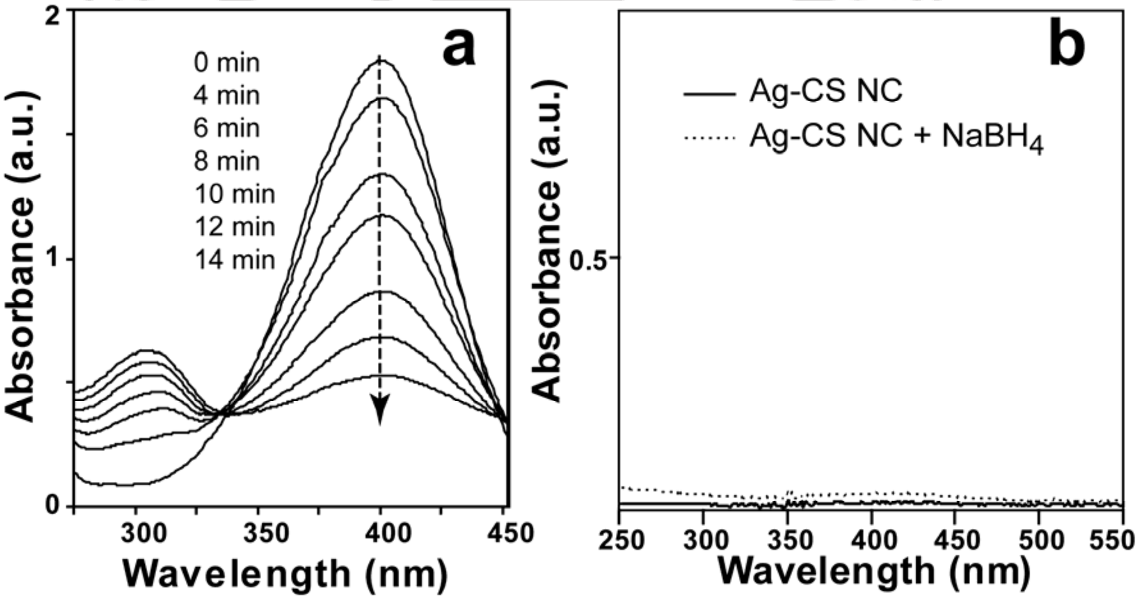

Figure 4.7. (a) Reduction of 4-NP by $NaBH_4$ in presence of 11.4 mgL^{-1} of Ag-CS NCs at room temperature. UV-visible spectra of 4-NP were recorded at different times as indicated in the graph. **(b)** UV-visible spectra of 49 mg L^{-1} Ag-CS NCs and 49 mg L^{-1} Ag-CS NCs incubated with 10 mM $NaBH_4$ for 30 min.

The catalytic rate of Ag-CS NCs in the present study can be evaluated by considering the rate kinetics of the catalytic reaction to be of pseudo-first order with respect to the concentration of 4-NP as the concentration of $NaBH_4$ used was in large excess compared to that of 4-NP. As the apparent rate constant, k_{app} should be proportional to the surface of the Ag NPs present in the system, the rate equation in the present study can be expressed as (Lu et al., 2006a, 2007):

$$-\frac{dC_t}{dt} = k_{app}C_t = kSC_t \qquad (2)$$

where k_{app} is the apparent rate constant, C_t is the concentration of 4-NP at time t, S is the surface area of Ag NPs normalized to unit volume of the system and k is the rate constant normalized to S. As the absorbance of 4-NP is directly proportional to its concentration in the reaction mixture, the ratio of the concentration (C_t) of 4-NP at time t to its value (C_0) at t_0 can be directly obtained from the ratio of the corresponding absorbance (A_t/A_0). The catalytic reduction of 4-NP by $NaBH_4$ in presence of different concentrations of Ag-CS NCs were followed and $\ln(C_t/C_0)$ versus reaction time t were plotted for each case (**Figure 4.8**). **Figure 4.8** demonstrated a linear relationship between $\ln(C_t/C_0)$ and time t in all the cases. Interestingly, an induction period for the catalytic reduction was observed in each case. This could be due to the time required for the activation of the Ag NPs in Ag-CS NCs in the reaction mixture. The same phenomenon has also been observed previously by others studying catalytic reduction of 4-NP by MNPs (Pradhan et al., 2002; Lu et al., 2006a, 2007; Murugadoss and Chattopadhyay, 2008). Moreover the duration of the induction period decreased gradually with increasing concentration of Ag-CS NCs in the system.

Figure 4.9a shows the plot of apparent rate constant k_{app} as a function of concentration of Ag-CS NCs present in the reaction medium. The apparent rate constants (k_{app}) were calculated form the curve of ln (C_t/C_0) versus time t by linear fit in each case. **Figure 4.9a** essentially reveals that k_{app} increased almost linearly with increasing concentration of Ag-CS NCs. In other words, increasing the amount of Ag NPs in the system leads to faster catalysis of 4-NP. **Figure 4.9b** shows the values of k_{app} as a function of theoretical surface area of Ag NPs present in unit volume of reaction medium (detailed calculations of theoretical surface area given in Appendix, **Table 4.A1**). The result demonstrates nearly linear dependency of k_{app} on the specific surface area of Ag NPs, consistent with the assumption made in equation (2). This also confirms the surface of the Ag NPs to be involved in the catalysis and the catalytic activity depends on the total surface area of Ag NPs immobilized in Ag-CS NCs per unit volume of the system.

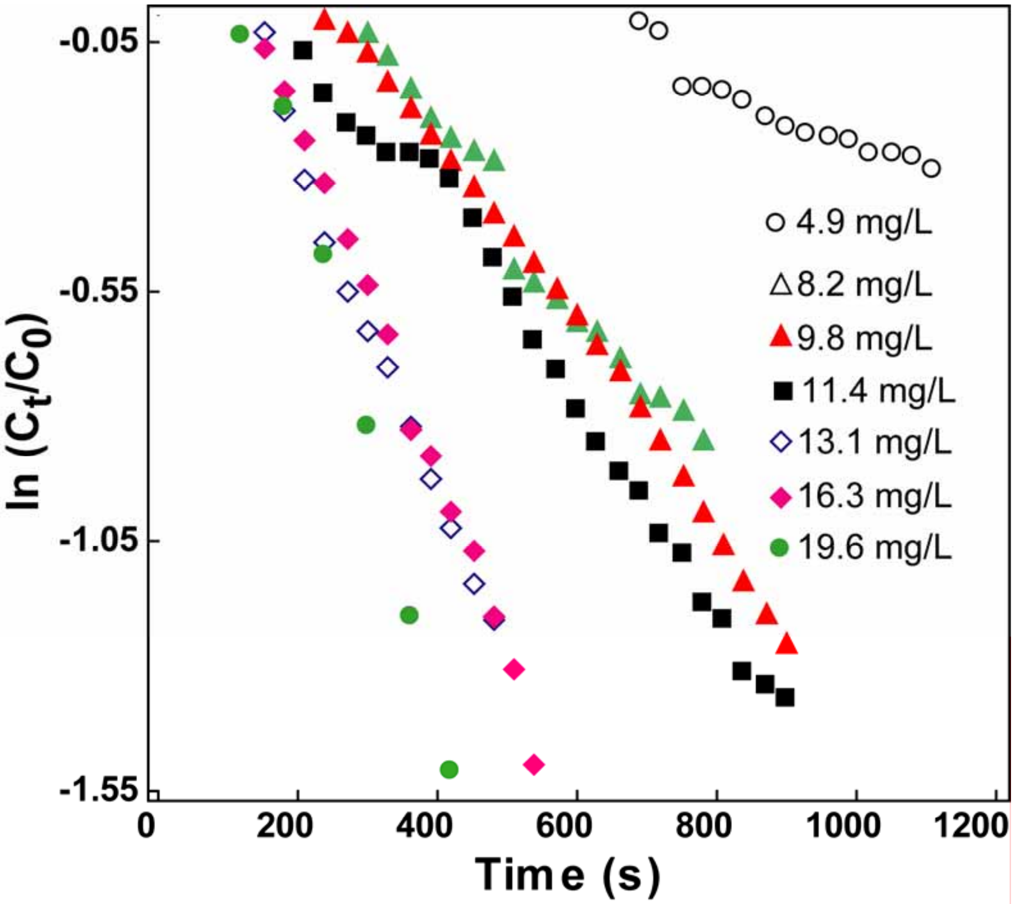

Figure 4.8. Effect of Ag-CS NC concentration on the reduction of 4-NP by $NaBH_4$ at room temperature. Concentration: [4-NP] = 0.1 mM, [$NaBH_4$] =10 mM.

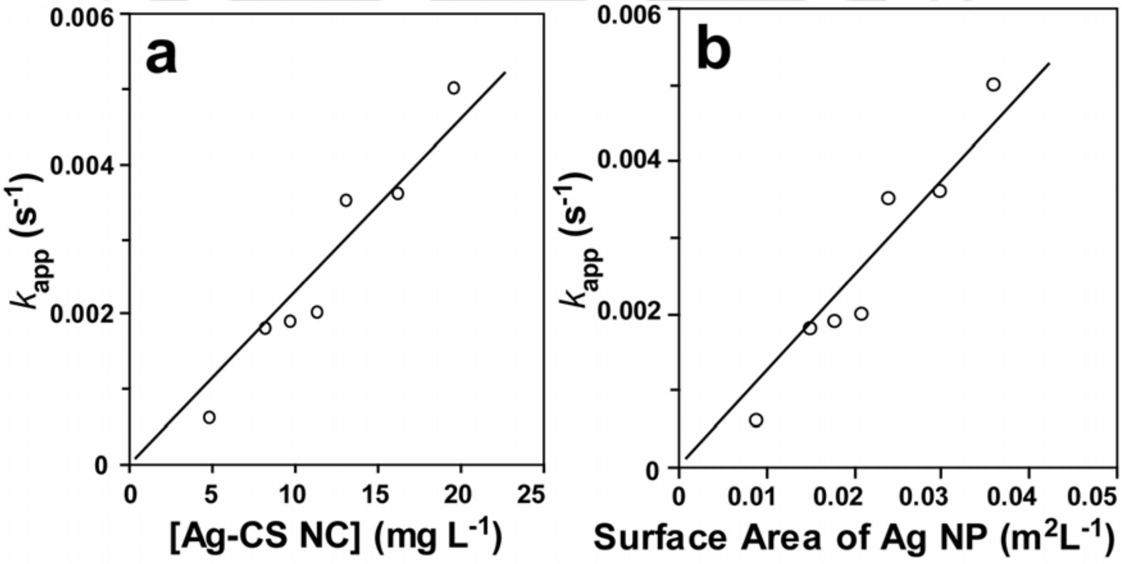

Figure 4.9. (a) Rate constant k_{app} as a function of the concentration of Ag-CS nanocarrier. **(b)** Rate constant k_{app} as a function of the surface area S of Ag NPs normalized to the unit volume of the reaction medium.

The rate constant normalized to the surface area of Ag NPs per unit volume of the reaction medium, *k* was calculated from the graph in **Figure 4.9b** to be 0.13 s^{-1} m^{-2} L for Ag-CS NCs. In order to evaluate the catalytic efficiency of the present system, the rate constants (normalized to the surface area of Ag NPs per unit volume) of other Ag NP –based systems together with the present study are summarized in **Table 4.2**.

Table 4.2: Catalytic Activity of Ag NPs in the Reduction of 4-Nitrophenol

Study	**Carrier System**	***d*** **[a] (nm)**	***k*** **($s^{-1}m^{-2}L$)**
Present study	Chitosan nanoparticles	4.9 ± 1.6	1.30 X 10^{-1}
Lu et al., 2006a	PS core - poly(N-isopropylacrylamide) (PS-NIPA) shell microgel	8.5 ± 1.5	5.02 X 10^{-2}
Lu et al., 2007a	PS core - poly(acrylic acid) polyelectrolyte brush particles	3 ± 1.2	7.81 X 10^{-2}
Lu et al., 2006b	PS core–highly branched poly(ethylene glycol) methacrylate (PEGMA) brush particle	7.5 ± 2	7.27 X 10^{-2}
Lu et al., 2007b	PVA hydrogel	45 ± 5	7.31 X 10^{-5}
	PVA/PS-PEGMA composite hydrogel	35 ± 5	7.80 X 10^{-5}
Pradhan et al., 2002	PVA polymer	25	3.78 X 10^{-7}

[a] Diameter of the Ag NPs. PS: polystyrene.

The value of *k* in the present study is quite high compared to previously reported data on the catalytic reduction of 4-NP in presence of Ag NP- based nanocarrier systems (Lu et al., 2006a, 2007a, 2007b). Turn over frequency (TOF) is another commonly used parameter to indicate the catalytic efficiency of a catalyst and can be defined as,

$$\mathrm{TOF} = \frac{N_r}{N_s t}$$

where N_r is the number of molecules (4-NP in the present study) reacting in the presence of catalyst in time t to produce the product, and N_s is the number of surface atoms of the catalyst involved in the reaction. TOF, for each concentration of Ag-CS NCs used, was calculated by considering the size of Ag NPs to be 4.9 nm as observed under TEM (Appendix, **Table 4.A2**). The average TOF for the Ag-CS NCs in the present study was estimated to be 0.4 ± 0.1 (including induction period) and 0.7 ± 0.1 (excluding induction period), which is much higher than previously reported value of $0.97 \pm 0.02 \times 10^{-3}$ and $1.5 \pm 0.3 \times 10^{-3}$, respectively, for bulk chitosan-Ag NP composite material (Murugadoss and Chattopadhyay, 2008). The high TOF value of Ag-CS NCs indicated excellent catalytic property of Ag NPs immobilized in chitosan nanoparticles in the present study. As indicated previously (Lu et al., 2007), the pronounced enhancement in the catalytic activity of Ag-CS NCs could be due to the fact that the polyelectrolyte nature of chitosan makes Ag-CS NCs to have open structures allowing reactant molecule to diffuse easily and reach Ag NPs quickly. Also, the dispersion of the NCs in the reaction medium makes the catalyst more efficient as the reaction occurs under micro-heterogeneous conditions rather than bulk precipitate where the reaction takes place under heterogeneous condition.

4.5. Conclusion

Well-dispersed nanocarriers for Ag NPs having average size of about 172.6 nm were prepared from biogenic polymer, chitosan in a completely 'green' method. TEM analysis demonstrated that monodispersed and crystalline Ag NPs of mean particle size of 4.9 ± 1.6 nm were uniformly impregnated in the chitosan nanocarriers, which led to increased amount of accessible surface of Ag NPs. Moreover, Ag-CS NCs showed excellent catalytic activity in $NaBH_4$-mediated reduction of 4-NP. The present study demonstrates that chitosan nanoparticles can work as excellent nanocarrier system for Ag NPs which has potential reusability in catalysis and other applications. Additionally, the method developed in the present study can easily be extended to prepare nanocarrier systems for other metal nanoparticles. Now, it will be interesting to study the interaction of Ag NPs embedded in this nanocarrier with the cancer cells for possible therapeutic implications.

4.6. Appendix

1. Calculation of Surface Area of Ag NPs in Ag-CS NCs

Diameter of a single Ag NP in Ag-CS NCs, d = 4.9 nm (Average particle size as observed under TEM) and density of a single Ag NP in Ag-CS NCs, ρ = 10500 kg/m^3 (Density of bulk metallic Ag),

So, Volume of a single Ag NP in Ag-CS NCs, $v = \frac{\pi d^3}{6} = 61.57\ \text{nm}^3$

Surface area of a single Ag NP in Ag-CS NCs, $s = \pi d^2 = 75.39\ \text{nm}^2$

Mass of a single Ag NP in Ag-CS NCs, $m = \rho v = 6.47 \times 10^{-10}$ ng

Now, Total volume of the reaction medium was 3.0 mL.

Table 4.A1. Calculated Specific Surface Area

[Ag-CS NC] (mgL^{-1})	Ag NP added (ng)[a]	No. of Ag NPs added	Total surface area (m^2)	Specific surface area, *S* (m^{2}L^{-1})
4.9	230	35.58 X 10^{10}	2.68 X 10^{-5}	0.008941
8.2	390	60.32 X 10^{10}	4.55 X 10^{-5}	0.015162
9.8	460	71.15 X 10^{10}	5.36 X 10^{-5}	0.017883
11.4	540	83.53 X 10^{10}	6.30 X 10^{-5}	0.020993
13.1	620	95.90 X 10^{10}	7.23 X 10^{-5}	0.024103
16.3	770	119.10 X 10^{10}	8.98 X 10^{-5}	0.029935
19.6	930	143.85 X 10^{10}	10.85 X 10^{-5}	0.036155

[a] Amount of Ag NPs in Ag-CS NC system was calculated theoretically to be 1.58% and Ag content in Ag-CS NC was measured in atomic absorption spectroscopy (AAS) to be 1.54 %. Ag content was, hence, considered to be 1.58% for further calculation.

2. Calculation of TOF

Final reaction volume = 3 mL and [4-nitrophenol] = 0.1 mM

So, no. of 4-nitrophenol molecule in the reaction medium, N_r = 1.8 X 10^{17}

As, the cross-sectional area of a single Ag atom = 0.08 nm^2 (diameter of Ag atom = 0.32 nm), no. of surface Ag atom per Ag NP = 943

Table 4.A2: Calculated TOF

[Ag-CS NC] (mgL^{-1})	No. of Ag NPs added ($\times 10^{10}$)	No. of surface Ag atoms (N_s) ($\times 10^{14}$)	Time, t (s) [a]		$TOF = \frac{N_r}{N_s t}$ (s^{-1})	
			Excluding IP [b]	Including IP	Excluding IP	Including IP
4.9	35.58	3.4	Not considered [c]			
8.2	60.32	5.7	480	780	0.7	0.4
9.8	71.15	6.7	450	720	0.6	0.4
11.4	83.53	7.9	420	630	0.5	0.4
13.1	95.90	9.0	210	360	0.9	0.6
16.3	119.10	11.2	210	360	0.8	0.4
19.6	143.85	13.6	180	300	0.7	0.4
		Average TOF			0.7 ± 0.1	0.4 ± 0.1

---

[a] Time , t was considered as the time needed for Abs_{400} to reach a value of 0.75. [b] IP: Induction period. [c] Ag – CS NC concentration of 4.9 mgL^{-1} was not considered as the Abs_{400} did not reach 0.75 within the experimental time.

CHAPTER 5

Induction of Apoptosis in Cancer Cells by Silver Nanoparticles using Chitosan Nanocarrier

This chapter describes the implication of the chitosan based nanocarrier of Ag NPs (Ag-CS NCs) in inducing apoptosis in HT 29 human colon cancer cells at a very low concentration of Ag NPs. While the characteristic morphological changes of apoptosis were evident in fluorescence and electron microscopy, flow cytometry confirmed the efficient induction of apoptosis by Ag-CS NCs. Intracellular ROS production was demonstrated to augment the apoptosis in HT 29 cells, in addition to classical mitochondria dependent caspase signaling pathway.

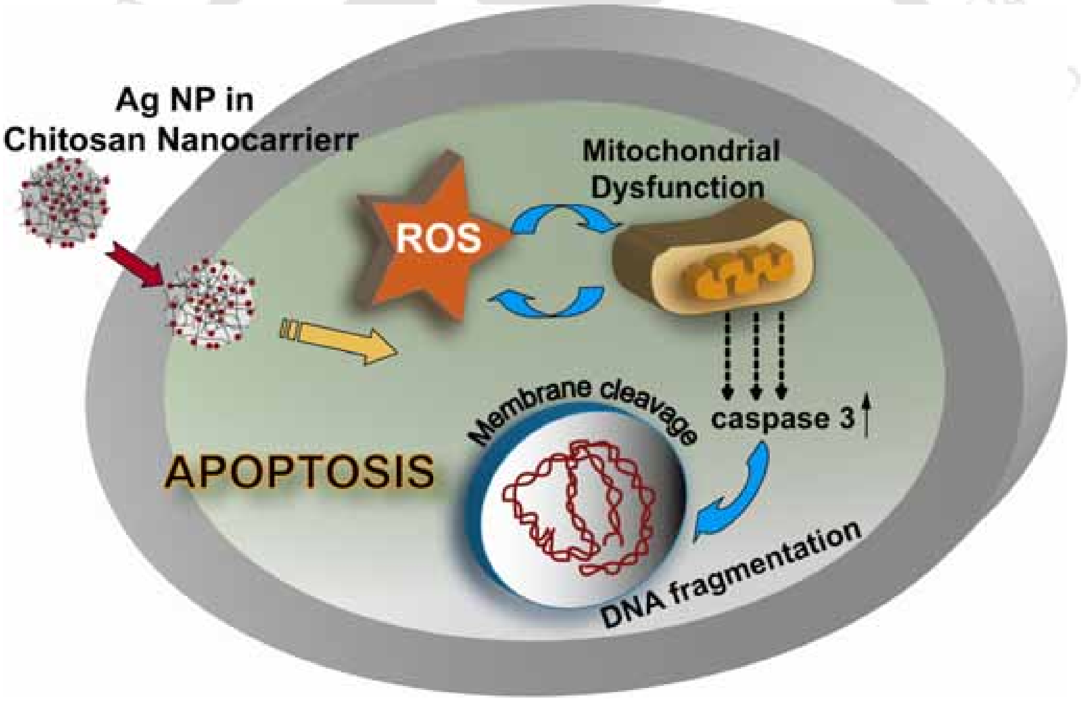

Chapter 5

INDUCTION OF APOPTOSIS IN CANCER CELLS BY SILVER NANOPARTICLES USING CHITOSAN NANOCARRIER

5.1. Introduction

The possibility of using silver nanoparticles (Ag NPs), by themselves or in combination with gene therapy, in order to induce apoptosis in mammalian cells has recently been explored (Gopinath et al., 2008, 2010) by our group. This therapeutically promising aspect of Ag NPs to induce apoptosis can effectively be exploited in the field of nanomedicine as the genetically programmed cell death or apoptosis, which eliminates the unwanted or damaged cells in the process of development or in response to infection or DNA damage (Newmeyer and Ferguson-Miller, 2003), is critical to develop viable therapeutics for fighting against killer diseases, such as cancer and autoimmune diseases (Thompson, 1995). The DNA damaging ability and possible genotoxicity of Ag NPs reported in recent studies (AshaRani et al, 2008, 2009) pose critical issues in the therapeutic implications of Ag NPs. However, the conventional anti-cancer therapies suffer from lack of generality, effectiveness in case of advanced stages of the disease and numerous toxic side effects caused by radiation or chemicals used in the process (Carr et al., 2008; Singal and Iliskovic, 1998). The level of toxicity associated with the use of Ag NPs, hence, may not necessarily be graver than those mentioned above and thus could be considered for alternative therapy. In this regard, nanocarriers (NCs) have recently emerged as potential drug-carriers in cancer therapy due to increased drug efficacy, low toxicity and continued steady-state therapeutic level of drug in drug–nanocarrier systems (Peer et al., 2007). The potential of chitosan for developing biocompatible NCs of conventional anti-cancer drugs, DNA and other therapeutically important molecules has already been well established (Kumar et al., 2004; Bhattarai et al., 2010). However, chitosan NCs have not been used as such for metal NP delivery. The development of chitosan based NC system for Ag NPs, thus, could lead to increased therapeutic index of Ag NPs as a result of improved bio-availability and thereby overall decrease in toxicity.

5.2. Outline of the Research Work

1) Induction of apoptosis in human HT 29 colon cancer cells by the Ag NPs confined within the biodegradable chitosan nanospheres (Ag-CS NCs) [reported in chapter 4].
2) The apoptotic cell death was investigated by conventional AO/EB dual staining as well as electron microscopy. Flow cytometric quantification of apoptosis along with cell viability assay revealed that the apoptosis could successfully be induced in HT 29 cells by Ag NPs (being present in the NC) at a concentration, way below the previously reported values.
3) The interplay of the pro-apoptotic caspase 3 and anti-apoptotic Bcl 2 in the apoptotic process was shown by semi-quantitative RT-PCR as well as quantitative real time RT-PCR.
4) In order to appreciate the multiplex origin of apoptosis, the effect of Ag-CS NCs on the cellular oxidative stress (ROS) and mitochondrial membrane potential (MMP) was also investigated.
5) The results indicate that the NCs are efficient in inducing programmed cell death with the minimization of toxicity at very low concentrations of Ag NPs.

5.3. Experimental Section

5.3.1. Synthesis of silver nanoparticle-chitosan nanocarrier (Ag-CS NC)

The synthesis and detailed characterization of Ag-CS NCs have been described in Experimental Section in Chapter 4.

5.3.2 Cell culture and Ag-CS NCs treatment

HT 29 cells (human adenocarcinoma) were procured from National Center for Cell Sciences (NCCS), Pune, India and were cultured in Dulbecco's modified Eagle's medium supplemented with L-glutamine (4 mM), penicillin (50 units mL^{-1}), streptomycin (50 mg mL^{-1}) and 10% (v/v) fetal bovine serum. Cells were maintained in 5% CO_2 humidified incubator at 37^{0}C. The stock solutions of Ag-CS NCs and blank CS NCs (2 mg mL^{-1}) were prepared in sterile phosphate buffered saline (PBS). Required volume of Ag-CS NCs and CS NCs stock solution were added to the cultures to obtain appropriate concentrations of nanocarriers and incubated for 24 h. DMEM was used to dilute the nanocarrier stock to required concentrations. After the treatment with Ag-CS NCs and CS NPs, HT 29 cells were observed under a phase contrast microscope (Nikon ECLIPSE, TS100, Tokyo) to identify the morphological changes as compared to the non-treated cells.

5.3.3. Lactate dehydrogenase (LDH) assay

The cytotoxicity of Ag-CS NCs and blank CS NCs was determined by measuring the activity of LDH enzyme, released in culture media due to the treatment, using CytoTox 96 Non-Radioactive Cytotoxicity Assay Kit (Roche Applied Science). 50.0 μL aliquots of culture media were collected at different time intervals, diluted with 1: 1 fresh medium and incubated with 50.0 μL of tetrazolium salt (INT) solution (substrate) for 30 min at room temperature. As LDH converted INT to the red formazon product, the LDH release was measured at 490 nm with a microplate reader (Bio-Rad Model 680; Bio-Rad, CA) as per manufacturer's instructions. The cells treated with 0.8 % (v/v) Triton X-100 were used as positive control whereas non-treated cells served as negative control. Cytotoxicity of the test materials were calculated as:

% cytotoxicity = (LDH release in treated cells – LDH release in negative control) / (LDH release in positive control – LDH release in negative control) × 100.

5.3.4. 5-carboxyfluorescein diacetate succinimidyl ester (cFDA) – propidium iodide (PI) staining

Viability of Ag-CS NC treated cells were microscopically examined by cFDA-SE (Sigma-Aldrich) staining. cFDA-SE is a membrane permeable nonfluorescent probe which intracellular esterases convert to a fluorescent derivative that in turn is covalently bound to intracellular proteins through the probe's succinimidyl group (Weston and Parish, 1990). The stock solution of cFDA-SE (100 μM) was prepared by dissolving in 20 μL dimethyl sulfoxide (Sigma-Aldrich) and then further diluted in 1 mL ethanol (Merck India Ltd.). The stock was filter sterilized and stored at -20°C. Following the nanocarrier treatment, 5 μM cFDA-SE was added to the culture plate and incubated for 30 min. The cells were then washed with PBS and fresh DMEM was added to the plates before observing under the fluorescence microscope (Nikon ECLIPSE, TS100, Tokyo).

5.3.5. Viability assay

Cell viability was quantified by measuring mitochondrial activity by CellTiter 96 Aqueous One Solution Assay kit (Promega, Madison, WI). Respiring mitochondria in viable cells convert tetrazolium compound, MTS [3-(4, 5-dimethylthiazol-2yl)-5-(3carboxymethoxyphenyl)-2-(4-sulfophenyl)-2H-tetrazolium] to formazon product in presence of an electron coupling reagent phenazine ethosulfate (PES). The quantity of formazon product as measured by the absorbance at 490 nm is directly proportional to the number of living cells in culture. For viability assay, HT 29 cells were seeded in 96 well microtitre plates followed by overnight incubation. After overnight incubation, the cells were treated with different concentrations of the Ag-CS NCs for another 12 h. 20 μL of Aqueous One solution was then directly added to individual well and further incubated for 2 h. The amount of formazon product was measured by recording A_{490} with a microplate reader (Bio-Rad Model 680; Bio-Rad, CA). The cell viability was calculated as:

$$\% \text{ cell viability} = (A_{490} \text{ in treated sample} / A_{490} \text{ in control sample}) \times 100.$$

5.3.6. Acridine orange /ethidium bromide (AO/EB) staining

The cells treated with Ag-CS NCs were stained with AO/EB (Sigma-Aldrich) dual dye in order to detect apoptotic or necrotic nuclei. Cells were grown in 6-well tissue culture plate for 24 h followed by the Ag-CS NC treatment at desired concentrations. The culture media were then removed and the cells were washed twice with PBS. Fresh media were added in each well and the cells were stained by adding 10 μL of AO/EB mix (10 mg mL^{-1} AO and 10 mg mL^{-1} EB in PBS). After 10 min of incubation, cells were washed with PBS before visualizing under a fluorescence microscope (Nikon ECLIPSE, TS100, Tokyo) with an excitation filter of 480/30 nm.

5.3.7. Scanning electron microscopy (SEM)

Cells were grown in 6 well tissue culture plates and treated with respective concentrations of Ag-CS NCs for 6 h. The cells were then washed with PBS followed by fixation in glutaraldehyde/paraformaldehyde solution. The fixed cells were dehydrated in graded ethanol solutions and air dried. Finally a heated metal cutter was used to cut out discs from the bottom of the wells on which the cells had been grown.

The cells attached on discs were coated with gold film in a Polaron in the sputter coater and examined in LEO 1430VP SEM.

5.3.8. Annexin V – PI staining

The induction of apoptosis in HT 29 cells by Ag-CS NCs was examined by FITC labeled annexin V (FITC-annexin V) staining of the treated cells. The cells were simultaneously stained with PI in order to differentiate the necrotic cells from the apoptotic ones based on the membrane integrity. Following the Ag-CS NC treatment, cells were harvested and washed with PBS. The cells were then stained with FITC-annexin V – PI as per manufacturer's instructions (FITC Annexin V Apoptosis Detection Kit, BD Pharmingen™, NJ) and analyzed in a FACS Calibur (BD Biosciences, NJ) flow cytometer. The data were collected with Cell Quest Pro software for 15,000 cells in each sample and subsequently analyzed with WinMDI software. Parallel set of FITC-annexin V – PI stained cells were also visualized for apoptosis under a fluorescence microscope (Nikon ECLIPSE, TS100, Tokyo).

5.3.9. Analysis of DNA fragmentation

Following the treatment with required concentrations of Ag-CS NCs for 12 h, HT 29 cells were collected, washed with PBS, and lyzed (Lysis solution: 10 mM Tris-HCl pH 7.4, 10 mM EDTA and 0.5% Triton X-100). Cell lysates were then incubated with RNase A (200 mg mL^{-1}; Bioline, USA) for 1 h, followed by proteinase K (200 mg mL^{-1}; Bioline, USA) treatment for 1 h at 37^{0}C. After extracting the samples with phenol/chloroform/isoamyl alcohol (25:24:1, v/v/v) followed by chloroform, DNA was precipitated in two volumes of ethanol in the presence of 0.3 mol/L sodium acetate at -20^{0}C. Finally the DNA samples were run on 1.5% agarose gel at 60 V and visualized by ethidium bromide staining under UV light.

5.3.10. Semi-quantitative RT-PCR and real time quantitative RT-PCR analysis

Expression of apoptotic signaling genes, Bcl2 and caspase-3 was examined using reverse transcriptase – polymerase chain reaction (RT-PCR). The housekeeping gene β actin was used as internal control. Total RNA was isolated using Tri reagent (Sigma-Aldrcih, USA). cDNA was generated from of total denatured RNA (3 µg) by reverse transcription performed at 37ºC for 50 min using M-MLV Reverse Transcriptase (Sigma-Aldrcih, USA) in a total mixture of 20 µl. Semi-quantitative PCR was carried out with 2 μl of the above RT product using the gene specific upstream and downstream primers in Gene Amp PCR system 9700, Applied Biosystems. Initial denaturation (94ºC for 2 min) was followed by a PCR cycle of denaturation (94ºC for 15 s), annealing (55ºC for 30 s), extension (68ºC for 1 minute) and final extension (68ºC for 5m). The PCR products were finally resolved on a 1.2% agarose gel and visualized by ethidium bromide staining under UV light.

For real time PCR reaction, reactions were performed with 2 μl of cDNA sample in a total volume of 25 μl including SYBR Green PCR master mix (Applied Biosystems, CA) according to manufacturer's instructions. Amplification was carried out in an Applied Biosystems 7500 Real-Time PCR System, keeping cycles parameters same as above except the initial denaturation was performed at 95 °C for 10 min (for activation of Ampli- Taq Gold present in SYBR Green PCR master mix). Each PCR reaction was performed in triplicate. Relative quantification of the target gene transcripts normalized to endogenous control β actin and relative to a calibrator (non-treated control cells) was calculated by SDS software (provided with the Applied Biosystems 7500 Real-Time PCR System) based on ΔΔCT method. Thus the gene expression in control sample has a value of 1 and expression in treated sample is expressed as an n-fold difference relative to control. The primers used were β actin – forward: 5′-CTGTCTGGCGGCACCACC AT-3′ and reverse: 5′-GCAACTAAGTCATAGTCCGC-3′, Bcl 2 – forward: 5′-AGA TGTCCAGCCAGCTGCACCTGAC-3′ and reverse: 5′-AGATAGGCACCCAGGGT GATGCAA GCT-3′ and caspase 3 –forward: 5′-TTTGTTTGTGTGCTTCTGAGCC-3′ and reverse: 5′-ATTCTGTTGCCACC TTTCGG-3′.

5.3.11. Determination of mitochondrial membrane potential (MMP)

HT 29 cells grown for 24 h were treated with appropriate concentrations of Ag-CS NCs for 3 h and then incubated with 5 μM of 5,5,6,6-tetrachloro-1,1,3,3-tetraethylbenzimidazolylcarbocyanine iodide (JC-1; Sigma-Aldrich, USA) for 30 min in the CO_2 incubator. After the incubation the cells were washed twice with prewarmed PBS, harvested and analyzed with a flow cytometer (FACSCalibur; BD Biosciences). The JC 1 fluorescence data were recorded with the CellQuest program (BD Biosciences) and subsequently analyzed by WinMDI software. A parallel batch of treated cells were stained with JC 1 and washed with PBS before visualizing under a fluorescence microscope (Nikon ECLIPSE, TS100, Tokyo).

5.3.12. Determination of reactive oxygen species (ROS)

The generation of ROS in Ag-CS NCs treated cells was determined by 2, 7-dichlorofluoresceindiacetate (DCFH-DA; Sigma-Aldrcih, USA) staining. DCFH-DA is non-fluorescent and can diffuse into the cell through the plasma membrane where it is hydrolysed to DCFH. Non-fluorescent DCFH is finally converted to green fluorescent dichlorofluorescein (DCF) upon intracellular oxidation. The cells, treated with different concentrations of Ag-CS NCs for 3 h, were harvested and washed twice with PBS. Finally the cells were resuspended in 1 mL DMEM with 5 μM DCFH-DA and incubated for 10 min at 37^0C. Stock (1 mM) solution of DCFH-DA was prepared in ethanol and stored under liquid nitrogen vapour. Immediately after the incubation, the samples were analyzed for DCF fluorescence in a flow cytometer (FacsCalibur, BD Biosciences, NJ) at an excitation wavelength of 488 nm and emission wavelengths of 530. Flow cytometric data were analyzed using WinMDI software and the ROS generation was expressed in terms of percentage of cells with DCF (green) fluorescence. A parallel batch of treated cells was stained with DCFH-DA visualized under a fluorescence microscope (Nikon ECLIPSE, TS100, Tokyo).

5.3.13. Cell cycle analysis

Cell cycle analysis was performed by measuring the DNA content of the treated as well as control cells in a flow cytometer. HT 29 cells were grown in 100-mm tissue culture dishes followed by Ag-CS NC treatment for 24 h. After treatment, the cells were harvested by trypsinization, washed with PBS, fixed by adding slowly 2 mL of cold 70% ethanol and finally stored at 4^0C. The cells were then centrifuged and washed in ice-cold PBS. Finally the cells were stained with PI in RNase (40 μg/mL PI and 100 μg/mL RNase A) and incubated at 37 °C for 30 min in the dark. Immediately after the incubation, the samples were analyzed in a FACSCalibur (BD Biosciences, NJ). Flow cytometric data were recorded with CellQuest software and subsequently re-analyzed by WinMDI software**.**

5.3.14. Statistical analysis

The values for all experiments are expressed as mean ± standard deviation (S.D.) of three or more individual experiments. The data were analyzed using *Student's t test* and statistically significant values are denoted by * ($p < 0.05$), ** ($p < 0.005$) and *** ($p < 0.001$).

5.4. Results and Discussion

5.4.1. Characterization of Ag-CS NCs

The Ag-CS NCs used in the present study were prepared via ionic gelation of bulk CS-Ag NP composite by TPP as described in Chapter 4. The detailed characterization of the Ag-CS NCs has been described in Results and Discussion section of Chapter 4. In brief, 172.6 nm Ag-CS NCs with homogenously impregnated Ag NPs (~ 4.9 nm) and 136.9 nm blank CS NCs (for control cytotoxicity experiments) were synthesized.

5.4.2. Cytotoxicity

In order to examine the cytotoxic effect of Ag CS NCs, the morphology of treated HT 29 cells were observed under phase contrast microscope and distinct morphological changes were detected in treated cells (**Figure 5.1**). More cells appeared to be rounded, shrunken and loosely attached to the surface as the concentration of the Ag-CS NCs increased up to 40 µg mL^{-1}. The Inter-cellular connections also decreased notably. At a concentration of 80 µg mL^{-1} or above, treated cells were mostly swollen and detached form neighbor cells with completely disintegrated membrane indicating extensive necrotic cell death at these concentrations. However, HT 29 cells treated with CS NCs (80 µg mL^{-1}) showed healthy and normal morphology as compared to the control cells.

The cytotoxicity of Ag-CS NCs on HT 29 cells were measured quantitatively by LDH assay. The results (**Figure 5.2**) demonstrate the concentration and time dependent leakage of LDH from HT 29 cells exposed to Ag CS NCs. Moreover, the insignificant LDH release in cells treated with blank CS NPs confirmed the cyto-compatibility of the chitosan nanocarriers (**Figure 5.2**, inset) in the present experimental concentration range.

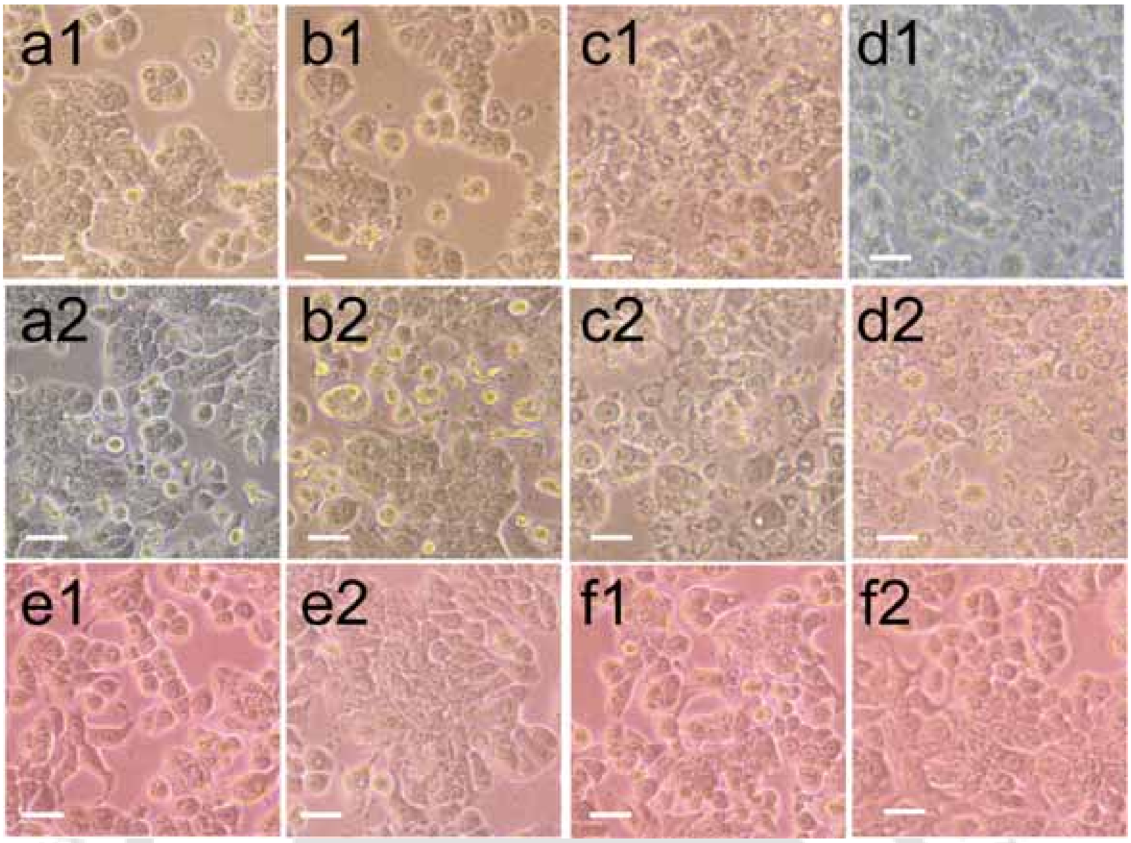

Figure 5.1. Morphology of HT 29 cells treated with 20 μg mL^{-1} **(a1, a2)**, 40 μg mL^{-1} **(b1, b2)**, 60 μg mL^{-1} **(c1, c2)** and 80 μg mL^{-1} **(d1, d2)** of Ag-CS NCs for 3 h **(a1, b1, c1**and **d1)** and 6 h **(a2, b2, c2** and **d2)**. Morphology of non-treated control cells (**e1**, 3 h and **e2**, 6 h) and CS NC (80 μg mL^{-1})-treated cells (**f1**, 3 h and **f2**, 6 h) are also shown. Scale bar: 20 μ

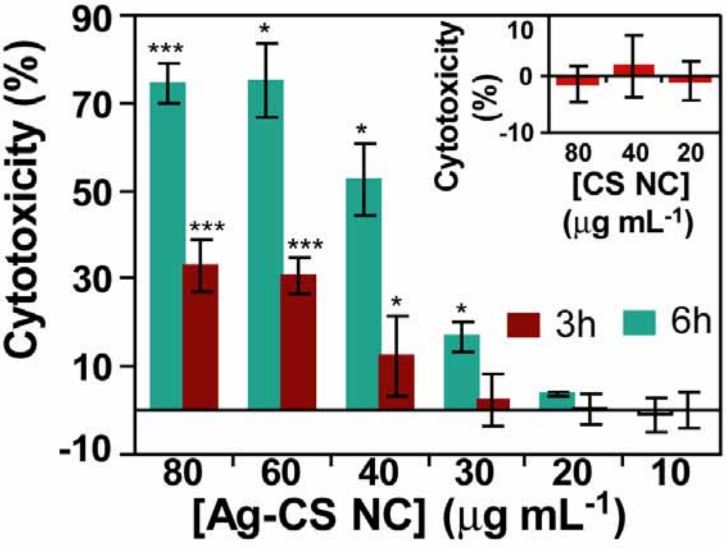

Figure 5.2. Cytotoxicity of different concentrations of Ag-CS NCs on HT 29 cells after 3 and 6 h of treatment, as calculated from the LDH assay. Cytotoxicity due to blank chitosan nanoparticles is shown in the inset. The values are represented as mean ± S.D. of three individual experiments. Statistical significance between non-treated control and treated sample is denoted by * ($p < 0.05$) and *** ($p < 0.001$).

5.4.3 Cell viability

The effect of Ag-CS NCs on the viability of HT 29 cells was assessed microscopically by cFDA/PI staining of the treated cells. The result of cFDA/PI staining (**Figure 5.3**) clearly shows that the number of viable cells decreased with increasing concentration of Ag CS NCs, as evident from the gradual increase in number of PI-stained (red) cells. Additionally, MTS assay was carried out in order to determine the cell viability quantitatively in Ag CS NCs-treated cells and the results are shown in **Figure 5.4**. The results show the inhibition of cell viability by Ag CS NCs in a concentration-dependent manner. The IC_{50} value of Ag CS NCs was calculated to be 22 μg mL^{-1}.

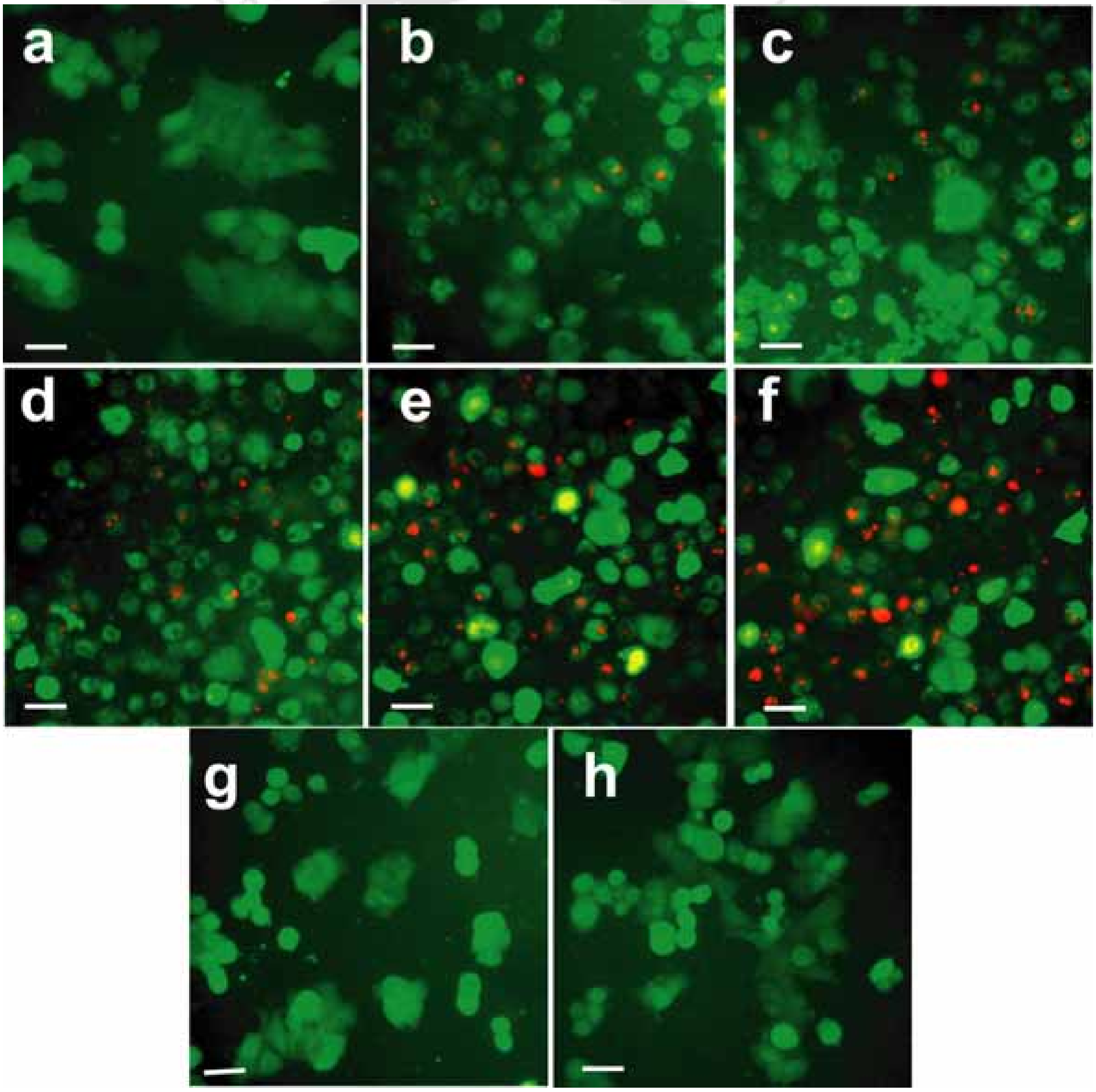

Figure 5.3. cFDA/PI staining of HT 29 cells treated with **(a)**10 μg mL^{-1}, **(b)** 20 μg mL^{-1}, **(c)** 30 μg mL^{-1}, **(d)** 40 μg mL^{-1}, **(e)** 60 μg mL^{-1} and **(f)** 80 μg mL^{-1} of Ag-CS NCs for 6 h. Morphology of **(g)** non-treated and **(h)** CS NC (80 μg mL^{-1}) -treated cells are also shown. Scale bar: 20 μ

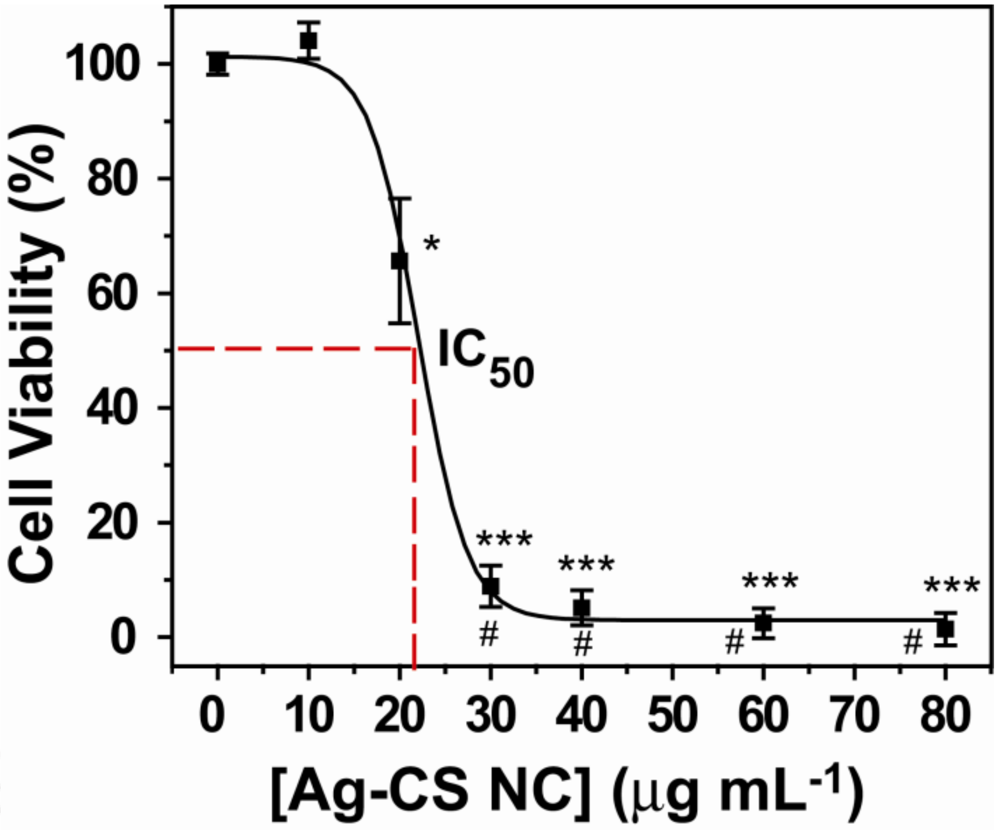

Figure 5.4. Cell viability of HT 29 cells after 12 h treatment with different concentrations of Ag-CS NCs, as calculated from the MTS assay. The values are represented as mean ± S.D. of three individual experiments. Statistical significance between non-treated control and treated sample is denoted by * ($p < 0.05$) and *** ($p < 0.001$); statistical significance compared to blank CS NPs (80 µg mL^{-1}) treated sample is denoted by # ($p < 0.05$).

Based on the IC$_{50}$ value, three different concentrations of Ag-CS NCs namely 12 µg mL^{-1} (~½ IC$_{50}$), 24 µg mL^{-1} (~IC$_{50}$) and 48 µg mL^{-1} (~2 IC$_{50}$) were chosen for further apoptosis experiments. It may be mentioned here that the concentration of Ag NPs in Ag-CS NCs at IC$_{50}$ value, as determined by atomic absorption spectroscopy (AAS), was found to be 330 ng mL^{-1}. The concentration of Ag NPs required to reduce cell viability by 50% in the present study is less than previously reported values (Gopinath et al., 2008; AshaRani et al, 2009; Jain et al., 2009; Hsin et al., 2008; Arora et al., 2008; Hussain et al., 2005) by orders of magnitude (**Table 5.1**). This extraordinarily high cell death caused by the Ag NPs in the present study could be due to the increased bio-availability of the Ag NPs impregnated in chitosan NCs which, unlike free Ag NPs, prevent Ag NPs from premature interaction with biological environment as well as help in intracellular uptake (Peer et al., 2007).

Table 5.1. IC_{50} values of different Ag NP systems

Study	**Carrier system**	**Particle Size (nm)**	**Cell Type**	**IC_{50} ($\mu g\ mL^{-1}$)**
Present	Chitosan NCs	4.9	HT 29	0.33
Gopinath et al., 2008		10-15	HT 29, BHK 21	27.0
Jain et al., 2009	Polymeric gel	16.6	Hep G2	251
Arora et al., 2008		7-20	A431	11.6
			HT-1080	10.6
AshaRani et al, 2009		6-20	IMR-90, U251	~ 400
Hussain et al., 2005		15	BRL3A	24.0
		100		19.0
Hsin et al., 2008		1-100	NIH3T3,A10, HCT116	~50.0

5.4.4. Mode of cell death

In order to investigate the mode of cell death (viz. apoptosis or necrosis) in HT 29 cells caused by the Ag-CS NCs, treated cells were stained with AO/EB dual dye and observed under the fluorescence microscope. **Figure 5.5b** shows that the cells treated with 12 $\mu g\ mL^{-1}$ Ag-CS NCs, like the non-treated ones (**Figure 5.5a**), are uniformly green with normal nuclear morphology and well-organized chromatin structure. However, extensive nuclear margination accompanied with chromatin condensation and fragmentation, distinctive of apoptotic cell death (Rello et al., 2005; Allen et al., 1997) was observed in treated cells at the Ag-CS NCs concentration of 24 $\mu g\ mL^{-1}$ and 48 $\mu g\ mL^{-1}$. The images in **Figure 5.5c** and **5.5d** clearly demonstrate the presence of early apoptotic cells having condensed chromatin as well as late apoptotic cells with fragmented chromatin and apoptotic bodies. The results of AO/EB nuclear staining indicated the induction of apoptosis in HT 29 cells by Ag-CS NCs.

In complementary to the AO/EB staining, Ag-CS NC treated HT 29 cells were further examined under the SEM in quest of the characteristic morphological changes observed during apoptosis. **Figure 5.6a** shows the typical morphology of healthy HT 29 cells that are well-attached to the surface. The cells treated with 12 $\mu g\ mL^{-1}$ (½ IC_{50}) Ag-CS NC showed healthy morphology (**Figure 5.6b**) whereas the cells treated with 24 $\mu g\ mL^{-1}$ (IC_{50}) and 48 $\mu g\ mL^{-1}$ (2 IC_{50}) of Ag-CS NC demonstrated round-shaped and loosely attached cells (**Figure 5.6c** and **5.6d**) as compared to non-treated cells. The occurrence of membrane blebbing as well as formation of apoptotic bodies, indicative of apoptotic cell death (Rello et al., 2005; Allen et al., 1997), were clearly detected in HT 92 cells treated with Ag-CS NCs (at IC_{50} and 2 IC_{50}).

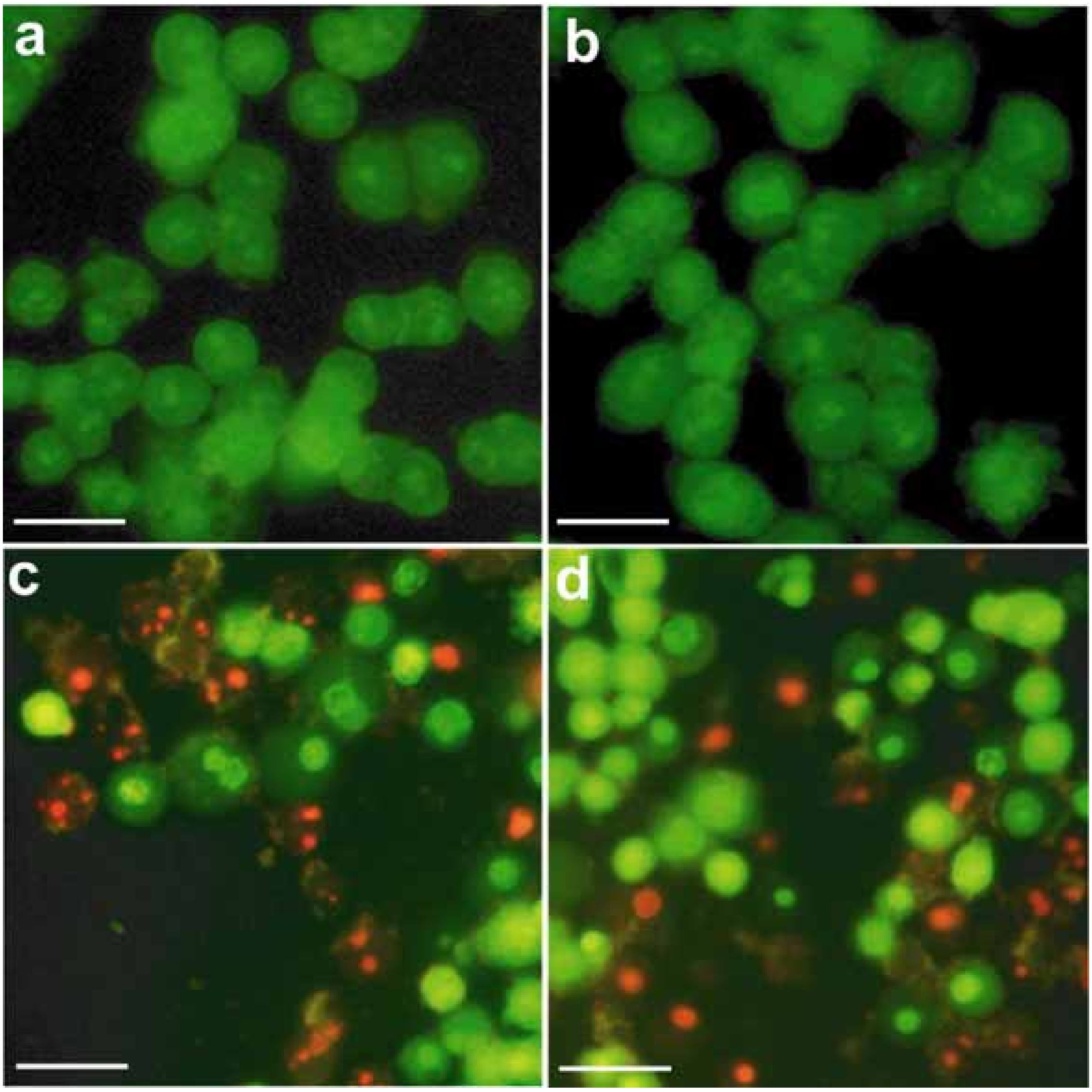

Figure 5.5. Representative images of AO/EB dual staining of (**a**) non-treated, (**b**) 12 µg mL^{-1} (~½ IC_{50}), (**c**) 24 µg mL^{-1} (~ IC_{50}) and (**d**) 48 µg mL^{-1} (~2 IC_{50}) Ag-CS NCs treated HT 29 cells after 6 h of treatment. Condensed chromatin in early apoptotic (EA) cells and fragmented chromatin in late apoptotic (LA) cells are clearly visible in (**c**) and (**d**). Scale bar: 20 µ

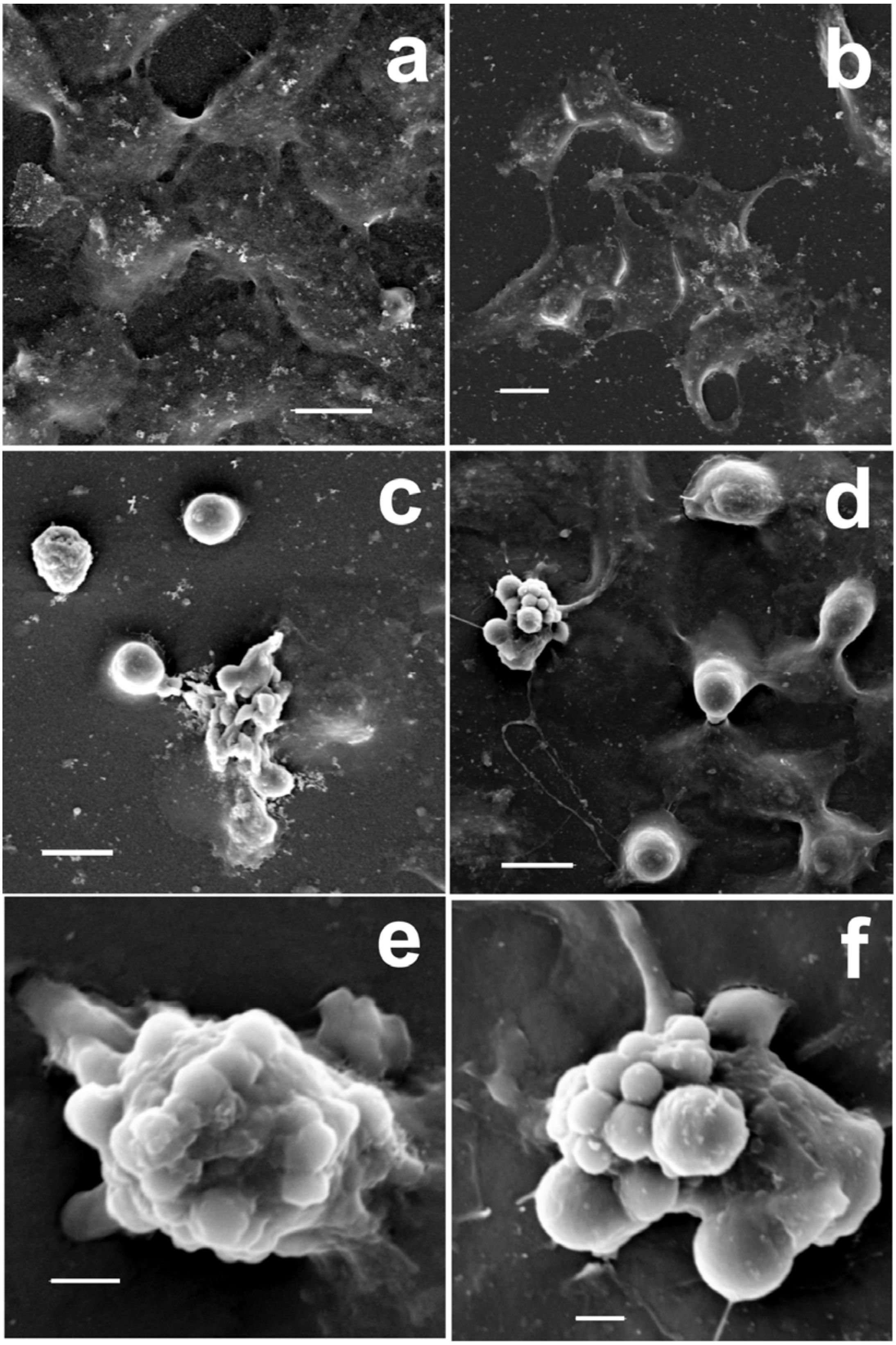

Figure 5.6. Representative SEM images of **(a)** non-treated HT 29 cells and cells treated with **(b)** 12 μg mL^{-1} (~½ IC$_{50}$), **(c)** 24 μg mL^{-1} (~ IC$_{50}$) and (**d**) 48 μg mL^{-1} (~2 IC$_{50}$) of Ag-CS NCs for 6 h. Image **(c)** and **(d)** are shown at higher magnification in **(e)** and **(f)**, respectively. Morphological changes associated with apoptosis viz. membrane blebbing and formation of apoptotic body are clearly detectable in (**c**) – (**f**). Scale bar: 10 μ (**a-d**) and 2 μ (**e, f**).

5.4.5. Anexin V- PI staining

The apoptotic cell death in HT 29 cells induced by Ag-CS NCs was confirmed and subsequently quantified by microscopic and flow cytometric analysis of anexin V-PI stained HT 29 cells, respectively. Early apoptotic cells can easily be identified by green fluorescence of FITC-conjugated anexin V as annexin V has a high affinity towards phosphatidyl serine (PS) residues which are externalized from inner to outer leaflet of the plasma membrane during early stages of apoptosis (Martin et al., 1995; Koopman et al., 1994). Due to its membrane impermeability, PI, on the other hand, helps in identifying the necrotic and late apoptotic cells having damaged plasma membrane (Allen et al., 1997; Koopman et al., 1994). The fluorescence microscopic images of FITC-anexinV – PI stained HT 29 cells (**Figure 5.7a-5.7h**) revealed that the cells treated with 12 μg mL^{-1} Ag-CS NCs were almost unaffected as compared to non-treated control cells. However, the induction of apoptosis in HT 29 cells by Ag-CS NCs at the concentrations of 24 μg mL^{-1} and 48 μg mL^{-1} is evident from the presence of green fluorescent early apoptotic cells and red - green dual fluorescent late apoptotic cells in **Figure 5.7c** and **5.7d**.

Figure 5.7i shows the results of flow cytometric analysis of FITC-anexin V – PI stained HT 29 cells treated with different concentrations of Ag-CS NCs. The percentage of apoptotic and necrotic population in treated as well as non-treated cells were calculated from the flow cytometric data and summarized in **Figure 5.7j**. **Figure 5.7j** clearly shows the dose dependent reduction in cell viability of HT 29 cells in presence Ag-CS NCs. Most importantly, the apoptotic population in HT 29 cells increased by ca. 34% and ca. 61% in presence of 24 μg mL^{-1} and 48 μg mL^{-1} Ag-CS NCs, respectively. On the other hand, an increase of ca. 8% and ca. 2.5%, respectively, was observed in necrotic population at these concentrations. The results of flow cytometric analysis clearly establish the efficient induction of apoptotic cell death in HT 29 cells by Ag-CS NCs.

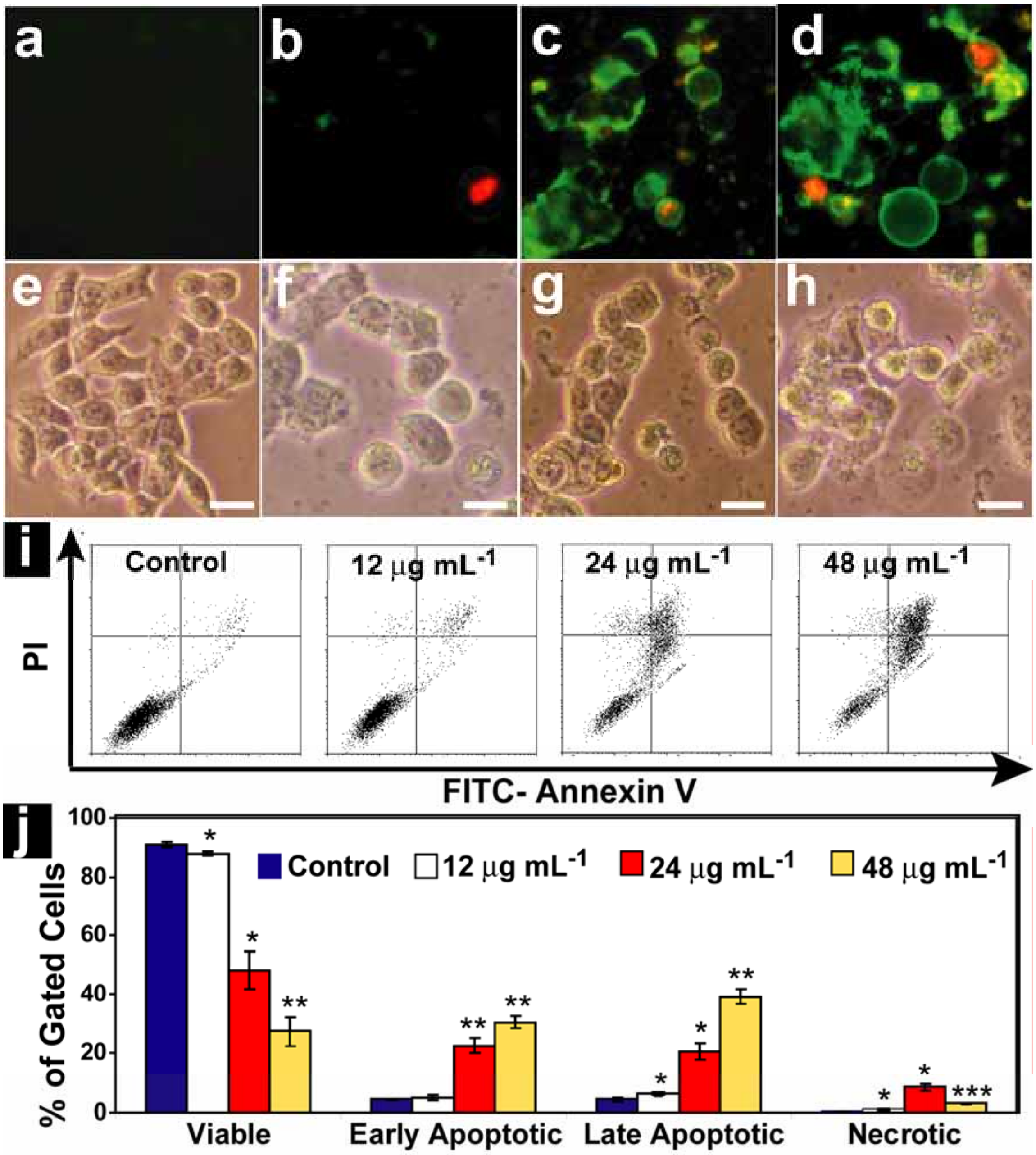

Figure 5.7. Representative images of FITC-annexin V – PI staining of (**a, e**) non-treated, (**b, f**) 12 μg mL^{-1} (~½ IC$_{50}$), (**c, g**) 24 μg mL^{-1} (~ IC$_{50}$) and (**d, h**) 48 μg mL^{-1} (~2 IC$_{50}$) Ag-CS NCs treated HT 29 cells after 6 h of treatment. The images in the lower panel (**e-h**) are corresponding bright field images. Scale bar: 10 μ. (**i**) Flow cytometric analysis of FITC-annexin V – PI stained HT 29 cells after Ag-CS NC treatment. (**j**) Apoptotic and necrotic population (%) in each sample were calculated from cytometric analysis. The values are represented as mean ± S.D. of three individual experiments. Statistical significance between non-treated control and treated sample is denoted by * (p < 0.05), ** (p < 0.005) and *** (p < 0.001).

5.4.6. DNA fragmentation and up-regulation of caspase 3

The formation of oligo-nucleosomal DNA fragments or ‘ladder’ due to the fragmentation of DNA is widely regarded as a biochemical hallmark of late apoptosis (Rello et al., 2005). The DNA fragmentation in the present study was verified by extracting DNA from HT 29 cells treated with Ag-CS NCs followed by detection in the agarose gel. **Figure 5.8a** clearly demonstrate the DNA ‘laddering’ pattern in HT 29 cells treated with 24 µg mL^{-1} (~IC_{50}) and 48 µg mL^{-1} (~2 IC_{50}) Ag-CS NCs. On the other hand, cells treated with 12 µg mL^{-1} (~½ IC_{50}) Ag-CS NCs did not produce detectable DNA ladder. These results are consistent with flow cytometric data of apoptosis in Ag-CS NC treated HT 29 cells.

Caspases are cysteine-aspartic acid proteases and well known for their vital role in the initiation as well as the execution of apoptosis (Nunez et al., 1998). Especially the activation of caspase-3 is crucial for cellular DNA fragmentation (Janicke et al., 1998). The role of caspase 3 in Ag-CS NC mediated apoptosis in HT 29 cells was investigated by conventional RT-PCR analysis. The results of semi-quantitative RT-PCR (**Figure 5.8b**) indicate up-regulation of caspase 3, as compared to house-keeping β actin gene, in HT 29 cells treated with 48 µg mL^{-1} (~IC_{50}) Ag-CS NCs. Additionally, quantitative real-time RT-PCR analysis (**Figure 5.8c**) clearly demonstrates that the expression level of caspase 3, normalized to β actin gene as internal control, increased after exposure to Ag-CS NCs. The results indicate the involvement of the caspase signaling pathway in the apoptotic cell death of HT 29 cells treated with Ag-CS NCs. The elevated caspase 3 activity in Ag NP treated mammalian cells has been also reported by others (Gopinath et al., 2008, 2010; Hsin et al., 2008; Arora et al., 2008). On the other hand, the changes in anti-apoptotic Bcl 2 expression in treated HT 29 cells were insignificant, as evident from RT-PCR and real-time quantitative RT-PCR analysis (**Figure 5.8b, 5.8c**). The importance of up-regulation of Bcl 2 in shielding the apoptotic responses of nano-silver in HCT 116 cells has recently been reported by Hsin et al. (2008). The RT-PCR results indicate that the absence of active up-regulation, although not down-regulated, of anti-apoptotic Bcl 2 plays a critical role in Ag-CS NC induced apoptosis in HT 29 cells.

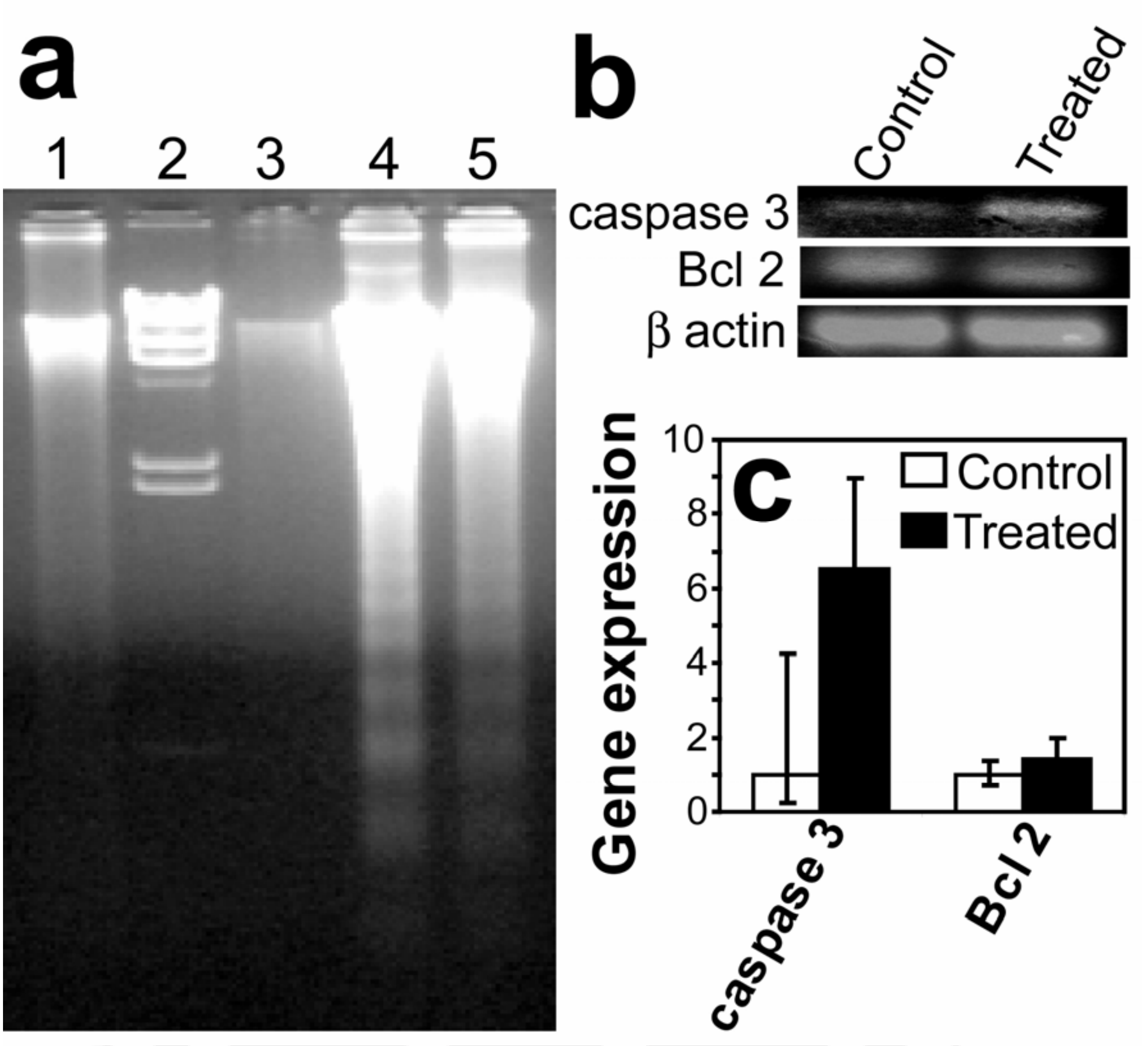

Figure 5.8. (a) DNA laddering assay of non-treated (lane 3), 12 μg mL^{-1} (lane 1), 24 μg mL^{-1} (lane 4) and 48 μg mL^{-1} (lane 5) Ag-CS NCs treated HT 29 cells. Lane 2: λ DNA/*Hind* III marker. **(b)** Semi-quantitative and **(c)** real time quantitative RT-PCR analysis of caspase 3 and Bcl 2 gene in HT 29 cells treated with Ag-CS NCs (24 μg mL^{-1}).

5.4.7. Effect on mitochondrial membrane potential (MMP)

Mitochondria play key role in the apoptotic pathway of cell death, and the changes in mitochondrial membrane permeability comprise the early events during apoptosis (Thresset al., 1999). As the mitochondrial inner membrane potential decreases during apoptosis, the effect of Ag-CS NC exposure on the mitochondrial membrane potential ($\Delta\psi_m$) of HT 29 cells in the present study were further investigated by JC 1 staining. JC 1 is a cationic lipophilic dye which stains polarized mitochondria in viable cells as red due to the formation of J-aggregates emitting red fluorescence (Cossarizza et al., 1993). On the other hand, due to the depolarization of mitochondrial membrane in apoptotic cells, JC 1 remains in its monomeric form and thereby emits green fluorescence. A reduction in the J-aggregate (red fluorescence) / monomer (green fluorescence) ratio, thus, indicates a drop in $\Delta\psi_m$. Fluorescence microscopic observation of control HT 29 cells (**Figure 5.9a**) showed completely polarized mitochondria forming J-aggregates as red dots. In contrast, the treatment with Ag-CS NCs resulted in the depolarization of the mitochondrial membrane in HT 29 cells, as evident from the loss of the red dots and simultaneous increase of green fluorescence (**Figure 5.9b-5.9d**). Quantitative analysis by flow cytometry showed that the MMP in HT 29 cells treated with 24 (IC_{50}) and 48 $\mu g\ mL^{-1}$ (2 IC_{50})of Ag-CS NCs decreased by 43% and 55%, respectively, as compared to that of the control cells. Preferential localization of nanoparticulate fullerenes (C_{60}) in mitochondria has already been reported by Foley et al (2002). As the mitochondrial respiratory chain is the main source of intracellular ROS production in aerobic cells, mitochondrial dysfunction due to NP immobilization may lead to oxidative stress. On the other hand, mitochondrial membrane is among the major susceptible targets of the deleterious effects associated with intracellular ROS. The present results indicate that the adverse changes in mitochondrial function due to Ag-CS NCs, with possible association of intracellular ROS production, trigger the apoptosis process.

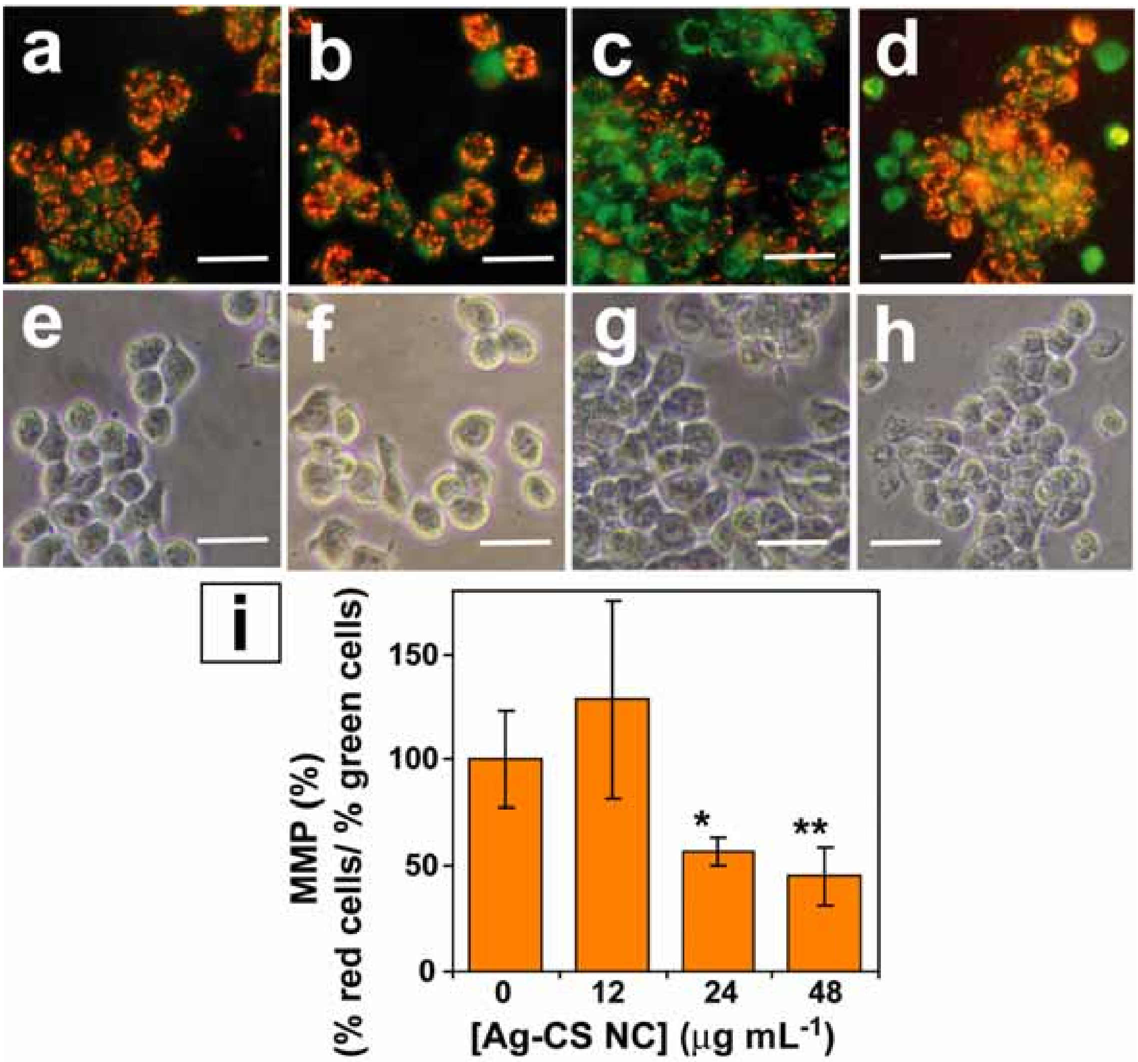

Figure 5.9. Microscopic image of JC 1 staining of **(a, e)** non-treated, **(b, f)** 12 μg mL^{-1} (~½ IC_{50}), **(c, g)** 24 μg mL^{-1} (~ IC_{50}) and **(d, h)** 48 μg mL^{-1} (~2 IC_{50}) Ag-CS NCs treated HT 29 cells. The images in the lower panel **(e-h)** are corresponding bright field images. Scale bar: 20 μ. **(i)** Flow cytometric analysis of MMP in presence of different concentration of Ag-CS NCs. The values are represented as mean ± S.D. of three individual experiments. Statistical significance between non-treated control and treated sample is denoted by * ($p < 0.05$) and ** ($p < 0.005$).

5.4.8 Role of ROS

The interaction of engineered nanoparticles with mammalian cells can induce oxidative stress by favoring the cellular ROS production over the cellular antioxidant defenses. Although the exact mechanism is still to be understood, the critical role of ROS in nanoparticle mediated cytotoxicity and genotoxicity has been recently reported by several researchers (Limbach et al., 2007; Sayes et al., 2005; Green et al., 2005; Park et al., 2008). In order to investigate the effect of Ag-CS NC on the cellular ROS production in the present study, the treated cells were examined under microscope for their ability to show green fluorescence of DCF, produced by the intracellular oxidation of DCFH-DA dye. **Figure 5.10** clearly shows the elevation in the ROS production in the Ag-CS NC treated cells compared to the non-treated cells. The increase in ROS generation in treated cells was quantified by determining the percentage of cells with increased green fluorescence in a flow cytometer. It is evident from the flow cytometric analysis (**Figure 5.10i**) that Ag-CS NC raised the level of intracellular ROS in a concentration dependent way and the percentage of cells with elevated ROS increased significantly at 24 and 48 µg mL^{-1} of Ag-CS NC. The present data indicates that Ag-CS NCs, at low concentrations (~ ½ IC_{50}), induce modest oxidative stress in HT 29 cells which can be efficiently repaired by intracellular antioxidant response. However, the intracellular ROS level in presence of Ag-CS NC at IC_{50} or more crossed an optimal limit which was toxic enough to augment the apoptotic cell death by damaging mitochondrial membrane integrity and increasing oxidative DNA damage (Ott et al., 2007). Similar role of ROS in ceramide induced apoptosis in U937 cells were reported previously by Quillet-Mary et al. (1997) where ROS scavengers such as dithiocarbamates (PDTC), N-acetylcysteine (thiol antioxidant), and a glutathione (GSH) precursor successfully inhibited the ceramide induced apoptosis.

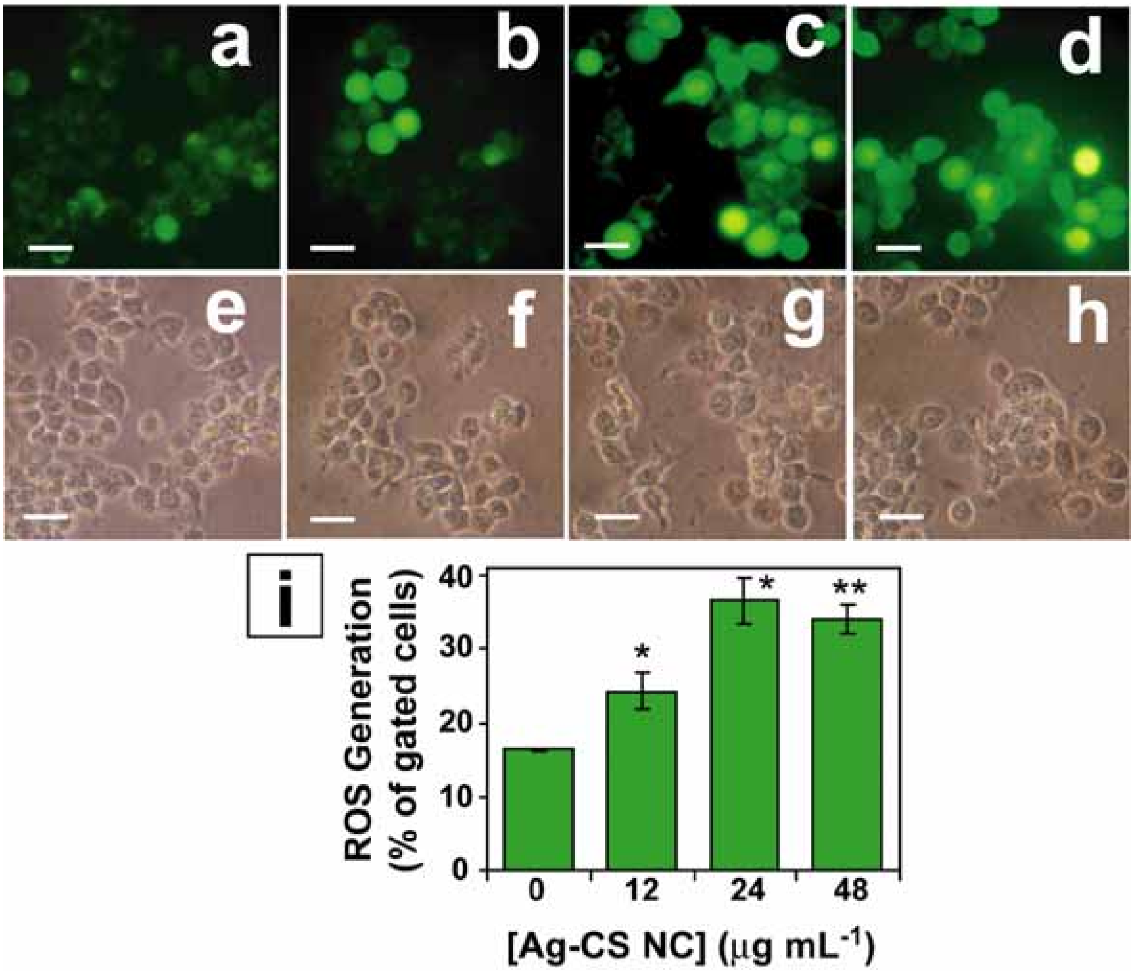

Figure 5.10. DCFH-DA staining of **(a, e)** non-treated, **(b, f)** 12 μg mL^{-1} (~½ IC$_{50}$), **(c, g)** 24 μg mL^{-1} (~ IC$_{50}$) and **(d, h)** 48 μg mL^{-1} (~2 IC$_{50}$) Ag-CS NCs treated HT 29 cells for visualization of cellular ROS production. The images in the lower panel **(e-h)** are corresponding bright field images. Scale bar: 20 μ. **(i)** Flow cytometric analysis of ROS production in presence of different concentration of Ag-CS NCs. The values are represented as mean ± S.D. of three individual experiments. Statistical significance between non-treated control and treated sample is denoted by * ($p < 0.05$) and ** ($p < 0.005$).

5.4.9. Effect on cell cycle

In order to investigate the possible DNA damage due to oxidative stress in Ag-CS NC treated HT 92 cells, the cell cycle distribution was monitored by measuring the DNA content in a flow cytometer. Flow cytometric analysis (**Figure 5.11**) shows that the cell populations in different phases of cell cycle (G_0/G_1, S and G_2/M) were mostly unaffected at lower Ag-CS NC concentrations (~½ IC and IC_{50}), as compared to the non-treated cells. The G_2/M population increase by ca. 3 % only when the cells were treated with 48 $\mu g\ mL^{-1}$ (~2 IC_{50}) Ag-CS NC. However, significant increase in sub G_0/G_1 population indicates the apoptotic cell death in Ag-CS NC treated cells. Recently, AshaRani et al (2009) has reported the profound effect of starch-capped Ag NPs on cell cycle progression, in the form of concentration dependent G_2/M arrest, in IMR-90 and U 251 cells and related this to the genotoxic effect of the Ag NPs. However, the absence of any significant G_2/M arrest in HT 29 cells the present study could be due to the fact that the concentrations of Ag NPs (in Ag-CS NCs) tested here are order of magnitude less. The present results are promising from therapeutic point of view as the detrimental geno-toxicity of Ag NPs could be avoided without compromising the beneficial apoptosis-inducing efficacy.

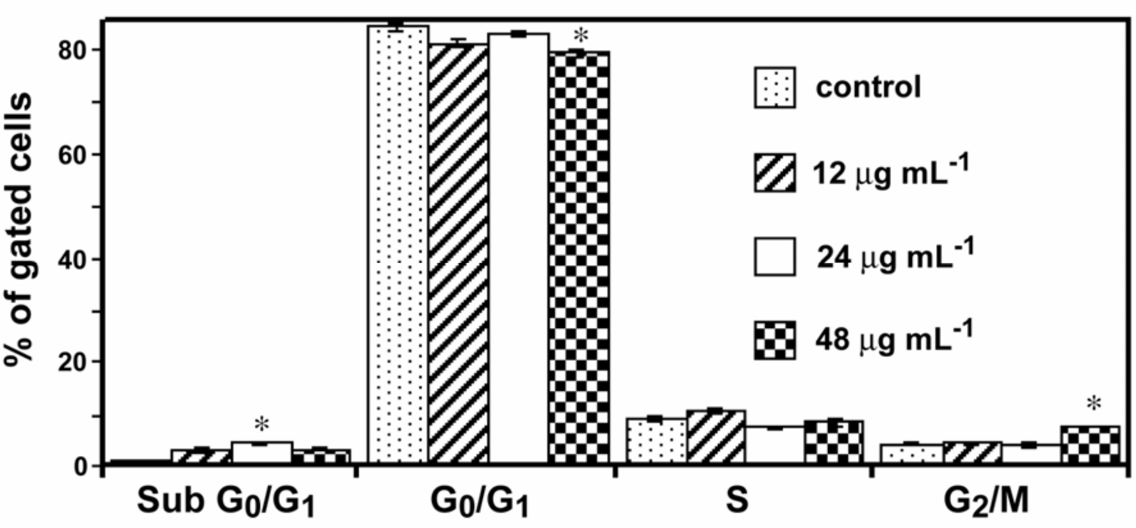

Figure 5.11. Effect of Ag-CS NCs on cell cycle in HT 29 cells was evaluated by calculating the percentage of cells in each phase from flow cytometric data. The values are represented as mean ± S.D. of three individual experiments. Statistical significance between non-treated control and treated sample is denoted by * ($p < 0.05$).

5.5. Conclusion

Ag-CS NCs, prepared in a completely ‘green’ method, were used for the successful delivery of Ag NPs to human HT 29 adenocarcinoma cells. The NCs were found to elicit anti-proliferative response at a much lower concentration of Ag NPs (330 ng mL^{-1} at IC_{50}) compared to previously reported data indicating the superior efficacy of the present system. Efficient induction of apoptosis, accompanied by insignificant necrosis, in HT 29 cells by Ag-CS NCs in the concentration range of 24 – 48 µg mL^{-1} was clearly demonstrated by flow cytometric analysis. The results may prove to be significant in therapeutic applications as the cell death induced by Ag-CS NCs could actually be directed to follow the apoptotic pathway by optimizing the concentration of Ag-CS NCs. The oxidative stress and mitochondrial dysfunction were shown to play important role in the apoptosis. The cell cycle progression was found to be unaffected by Ag NPs indicating the intimidation of carcinogenesis and genotoxicity being at minimum. The implication of the present findings seems to be promising for the possible application of chitosan based nanocarriers of Ag NPs to cancer cells, where synergistic effect of two separate mechanistic pathways – caspase signaling pathway and ROS production – leads to efficient apoptosis. Additionally, this could also help in the wound healing process which is otherwise affected by the inflammatory response elicited by the necrotic cell death. An important continuation of the present study would be the incorporation of fluorophores, such as quantum dots (QDs), in the chitosan matrix in order to monitor effects of nanoparticles in real time *in vitro*.

CHAPTER 6

Incorporation of Gene Therapy Vector in Chitosan Stabilized ZnS:Mn^{2+} Quantum Dots

Chapter 6 describes the synthesis of chitosan stabilized and water dispersible ZnS:Mn^{2+} *quantum dots (QDs) of ca. 3.6 nm, having strong orange fluorescence, in an environment friendly method. Binding of plasmid DNA containing CD-UPRT gene, having therapeutic importance in suicide gene therapy, has been investigated. These chitosan stabilized QDs could be a promising alternative to conventional organic fluorophore-tagged gene delivery systems for real-time monitoring in gene therapy applications.*

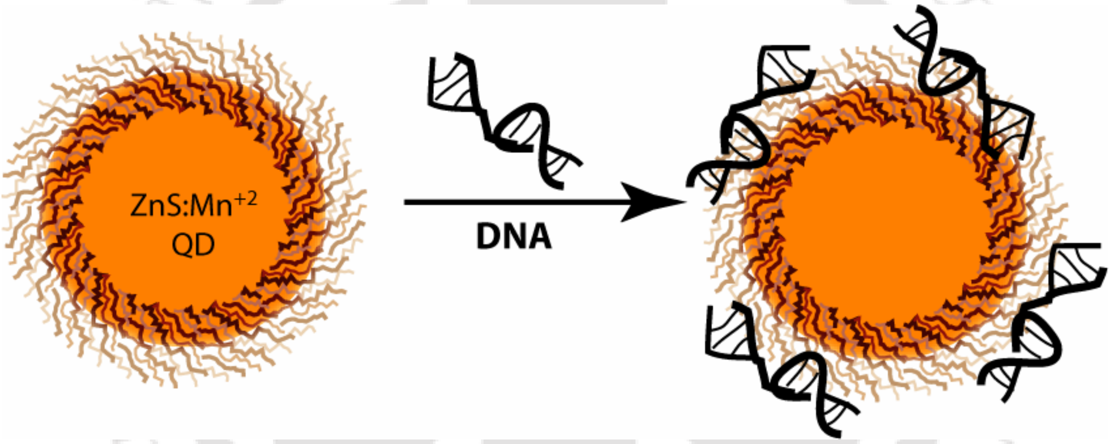

Chapter 6

INCORPORATION OF GENE THERAPY VECTOR IN CHITOSAN STABILIZED ZnS:Mn^{2+} QUANTUM DOTS

6.1. Introduction

Development of newer biocompatible gene delivery vehicles with potential implication in cancer gene therapy is an emerging area of research (Park et al., 2006). On the other hand, monitoring transport and sustained release of therapeutic gene(s) in real-time has also been a critical issue in unveiling the enigma of intracellular transport mechanism of trans-gene expression (Suh et al, 2003). In this regard, biocompatible nanocomposites consisting of quantum dots (QDs) would constitute ideal choices as delivery vehicles that are easily traceable. Recently, our laboratory has developed a potent gene therapy system associated with bifunctional cytosine deaminase – uracilphosphoribosyl transferase gene (CD-UPRT), which converts prodrug 5-fluorocytosine (5-FC) to 5-fluorouracil (5-FU) and other toxic metabolites useful for anticancer therapy (Gopinath and Ghosh, 2008). The molecular mechanism leading to apoptotic cell death due to 5-FC/CD-UPRT gene therapy has been established (Gopinath and Ghosh, 2009). Hence, development of suitable delivery vehicle, with the possibility of tracking by fluorescence of QDs, for 5-FC/CD-UPRT system is important in order to further enhance the efficacy of this system.

6.2. Outline of the Research Work

1) A novel chitosan stabilized Mn^{2+} doped ZnS QDs having excellent water solubility was synthesized and subsequently characterized.
2) The binding capacity of these QDs with plasmid carrying cytosine deaminase – uracilphosphoribosyl transferase (pCD-UPRT), having therapeutic importance in suicide gene therapy, was investigated thoroughly and was shown to follow the Langmuir reversible adsorption model.

3) The biocompatibility of the composite on human colon adenocarcinoma (HT 29) cells was confirmed by cell viability assay.
4) The chitosan stabilized ZnS:Mn^{2+} QDs synthesized in the present work could be a promising alternative to conventional organic fluorophore-tagged gene delivery systems for real-time monitoring in gene therapy applications.

6.3. Experimental Section

6.3.1 Synthesis of chitosan stabilized Mn^{2+} doped ZnS QDs

The wet chemical synthesis method used for the preparation of ZnS: Mn^{2+} QDs was based on a previous report (Warad et al., 2007) with some modifications. Briefly, 10 mM zinc acetate (Sigma-Aldrich) and 2.5 mM manganese chloride (Sigma-Aldrich) were mixed together in 10 mL of aqueous solution of 0.5 mg mL^{-1} chitosan (Sigma) and heated at 80°C for 15 min under constant stirring. After cooling to room temperature, freshly prepared 10 mM sodium sulfide (Merck India Ltd.) solution was added drop wise in the reaction mixture kept in an ice bath under constant stirring. The clear solution started turning milky white indicating the formation of ZnS: Mn^{2+} QDs. The QDs were precipitated at 10,000 rpm, washed and resuspended in MiliQ water.

6.3.2. Characterization of QDs

The UV-visible spectrum of colloidal QDs was recorded in a Cary 100 UV-visible spectrophotometer (Varian Inc.). Fluorescence emission spectrum was recorded in a Fluoro Max-3 (HORIBA Jobin Yvon) fluorescence spectrophotometer at an excitation wavelength of 318 nm. For X-ray Diffraction (XRD), colloidal solution of ZnS: Mn^{2+} QDs was freeze-dried and subsequently analyzed in a Bruker D8 ADVANCE (Bruker AXS Inc.) X-ray powder diffractometer using Cu$K\alpha$ (λ = 1.54 Å) source. For transmission electron microscopic (TEM) analysis, 5 μL of as prepared colloidal solution of QDs was drop cast on carbon coated Cu TEM grids followed by air-drying. The grids were then analyzed by a JEOL 2100 UHR-TEM instrument operating at an accelerating voltage of 200 KeV.

6.3.3. DNA binding study

Binding of DNA to QDs was investigated using pCD-UPRT (an expression vector developed in our laboratory (Gopinath and Ghosh, 2008) containing *E. coli* hybrid cytosine deaminase and phosphoribosyltransferase gene) and checked by gel retardation assay. For this purpose, different amount of pCD-UPRT DNA were incubated with the 2 μg of QDs for 1h at room temperature and then electrophoresed in a 0.8 % agarose gel at 70 mV. The gel was subsequently stained with ethidium bromide and visualized under UV transilluminator.

For quantitative study of DNA binding to the chitosan stabilized QDs, different amount of pCD-UPRT DNA were added to 1 mL Mili-Q water containing 5 μg of QDs. The pH of the solution was adjusted at 5.5 and incubated for 1 h at room temperature. The samples were then spun at 10,000 rpm for 20 minutes to precipitate the QDs as well as pCD-UPRT DNA bound onto them. The free DNA in the supernatant was quantified spectrophotometrically by taking absorbance at 260 nm (A_{260}). The amount of bound DNA was calculated by subtracting the amount of free DNA from that of initial DNA added.

6.3.4. Cell viability assay

The cytotoxicity of ZnS:Mn^{2+} QDs was tested on HT 29 cell line maintained in complete DMEM medium supplemented with 10% FBS, 50 U mL^{-1} penicillin and 50 mg mL^{-1} streptomycin in a humidified atmosphere containing 5% CO_2 at 37^0C. For cell viability assay, HT 29 cells were seeded into 96-well plate at a density of 1×10^4 cells/well and grown overnight. Then different concentrations of QDs were added to the cells and incubated another 24 or 48 h. After the treatment of HT 29 cells with QDs, MTS based cell proliferation assay was carried out with CellTiter 96 Aqueous One Solution Assay kit (Promega, Madison, WI) as per manufacturer's instructions.

6.4. Results and Discussion

6.4.1 Characterization of chitosan stabilized ZnS: Mn^{2+} QDs

The UV-visible absorption spectrum (**Figure 6.1a**) of chitosan stabilized ZnS:Mn^{2+} QDs shows absorption edge at ca. 315 nm, considerably blue-shifted compared to that of bulk ZnS occurring at 340 nm (Sapra et al., 2005). In nano-crystalline ZnS, the particle radius r (nm) is related to band gap E (eV) by the equation,

$$r = \frac{0.32 - 2.9\sqrt{E - 3.49}}{2(3.5 - E)} \tag{1}$$

as reported previously (Suyver et al., 2001). The size of the ZnS:Mn^{2+} QDs were calculated from equation (1) to be 3.7 nm.

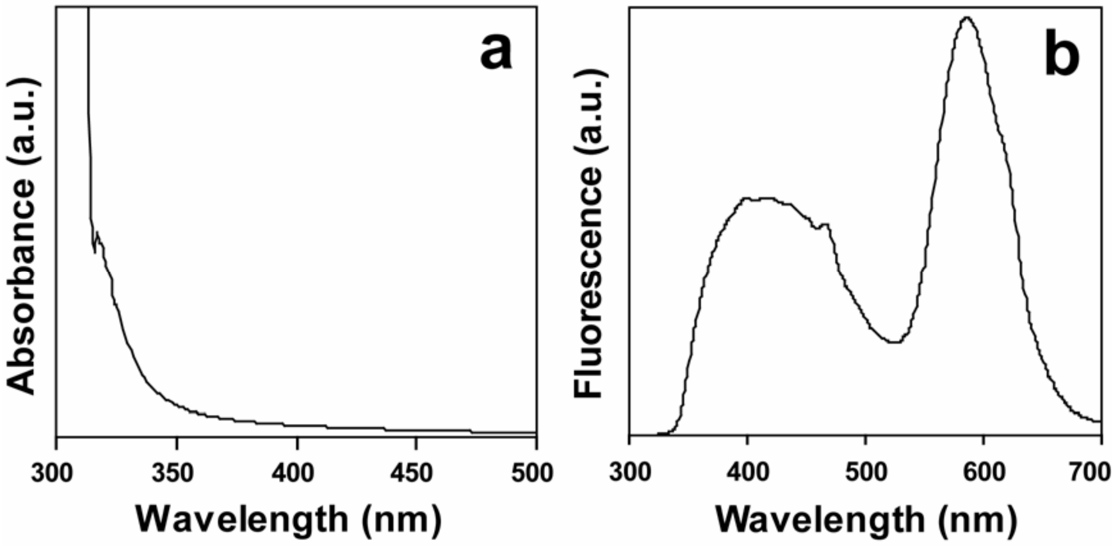

Figure 6.1. (a) UV-visible absorption and **(b)** fluorescence emission spectrum of chitosan stabilized ZnS: Mn^{2+} QDs.

Figure 6.1b shows the fluorescence emission spectra of the chitosan stabilized ZnS:Mn^{2+} QDs with two emission peaks at around 409 nm and 586 nm respectively. However, the undoped ZnS QDs showed only one emission peak at about 409 nm due to radiative recombination as a result of defect states in the ZnS nanocrystals (Sapra et al., 2005). In Mn^{2+} doped QDs, the first emission peak at 409 nm was due to host ZnS, but the second emission peak at 586 nm was due to $^4T_1 \rightarrow {}^6A_1$ transition within the 3d shell of Mn^{2+} ions doped into ZnS lattice. Incorporation of Mn^{2+} into nanocrystalline ZnS allows d electrons of Mn^{2+} to interact strongly with the s-p electronic states of ZnS (Sapra et al., 2005; Bhargava et al., 1994). This perturbation partially allows otherwise spin forbidden $^4T_1 \rightarrow {}^6A_1$ transition to occur resulting into the characteristics orange colored emission.

The XRD pattern of ZnS:Mn^{2+} QDs, shown in **Figure 6.2**, consists of characteristic peaks at 28^0, 48^0 and 56.5^0 corresponding to principal Bragg reflections in (111), (220) and (311) lattice planes, respectively, of bulk ZnS crystallizing in Wurtzite structure according to the JCPDS-ICDD database. The mean crystallite size *d* was calculated according to Scherrer equation (Cullity, 1978),

$$d = \frac{0.9\lambda}{\beta \cos\theta} \qquad (2)$$

where λ is the X-ray wavelength, β is the full width at half maxima (FWHM) of the diffraction peak and θ is the diffraction angle. Based on the diffraction peak corresponding to (220) plane, the average crystallite size of ZnS QDs was estimated to be 3.5 nm, in good agreement with UV-visible absorption data.

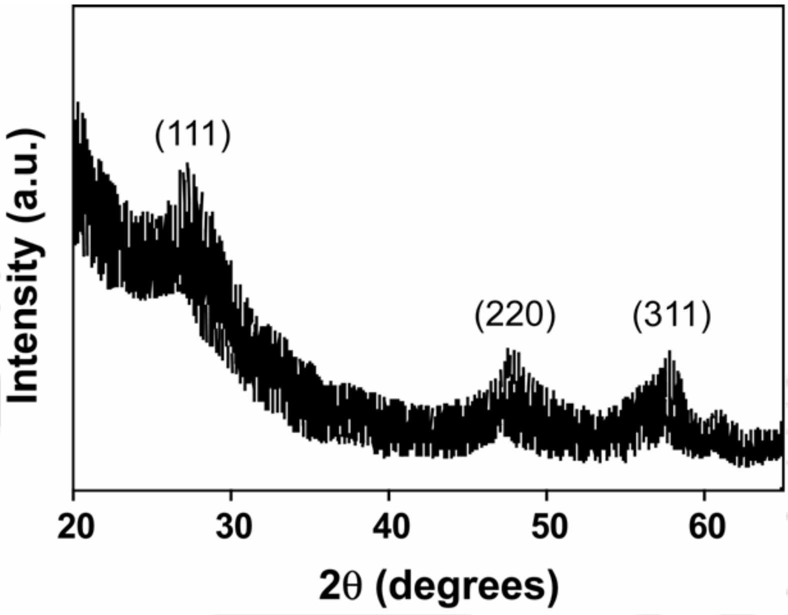

Figure 6.2. XRD pattern of chitosan stabilized ZnS:Mn^{2+} QDs.

TEM images of ZnS:Mn^{2+} QDs (**Figure 6.3a**) shows that QDs are nearly spherical in shape and have an average size of 3.6 nm, calculated based on the corresponding particle size distribution shown in **Figure 6.3b**. Under high resolution TEM (HRTEM), the lattice-resolved image of Mn^{2+}:ZnS QDs (**Figure 6.3c**) revealed typical lattice spacing of about 1.2 Å and 1.7 Å corresponding to the (111) and (220) planes of the crystal respectively. Furthermore, energy dispersive X- ray spectrum (EDX) confirmed the presence of Mn in QDs.

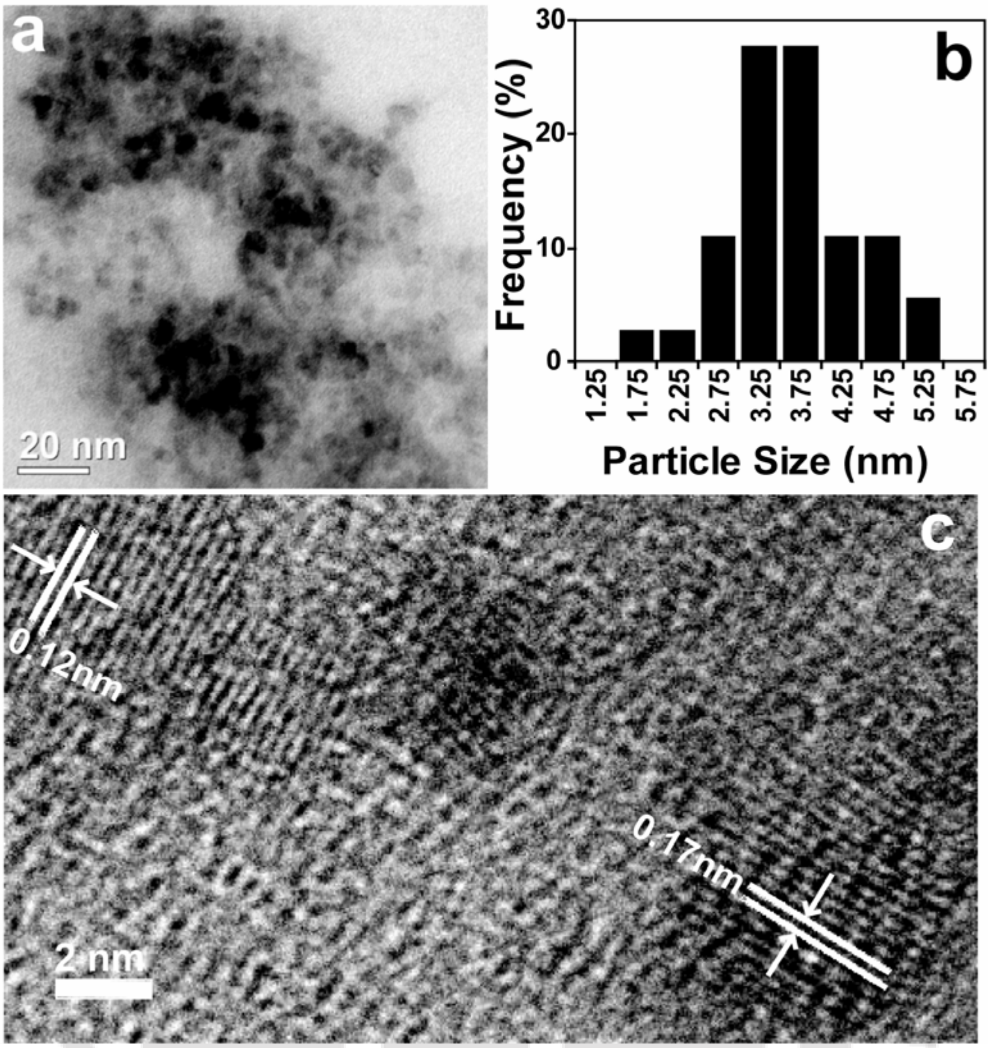

Figure 6.3. **(a)** TEM image of chitosan stabilized ZnS:Mn^{2+} QDs. **(b)** Size distribution of ZnS: Mn^{2+} QDs, calculated based on several frame of images; **(c)** The separation between individual lattice planes in QDs were calculated in a lattice resolved image under HRTEM and corresponding Bragg planes were identified.

6.4.2. DNA binding with the chitosan stabilized ZnS: Mn^{2+} QDs

The binding of pCD-UPRT DNA to chitosan stabilized Mn^{2+} doped ZnS QDs was examined qualitatively by gel-retardation assay. **Figure 6.4** clearly shows that the DNA samples, incubated with QDs, remained almost completely in the wells demonstrating efficient binding of DNA onto the chitosan –QD composite. Interestingly the presence of a faint band, corresponding to free DNA, in lane 5 indicated that about 4 µg of pCD-UPRT was sufficient to saturate 2 µg composite. In other words, the band is due to the excess of DNA that could not bind with the composite.

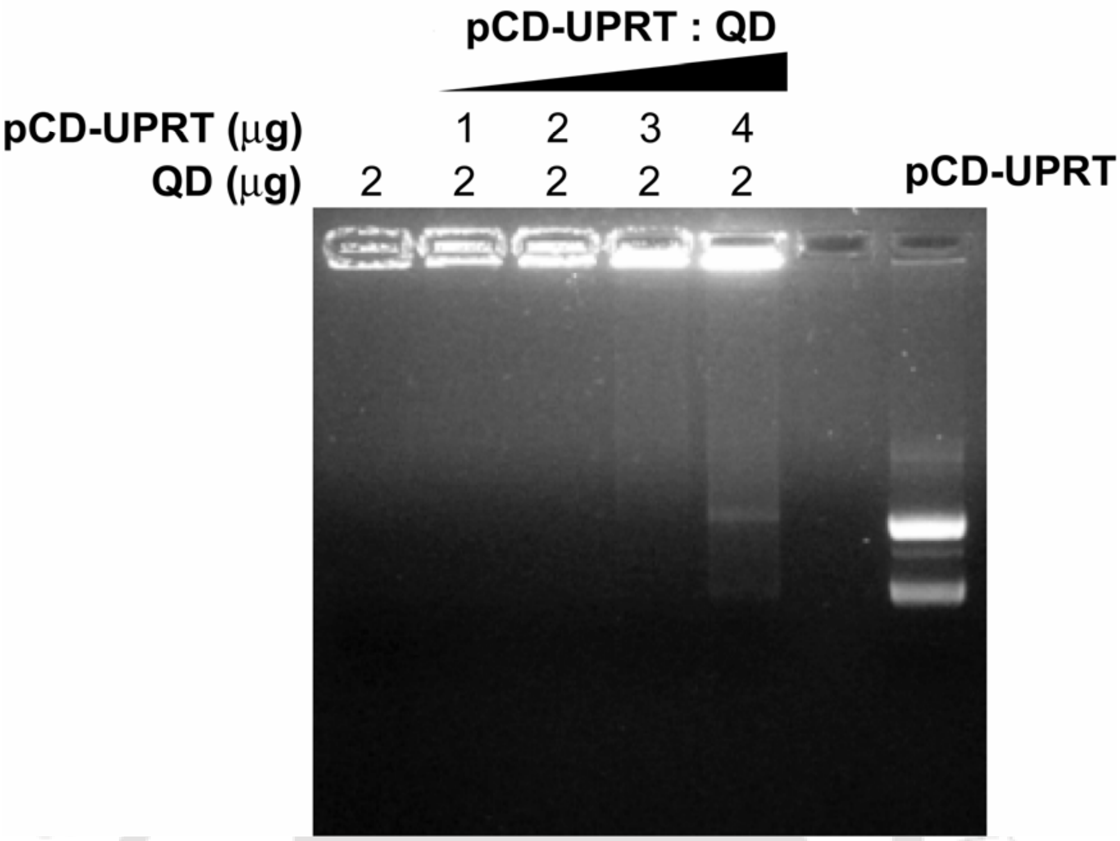

Figure 6.4. Gel retardation assay of pCD-UPRT incubated with chitosan stabilized ZnS: Mn^{2+} QDs (lane 2-5). Lane 1 and 7 corresponds to QDs and pDNA control, respectively.

In order to investigate the DNA binding capacity of the chitosan-QD composite further, the amount of DNA bound to 5 μg of the composite with varying dose of initial DNA were measured quantitatively. The results (**Figure 6.5a**) showed that amount of bound DNA initially increased linearly with increasing amount of initial pCD-UPRT up to 4.16 μg of initial dose. DNA binding reached a plateau at 5.2 μg or greater amount of initial DNA indicating the saturation of pCD-UPRT DNA binding on chitosan stabilized QDs. **Figure 6.5b** shows the effect of weight ratio of initial pCD-UPRT DNA to the composite on the DNA-loading efficiency of the composite. Initially the DNA-loading efficiency increased form 80% to almost 100% with increasing DNA/composite ratio from 0.62 to 0.83. Beyond this value, however, the loading efficiency decreased linearly with increasing DNA/composite ratio simply because of the saturation of the composite with plasmid DNA.

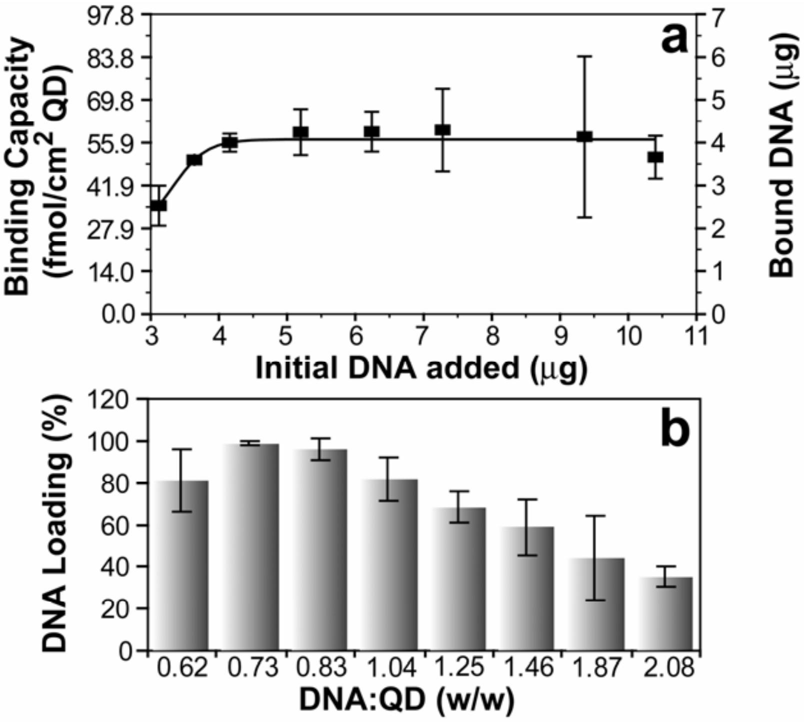

Figure 6.5. (a) DNA binding isotherm of chitosan stabilized ZnS:Mn^{2+} QDs conducted at pH 5.5 with 5 µg of QDs. **(b)** Effect of DNA: chitosan-QD composite weight ratio on DNA loading efficiency.

The amino groups of chitosan are expected to be protonated at pH 5.5 as the pK$_a$ value of the chitosan amino group is estimated to be at ~6.3 (Kumar et al., 2004). Therefore, the binding of pCD-UPRT DNA onto the chitosan stabilized QDs in the present study was possibly due to the positively charged NH_3^+ groups on the surface of the composite. Recently chitosan coated silica beads have been successfully applied in microfluidic devices for solid phase extraction of DNA and RNA based on the same principle (Cao et al., 2006; Hagan et al., 2009). Previous studies (Tanaka et al., 2009; Balladur et al., 1997; Chan et al., 1997) have shown that the adsorption of high molecular weight double stranded DNA (dsDNA) or single stranded oligonucleotides onto aminosilane-modified surface follows a Langmuir reversible adsorption model. In equilibrium, Langmuir reversible adsorption equation can be written as:

$$Q = Q_{\max} \frac{KC_{eq}}{1 + KC_{eq}} \tag{3}$$

where Q is the amount of adsorbed DNA (fmol cm^{-2}), C$_{eq}$ (fmol µL^{-1}) is the equilibrium DNA concentration in the solution, Q$_{max}$ (fmol cm^{-2}) is the maximum DNA adsorbed and K (cm^3 mol^{-1}) is the adsorption equilibrium constant. The Langmuir equation can be linearized into the form of:

$$\frac{C_{eq}}{Q} = \frac{1}{Q_{\max}} C_{eq} + \frac{1}{KQ_{\max}} \qquad (4).$$

The values of C_{eq}/Q versus C_{eq}, calculated from the present experimental dada, are plotted in 3d and a linear regression is performed. **Figure 6.6** shows that experimental data fitted quite well to the Langmuir adsorption model ($R > 0.95$). The maximum amount of bound DNA (Q_{max}) and equilibrium binding constant (K) were calculated from the graph to be 60.24 fmol cm^{-2} and 4.6×10^{12} cm^3 mol^{-1}, respectively. The Q_{max} value is greater than previously reported 0.85 fmol cm^{-2} by Tanaka et. al. (2009) or 1.1 fmol cm^{-2} by Benzanilla et al. (1995) for 2961 bp plasmid, but still less than that (0.5 or 19 pmol cm^{-2}) for single stranded oligonucleotides (Balladur et al., 1997; Chan et al., 1997). The difference in Q_{max} value can be attributed to the fact that Q_{max} strongly depends on the surface charge density of the adsorbent, nature of bound DNA and the experimental condition (Balladur et al., 1997). Further, the equilibrium binding constant K, the ratio of the adsorption and desorption rate constants, was found to be very high in the present study indicating very rapid binding of plasmid DNA to the chitosan-QD composite.

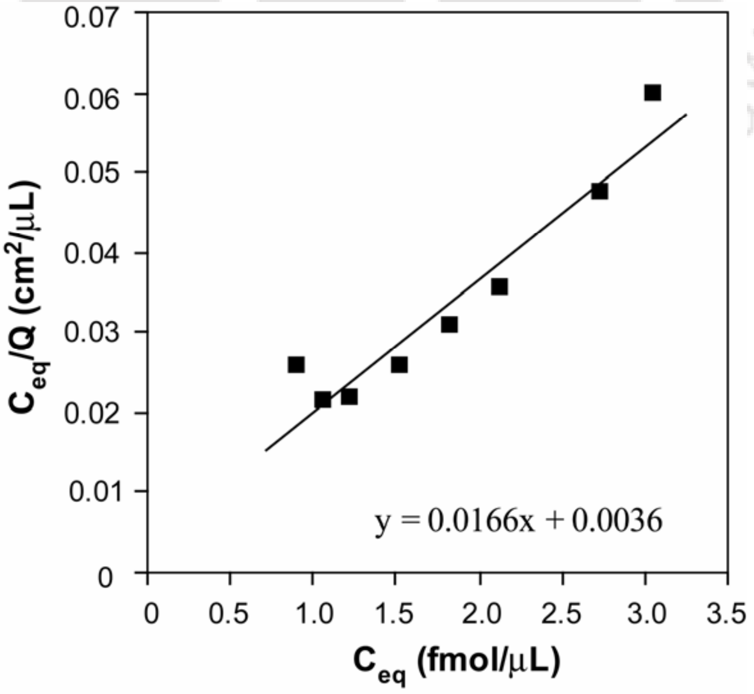

Figure 6.6. Linear regression of C_{eq}/Q as a function of C_{eq} of the DNA binding onto chitosan-QD composite.

6.4.3. Cytotoxicity of the QDs

The cytotoxicity of the chitosan stabilized ZnS:Mn^{2+} QDs are critical for successful application of these QDs in DNA delivery system. MTS assay was carried out in order to evaluate the cytotoxicity of the composite on HT 29 cells and results are shown in Figure 6.7. Figure 6.7 clearly shows that the composite had hardly any effect on the cell viability after 24 h of treatment and viability decreased only by 5-10 % after 48 h of treatment. More than 90% cells were viable even after 48 h in all the concentrations of the composite tested indicating excellent biocompatibility of the chitosan stabilized QDs.

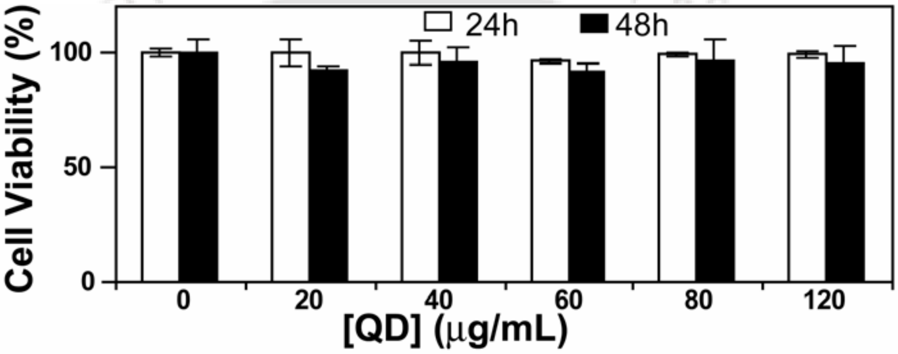

Figure 6.7. Cell viability of HT 29 cells treated with different concentration of chitosan stabilized ZnS:Mn^{2+} QDs for 24h or 48h. Viability of control cells was considered 100%.

6.5. Conclusions

In summary, chitosan stabilized Mn^{2+} doped ZnS QDs, having excellent stability in aqueous solution and strong orange-colored photoluminescence ($\lambda_{emission}$ = 586 nm), have been synthesized. pCD-UPRT, a therapeutically important plasmid having practical application in suicide gene therapy, has been shown to efficiently bind onto the surface of the chitosan stabilized ZnS:Mn^{2+} QDs following a Langmuir reversible adsorption model with a high equilibrium binding constant The excellent biocompatibility of the composite synthesized in the present study has also been demonstrated. The results and the insight gained in the present study could be critical in developing a ‘self-tracking’ non-viral gene delivery system for bifunctional CD-UPRT mediated suicide gene therapy. Nevertheless, the immediate use of these QDs in gene delivery system, as biocompatible fluorescent probe, or even colloidal phase for DNA adsorption in microfluidic devices has potential implications in therapeutics and biodiagnostics.

CHAPTER 7

Concluding Remarks

A summary of the present study and scopes for the future work are described in this chapter.

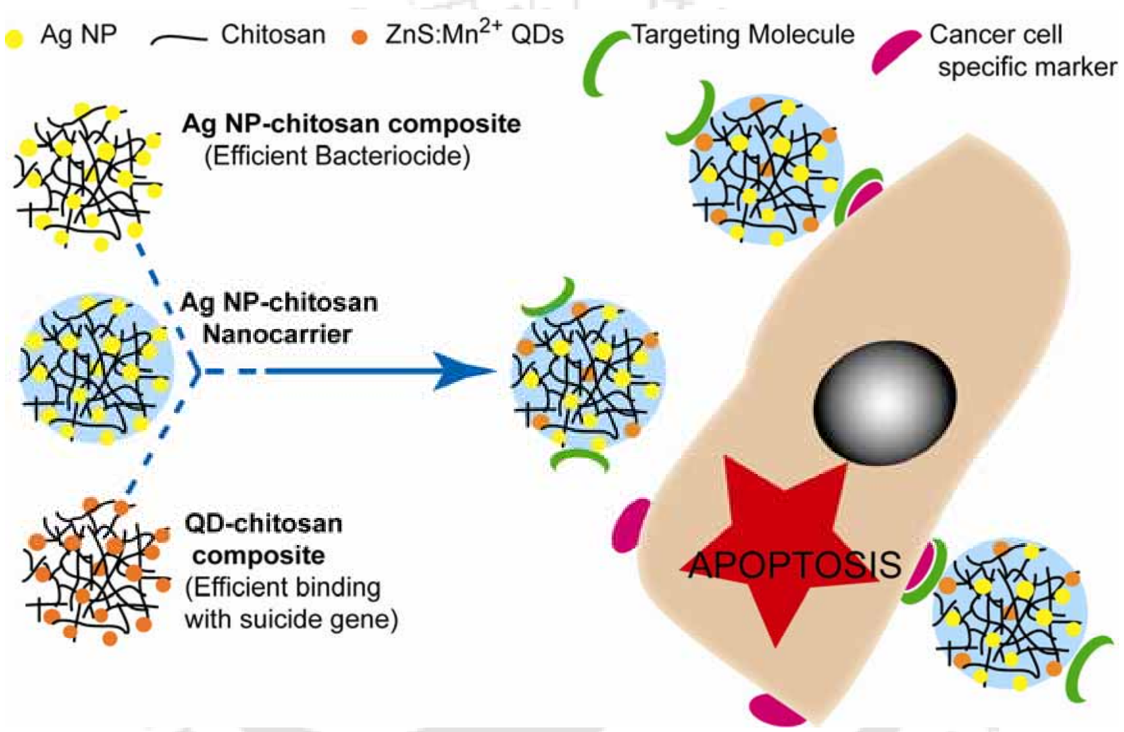

Chapter 7

CONCLUDING REMARKS

7.1. Summary of the Present Work

The work involved in the present thesis consisted of development of novel methods of preparing polymer–based nanocomposite materials and investigation of the usefulness of these nanocomposites on the biological systems, with special emphasis on therapeutic implications.

A single step biochemical route has been developed to prepare Au NPs with extraordinary size specificity (~2.2 nm) in aqueous medium with the use of purified GFP. The role of cysteine residues in the formation of Au NPs has been established. The fluorescence of GFP has been monitored in order to study the concomitant changes in the protein during the synthesis. The polyacrylamide gel electrophoresis of GFP revealed the protein denaturation during the formation of Au NPs. In addition to the establishment of a green method of synthesizing uniform small-sized Au NPs, the results would enrich our knowledge about the 'protein–metal NP' interaction especially during the synthesis of the NPs.

Further, the antibacterial potential of a novel chitosan-Ag NP nanocomposite has been investigated against GFP–expressing *E. coli*. The composite was found to have significantly higher bactericidal activity than its components at their respective concentrations present in the composite. The results indicate the potential of the chitosan-Ag NP nanocomposite in various biomedical and therapeutic applications as an efficient antibacterial agent.

In addition, a novel biodegradable chitosan based nanocarrier (NC) system ca. 172.6 nm in size for Ag NPs has been developed. Electron microscopy and spectroscopic investigations revealed that Ag NPs (~4.9 nm) were homogenously impregnated the polymer NCs and were unaffected during the preparation of the NCs, indicating excellent applicability of the present method to develop NCs for metal NPs. The catalytic activity of the Ag NP–containing NC system was found to be much higher than that of the bulk polymer-Ag NP composite, showing their potential, in catalysis applications.

Moreover, the potential of the chitosan based NC of Ag NPs (Ag-CS NCs) in inducing apoptosis in human colon cancer cells at a very low concentration of the Ag NPs has been demonstrated. The corresponding IC_{50} of Ag NPs was found to be 0.33 $\mu g\ mL^{-1}$, much less than previously reported value of 27 $\mu g\ mL^{-1}$ in case of free Ag NPs by our laboratory. In addition to the involvement of mitochondrial pathway and up-regulation of caspase 3 expression, the important role of oxidative stress (ROS) in the apoptotic cell death has also been revealed. The chitosan based NCs of Ag NPs, after appropriate *in vivo* experiments, could open novel strategies of cancer therapy.

Finally, Mn^{2+} doped ZnS QDs showing strong orange fluorescence and excellent water dispersibility were synthesized in an environment friendly method using chitosan as the stabilizing agent. Efficient binding of plasmid DNA containing bifunctional suicide gene to the composite has been demonstrated and shown to follow the Langmuir reversible adsorption model. Moreover, the *in vitro* biocompatibility of the chitosan – $ZnS:Mn^{2+}$ QDs composite was confirmed by viability assay. The chitosan stabilized $ZnS:Mn^{2+}$ QDs synthesized in the present study could be a promising alternative to conventional organic fluorophore-tagged gene delivery systems for real-time monitoring in gene therapy applications.

7.2. Scope for Future Work

- Films, based on chitosan-Ag NP composite material, can be developed in order to prepare novel antibacterial packaging material for food industries.
- Scaffolds can be made from chitosan-Ag NP composite material to provide efficient biocompatible dressing material for wounds.
- The methodologies for preparing chitosan based nanocarriers for Ag NPs developed in the present study can easily be extended to produce nanocarriers for other metal NPs.
- The chitosan based nanocarriers for Ag NPs can be further pursued in animal models for their *in vivo* efficacy of inducing apoptosis.
- The chitosan nanocarrier can be conjugated with cancer cell specific markers in order to achieve ‘active targeting’ of these nanocarriers toward cancer cells.

REFERENCES

Achermann, M.; Petruska, M.A.; Crooker, S.A.; Klimov, V.I. Picosecond energy transfer in quantum dot Langmuir−Blodgett nanoassemblies, *J. Phys. Chem. B* **2003**, *107*, 13782-13787.

Agnihotri, S.A.; Mallikarjuna, N.N.; Aminabhavi, T.M. Recent advances on chitosan based micro and nanoparticles in drug delivery. *J. Controlled Release* **2004**, *100*, 5-28.

Akerman, M.E.; Chan, W.C.W.; Laakkonen, P.; Bhatia, S.N.; Ruoslahti, E. Nanocrystal targeting *in vivo*. *Proc. Natl. Acad. Sci. U. S. A.* **2002**, *99*, 12617-12621.

Alivisatos, A.P. Semiconductor clusters, nanocrystals, and quantum dots. *Science* **1996**, *271*, 933-937.

Allen, R.T.; Hunter III, W.J.; Agrawal, D.K. Morphological and biochemical characterization and analysis of apoptosis. *J. Pharmacol. Toxicol. Methods* **1997**, *37*, 215-228.

Arora, S.; Jain, J.; Rajwade, J.M.; Paknikar, K.M. Cellular responses induced by silver nanoparticles: *in vitro* studies. *Toxicol. Lett.* **2008**, *179*, 93–100.

AshaRani, P.V.; Mun, G.L.K.; Hande, M.P.; Valiyaveettil, S. Cytotoxicity and genotoxicity of silver nanoparticles in human cells. *ACS Nano* **2009**, *3*, 279-290.

Asharani, P.V.; Wu, Y.L.; Gong, Z.; Valiyaveettil, S. Toxicity of silver nanoparticles in zebrafish models. *Nanotechnology* **2008**, *19*, 255102-255109.

Asuri, P.; Karajanagi, S.S.; Yang, H.; Yim, T.-J.; Kane, R.S.; Dordick, J.S. Increasing protein stability through control of the nanoscale environment. *Langmuir* **2006**, *22*, 5833-5836.

Baker, C.; Pradhan, A.; Pakstis, L.; Pochan, D.J.; Shah, S.I. Synthesis and antibacterial properties of silver nanoparticles. *J. Nanosci. Nanotechnol.* **2005**, *5*, 244–249.

Balladur, V., Theretz, A.; Mandrand, B. Determination of the main forces driving DNA oligonucleotide adsorption onto aminated silica wafers. *J. Colloid Interface Sci.* **1997**, *194*, 408-418.

Ballou, B.; Ernst, L.A.; Andreko, S.; Harper, T.; Fitzpatrick, J.A.J.; Waggoner, A.S.; Bruchez, M.P. Sentinel lymph node imaging using quantum dots in mouse tumor models. *Bioconjug. Chem.* **2007**, *18*, 389-396.

Bezanilla, M.; Manne, S.; Laney, D.E.; Lyubchenko, Y.L.; Hansma, H.G. Adsorption of DNA to mica, silylated mica, and minerals: characterization by atomic force microscopy. *Langmuir* **1995**, *11*, 655-659.

Bhargava, R.N.; Gallagher, D.; Hong, X.; Nurmiko, A. Optical properties of manganese-doped nanocrystals of ZnS. *Phys. Rev. Lett.* **1994**, *72*, 416-419.

Bhattarai, N.; Gunn, J.; Zhang, M. Chitosan-based hydrogels for controlled, localized drug delivery. *Adv. Drug Deliv. Rev.* **2010**, *62*, 83-99.

Bhumkar, D.R.; Joshi, H.M.; Sastry, M.; Pokharkar, V.B. Chitosan reduced gold nanoparticles as novel carriers for transmucosal delivery of insulin. *Pharm. Res.* **2007**, *24*, 1415-1426.

Blaker, J.J.; Maquet, V.; Jerome, R.; Boccaccini, A.R.; Nazhat, S.N. Mechanical properties of highly porous PDLLA/Bioglass® composite foams as scaffolds for bone tissue engineering. *Acta Biomater.* **2005**, *1*, 643-652.

Bodmeier, R.; Oh, K.H.; Pramar, Y., Preparation and evaluation of drug-containing chitosan beads. *Drug Dev. Ind. Pharm.* **1989**, *15*, 1475-1494.

Bodnar, M.; Hartmann, J.F.; Borbely, J. Preparation and characterization of chitosan based nanoparticles. *Biomacromolecules* **2005**, *6*, 2521-2527.

Boussif, O.; Lezoualch, F.; Zanta, M.A.; Mergny, M.D.; Scherman, D.; Demeneix, B.; Behr, J.P. A versatile vector for gene and oligonucleotide transfer into cells in culture and in-vivo — polyethylenimine. *Proc. Natl. Acad. Sci. U. S. A.* **1995**, *92*, 7297-7301.

Braydich-Stolle, L.; Hussain, S.; Schlager, J.J.; Hofmann, M.C. In vitro cytotoxicity of nanoparticles in mammalian germline stem cells. *Toxicol. Sci.* **2005**, *88*, 412-419.

Bruchez, M.Jr.; Moronne, M.; Gin, P.; Weiss, S.; Alivisatos, A.P. Semiconductor nanocrystals as fluorescent biological labels. *Science* **1998**, *281*, 2013-2016.

Brus, L.E. A simple model for the ionization potential, electron affinity, and aqueous redox potentials of small semiconductor crystallites. *J. Chem. Phys.* **1983**, *79*, 5566-5571.

Budhlall, B.M.; Marquez, M.; Velev, O.D. Microwave, photo- and thermally responsive PNIPAm−gold nanoparticle microgels. *Langmuir* **2008**, *24*, 11959-11966.

Byrne, J.D.; Betancourt, T.; Peppas, L.B. Active targeting schemes for nanoparticle systems in cancer therapeutics. *Adv. Drug Deliv. Rev.* **2008**, *60*, 1615-1626.

Cai, J.; Kimura, S.; Wada, M.; Kuga, S. Nanoporous cellulose as metal nanoparticles support. *Biomacromolecules* **2009**, *10*, 87-94.

Calvo, P.; Remunan-Lopez, C.; Vila-Jato, J.L.; Alonso, M.J., Novel hydrophilic chitosan-polyethylene oxide nanoparticles as protein carriers. *J. Appl. Pol. Sci.* **1997**, *63*, 125-132.

Camerin, M.; Rello, S.; Villanueva, A.; Ping, X.; Kenney, M.E.; Rodgers, M.A.J.; Jori, G. Photothermal sensitisation as a novel therapeutic approach for tumours: studies at the cellular and animal level. *Eur. J. Cancer* **2005**, *41*, 1203-1212.

Cao, W.; Easley, C.J.; Ferrance, J.P.; Landers, J.P. Chitosan as a polymer for pH-induced DNA capture in a totally aqueous system. *Anal. Chem.* **2006**, *78*, 7222-7228.

Carr, C.; Ng, J.; Wigmore, T. The side effects of chemotherapeutic agents. *Curr. Anaesthesia Critical Care* **2008**, *19*, 70-79.

Caruso, E.B.; Petralia, S.; Conoci, S.; Giuffrida, S.; Sortino, S. Photodelivery of nitric oxide from water-soluble platinum nanoparticles. *J. Am. Chem. Soc.* **2007**, *129*, 480-481.

Castellano, J.J.; Shafii, S.M.; Ko, F.; Donate, G.; Wright, T.E.; Mannari, R.J. Comparative evaluation of silver-containing antimicrobial dressings and drugs. *Int. Wound J.* **2007**, *4*, 114–122.

Chan, V.; Graves, D.J.; Fortina, P.; McKenzie, S.E. Adsorption and surface diffusion of DNA oligonucleotides at liquid/solid interfaces. *Langmuir* **1997**, *13*, 320-329.

Chan, W.C.W.; Maxwell, D.J.; Gao, X.; Bailey, R.E.; Han, M.; Nie, S. Luminescent quantum dots for multiplexed biological detection and imaging. *Curr. Opin. Biotechnol.* **2002**, *13*, 40-46.

Chan, W.C.W.; Nie, S. Quantum dot bioconjugates for ultrasensitive nonisotopic detection, *Science* **1998**, *281*, 2016-2018.

Chang, E.; Thekkek, N.; Yu, W.W.; Colvin, V.L.; Drezek, R. Evaluation of quantum dot cytotoxicity based on intracellular uptake. *Small* **2006**, *2*, 1412-1417.

Chen, C.W.; Serizawa, T.; Akashi, M. In situ formation of Au/Pt bimetallic colloids on polystyrene microspheres: control of particle growth and morphology. *Chem. Mater.* **2002**, *14*, 2232-2239.

Chen, H.F.; Titushkin, I.; Stroscio, M.; Cho, M. Altered membrane dynamics of quantum dot-conjugated integrins during osteogenic differentiation of human bone marrow derived progenitor cells. *Biophys. J.* **2007**, *92*, 1399-1408.

Chen, J.; Wiley, B.; Li, Z.Y.; Campbell, D.; Saeki, F.; Cang, H.; Au, L.; Lee, J.; Li, X.; Xie, Y. Gold nanocages: engineering their structure for biomedical applications. *Adv. Mater.* **2005**, *17*, 2255-2261.

Chen, Y.H.; Tsai, C.Y.; Huang, P.Y.; Chang, M.Y.; Cheng, P.C.; Chou, C.H.; Chen, D.H.; Wang, C.R.; Shiau, A.L.; Wu, C.L. Methotrexate conjugated to gold nanoparticles inhibits tumor growth in a syngeneic lung tumor model. *Mol. Pharm.* **2007**, *4*, 713-722.

Cheng, Y.; Samia, A.C.; Meyers, J.D.; Panagopoulos, I.; Fei, B.; Burda, C. Highly efficient drug delivery with gold nanoparticle vectors for in vivo photodynamic therapy of cancer. *J. Am. Chem. Soc.* **2008**, *130*, 10643-10647.

Chenite, A.; Chaput, C.; Wang, D.; Combes, C.; Buschmann, M.D.; Hoemann, C.D.; Leroux, J.C.; Atkinson, B.L.; Binette, F.; Selmani, A. Novel injectable neutral solutions ofchitosan form biodegradable gels in situ. *Biomaterials* **2000**, 21, 2155-2161.

Cho, S.J.; Maysinger, D.; Jain, M.; Roder, B.; Hackbarth, S.; Winnik, F.M. Long-term exposure to CdTe quantum dots causes functional impairments in live cells. *Langmuir* **2007**, *23*, 1974-1980.

Chung, T.-W.; Lu, Y.-F.; Wang, S.-S.; Lin, Y.-S.; Chu, S.-H. Growth of human endothelial cells on photochemically grafted Gly–Arg–Gly–Asp (GRGD) chitosans. *Biomaterials* **2002**, *23*, 4803-4809.

Chung, T.W.; Yang, J.; Akaike, T.; Cho, K.Y.; Nah, J.W.; Kim, S.I.; Cho, C.S. Preparation of alginate/galactosylated chitosan scaffold for hepatocyte attachment. *Biomaterials* **2002**, *23*, 2827-2834.

Chung, Y.-C.; Wang, H.-L.; Chen, Y.-M.; Li, S.-L. Effect of abiotic factors on the antibacterial activity of chitosan against waterborne pathogens. *Biores. Tech.* **2003**, *88*, 179-184.

Cossarizza, A.; Baccarani-Contri, M.; Kalashnikova, G.; Franceschi, C. A new method for the cytofluorometric analysis of mitochondrial membrane potential using the J-aggregate forming lipophilic cation 5,5′,6,6′-Tetrachloro-1,1′,3,3′-tetraethylbenz-imidazolcarbocyanine iodide (JC-1). *Biochem. Biophys. Res. Comm.* **1993**, *197*, 40-45.

Cullity, B.D. Elements of X-ray Diffraction. Addison-Wesley, Massachusetts, **1978**.

Dahan, M.; Levi, S.; Luccardini, C.; Rostaing, P.; Riveau, B.; Triller, A. Diffusion dynamics of glycine receptors revealed by single-quantum dot tracking. *Science* **2003**, *302*, 442-445.

Dameron, C.T.; Reese, R.N.; Mehra, R.K.; Kortan, A.R.; Carroll, P.J.; Steigerwald, M.L.; Brus, L.E.; Winge, D.R. Biosynthesis of cadmium sulphide quantum semiconductor crystallites. *Nature* **1989**, *338*, 596-597.

Daniel M.C.; Astruc, D. Gold nanoparticles: assembly, supramolecular chemistry, quantum-size-related properties, and applications toward biology, catalysis, and nanotechnology. *Chem. Rev.* **2004**, *104*, 293-346.

Darouiche, R.O.; Raad, I.I.; Heard, S.O.; Thornby, J.I.; Wenker, O.C.; Gabrielli, A. Comparison of two antimicrobial impregnated central venous catheters. *New Engl. J. Med.* **1999**, *340*, 1–8.

Davies, D.H.; Elson, C.M.; Hayes, E.R. In Chitin and Chitosan; Skjak-Braek, G., Anthonsen, T., Sandford, P., Eds.; *Elsevier Applied Science: London*, **1989**, pp 467-472.

de la Fuente, J.M.; Berry, C.C.; Tat peptide as an efficient molecule to translocate gold nanoparticles into the cell nucleus. *Bioconjug. Chem.* **2005**, *16*, 1176-1180.

Delehanty, J.B.; Medintz, I.L.; Pons, T.; Brunel, F.M.; Dawson, P.E.; Mattoussi, H. Self assembled quantum dot–peptide bioconjugates for selective intracellular delivery. *Bioconjug. Chem.* **2006**, *17*, 920-927.

Derfus, A.M.; Chan, W.C.W.; Bhatia, S.N. Probing the cytotoxicity of semiconductor quantum dots. *Nano Lett.* **2004**, *4*, 11-18.

Detty, M.R.; Gibson, S.L.; Wagner, S.J. Current clinical and preclinical photosensitizers for use in photodynamic therapy. *J. Med. Chem.* **2004**, *47*, 3897-3915.

Ding, W.; Lian, Q.; Samuels, R.J.; Polk, M.B., Synthesis and characterization of a novel derivative of chitosan. *Polymer* **2003**, *44*, 547-556.

Dixit, V.; Bossche, J.V.; Sherman, D.M.; Thompson, D.H.; Andres, R.P. Synthesis and grafting of thioctic acid–PEG–folate conjugates onto Au nanoparticles for selective targeting of folate receptor-positive tumor cells. *Bioconjug. Chem.* **2006**, *17*, 603-609.

Duan, H.W.; Nie, S.M. Cell-penetrating quantum dots based on multivalent and endosome-disrupting surface coatings. *J. Am. Chem. Soc.* **2007**, *129*, 3333-3338.

Echarte, M.M.; Bruno, L.; Arndt-Jovin, D.J.; Jovin, T.M.; Pietrasanta, L.I. Quantitative single particle tracking of NGF-receptor complexes: transport is bidirectional but biased by longer retrograde run lengths. *FEBS Lett.* **2007**, *581*, 2905-2913.

El Ghaouth, A.J.; Asselin, A. In Advances in chitin and chitosan; Brine, C. J., Sandford, P. A., Zikakis, J. P., Eds.; *Elsevier: Amsterdam*, **1992**, pp 440.

Elechiguerra, J.L.; Burt, J.L.; Morones, J.R.; Bragado, A.C.; Gao, X.; Lara, H.H. Interaction of silver nanoparticles with HIV-1. *J. Nanobiotechnol.* **2005**, 3:6.

El-Sayed, I.H.; Huang, X.; El-Sayed, M.A. Selective laser photo-thermal therapy of epithelial carcinoma using anti-EGFR antibody conjugated gold nanoparticles. *Cancer Lett.* **2006**, *239*, 129-135.

El-Sayed, M.A. Some interesting properties of metals confined in time and nanometer space of different shapes. *Acc. Chem. Res.* **2001**, *34*, 257-264.

Empedocles, S.A.; Norris, D.J.; Bawendi, M.G. Photoluminescence spectroscopy of single CdSe nanocrystallite quantum dots. *Phys. Rev. Lett.* **1996**, *77*, 3873-3876.

Engin, K.; Leeper, D.B.; Cater, J.R.; Thistlethwaite, A.J.; Tupchong, L.; Mcfarlane, J.D. Extracellular pH distribution in human tumors. *Int. J. Hypertherm.* **1995**, *11*, 211-216.

Esumi, K.; Suzuki, A.; Yamahira, A.; Torigoe, K. Role of poly(amidoamine) dendrimers for preparing nanoparticles of gold, platinum, and silver. *Langmuir* **2000**, *16*, 2604-2608.

Fan, H.; Yang, K.; Boye, D.M.; Sigmon, T.; Malloy, K.J.; Xu, H.; López, G.P.; Brinker, C.J. Self-assembly of ordered, robust, three-dimensional gold nanocrystal/silica Arrays. *Science* **2004**, *304*, 567-571.

Faraday, M. Experimental relations of gold (and other metals) to light. *Philos. Trans. R. Soc.* London **1857**, *147*, 145-181.

Feng, Q.L.; Wu, J.; Chen, G.Q.; Cui, F.Z.; Kim, T.N.; Kim, J.O. A mechanistic study of the antibacterial effect of silver ions on *Escherichia coli* and *Staphylococcus aureus*. *J. Biomed. Mater. Res.* **2000**, *52*, 662-668.

Foley, S.; Crowley, C.; Smaihi, M.; Bonfils, C.; Erlanger, B.F.; Seta, P.; Larroque, C. Cellular localisation of a water-soluble fullerene derivative. *Biochem. Biophys. Res. Comm.* **2002**, *294*, 116-119.

Fox, C.L. Silver sulfadiazine: a new topical therapy for *Pseudomonas* in burns. *Arch. Surg.* **1968**, *96*, 184–188.

Fujimoto, T.; Tsuchiya, Y.; Terao, M.; Nakamura, K.; Yamamoto, M. Antibacterial effects of chitosan solution® against *Legionella pneumophila*, *Escherichia coli*, and *Staphylococcus aureus*. *Int. J. Food Microbiol.* **2006**, *112*, 96-101.

Furno, F.; Morley, K.S.; Wong, B.; Sharp, B.L.; Arnold, P.L.; Howdle, S.M. Silver nanoparticles and polymeric medical devices: a new approach to prevention of infection? *J. Antimicrob. Chemother.* **2004**, *54*, 1019–1024.

Gao, J.; Liang, G.; Zhang, B.; Kuang, Y.; Zhang, X.; Xu, B. FePt@CoS(2) yolk–shell nanocrystals as a potent agent to kill HeLa cells. *J. Am. Chem. Soc.* **2007**, *129*, 1428-1433.

Gao, X.H.; Cui, Y.Y.; Levenson, R.M.; Chung, L.W.K.; Nie, S.M. In vivo cancer targeting and imaging with semiconductor quantum dots. *Nat. Biotechnol.* **2004**, *22*, 969-976.

Gill, I.; Ballesteros, A. Bioencapsulation within synthetic polymers (Part 1): sol–gel encapsulated biologicals. *Trends in Biotechnol.* **2000**, *18*, 282-296.

Gogoi, S.K.; Gopinath, P.; Paul, A.; Ramesh, A.; Ghosh, S.S.; Chattopadhyay, A. Green fluorescent protein-expressing Escherichia coli as a model system for investigating the antimicrobial activities of silver nanoparticles. *Langmuir* **2006**, *22*, 9322–9328.

Gong, P.; Li, H.; He, X.; Wang, K.; Hu, J.; Tan, W. Preparation and antibacterial activity of Fe3O4@Ag nanoparticles. *Nanotechnology* **2007**, *18*, 604–611

Gopinath, P.; Ghosh, S.S. Apoptotic induction with bifunctional *E.coli* cytosine deaminase-uracil phosphoribosyltransferase mediated suicide gene therapy is synergized by curcumin treatment in vitro. *Mol. Biotechnol.* **2008**, *39*, 39-48.

Gopinath, P.; Ghosh, S.S. Understanding apoptotic signaling pathways in cytosine deaminase-uracil phosphoribosyl transferase-mediated suicide gene therapy in vitro. *Mol. Cell. Biochem.* **2009**, *324*, 21-29.

Gopinath, P.; Gogoi, S.K.; Chattopadhyay, A.; Ghosh, S.S. Implications of silver nanoparticle induced cell apoptosis for in vitro gene therapy. *Nanotechnology* **2008**, *19*, 75104-75114.

Gopinath, P.; Gogoi, S.K.; Sanpui, P.; Paul, A.; Chattopadhyay, A.; Ghosh, S.S. Signaling gene cascade in silver nanoparticle induced apoptosis. *Colloid Surface B: Biointreface* **2010**, *77*, 240–245.

Green, M.; Howman, E. Semiconductor quantum dots and free radical induced DNA nicking. *Chem. Commun.* **2005**, *121*, 121-123.

Guerin P. Use of synthetic polymers for biomedical application. *P.A.C.E.* **1983**, *6*, 449-453.

Guo G.N.; Liu, W.; Liang, J.G.; He, Z.K.; Xu, H.B.; Yang, X.L. Probing the cytotoxicity of CdSe quantum dots with surface modification. *Mater. Lett.* **2007**, *61*, 1641-1644.

Hagan, K.A.; Meier, W.M.; Ferrance, J.P.; Landers, J.P. Chitosan-coated silica as a solid phase for RNA purification in a microfluidic device. *Anal. Chem.* **2009**, *81*, 5249-5256.

Haipeng, G.; Zhong, Y.; Li, J.; Gong, Y.; Zhao, N.; Zhang, X. Studies on nerve cell affinity of chitosan-derived materials. *J. Biomed. Mater. Res.* **2000**, *52*, 285-295.

Hama, Y.; Koyama, Y.; Urano, Y.; Choyke, P.L.; Kobayashi, H. Simultaneous two-color spectral fluorescence lymphangiography with near infrared quantum dots to map two lymphatic flows from the breast and the upper extremity. *Breast Cancer Res. Treat.* **2007**, *103*, 23-28.

Hamilton S.J. Review of selenium toxicity in the aquatic food chain. *Sci Total Environ*. **2004**, *326*, 1-31.

Han, G.; Chari, N.S.; Verma, A.; Hong, R.; Martin, C.T.; Rotello, V.M. Controlled recovery of the transcription of nanoparticle-bound DNA by intracellular concentrations of glutathione. *Bioconjug. Chem.* **2005**, *16*, 1356-1359.

Han, G.; Martin, C.T.; Rotello, V.M. Stability of gold nanoparticle-bound DNA toward biological, physical, and chemical agents. *Chem. Biol. Drug Des.* **2006b** *67*, 78-82.

Han, G.; You, C.C.; Kim, B.J.; Turingan, R.S.; Forbes, N.S.; Martin, C.T.; Rotello, V.M. Light regulated release of DNA and its delivery to nuclei by means of photolabile gold nanoparticles. *Angew. Chem.* **2006a**, *45*, 3165-3169.

Hanaki, K.; Momo, A.; Oku, T.; Komoto, A.; Maenosono, S.; Yamaguchi, Y.; Yamamoto, K. Semiconductor quantum dot/albumin complex is a long-life and highly photostable endosome marker. *Biochem. Biophys. Res. Commun.* **2003**, *302*, 496-501.

Hans, M.L.; Lowman, A.M. Biodegradable nanoparticles for drug delivery and targeting. *Curr. Opin. Solid State Mater. Sci.* **2002**, *6*, 319-327.

He, X.; Bischof, J.C. Quantification of temperature and injury response in thermal therapy and cryosurgery. *Crit. Rev. Biomed. Eng.* **2003**, *31*, 355-422.

Helander, I.M.; Nurmiaho-Lassila, E.-L.; Ahvenainen, R.; Rhoades, J.; Roller, S. Chitosan disrupts the barrier properties of the outer membrane of Gram-negative bacteria. *Int. J. Food Microbiol.* **2001**, *71*, 235-244.

Heras, A.; Rodriguez, N.M.; Ramos, V.M.; Agullo, E. N-methylene phosphonic chitosan: a novel soluble derivative, *Carbohydr. Polym*. **2001**, *44*, 1-8.

Hines, M.A.; Guyot-Sionnest, P. Synthesis and characterization of strongly luminescing ZnS-capped CdSe nanocrystals. *J. Phys. Chem.* **1996**, *100*, 468-71.

Hirano, S.; Zhang, M.; Nakagawa, M. Release of glycosaminoglycans in physiological saline and water by wet-spun chitin-acid glycosaminoglycan fibers. *J. Biomed. Mater. Res.* **2001**, *56*, 556–561.

Hlady, V.; Buijs, J. Protein adsorption on solid surfaces. *Curr. Opin. Biotechnol.* **1996**, *7*, 72-77.

Hone, D.C., Walker, P.I., Evans-Gowing, R.; FitzGerald, S.; Beeby, A.; Chambrier, I.; Cook, M.J.; Russell, D.A. Generation of cytotoxic singlet oxygen via phthalocyanine stabilized gold nanoparticles: a potential delivery vehicle for photodynamic therapy. *Langmuir* **2002**, *18,* 2985-2987.

Hsin, Y.-H.; Chen, C.-F.; Huang, S.; Shih, T.-S.; Lai, P.-S.; Chueh, P.J. The apoptotic effect of nanosilver is mediated by a ROS- and JNK-dependent mechanism involving the mitochondrial pathway in NIH3T3 cells. *Toxicol. Lett.* **2008**, *179*, 130-139.

Hu, M.; Petrova, H.; Chen, J.; McLellan, J.M.; Siekkinen, A.R.; Marquez, M.; Li, X.; Xia, Y.; Hartland, G.V. Ultrafast laser studies of the photothermal properties of gold nanocages. *J. Phys. Chem. B* **2006**, *110*, 1520-1524.

Hu, Q.; Li, B.; Wang, M.; Shen, J. Preparation and characterization of biodegradable chitosan/hydroxyapatite nanocomposite rods via in situ hybridization: a potential material as internal fixation of bone fracture. *Biomaterials* **2004**, *25*, 779-785.

Huang, H.; Yang, X. Synthesis of polysaccharide-stabilized gold and silver nanoparticles: a green method. *Carbohydr. Res.* **2004**, *339*, 2627-2631.

Huang, X.; Jain, P.K.; El-Sayed, I.H.; El-Sayed, M.A, Determination of the minimum temperature required for selective photothermal destruction of cancer cells using immunotargeted gold nanoparticles. *Photochem. Photobiol.* **2006**, *82*, 412-417

Huff, T.B.; Tong, L.; Zhao, Y.; Hansen, M.N.; Cheng, J.X.; Wei, A. Hyperthermic effects of gold nanorods on tumor cells. *Nanomedicine* **2007**, *2*, 125-132.

Hussain, S.M.; Hess, K.L.; Gearhart, J.M.; Geiss, K.T.; Schlager, J.J. In vitro toxicity of nanoparticles in BRL 3A rat liver cells. *Toxicol. in Vitro* **2005**, *19*, 975-983.

Ignarro, L.J. Nitric Oxide, Biology and Pathobiology; Academic Press: San Diego, CA, **2000**.

Jain, J.; Arora, S.; Rajwade, J.M.; Omray, P.; Khandelwal, S.; Paknikar, K.M. Silver nanoparticles in therapeutics: development of an antimicrobial gel formulation for topical use. *Mol. Pharm.* **2009**, *6*, 1388-1401.

Jain, R.K. Transport of molecules, particles, and cells in solid tumors. *Annu. Rev. Biomed. Eng.* **1999**, *1*, 241-263.

Jain, S.; Singh, R.; Gupta, M.N. Purification of recombinant green fluorescent protein by three-phase partitioning. *J. Chromat. A* **2004**, *1035*, 83-86.

Jain,P.; Pradeep, T. Potential of silver nanoparticle-coated polyurethane foam as an antibacterial water filter. *Biotechnol. Bioeng.* **2005**, *90*, 59-63.

Jaiswal, J.K.; Mattoussi, H.; Mauro, J.M.; Simon, S.M. Long-term multiple color imaging of live cells using quantum dot bioconjugates. *Nat. Biotechnol.* **2003**, *21*, 47-51.

Janes, K.A.; Fresneau, M.P.; Marazuela, A.; Fabra, A. Alonso, M.J. Chitosan nanoparticles as delivery systems for doxorubicin. *J. Controlled Release* **2001**, *73*, 255-267.

Janicke, R.U.; Sprengart, M.L.; Wati, M.R.; Porter, A.G. Caspase-3 is required for DNA fragmentation and morphological changes associated with apoptosis. *J. Biol. Chem.* **1998**, *273*, 9357-9360.

Jia, Z.; Shen, D.; Xu, W. Synthesis and antibacterial activities of quaternary ammonium salt of chitosan. *Carbohydr. Res.* **2001**, *333*, 1-6.

Jin, R.; Cao, Y.; Mirkin, C.A.; Kelly, K.L.; Schatz, G.C.; Zheng, J.G. Photoinduced conversion of silver nanospheres to nanoprisms. *Science* **2001**, *294*, 1901-1903.

Jori, G.; Spikes, J.D. Photothermal sensitizers: possible use in tumor therapy. *J Photochem. Photobiol. B Biol.* **1990**, *6*, 93-101.

Jun, J.; Yuan-Yuan, D.; Shao-hai, W.; Shao-feng, Z.; Zhong-yi, W. Preparation and characterization of antibacterial silver-containing nanofibers for wound dressing applications. *J. US-China Med. Sci.* **2007**, *4*, 52–54.

Kagan, C.R.; Murray, C.B.; Nirmal, M.; Bawendi, M.G. Electronic energy transfer in CdSe quantum dot solids. *Phys. Rev. Lett.* **1996**, *76*, 1517-1520.

Karajanagi, S.S.; Vertegel, A.A.; Kane, R.S.; Dordick, J.S. Structure and function of enzymes adsorbed onto single-walled carbon nanotubes. *Langmuir* **2004**, *20*, 11594-11599.

Kato, Y.; Onishi, H.; Machida, Y. Contribution of chitosan and its derivatives to cancer chemotherapy. *In Vivo* **2005**, *19*, 301-310.

Kelly, K.L.; Coronado, E.; Zhao, L.L.; Schatz, G.C. The optical properties of metal nanoparticles: The influence of size, shape, and dielectric environment. *J. Phys. Chem. B* **2003**, *107*, 668-677.

Khlebtsov, B.; Zharov, V.; Melnikov, A.; Tuchin, V.; Khlebtsov, N. Optical amplification of photothermal therapy with gold nanoparticles and nanoclusters. *Nanotechnology* **2006**, *17*, 5167-5179.

Khor, E.; Lim, L.Y. Implantable applications of chitin and chitosan. *Biomaterials* **2003**, *24*, 2339-2349.

Kim, J.H.; Kim, Y.S.; Kim, S.; Park, J.H.; Kim, K.; Choi, K.; Chung, H.; Jeong, S.Y.; Park, R.W.; Kim, I.S.; Kwon, I.C. Hydrophobically modified glycol chitosan nanoparticles as carriers for paclitaxel. *J. Controlled Release* **2006**, *111*, 228-234.

Kim, J.H.; Kim, Y.S.; Park, K.; Kang, E.; Lee, S.; Nam, H.Y.; Kim, K.; Park, J.H.; Chi, D.Y.; Park, R.W.; Kim, I.S.; Choi, K., Kwon, I.C. Self-assembled glycol chitosan nanoparticles for the sustained and prolonged delivery of antiangiogenic small peptide drugs in cancer therapy. *Biomaterials* **2008**, *29*, 1920-1930.

Kim, J.S.; Kuk, E.; Yu, K.N.; Kim, J.H.; Park, S.J.; Lee, H.J. Antimicrobial effects of silver nanoparticles. *Nanomed. Nanotechnol. Biol. Med.* **2007**, *3*, 95-101.

Kim, S.; Lim, Y.T.; Soltesz, E.G.; De Grand, A.M.; Lee, J.; Nakayama, A.; Parker, J.A.; Mihaljevic, T.; Laurence, R.G.; Dor, D.M.; Cohn, L.H.; Bawendi, M.G.; Frangioni, J.V. Nearinfrared fluorescent type II quantum dots for sentinel lymph node mapping. *Nat. Biotechnol.* **2004**, *22*, 93-97.

Kim, Y.H.; Lee, D.K.; Cha, H.G.; Kim, C.W.; Kang, Y.C.; Kang, Y.S. Preparation and characterization of the antibacterial Cu nanoparticle formed on the surface of SiO2 nanoparticles. *J. Phys. Chem. B* **2006**, *110*, 24923-24928.

Kirchner, C.; Liedl, T.; Kudera, S.; Pellegrino, T.; Javier, A.M.; Gaub, H.E.; Stolzle, S.; Fertig, N.; Parak, W.J. Cytotoxicity of colloidal CdSe and CdSe/ZnS nanoparticles. *Nano Lett.* **2005**, *5*, 331-338.

Klaus, T.; Joerger, R.; Olsson, E.; Granqvist, C.-G. Silver-based crystalline nanoparticles, microbially fabricated. *Proc. Natl. Acad. Sci. USA* **1999**, *96*, 13611-13614.

Kobayashi, H.; Hama, Y.; Koyama, Y.; Barrett, T.; Regino, C.A.S.; Urano, Y.; Choyke, P.L. Simultaneous multicolor imaging of five different lymphatic basins using quantum dots. *Nano Lett.* **2007**, *7*, 1711-1716.

Koeppel, F.; Jaiswal, J.K.; Simon, S.M. Quantum dot-based sensor for improved detection of apoptotic cells. *Nanomedicine* **2007**, *2*, 71-78.

Kondoh, M.; Araragi, S.; Sato, K.; Higashimoto, M.; Takiguchi, M.; Sato, M. Cadmium induces apoptosis partly via caspase-9 activation in HL-60 cells. *Toxicology* **2002**, *170*, 111-117.

Koopman, G.; Reutelingsperger, C.P.; Kuijten, G.A.; Keehnen, R.M.; Pals, S.T.; van Oers, M.H. Annexin V for flow cytometric detection of phosphatidylserine expression on B cells undergoing apoptosis. *Blood* **1994**, *84*, 532-540.

Kowshik, M.; Vogel, W.; Urban, J.; Kulkarni, S.K.; Paknikar, K.M. Microbial synthesis of semiconductor PbS nanocrystallites. *Adv. Mater.* **2002**, *14*, 815-818.

Kreuter, J. Nanoparticulate systems for brain delivery of drugs. *Adv. Drug Deliv. Rev.* **2001**, 47, 65-81.

Kumar, M.N.V.R.; Muzzarelli, R.A.A.; Muzzarelli, C.; Sashiwa, H.; Domb A.J. Chitosan chemistry and pharmaceutical perspectives. *Chem. Rev.* **2004**, *104*, 6017-6084.

Kurita, K.; Ikeda, H.; Yoshida, Y.; Shimojoh, M.; Harata, M. Chemoselective protection of the amino groups of chitosan by controlled phthaloylation: Facile preparation of a precursor useful for chemical modifications. *Biomacromolecules* **2002**, *3*, 1-4.

Laflamme, P.; Benhamou, N.; Bussieres, G.; Dessureault, M. Differential effect of chitosan on root rot fungal pathogens in forest nurseries. *Can. J. Bot.* **1999**, *77*, 1460-1468.

Lagerholm, B.; Wang, M.; Ernst, L.; Ly, D.; Liu, H.; Bruchez, M.; Waggoner, A. Multicolor coding of cells with cationic peptide coated quantum dots. *Nano Lett.* **2004**, *4*, 2019-2022.

Larson, D.R.; Zipfel, W.R.; Williams, R.M.; Clark, S.W.; Bruchez, M.P.; Wise, F.W.; Webb, W.W. Water-soluble quantum dots for multiphoton fluorescence imaging in vivo. *Science* **2003**, *300*, 1434-1436.

Laudenslager, M.J.; Schiffman, J.D.; Schauer, C.L. Carboxymethyl chitosan as a matrix material for platinum, gold, and silver nanoparticles. *Biomacromolecules* **2008**, *9*, 2682-2685.

Le Gac, S.; Vermes, I.; van den Berg, A. Quantum dots based probes conjugated to annexin V for photostable apoptosis detection and imaging. *Nano Lett.* **2006**, *6*, 1863-1869.

Lee, D.; Cohen, R.E.; Rubner, M.F. Antibacterial properties of Ag nanoparticle loaded multilayers and formation of magnetically directed antibacterial microparticles. *Langmuir* **2005**, *21*, 9651-9659.

Lee, K.Y.; Jo, W.H.; Kwon, I.C.; Kim, Y.H.; Jeong, S.Y. Physico-chemical characteristics of self-aggregates of hydrophobically modified chitosans. *Langmuir* **1998**, *14*, 2329-2332.

Lee, Y.M.; Kim, S.S.; Park, M.H.; Song, K.W.; Sung, Y.K.; Kang, I.K. β-Chitin-based wound dressing containing sulfurdiazine. *J. Mater. Sci. Mater. Med.* **2000**, *11*, 817–823.

Lenoir, S.; Pagnoulle, C.; Detrembleur, C.; Galleni, M.; Jerome, R. New antibacterial cationic surfactants prepared by atom transfer radical polymerization. *J. Polym. Sci. Part A Polym. Chem.* **2006**, *44*, 1214-1224.

Li, J.J.; Wang, Y.A.; Guo, W.; Keay, J.C.; Mishima, T.D.; Johnson, M.B.; Peng, X. Large-scale synthesis of nearly monodisperse CdSe/CdS core/shell nanocrystals using air-stable reagents via successive ion layer adsorption and reaction. *J. Am. Chem. Soc.* **2003**, *125*, 12567-12575.

Liau, S.Y.; Read, D.C.; Pugh, W.J.; Furr, J.R.; Russell, A.D. Interaction of silver nitrate with readily identifiable groups: relationship to the antibacterialaction of silver ions. *Lett. Appl. Microbiol.* **1997**, *25*, 279-283.

Lidke, D.S.; Nagy, P.; Heintzmann, R.; Arndt-Jovin, D.J.; Post, J.N.; Grecco, H.E.; Jares-Erijman, E.A.; Jovin, T.M. Quantum dot ligands provide new insights into erbB/HER receptor-mediated signal transduction, *Nat. Biotechnol.* **2004**, *22*, 198-203.

Lieleg, O.; Lopez-Garcia, M.; Semmrich, C.; Auernheimer, J.; Kessler, H.; Bausch, A.R. Specific integrin labeling in living celts using functionalized nanocrystals. *Small* **2007**, *3*, 1560-1565.

Lim, Y.T.; Kim, S.; Nakayama, A.; Stott, N.E.; Bawendi, M.G.; Frangioni, J.V. Selection of quantum dot wavelengths for biomedical assays and imaging. *Mol. Imaging* **2003**, *2*, 50-64.

Limbach, L.K.; Wick, P.; Manser, P.; Grass, R.N.; Bruinink, A.; Stark, W.J. Exposure of engineered nanoparticles to human lung epithelial cells: Influence of chemical composition and catalytic activity on oxidative stress. *Environ. Sci. Technol.* **2007**, *41*, 4158-4163.

Liu, N.; Chen, X.-G.; Park, H.-J.; Liu, C.-G.; Liu, C.-S.; Meng, X.-H.; Yu, L.-J. Effect of MW and concentration of chitosan on antibacterial activity of *Escherichia coli*. *Carbohydr. Polym.* **2006**, 64, 60-65.

Liu, X.F.; Guan, Y.L.; Yang, D.Z.; Li, Z.; Yao, K.D. Antibacterial action of chitosan and carboxymethylated chitosan. *J. Appl. Polym. Sci.* **2001**, *79*, 1324-1335.

Loo, C.; Lowery, A.; Halas, N.J.; West, J.L.; Drezek, R. Immunotargeted nanoshells for integrated cancer imaging and therapy. *Nano Lett.* **2005**, *5*, 709-711.

Lopez-Leon, T.; Carvalho, E.L.; Seijo, B.; Ortega-Vinuesa, J.L.; Bastos-Gonzalez, D. Physicochemical characterization of chitosan nanoparticles: Electrokinetic and stability behavior. *J. Colloid Interface Sci.* **2005**, 283, 344-351.

Lu, Y.; Mei, Y.; Ballauff, M.; Drechsler, M. Thermosensitive core−shell particles as carrier systems for metallic nanoparticles. *J. Phys. Chem. B* **2006a**, *110*, 3930-3937.

Lu, Y.; Mei, Y.; Schrinner, M.; Ballauff, M.; Mller, M.W.; Breu, J. In situ formation of Ag nanoparticles in spherical polyacrylic acid brushes by UV irradiation. *J. Phys. Chem. C* **2007a**, *111*, 7676-7681.

Lu, Y.; Mei, Y.; Walker, R.; Ballauff, M.; Drechsler, M., 'Nano-tree'—type spherical polymer brush particles as templates for metallic nanoparticles. *Polymer* **2006b**, *47*, 4985-4995.

Lu, Y.; Proch, S.; Schrinner, M.; Drechsler, M.; Kempe, R.; Ballauff, M., Thermosensitive core-shell microgel as a nanoreactor for catalytic active metal nanoparticles. *J. Mater. Chem.* **2009**, *19*, 3955-3961.

Lu, Y.; Spyra, P.; Mei, Y.; Ballauff, M.; Pich, A., Composite hydrogels: robust carriers for catalytic nanoparticles. *Macromol. Chem. Phys.* **2007b**, *208*, 254-261.

Lundqvist, M.; Sethson, I.; Jonsson, B.-H. Protein adsorption onto silica nanoparticles: conformational changes depend on the particles' curvature and the protein stability. *Langmuir* **2004**, *20*, 10639-10647.

Ma, J.; Wang, H.; He, B.; Chen, J. A preliminary in vitro study on the fabrication and tissue engineering applications of a novel chitosan bilayer material as a scaffold of human neofetal dermal fibroblasts. *Biomaterials* **2001**, *22*, 331-336.

Maeda, H.; Wu, J.; Sawa, T.; Matsumura, Y.; Hori, K. Tumor vascular permeability and the EPR effect in macromolecular therapeutics: a review. *J. Control. Release* **2000**, *65*, 271-284.

Majeti, N.V.; Kumar, R. A review of chitin and chitosan applications. *React. Funct. Polym.* **2000**, *46*, 1-27.

Maneerung, T.; Tokura, S.; Rujiravanit, R. Impregnation of silver nanoparticles into bacterial cellulose for antimicrobial wound dressing. *Carbo. Poly.* **2008**, *72*, 43–51.

Manna, A.; Imae, T.; Aoi, K.; Okada, M.; Yogo, T. Synthesis of dendrimer-passivated noble metal nanoparticles in a polar medium: comparison of size between silver and gold particles. *Chem. Mater.* **2001**, *13*, 1674-1681.

Martin, S.J.; Reutelingsperger, C.P.M.; McGahon, A.J.; Radar, A.; van-Schie, R.C.; LaFace, D.M.; Green, D.R. Early distribution of plasma membrane phosphatidylscrine is a general feature of apoptosis regardless of the initiating stimulus: inhibition by overexpression of Bcl-2 and Abl. *J. Exp. Med.* **1995**, *182*, 1545-1556.

Martino, A.D.; Sittinger, M.; Risbud, M.V. Chitosan: A versatile biopolymer for orthopaedic tissue-engineering. *Biomaterials* **2005**, *26*, 5983-5990.

Masala, O.; Seshadri, R. Synthesis routes for large volumes of nanoparticles. *Ann. Rev. Mater. Res.* **2004**, *34*, 41-81.

Matsumura, Y.; Maeda, H. A new concept for macromolecular therapeutics in cancer-chemotherapy — mechanism of tumoritropic accumulation of proteins and the antitumor agent smancs. *Cancer Res.* **1986**, *46*, 6387-6392.

Maysinger, D.; Behrendt, M.; Lalancette-Herbert, M.; Kriz, J. Real-time imaging of astrocyte response to quantum dots: in vivo screening model system for biocompatibility of nanoparticles. *Nano Lett.* **2007**, *7*, 2513-2520.

McIntosh, C.M.; Esposito, E.A.; Boal, A.K.; Simard, J.M.; Martin, C.T.; Rotello, V.M. Inhibition of DNA transcription using cationic mixed monolayer protected gold clusters. *J. Am. Chem. Soc.* **2001**, *123*, 7626-7629.

McRae, S.R.; Brown, C.L.; Bushell, G.R. Rapid purifcation of EGFP, EYFP, and ECFP with high yield and purity. *Protein Expr. Purif.* **2005**, *41*, 121-127.

Mellman, I.; Fuchs, R.; Helenius, A. Acidification of the endocytic and exocytic pathways. *Ann. Rev. Biochem.* **1986**, *55*, 663-700.

Mi, F.L.; Shyu, S.S.; Wu, Y.B.; Lee, S.T.; Shyong, J.Y.; Ro Huang, R.N. Fabrication and characterization of a sponge-like asymmetric chitosan membrane as a wound dressing. *Biomaterials* **2001**, *22*, 165-173.

Mie, G. Beitrage zur Optik truber Medien speziell kolloidaler Metallosungen, *Ann. Phys.* **1908**, *25*, 377-445.

Min, K.H.; Park, K.; Kim, Y.S.; Bae, S.M.; Lee, S.; Jo, H.;G.; Park, R.W.; Kim, I.S.; Jeong, S.Y.; Kim, K.; Kwon, I.C. Hydrophobically modified glycol chitosan nanoparticles-encapsulated camptothecin enhance the drug stability and tumor targeting in cancer therapy. *J. Controlled Release* **2008**, *127*, 208-218.

Mitra, S.; Gaur, U.; Ghosh, P.C.; Maitra, A.N. Tumour targeted delivery of encapsulated dextran–doxorubicin conjugate using chitosan nanoparticles as carrier. *J. Controlled Release* **2001**, *74*, 317-323.

Morones, J.R.; Elechiguerra, J.L.; Camacho, A.; Holt, K.; Kouri, J.B.; Ramírez, J.T.; Yacaman, M.J. The bactericidal effect of silver nanoparticles. *Nanotechnology* **2005**, *16*, 2346-2353.

Moyer, C.A.; Brentano, L.; Gravens, D.L.; Margraf, H.W.; Monafo, W.W. Treatment of large human burns with 0.5% silver nitrate solution. *Arch. Surg.* **1965**, *90*, 812–867.

Mukherjee, P.; Ahmad, A.; Mandal, D.; Senapati, S.; Sainkar, S.R.; Khan, M.I.; Ramani, R.; Parischa, R.; Ajayakumar, P.V.; Alam, M.; Sastry, M.; Kumar, R. Bioreduction of $AuCl_4^-$ ions by the fungus, *Verticillium sp.* and surface trapping of the gold nanoparticles formed. *Angew. Chem. Int. Ed.* **2001**, *40*, 3585-3588.

Murray, C.B.; Norris, D.J.; Bawendi, M.G. Synthesis and characterization of nearly monodisperse CdE (E = sulfur, selenium, tellurium) semiconductor nanocrystallites. *J. Am. Chem. Soc.* **1993**, *115*, 8706-8715.

Murugadoss, A.; Chattopadhyay, A. A 'green' chitosan–silver nanoparticle composite as a heterogeneous as well as micro-heterogeneous catalyst. *Nanotechnology* **2008**, *19*, 015603/1-015603/9.

Muzzarelli, R.A.A. Chitin in nature and technology; *Plenum Press: New York*, *London*, **1986**.

Muzzarelli, R.A.A. Modified chitosans carrying sulfonic acid groups. *Carbohydr. Polym.* **1992**, *19*, 231-236.

Naik, R.R.; Stringer, S.J.; Agarwal, G.; Jones, S.E.; Stone, M.O. Biomimetic synthesis and patterning of silver nanoparticles *Nat. Mater.* **2002**, *1*, 169-172.

Nair, B.; Pradeep, T. Coalescence of nanoclusters and formation of submicron crystallites assisted by *Lactobacillus* strains. *Cryst. Growth Des.* **2002**, *2*, 293-298.

Nan, X.L.; Sims, P.A.; Chen, P.; Xie, X.S. Observation of individual microtubule motor steps in living cells with endocytosed quantum dots. *J. Phys. Chem. B* **2005**, *109*, 24220-24224.

Neto, C.G.T.; Giacometti, J.A.; Job, A.E.; Ferreira, F.C.; Fonseca, J.L.C.; Pereira, M.R. Thermal analysis of chitosan based networks. *Carbohydrate Polymers* **2005**, *62*, 97-103.

Neu, M.; Fischer, D.; Kissel, T. Recent advances in rational gene transfer vector design based on poly(ethyleneimine) and its derivatives, *J. Gene Med.* **2005**, *7*, 992-1009.

Newman, G.R.; Walker, M.; Hobot, J.A.; Bowler, P.G. Visualisation of bacterial sequestration and bactericidal activity within hydrating Hydrofibers® wound dressings. *Biomaterials* **2006**, *27*, 1129-1139.

Newmeyer, D.D.; Ferguson-Miller, S. Mitochondria. *Cell* **2003**, *112*, 481-490.

Niemeyer, C.M. Nanoparticles, proteins, and nucleic acids: Biotechnology meets materials science. *Angew. Chem. Int. Ed.* **2001**, *40*, 4128–4158.

Niemeyer, C.M. Self-assembled nanostructures based on DNA: towards the development of nanobiotechnology. *Curr. Opin. Chem. Biol.* **2000**, *4*, 609-618.

No, H.K.; Park, N.Y.; Lee, S.H.; Meyers, S.P. Antibacterial activity of chitosans and chitosan oligomers with different molecular weights. *Int. J. Food Microbiol.* **2002**, *74*, 65-72.

Novak, J.P.; Feldheim, D.L. Assembly of phenylacetylene-bridged silver and gold nanoparticle arrays. *J. Am. Chem. Soc.* **2000**, *122*, 3979-3980.

Nunez, G.; Benedict, M.A.; Hu, Y.; Inohara, N. Caspases: the proteases of the apoptotic pathway. *Oncogene* **1998**, *17*, 3237-3245.

O'Neal, D.P.; Hirsch, L.R.; Halas, N.J.; Payne, J.D.; West, J.L. Photothermal tumor ablation in mice using near infrared absorbing nanoshells. *Cancer Lett.* **2004**, *209*, 171-176.

Oberdorster, G.; Oberdorster, E.; Oberdorster, J. Nanotoxicology: An emerging discipline evolving from studies of ultrafine particles. *Environ. Health Perspect.* **2005**, *113*, 823-839.

Oishi, M.; Nakaogami, J.; Ishii, T.; Nagasaki, Y. Smart PEGylated gold nanoparticles for the cytoplasmic delivery of siRNA to induce enhanced gene silencing. *Chem. Lett.* **2006**, *35,* 1046-1047.

Oleinick, N.L.; Antunez, A.R.; Clay, M.E.; Rihter, B.D.; Kenney, M.E. New phthalocyanine photosensitizers for photodynamic therapy. *Photochem. Photobiol.* **1993**, *57*, 242-247.

Oo, M.K.K.; Yang, X.; Du, H.; Wang, H. 5-aminolevulinic acid-conjugated gold nanoparticles for photodynamic therapy of cancer. *Nanomedicine* **2008**, *3*, 777-786.

Ott, M.; Gogvadze, V.; Orrenius, S.; Zhivotovsky, B. Mitochondria, oxidative stress and cell death. *Apoptosis* **2007**, *12*, 913-922.

Paciotti, G.F.; Kingston, D.G.I.; Tamarkin, L. Colloidal gold nanoparticles: a novel nanoparticle platform for developing multifunctional tumor-targeted drug delivery vectors. *Drug Dev. Res.* **2006**, *67*, 47-54.

Paciotti, G.F.; Myer, L.; Weinreich, D.; Goia, D.; Pavel, N.; McLaughlin, R.E.; Tamarkin, L. Colloidal gold: a novel nanoparticle vector for tumor directed drug delivery. *Drug Deliv.* **2004**, *11*, 169-183.

Pack, D.W.; Hoffman, A.S.; Pun, S.; Stayton, P.S. Design and development of polymers for gene delivery. *Nat. Rev. Drug Discov.* **2005**, *4*, 581-593.

Pal, S.; Tak, Y.K.; Song, J.M. Does the antibacterial activity of silver nanoparticles depend on the shape of the nanoparticle? A study of the gram-negative bacterium Escherichia coli. *Appl Environ. Microbiol.* **2007**, *27*, 1712–1720.

Palioura, D.; Armes, S.P.; Anastasiadis, S.H.; Vamvakaki, M. Metal nanocrystals incorporated within pH-responsive microgel particles. *Langmuir* **2007**, *23*, 5761-576.

Panacek, A.; Kvitek, L.; Prucek, R.; Kolar, M.; Vecerova, R.; Pizurova, N. Silver colloid nanoparticles: synthesis, characterization, and their antibacterial activity. *J. Phys. Chem.* **2006**, *110*,16248–16253.

Panyam, J.; Labhasetwar, V. Biodegradable nanoparticles for drug and gene delivery to cells and tissue. *Adv. Drug Deliv. Rev.* **2003**, *55*, 329-347.

Papineau, A.M.; Hoover, D.G.; Knorr, D.; Farkas, D.F., Antimicrobial effect of water-soluble chitosan with high hydrostatic pressure. *Food Biotechnol.* **1991**, 5, 45-57.

Parak, W.J.; Boudreau, R.; Le Gros, M.; Gerion, D.; Zanchet, D.; Micheel, C.M.; Williams, S.C.; Alivisatos, A.P.; Larabell, C. Cell motility and metastatic potential studies based on quantum dot imaging of phagokinetic tracks, *Adv. Mater.* **2002**, *14*, 882-885.

Park, E.J.; Choi, J.; Park, Y.; Park, K. Oxidative stress induced by cerium oxide nanoparticles in cultured BEAS-2B cells. *Toxicology* **2008**, *245*, 90-100.

Park, T.G.; Jeong, J.H.; Kim, S.W. Current status of polymeric gene delivery systems. *Adv. Drug Deliv. Rev.* **2006**, *58*, 467-486.

Parungo, C.; Colson, Y.; Kim, S.; Kim, S.; Cohn, L.; Bawendi, M.; Frangioni, J. Sentinel lymph node mapping of the pleural space. *Chest* **2005**, *127*, 1799-1804.

Parungo, C.; Ohnishi, S.; Kim, S.; Kim, S.; Laurence, R.; Soltesz, E.; Chen, F.; Colson, Y.; Cohn, L.; Bawendi, M.; Frangioni, J. Intraoperative identification of esophageal sentinel lymph nodes with near-infrared fluorescence imaging. *J. Thorac. Cardiovasc. Surg.* **2005**, *129*, 844-850.

Peer, D.; Karp, J.M.; Hong, S.; Farokhzad, O.C.; Margalit, R.; Langer, R. Nanocarriers as an emerging platform for cancer therapy. *Nat. Nanotechnol.* **2007**, *2*, 751-760.

Perez-Juste, J.; Pastoriza-Santos I.; Liz-Marzan, L.M., Mulvaney, P. Gold nanorods: Synthesis, characterization and applications. *Coordination Chemistry Reviews* **2005**, *249* 1870–1901.

Pillai, O.; Panchagnula, R. Polymers in drug delivery. *Curr. Opin. Chem. Biol.* **2001**, *5*, 447-451.

Poliandri, A.H.; Cabilla, J.P.; Velardez, M.O.; Bodo, C.C.; Duvilanski, B.H. Cadmium induces apoptosis in anterior pituitary cells that can be reversed by treatment with antioxidants. *Toxicol. Appl. Pharmacol.* **2003**, *190*, 17-24.

Polizzi, M.A.; Stasko, N.A.; Schoenfisch, M.H. Water-soluble nitric oxide-releasing gold nanoparticles. *Langmuir* **2007**, *23,* 4938–4943.

Pradhan, N.; Goorskey, D.; Thessing, J.; Peng, X. An alternative of CdSe nanocrystal emitters: Pure and tunable impurity emissions in ZnSe nanocrystals. *J. Am. Chem. Soc.* **2005**, *127*, 17586-17587.

Pradhan, N.; Pal, A.; Pal, T., Silver nanoparticle catalyzed reduction of aromatic nitro compounds. *Colloids Surf. A* **2002**, *196*, 247-257.

Prescott, L.M.; Harley, J.P.; Klein, D.A. Microbiology, 5th ed.; The McGraw-Hill Companies: New York, **2002**, pp 46-61.

Pridgen, E.M.; Langer, R.; Farokhzad, O.C. Biodegradable, polymeric nanoparticle delivery systems for cancer therapy. *Nanomedicine* **2007**, *2*, 669-680.

Quillet-Mary, A.; Jaffre´zou, J.-P.; Mansat, V.; Bordier, C.; Naval, J.; Laurent, G. Implication of mitochondrial hydrogen peroxide generation in ceramide-induced apoptosis. *J. Biol. Chem.* **1997**, *272*, 21388-21395.

Rabea, E.I.; Badawy, M.E.-T.; Stevens, C.V.; Smagghe, G.; Steurbaut, W. Chitosan as antimicrobial agent: applications and mode of action. *Biomacromolecules* **2003**, *4*, 1457-1465.

Radomski, M.W.; Rees, D.D.; Dutra, A.; Moncada, S. S-nitroso-glutathione inhibits platelet activation in vitro and in vivo. *Br. J. Pharmacol.* **1992**, *107*, 754−749.

Rajan, S.S.; Vu, T.Q. Quantum dots monitor TrkA receptor dynamics in the interior of neural PC12 cells. *Nano Lett.* **2006**, *6*, 2049-2059.

Ramos, V.M.; Rodriguez, N.M.; Diaz, M.F.; Rodriguez, M.S.; Heras, A.; Agullo, E. N-methylene phosphonic chitosan. Effect of preparation methods on its properties. *Carbohydr. Polym.* **2003**, *52*, 39-46.

Rangnekar, A.; Sarma, T.K.; Singh, A.K.; Deka, J.; Ramesh, A.; Chattopadhyay, A. Retention of enzymatic activity of α-Amylase in the reductive synthesis of gold nanoparticles. *Langmuir* **2007**, *23*, 5700-5706.

Raveendran, P.; Fu, J.; Wallen, S.L. Completely "green" synthesis and stabilization of metal nanoparticles. *J. Am. Chem. Soc.* **2003**, *125*, 13940-13941.

Ravi, K.M.N.V.; Muzzarelli, R.A.A.; Muzzarelli, C.; Sashiwa, H.; Domb, A.J. Chitosan chemistry and pharmaceutical perspectives. *Chem. Rev.* **2004**, *104*, 6017-6084.

Rello, S.; Stockert, J.C.; Moreno, V.; G´amez, A.; Pacheco, M.; Juarranz, A.; Canete M.; Villanueva A. Morphological criteria to distinguish cell death induced by apoptotic and necrotic treatments. *Apoptosis* **2005**, *10*, 201-208.

Rhim, J.-W.; Hong, S.-I.; Park, H.-M.; Ng, P.K.W. Preparation and characterization of chitosan-based nanocomposite films with antimicrobial activity. *J. Agric. Food Chem.* **2006**, *54*, 5814-5822.

Risbud, M.; Bhonde, M.R.; Bhonde, R.R. Effect of chitosanpolyvinyl pyrrolidone hydrogel on proliferation and cytokine expression of endothelial cells: implications in islet immunoisolation. *J. Biomed. Mater. Res.* **2001**, *57*, 300-305.

Risbud, M.; Endres, M.; Ringe, J.; Bhonde, R.; Sittinger, M. Biocompatible hydrogel supports the growth of respiratory epithelial cells: possibilities in tracheal tissue engineering. *J. Biomed. Mater. Res.* **2001**, *56*, 120-127.

Risbud, M.; Ringe, J.; Bhonde, R.; Sittinger, M. In vitro expression of cartilage-specific markers by chondrocytes on a biocompatible hydrogel: implications for engineering cartilage tissue. *Cell Transplant* **2001**, *10*, 755–763.

Roach, P.; Farrar, D.; Perry, C.C. Interpretation of protein adsorption: surface-induced conformational changes. *J. Am. Chem. Soc.* **2005**, *127*, 8168-8173.

Roller, S.; Covill, N. The antifungal properties of chitosan in laboratory media and apple juice. *Int. J. Food Microbiol.* **1999**, *47*, 67-77.

Ronghua, H.; Yumin, D.; Jianhong, Y., Preparation and anticoagulant activity of carboxybutyrylated hydroxyethyl chitosan sulfates. *Carbohydr. Polym.* **2003**, *51*, 431-438.

Rosi, N.L.; Mirkin, C.A. Nanostructures in Biodiagnostics. *Chem. Rev.* **2005**, *105*, 1547-1562.

Rothrock, A.R.; Donkers, R.L.; Schoenfisch M.H. Synthesis of Nitric Oxide-Releasing Gold Nanoparticles. *J. Am. Chem. Soc.* **2005**, *127*, 9362-9363.

Roy, K.; Mao, H.-Q.; Huang, S.-K.; Leong, K.W. Oral gene delivery with chitosan–DNA nanoparticles generates immunologic protection in a murine model of peanut allergy. *Nat. Med.* **1999**, *5*, 387-391.

Sambhy, V.; MacBride, M.M.; Peterson, B.R.; Sen, A. Silver bromide nanoparticle/polymer composites: Dual action tunable antimicrobial materials. *J. Am. Chem. Soc.* **2006**, *128*, 9798-9808.

Sandhu, K.K.; McIntosh, C.M.; Simard, J.M.; Smith, S.W.; Rotello, V.M. Gold nanoparticle-mediated transfection of mammalian cells. *Bioconjug. Chem.* **2002**, *13,* 3-6.

Sapra, S.; Prakash, A.; Ghangrekar, A.; Periasamy, N.; Sarma, D.D. Emission properties of manganese-doped ZnS nanocrystals. *J. Phys. Chem. B* **2005**, *109*, 1663-1668.

Sashiwa, H.; Aiba, S. Chemically modified chitin and chitosan as biomaterials. *Prog. Polym. Sci.* **2004**, *29*, 887-908.

Sashiwa, H.; Saimoto, H.; Shigemasa, Y.; Ogawa, R.; Tokura, S. Lysozyme susceptibility of partially deacetylated chitin. *Int. J. Biol. Macromol.* **1990**, *12*, 295-296.

Sayes, C.M.; Gobin, A.M.; Ausman, K.D.; Mendez, J.; West, J.L.; Colvin, V.L. Nano-C60 cytotoxicity is due to lipid peroxidation. *Biomaterials* **2005**, *26*, 7587-7595.

Shahverdi, A.R.; Fakhimi, A.; Shahverdi, H.R.; Minaian, S. Synthesis and effect of silver nanoparticles on the antibacterial activity of different antibiotics against Staphylococcus aureus and Escherichia coli. *Nanomed: Nanotechnol. Biol. Med.* **2007**, *3*, 168–171.

Shang, W.; Nuffer, J.H.; Dordick, J.S.; Siegel, R.W. Unfolding of ribonuclease A on silica nanoparticle surfaces. *Nano Lett.* **2007**, *7*, 1991-1995.

Shankar, S.S.; Rai, A.; Ankamwar, B.; Singh, A.; Ahmad, A.; Sastry, M. Biological synthesis of triangular gold nanoprisms. *Nat. Mater.* **2004**, *3*, 482-488.

Shi, Z.; Neoh, K.G.; Kang, E.T.; Wang, W. Antibacterial and mechanical properties of bone cement impregnated with chitosan nanoparticles. *Biomaterials* **2006**, *27*, 2440-2449.

Shigemasa, Y.; Saito, K.; Sashiwa, H.; Saimoto, H. Enzymatic degradation of chitins and partially deacetylated chitins. *Int. J. Biol. Macromol.* **1994**, *16*, 43-49.

Shukla, R.; Bansal, V.; Chaudhary, M.; Basu, A.; Bhonde R.B.; Satry, M. Biocompatibility of gold nanoparticles and their endocytotic fate inside the cellular compartment: a microscopic overview. *Langmuir* **2005**, *21*, 10644-10654.

Singal, P.K.; Iliskovic N. Doxorubicin-induced cardiomyopathy. *New Engl. J. Med.* **1998**, *339*, 900-905.

Sinha, V.R.; Singla, A.K.; Wadhawan, S.; Kaushik, R.; Kumria, R.; Bansal, K.; Dhawan, S. Chitosan microspheres as a potential carrier for drugs. *Int. J. Pharm.* **2004**, *274*, 1-33.

Soltesz, E.; Kim, S.; Laurence, R.; DeGrand, A.; Parungo, C.; Dor, D.; Cohn, L.; Bawendi, M.; Frangioni, J.; Mihaljevic, T. Intraoperative sentinel lymph node mapping of the lung using near-infrared fluorescent quantum dots. *Ann. Thorac. Surg.* **2005**, *79*, 269-277.

Soncin, M.; Busetti, A.; Fusi, F.; Jori, G.; Rodgers, M.A.J. Irradiation of amelanotic melanoma cells with 532 nm high peak power pulsed laser radiation in the presence of the photothermal sensitiser Cu [II]-haematoporphyrin: a new approach to cell photoinactivation. *Photochem. Photobiol.* **1999**, *69*, 708-712.

Sondi, I.; Salopek-Sondi, B. Silver nanoparticles as antimicrobial agent: A case study on *E. coli* as a model for gram-negative bacteria. *J. Colloid Interface Sci.* **2004**, *275*, 177-82.

Soppimath, K.; Aminabhavi, T.; Kulkarni, A.; Rudzinski, W. Biodegradable polymeric nanoparticles as drug delivery devices. *J. Controlled Release* **2001**, *70*, 1-20.

Springer, C.J.; Duvaz, I.N. Prodrug-activating systems in suicide gene therapy. *J. Clin. Invest.* **2000**, *105*, 1161-1167.

Stossel, P.; Leuba, J.L. Effect of chitosan, chitin and some amino-sugars on growth of various soil borne phytopathogenic fungi. *Physiopathology* **1984**, *111*, 82-90.

Sturersson, C.; Andersson-Engels, S. A mathematical model for predicting the temperature distribution in laser-induced hyperthermia. Experimental evaluation and applications. *Phys. Med. Biol.* **1995**, *40*, 2037-2052.

Sudarshan, N.R.; Hoover, D.G.; Knorr, D. Antibacterial action of chitosan, *Food Biotechnol.* **1992**, *6*, 257-272.

Suh, J.; Wirtz, D.; Hanes, J. Efficient active transport of gene nanocarriers to the cell nucleus. *Proc. Natl. Acad. Sci. USA* **2003**, *100*, 3878-3882.

Sun Y.; Xia, Y. Increased sensitivity of surface plasmon resonance of gold nanoshells compared to that of gold solid colloids in response to environmental changes. *Anal. Chem.* **2002**, *74*, 5297-5305.

Sun, R.W.Y.; Chen, R.; Chung, N.P.-Y.; Ho, C.-M.; Lin, C.-L.S.; Che, C.-M. Silver nanoparticles fabricated in Hepes buffer exhibit cytoprotective activities toward HIV-1 infected cells. *Chem. Comm.* **2005**, *40*, 5059-5061.

Sun, Y.; Mayers, B.; Xia, Y. Transformation of silver nanospheres into nanobelts and triangular nanoplates through a thermal process. *Nano Lett.* **2003**, *3*, 675-679.

Suyver, J.F.; Wuister, S.F.; Kelly, J.J.; Meijerink, A. Synthesis and photoluminescence of nanocrystalline ZnS:Mn^{2+}. *Nano Lett.* **2001**, *1*, 429-433.

Takahashi, H.; Niidome, T.; Nariai, A.; Niidome, Y.; Yamada, S. Photothermal reshaping of gold nanorods prevents further cell death. *Nanotechnology* **2006a**, *17*, 4431-4435.

Tamai, T.; Watanabe, M.; Hatanaka, Y.; Tsujiwaki, H.; Nishioka, N.; Matsukawa, K. Formation of metal nanoparticles on the surface of polymer particles incorporating polysilane by UV irradiation. *Langmuir* 2008, *24*, 14203-14208.

Tanaka, T.; Sakai, R.; Kobayashi, R.; Hatakeyama, K.; Matsunaga, T. Contributions of phosphate to DNA adsorption/desorption behaviors on aminosilane-modified magnetic nanoparticles. *Langmuir* **2009**, *25*, 2956-2961.

Thomas, M.; Klibanov, A.M. Conjugation to gold nanoparticles enhances polyethylenimine's transfer of plasmid DNA into mammalian cells. *Proc. Natl. Acad. Sci. U. S. A.* **2003**, *100*, 9138-9143.

Thompson, C.B. Apoptosis in the pathogenesis and treatment of disease. *Science* **1995**, *267*, 1456-1462.

Thress, K.; Kornbluth, S.; Smith, J.J. Mitochondria at the crossroad of apoptotic cell death. *J. Bioenergetics Biomembranes* **1999**, *31*, 321 – 326.

Tomczak, M.M.; Slocik, J.M.; Stone, M.O.; Naik, R.R. Bio-based approaches to inorganic material synthesis. *Biochem. Soc. Trans.* **2007**, *35*, 512-515.

Turkevich, J.; Stevenson, P.C.; Hillier, J. A study of the nucleation and growth processes in the synthesis of colloidal gold. *Discuss. Faraday. Soc.* **1951**, *11*, 55-75.

Tuzlakoglu, K.; Alves, C.M.; Mano, J.F.; Reis, R.L. Production and characterization of chitosan fibers and 3-D fiber mesh scaffolds for tissue engineering applications. *Macromol. Biosci.* **2004**, *4*, 811–819.

Uhrich, K.E.; Cannizzaro, S.M.; Langer, R.S.; Shakesheff, K.M. Polymeric systems for controlled drug release. *Chem. Rev.* **1999**, *99*, 3181-3198.

Varma, A.J.; Deshpande, S.V.; Kennedy, J.F. Metal complexation by chitosan and its derivatives: a review. *Carbohydr. Polym.* **2004**, *55*, 77-93.

Verma, A.; Simard, J.M.; Worrall, J.W.E.; Rotello, V.M. Tunable reactivation of nanoparticle-inhibited beta-galactosidase by glutathione at intracellular concentrations. *J. Am. Chem. Soc.* **2004**, *126*, 13987-13991.

Vertegel, A.A.; Siegel, R.W.; Dordick, J.S. Silica nanoparticle size influences the structure and enzymatic activity of adsorbed lysozyme. *Langmuir* **2004**, *20*, 6800-6807.

Vila, A.; Sánchez, A.; Tobío, M.; Calvo, P.; Alonso, M.J. Design of biodegradable particles for protein delivery. *J. Controlled Release* **2002**, *78*, 15-24.

Vold, I.M.N.; Vårum, K.M.; Guibal, E.; Smidsrød, O. Binding of ions to chitosan-selectivity studies. *Carbohydr. Polym.* **2003**, *54*, 471-477.

Walker, M.; Hobot, J.A.; Newman, G.R.; Bowler, P.G. Scanning electron microscopic examination of bacterial immobilisation in a carboxymethyl cellulose (AQUACEL®) and alginate dressings. *Biomaterials* **2003**, *24*, 883-890.

Wan, Y.; Lu, X.; Dalai, S.; Zhang, J. Thermophysical properties of polycaprolactone/ chitosan blend membranes. *Thermochimica Acta* **2009**, *487*, 33-38.

Wang, L.S.; Khor, E.; Lim, L.Y. Chitosan-alginate-CaCl2 system for membrane coat application. *J. Pharm. Sci.* **2001**, *90*, 1134-1142.

Wang, S.F.; Shen, L.; Zhang, W.D.; Tong, Y.J. Preparation and mechanical properties of chitosan/carbon nanotubes composites. *Biomacromolecules* **2005**, *6*, 3067-3072.

Wang, X.; Du, Y.; Liu, H. Preparation, characterization and antimicrobial activity of chitosan–Zn complex. *Carbohydr. Polym.* **2004**, *56*, 21-26.

Wang, Y.S.; Liu, L.R.; Jiang, Q.; Zhang, Q.Q. Self-aggregated nanoparticles of cholesterol modified chitosan conjugate as a novel carrier of epirubicin. *European Polym. J.* **2007**, *43*, 43-51.

Warad, H.C.; Thanachayanont, C.; Tumcharern, G.; Dutta, J. Chitosan clad manganese doped zinc suiphide nanoparticles as biological labels. *Proceedings of the 2nd IEEE International Conference on Nano/Micro Engineered and Molecular System*; Bangkok, Thailand, **2007**.

Warren, S.; Patel, S.; Kapron, C.M. The effect of vitamin E exposure on cadmium toxicity in mouse embryo cells in vitro. *Toxicology* **1999**, *142*, 119-126.

Weishaupt, K.R.; Gomer, C.J.; Dougherty, T.J. Identification of singlet oxygen as cytotoxic agent in photo-inactivation of a murine tumor. *Cancer Res.* **1976,** *36,* 2326-2329.

Weissleder, R. A clearer vision for in vivo imaging. *Nat. Biotechnol.* **2001**, *19*, 316-317.

Wen, F.; Zhang, W.; Wei, G.; Wang, Y.; Zhang, J.; Zhang, M.; Shi, L. Synthesis of noble metal nanoparticles embedded in the shell layer of core−shell poly(styrene-co-4-vinylpyridine) micospheres and their application in catalysis. *Chem. Mater.* **2008**, *20*, 2144-2150.

Weston, S.A.; Parish, C.R. New fluorescent dyes for lymphocyte migration studies: analysis by flow cytometry and fluorescent microscopy. *J. Immunol. Methods* **1990**, *133*, 87-97.

Wieder, M.E.; Hone, D.C.; Cook, M. J.; Handsley, M.M.; Gavrilovic, J.; Russell D.A. Intracellular photodynamic therapy with photosensitizer-nanoparticle conjugates: cancer therapy using a ‘Trojan horse’. *Photochem. Photobiol. Sci.* **2006**, *5,* 727-734.

Wilcox, M.; Kite, P.; Dobbins, B. Antimicrobial intravascular catheters-which surface to coat? *J. Hospital Infec.* **1998**, *40*, 322–323.

Williams, D.L.H. A chemist’s view of the nitric oxide story. *Org. Biomol. Chem.* **2003**, *1*, 441-449.

Wu, L.-Q.; Gadre, A.P.; Yi, H.; Kastantin, M.J.; Rubloff, G.W.; Bentley, W.E.; Payne, G.F.; Ghodssi, R. Voltage-dependent assembly of the polysaccharide chitosan onto an electrode surface. *Langmuir* **2002**, *18*, 8620-8625.

X.F. Yu, L.D. Chen, K.Y. Li, Y. Li, S. Xiao, X. Luo, J. Liu, L. Zhou, Y.L. Deng, D.W. Pang, Q.Q. Wang, Immunofluorescence detection with quantum dot bioconjugates for hepatoma in vivo, *J. Biomed. Opt.* **2007**, *12*, 014008-1–014008-5.

Xia, W.; Liu, W.; Cui, L.; Liu, Y.; Zhong, W.; Liu, D.; Wu, J.; Chua, K.; Cao, Y. Tissue engineering ofcartilage with the use of chitosan–gelatin complex scaffolds. *J. Biomed. Mater. Res.* **2004**, *71*, 373–380.

Yan, X.-L.; Khor, E.; Lim, L.Y. Chitosan-alginate films prepared with chitosans of different molecular weights. *J. Biomed. Mater. Res.* **2001**, *58*, 358-365.

Yang, F.; Moss, L.G.; Phillips, G.N. The molecular structure of green fluorescent protein. *Nat. Biotechnol.* **1996**, *14*, 1246-1251.

Yazawa, K.; Fisher, W.; Brunicardi, F.C. Current progress in suicide gene therapy for cancer. *World J. Surg.* **2002**, 26, 783-789.

Ye, W.J.; Leung, M.F.; Xin, J.; Kwong, T.L.; Lee, D.K.L.; Li, P. Novel core-shell particles with poly(n-Butyl Acrylate) cores and chitosan shells as an antibacterial coating for textiles. *Polymer* **2005**, *46*, 10538-10543.

Yi, Y.; Wang, Y.; Liu, H. Preparation of new crosslinked chitosan with crown ether and their adsorption for silver ion for antibacterial activities. *Carbohydr. Polym.* **2003**, *53*, 425-430.

Young, S.H.; Rozengurt, E. Qdot nanocrystal conjugates conjugated to bombesin or ANG II label the cognate G protein-coupled receptor in living cells. *Am. J. Physiol. Cell Physiol.* **2006**, *290*, C728-C732.

Zhang, L.; Gu, F.X.; Chan, J.M.; Wang, A.Z.; Langer, R.S.; Farokhzad, O.C. Nanoparticles in medicine: therapeutic applications and developments. *Clin. Pharmacol. Ther.* **2008**, *83*, 761-769.

Zhang, P.; Sham, T.K. X-ray studies of the structure and electronic behavior of alkanethiolate-capped gold nanoparticles: the interplay of size and surface effects. *Phy. Rev. Lett.* **2003**, *90*, 245502-1-245502-4.

Zhang, Y.; Peng, H.; Huang, W.; Zhou, Y.; Zhang, X.; Yan, D. Hyperbranched poly(amidoamine) as the stabilizer and reductant to prepare colloid silver nanoparticles in situ and their antibacterial activity, *J. Phys. Chem. C* **2008**, *112*, 2330-2336.

Zhang, Y.; Zhang, M. Cell growth and function on calcium phosphate reinforced chitosan scaffolds. *J. Mater. Sci. Mater. Med.* **2004**, *15*, 255–260.

Zhou, Y.; Chen, W.; Itoh, H.; Naka, K.; Ni, Q.; Yamane, H.; Chujo, Y. Preparation of a novel core–shell nanostructured gold colloid–silk fibroin bioconjugate by the protein in situ redox technique at room temperature. *Chem. Commun.* **2001**, *23*, 2518-2519.

Zhu, A.; Zhang, M.; Wu. J.; Shen, J. Covalent immobilization of chitosan/heparin complex with a photosensitive hetero-bifunctional crosslinking reagent on PLA surface. *Biomaterials* **2002**, *23*, 4657-4665.

Zhu, H.; Ji, J.; Lin, R.; Gao, C.; Feng, L.; Shen, J. Surface engineering of poly(d,l-lactic acid) by entrapment of chitosan-based derivatives for the promotion of chondrogenesis. *J. Biomed. Mater. Res.* **2002**, *62*, 532–539.

Zimmer, M. Green fluorescent protein (GFP): applications, structure, and related photophysical behavior. *Chem. Rev.* **2002**, *102*, 759-781.

LIST OF PUBLICATIONS

Journal Publication

1) **Pallab Sanpui**, Shivendra B. Pandey, Siddhartha Sankar Ghosh and Arun Chattopadhyay; Green fluorescent protein for in situ synthesis of highly uniform Au nanoparticles and monitoring protein denaturation *Journal of Colloid and Interface Science* **2008**, *326*, 129–137.
2) **Pallab Sanpui**, A. Murugadoss, P.V. Durga Prasad, Siddhartha Sankar Ghosh and Arun Chattopadhyay; The antibacterial properties of a novel chitosan–Ag-nanoparticle composite *International Journal of Food Microbiology* **2008**, *124*, 142-146.
3) P. Gopinath, Sonit Kumar Gogoi, **Pallab Sanpui**, Anumita Paul, Arun Chattopadhyay and Siddhartha Sankar Ghosh; Signaling Gene Cascade in Silver Nanoparticle Induced Apoptosis. *Colloids and Surfaces B: Biointerfaces* **2010**, *77*, 240-245.
4) **Pallab Sanpui**, Shivendra B. Pandey, Arun Chattopadhyay and Siddhartha Sankar Ghosh. A Chitosan-Based Nanocarrier for Silver Nanoparticles with Enhanced Catalytic Activity. (Submitted)
5) **Pallab Sanpui**, Arun Chattopadhyay and Siddhartha Sankar Ghosh. Induction of Apoptosis in cancer cells by chitosan based nanocarrier of silver nanoparticle. (Submitted)
6) **Pallab Sanpui**, Shivendra B. Pandey, Arun Chattopadhyay and Siddhartha Sankar Ghosh; Incorporation of Gene Therapy Vector in Chitosan Containing Mn^{2+}- doped ZnS Quantum Dot. (Submitted)
7) Amit Jaiswal, **Pallab Sanpui**, Arun Chattopadhyay and Siddhartha Sankar Ghosh. Investigating Fluorescence Quenching of ZnS Quantum Dots by Silver Nanoparticles. (Submitted)

Conference Publication

1) Shivendra B. Pandey, **Pallab Sanpui**, Arun Chattopadhyay and Siddhartha Sankar Ghosh. (2009) Chitosan–Mn^{2+}-doped ZnS quantum dot nanocomposites for Carrying Suicide Genes, *International Conference on Advanced Nanomaterials and Nanotechnology* 2009, IIT Guwahati.

PERMISSION

This section contains the copies of original *permissions obtained for reproducing Figures* in **Chapter 1** from other sources, as listed below:

Figure No.	Page No.	Source
1.1 (b)	4	Perez-Juste, J.; Pastoriza-Santos I.; Liz-Marzan, L.M., Mulvaney, P. Gold nanorods: Synthesis, characterization and applications. *Coordination Chemistry Reviews* **2005**, *249*, 1870–1901.
1.3 (b)	12	Medintz, I.L.; Uyeda, H.T.; Goldman, E.R.; Mattoussi. H. Quantum dot bioconjugates for imaging, labelling and sensing. *Nature Materials* **2005**, *4*, 435 – 446.
1.3 (c)	12	Quantum Dot Corp. & Medintz, I.L.; Uyeda, H.T.; Goldman, E.R.; Mattoussi. H. Quantum dot bioconjugates for imaging, labelling and sensing. *Nature Materials* **2005**, *4*, 435 – 446.
1.5	19	Peer, D.; Karp, J.M.; Hong, S.; Farokhzad, O.C.; Margalit, R.; Langer, R. Nanocarriers as an emerging platform for cancer therapy. *Nat. Nanotechnol.* **2007**, *2*, 751-760.
1.7	23	Martino, A.D.; Sittinger, M.; Risbud, M.V. Chitosan: A versatile biopolymer for orthopaedic tissue-engineering. *Biomaterials* **2005**, *26*, 5983-5990

ELSEVIER LICENSE
TERMS AND CONDITIONS

Dec 06, 2010

This is a License Agreement between Pallab Sanpui ("You") and Elsevier ("Elsevier") provided by Copyright Clearance Center ("CCC"). The license consists of your order details, the terms and conditions provided by Elsevier, and the payment terms and conditions.

All payments must be made in full to CCC. For payment instructions, please see information listed at the bottom of this form.

Supplier	Elsevier Limited The Boulevard,Langford Lane Kidlington,Oxford,OX5 1GB,UK
Registered Company Number	1982084
Customer name	Pallab Sanpui
Customer address	Centre for Nanotechnology Guwahati, other 781039
License number	2563071237404
License date	Dec 06, 2010
Licensed content publisher	Elsevier
Licensed content publication	Coordination Chemistry Reviews
Licensed content title	Gold nanorods: Synthesis, characterization and applications
Licensed content author	Jorge Pérez-Juste, Isabel Pastoriza-Santos, Luis M. Liz-Marzán, Paul Mulvaney
Licensed content date	September 2005
Licensed content volume number	249
Licensed content issue number	17-18
Number of pages	32
Start Page	1870
End Page	1901
Type of Use	reuse in a thesis/dissertation
Intended publisher of new work	other
Portion	figures/tables/illustrations
Number of figures/tables /illustrations	1
Format	both print and electronic
Are you the author of this Elsevier article?	No
Will you be translating?	No
Order reference number	

Title of your thesis/dissertation	Implications of Nanoparticle-Polymer Composites as Probes and Therapeutic Agents
Expected completion date	Jan 2011
Estimated size (number of pages)	145
Elsevier VAT number	GB 494 6272 12
Permissions price	0.00 USD
Value added tax 0.0%	0.0 USD / 0.0 GBP
Total	0.00 USD

Terms and Conditions

INTRODUCTION

1. The publisher for this copyrighted material is Elsevier. By clicking "accept" in connection with completing this licensing transaction, you agree that the following terms and conditions apply to this transaction (along with the Billing and Payment terms and conditions established by Copyright Clearance Center, Inc. ("CCC"), at the time that you opened your Rightslink account and that are available at any time at http://myaccount.copyright.com).

GENERAL TERMS

2. Elsevier hereby grants you permission to reproduce the aforementioned material subject to the terms and conditions indicated.

3. Acknowledgement: If any part of the material to be used (for example, figures) has appeared in our publication with credit or acknowledgement to another source, permission must also be sought from that source. If such permission is not obtained then that material may not be included in your publication/copies. Suitable acknowledgement to the source must be made, either as a footnote or in a reference list at the end of your publication, as follows:

“Reprinted from Publication title, Vol /edition number, Author(s), Title of article / title of chapter, Pages No., Copyright (Year), with permission from Elsevier [OR APPLICABLE SOCIETY COPYRIGHT OWNER].” Also Lancet special credit - “Reprinted from The Lancet, Vol. number, Author(s), Title of article, Pages No., Copyright (Year), with permission from Elsevier.”

4. Reproduction of this material is confined to the purpose and/or media for which permission is hereby given.

5. Altering/Modifying Material: Not Permitted. However figures and illustrations may be altered/adapted minimally to serve your work. Any other abbreviations, additions, deletions and/or any other alterations shall be made only with prior written authorization of Elsevier Ltd. (Please contact Elsevier at permissions@elsevier.com)

6. If the permission fee for the requested use of our material is waived in this instance, please be advised that your future requests for Elsevier materials may attract a fee.

7. Reservation of Rights: Publisher reserves all rights not specifically granted in the combination of (i) the license details provided by you and accepted in the course of this

licensing transaction, (ii) these terms and conditions and (iii) CCC's Billing and Payment terms and conditions.

8. License Contingent Upon Payment: While you may exercise the rights licensed immediately upon issuance of the license at the end of the licensing process for the transaction, provided that you have disclosed complete and accurate details of your proposed use, no license is finally effective unless and until full payment is received from you (either by publisher or by CCC) as provided in CCC's Billing and Payment terms and conditions. If full payment is not received on a timely basis, then any license preliminarily granted shall be deemed automatically revoked and shall be void as if never granted. Further, in the event that you breach any of these terms and conditions or any of CCC's Billing and Payment terms and conditions, the license is automatically revoked and shall be void as if never granted. Use of materials as described in a revoked license, as well as any use of the materials beyond the scope of an unrevoked license, may constitute copyright infringement and publisher reserves the right to take any and all action to protect its copyright in the materials.

9. Warranties: Publisher makes no representations or warranties with respect to the licensed material.

10. Indemnity: You hereby indemnify and agree to hold harmless publisher and CCC, and their respective officers, directors, employees and agents, from and against any and all claims arising out of your use of the licensed material other than as specifically authorized pursuant to this license.

11. No Transfer of License: This license is personal to you and may not be sublicensed, assigned, or transferred by you to any other person without publisher's written permission.

12. No Amendment Except in Writing: This license may not be amended except in a writing signed by both parties (or, in the case of publisher, by CCC on publisher's behalf).

13. Objection to Contrary Terms: Publisher hereby objects to any terms contained in any purchase order, acknowledgment, check endorsement or other writing prepared by you, which terms are inconsistent with these terms and conditions or CCC's Billing and Payment terms and conditions. These terms and conditions, together with CCC's Billing and Payment terms and conditions (which are incorporated herein), comprise the entire agreement between you and publisher (and CCC) concerning this licensing transaction. In the event of any conflict between your obligations established by these terms and conditions and those established by CCC's Billing and Payment terms and conditions, these terms and conditions shall control.

14. Revocation: Elsevier or Copyright Clearance Center may deny the permissions described in this License at their sole discretion, for any reason or no reason, with a full refund payable to you. Notice of such denial will be made using the contact information provided by you. Failure to receive such notice will not alter or invalidate the denial. In no event will Elsevier or Copyright Clearance Center be responsible or liable for any costs, expenses or damage incurred by you as a result of a denial of your permission request, other than a refund of the amount(s) paid by you to Elsevier and/or Copyright Clearance Center for denied permissions.

LIMITED LICENSE

TH-964_05615301

The following terms and conditions apply only to specific license types:

15. **Translation**: This permission is granted for non-exclusive world **English** rights only unless your license was granted for translation rights. If you licensed translation rights you may only translate this content into the languages you requested. A professional translator must perform all translations and reproduce the content word for word preserving the integrity of the article. If this license is to re-use 1 or 2 figures then permission is granted for non-exclusive world rights in all languages.

16. **Website**: The following terms and conditions apply to electronic reserve and author websites:
Electronic reserve: If licensed material is to be posted to website, the web site is to be password-protected and made available only to bona fide students registered on a relevant course if:
This license was made in connection with a course,
This permission is granted for 1 year only. You may obtain a license for future website posting,
All content posted to the web site must maintain the copyright information line on the bottom of each image,
A hyper-text must be included to the Homepage of the journal from which you are licensing at http://www.sciencedirect.com/science/journal/xxxxx or the Elsevier homepage for books at http://www.elsevier.com , and
Central Storage: This license does not include permission for a scanned version of the material to be stored in a central repository such as that provided by Heron/XanEdu.

17. **Author website** for journals with the following additional clauses:

All content posted to the web site must maintain the copyright information line on the bottom of each image, and
he permission granted is limited to the personal version of your paper. You are not allowed to download and post the published electronic version of your article (whether PDF or HTML, proof or final version), nor may you scan the printed edition to create an electronic version,
A hyper-text must be included to the Homepage of the journal from which you are licensing at http://www.sciencedirect.com/science/journal/xxxxx , As part of our normal production process, you will receive an e-mail notice when your article appears on Elsevier's online service ScienceDirect (www.sciencedirect.com). That e-mail will include the article's Digital Object Identifier (DOI). This number provides the electronic link to the published article and should be included in the posting of your personal version. We ask that you wait until you receive this e-mail and have the DOI to do any posting.
Central Storage: This license does not include permission for a scanned version of the material to be stored in a central repository such as that provided by Heron/XanEdu.

18. **Author website** for books with the following additional clauses:
Authors are permitted to place a brief summary of their work online only.
A hyper-text must be included to the Elsevier homepage at http://www.elsevier.com

All content posted to the web site must maintain the copyright information line on the bottom of each image
You are not allowed to download and post the published electronic version of your chapter,

nor may you scan the printed edition to create an electronic version.
Central Storage: This license does not include permission for a scanned version of the material to be stored in a central repository such as that provided by Heron/XanEdu.

19. **Website** (regular and for author): A hyper-text must be included to the Homepage of the journal from which you are licensing at http://www.sciencedirect.com/science/journal/xxxxx. or for books to the Elsevier homepage at http://www.elsevier.com

20. **Thesis/Dissertation**: If your license is for use in a thesis/dissertation your thesis may be submitted to your institution in either print or electronic form. Should your thesis be published commercially, please reapply for permission. These requirements include permission for the Library and Archives of Canada to supply single copies, on demand, of the complete thesis and include permission for UMI to supply single copies, on demand, of the complete thesis. Should your thesis be published commercially, please reapply for permission.

21. **Other Conditions**:

v1.6

Gratis licenses (referencing $0 in the Total field) are free. Please retain this printable license for your reference. No payment is required.

If you would like to pay for this license now, please remit this license along with your payment made payable to "COPYRIGHT CLEARANCE CENTER" otherwise you will be invoiced within 48 hours of the license date. Payment should be in the form of a check or money order referencing your account number and this invoice number RLNK10895010.
Once you receive your invoice for this order, you may pay your invoice by credit card. Please follow instructions provided at that time.

Make Payment To:
Copyright Clearance Center
Dept 001
P.O. Box 843006
Boston, MA 02284-3006

If you find copyrighted material related to this license will not be used and wish to cancel, please contact us referencing this license number 2563071237404 and noting the reason for cancellation.

Questions? customercare@copyright.com or +1-877-622-5543 (toll free in the US) or +1-978-646-2777.

NATURE PUBLISHING GROUP LICENSE
TERMS AND CONDITIONS

Dec 06, 2010

This is a License Agreement between Pallab Sanpui ("You") and Nature Publishing Group ("Nature Publishing Group") provided by Copyright Clearance Center ("CCC"). The license consists of your order details, the terms and conditions provided by Nature Publishing Group, and the payment terms and conditions.

All payments must be made in full to CCC. For payment instructions, please see information listed at the bottom of this form.

License Number	2563100093955
License date	Dec 06, 2010
Licensed content publisher	Nature Publishing Group
Licensed content publication	Nature Materials
Licensed content title	Quantum dot bioconjugates for imaging, labelling and sensing
Licensed content author	Igor L. Medintz, H. Tetsuo Uyeda, Ellen R. Goldman, Hedi Mattoussi
Licensed content date	Jun 1, 2005
Type of Use	reuse in a thesis/dissertation
Requestor type	academic/educational
Format	print and electronic
Portion	figures/tables/illustrations
Number of figures/tables /illustrations	1
High-res required	no
Figures	Figure 1c
Author of this NPG article	no
NPG Code	
Title of your thesis / dissertation	Implications of Nanoparticle-Polymer Composites as Probes and Therapeutic Agents
Expected completion date	Jan 2011
Estimated size (number of pages)	145
Total	0.00 USD
Terms and Conditions	

Terms and Conditions for Permissions

Nature Publishing Group hereby grants you a non-exclusive license to reproduce this material for this purpose, **and for no other use**, subject to the conditions below:

1. NPG warrants that it has, to the best of its knowledge, the rights to license reuse of this material. However, you should ensure that the material you are requesting is original to Nature Publishing Group and does not carry the copyright of another entity (as

credited in the published version). If the credit line on any part of the material you have requested indicates that it was reprinted or adapted by NPG with permission from another source, then you should also seek permission from that source to reuse the material.

2. Permission granted free of charge for material in print is also usually granted for any electronic version of that work, provided that the material is incidental to the work as a whole and that the electronic version is essentially equivalent to, or substitutes for, the print version.

   Where print permission has been granted for a fee, separate permission must be obtained for any additional, electronic re-use (unless, as in the case of a full paper, this has already been accounted for during your initial request in the calculation of a print run).

   NB: In all cases, web-based use of full-text articles must be authorized separately through the 'Use on a Web Site' option when requesting permission.

3. Permission granted for a first edition does not apply to second and subsequent editions and for editions in other languages (except for signatories to the STM Permissions Guidelines, or where the first edition permission was granted for free).

4. Nature Publishing Group's permission must be acknowledged next to the figure, table or abstract in print. In electronic form, this acknowledgement must be visible at the same time as the figure/table/abstract, and must be hyperlinked to the journal's homepage.

5. The credit line should read:

   Reprinted by permission from Macmillan Publishers Ltd: [JOURNAL NAME] (reference citation), copyright (year of publication)

   For AOP papers, the credit line should read:

   Reprinted by permission from Macmillan Publishers Ltd: [JOURNAL NAME], advance online publication, day month year (doi: 10.1038/sj.[JOURNAL ACRONYM].XXXXX)

6. Adaptations of single figures do not require NPG approval. However, the adaptation should be credited as follows:

   Adapted by permission from Macmillan Publishers Ltd: [JOURNAL NAME] (reference citation), copyright (year of publication)

7. Translations of up to a whole article do not require NPG approval. The translation should be credited as follows:

   Translated by permission from Macmillan Publishers Ltd: [JOURNAL NAME] (reference citation), copyright (year of publication)

We are certain that all parties will benefit from this agreement and wish you the best in the

TH-964_05615301

use of this material. Thank you.

Gratis licenses (referencing $0 in the Total field) are free. Please retain this printable license for your reference. No payment is required.

If you would like to pay for this license now, please remit this license along with your payment made payable to "COPYRIGHT CLEARANCE CENTER" otherwise you will be invoiced within 48 hours of the license date. Payment should be in the form of a check or money order referencing your account number and this invoice number RLNK10895046.
Once you receive your invoice for this order, you may pay your invoice by credit card. Please follow instructions provided at that time.

Make Payment To:
Copyright Clearance Center
Dept 001
P.O. Box 843006
Boston, MA 02284-3006

If you find copyrighted material related to this license will not be used and wish to cancel, please contact us referencing this license number 2563100093955 and noting the reason for cancellation.

Questions? customercare@copyright.com or +1-877-622-5543 (toll free in the US) or +1-978-646-2777.

---

pallab sanpui <pallabsanpui@gmail.com>

Molecular Probes

4 messages

Cholewa, Olivia <Olivia.Cholewa@lifetech.com> **Tue, Dec 7, 2010 at 10:32 PM**
To: "pallabsanpui@gmail.com" <pallabsanpui@gmail.com>

Dear Dissertator,

Please list the image(s) that you wish to publish and in what document (journal publication, thesis, etc.).

Sincerely,

Olivia Cholewa, Ph.D
Technical Application Specialist
Molecular Probes Labeling & Detection Technologies, Cell Systems Division

T 541 335 0353 • F 541 335 0238
29851 Willow Creek Road • Eugene • OR • 97402-9132
olivia.cholewa@lifetech.com
www.invitrogen.com

---

pallab sanpui <pallabsanpui@gmail.com> **Wed, Dec 8, 2010 at 2:34 PM**
To: "Cholewa, Olivia" <Olivia.Cholewa@lifetech.com>

Respected Madam,
Thank you for your kind reply. Actually I want to use a image published in a review article and was, in fact, taken from Quantum Dot corp. The details of the article:
Medintz IL, Uyeda HT, Goldman ER et al. (2005) Quantum dot bioconjugates for imaging, labelling and sensing [review]. Nat Materials 435–446.

The review article is attached for your kind perusal. I want use the **Figure 3b** in the article (highlighted) both in **print and electronic format for in my THESIS**. The same article has also been enlisted in the 'Qdot citation list' provided by Invitrogen. The same list is also attached here for your convenience.
I have already requested the Nature Publishing Group (Publisher of the specific article) for the permission and I was directed to contact you as the original image was taken from Quantum Dot Corp. I will be grateful if you please provide me the necessary permission. Thanking you in advance,

Sincerely,

Pallab Sanpui
PhD Scholar, Centre for Nanotechnology,
Indian Institute of Technology Guwahati,
Assam - 781039, India.

[Quoted text hidden]

---

2 attachments

Mednitz Nat. Mater..pdf
3034K

Qdot-citations.pdf
155K

Cholewa, Olivia <Olivia.Cholewa@lifetech.com> **Thu, Dec 9, 2010 at 4:46 AM**
To: pallab sanpui <pallabsanpui@gmail.com>

Dear Dr. Sanpui,

You have permission to include the requested images into your dissertation (but not in other documents or formats). You will need cite the paper reference, and also reference “Molecular Probes® by Life Technologies” directly by the image.

I hope this information is of some assistance.

Sincerely,

Olivia Cholewa, Ph.D
Technical Application Specialist
Molecular Probes Labeling & Detection Technologies, Cell Systems Division

T 541 335 0353 • F 541 335 0238
29851 Willow Creek Road • Eugene • OR • 97402-9132
olivia.cholewa@lifetech.com
www.invitrogen.com

life technologies AB applied biosystems | invitrogen

From: pallab sanpui [mailto:pallabsanpui@gmail.com]
Sent: Wednesday, December 08, 2010 1:05 AM
To: Cholewa, Olivia
Subject: Re: Molecular Probes

[Quoted text hidden]

pallab sanpui <pallabsanpui@gmail.com> **Thu, Dec 9, 2010 at 2:56 PM**
To: "Cholewa, Olivia" <Olivia.Cholewa@lifetech.com>

Respected Madam,

Thank you very much for your help. I will use the image accordingly and the reference Molecular Probes as well as the paper will definitely be indicated. Thanking you once again,

Sincerely,
Pallab Sanpui

[Quoted text hidden]

NATURE PUBLISHING GROUP LICENSE
TERMS AND CONDITIONS

Dec 06, 2010

This is a License Agreement between Pallab Sanpui ("You") and Nature Publishing Group ("Nature Publishing Group") provided by Copyright Clearance Center ("CCC"). The license consists of your order details, the terms and conditions provided by Nature Publishing Group, and the payment terms and conditions.

All payments must be made in full to CCC. For payment instructions, please see information listed at the bottom of this form.

License Number	2563100791602
License date	Dec 06, 2010
Licensed content publisher	Nature Publishing Group
Licensed content publication	Nature Nanotechnology
Licensed content title	Nanocarriers as an emerging platform for cancer therapy
Licensed content author	Dan Peer ,Jeffrey M. Karp ,Seungpyo Hong ,Omid C. Farokhzad ,Rimona Margalit et al.
Licensed content date	Dec 1, 2007
Volume number	2
Issue number	12
Type of Use	reuse in a thesis/dissertation
Requestor type	academic/educational
Format	print and electronic
Portion	figures/tables/illustrations
Number of figures/tables /illustrations	1
High-res required	no
Figures	Figure 1
Author of this NPG article	no
NPG Code	
Title of your thesis / dissertation	Implications of Nanoparticle-Polymer Composites as Probes and Therapeutic Agents
Expected completion date	Jan 2011
Estimated size (number of pages)	145
Total	0.00 USD
Terms and Conditions	

Terms and Conditions for Permissions

Nature Publishing Group hereby grants you a non-exclusive license to reproduce this material for this purpose, **and for no other use**, subject to the conditions below:

1. NPG warrants that it has, to the best of its knowledge, the rights to license reuse of this material. However, you should ensure that the material you are requesting is original to Nature Publishing Group and does not carry the copyright of another entity (as credited in the published version). If the credit line on any part of the material you have requested indicates that it was reprinted or adapted by NPG with permission from another source, then you should also seek permission from that source to reuse the material.

2. Permission granted free of charge for material in print is also usually granted for any electronic version of that work, provided that the material is incidental to the work as a whole and that the electronic version is essentially equivalent to, or substitutes for, the print version.

   Where print permission has been granted for a fee, separate permission must be obtained for any additional, electronic re-use (unless, as in the case of a full paper, this has already been accounted for during your initial request in the calculation of a print run).

   NB: In all cases, web-based use of full-text articles must be authorized separately through the 'Use on a Web Site' option when requesting permission.

3. Permission granted for a first edition does not apply to second and subsequent editions and for editions in other languages (except for signatories to the STM Permissions Guidelines, or where the first edition permission was granted for free).

4. Nature Publishing Group's permission must be acknowledged next to the figure, table or abstract in print. In electronic form, this acknowledgement must be visible at the same time as the figure/table/abstract, and must be hyperlinked to the journal's homepage.

5. The credit line should read:

   Reprinted by permission from Macmillan Publishers Ltd: [JOURNAL NAME] (reference citation), copyright (year of publication)

   For AOP papers, the credit line should read:

   Reprinted by permission from Macmillan Publishers Ltd: [JOURNAL NAME], advance online publication, day month year (doi: 10.1038/sj.[JOURNAL ACRONYM].XXXXX)

6. Adaptations of single figures do not require NPG approval. However, the adaptation should be credited as follows:

   Adapted by permission from Macmillan Publishers Ltd: [JOURNAL NAME] (reference citation), copyright (year of publication)

7. Translations of up to a whole article do not require NPG approval. The translation should be credited as follows:

   Translated by permission from Macmillan Publishers Ltd: [JOURNAL NAME]

(reference citation), copyright (year of publication)

We are certain that all parties will benefit from this agreement and wish you the best in the use of this material. Thank you.

Gratis licenses (referencing $0 in the Total field) are free. Please retain this printable license for your reference. No payment is required.

If you would like to pay for this license now, please remit this license along with your payment made payable to "COPYRIGHT CLEARANCE CENTER" otherwise you will be invoiced within 48 hours of the license date. Payment should be in the form of a check or money order referencing your account number and this invoice number RLNK10895058.
Once you receive your invoice for this order, you may pay your invoice by credit card. Please follow instructions provided at that time.

Make Payment To:
Copyright Clearance Center
Dept 001
P.O. Box 843006
Boston, MA 02284-3006

If you find copyrighted material related to this license will not be used and wish to cancel, please contact us referencing this license number 2563100791602 and noting the reason for cancellation.

Questions? customercare@copyright.com or +1-877-622-5543 (toll free in the US) or +1-978-646-2777.

TH-964_05615301

ELSEVIER LICENSE
TERMS AND CONDITIONS

Dec 06, 2010

This is a License Agreement between Pallab Sanpui ("You") and Elsevier ("Elsevier") provided by Copyright Clearance Center ("CCC"). The license consists of your order details, the terms and conditions provided by Elsevier, and the payment terms and conditions.

All payments must be made in full to CCC. For payment instructions, please see information listed at the bottom of this form.

Supplier	Elsevier Limited The Boulevard,Langford Lane Kidlington,Oxford,OX5 1GB,UK
Registered Company Number	1982084
Customer name	Pallab Sanpui
Customer address	Centre for Nanotechnology Guwahati, other 781039
License number	2563050872588
License date	Dec 06, 2010
Licensed content publisher	Elsevier
Licensed content publication	Biomaterials
Licensed content title	Chitosan: A versatile biopolymer for orthopaedic tissue-engineering
Licensed content author	Alberto Di Martino, Michael Sittinger, Makarand V. Risbud
Licensed content date	October 2005
Licensed content volume number	26
Licensed content issue number	30
Number of pages	8
Start Page	5983
End Page	5990
Type of Use	reuse in a thesis/dissertation
Portion	figures/tables/illustrations
Number of figures/tables /illustrations	1
Format	both print and electronic
Are you the author of this Elsevier article?	No
Will you be translating?	No
Order reference number	
Title of your thesis/dissertation	Implications of Nanoparticle-Polymer Composites as Probes and Therapeutic Agents

Expected completion date	Jan 2011
Estimated size (number of pages)	145
Elsevier VAT number	GB 494 6272 12
Permissions price	0.00 USD
Value added tax 0.0%	0.0 USD / 0.0 GBP
Total	0.00 USD

Terms and Conditions

INTRODUCTION

1. The publisher for this copyrighted material is Elsevier. By clicking "accept" in connection with completing this licensing transaction, you agree that the following terms and conditions apply to this transaction (along with the Billing and Payment terms and conditions established by Copyright Clearance Center, Inc. ("CCC"), at the time that you opened your Rightslink account and that are available at any time at http://myaccount.copyright.com).

GENERAL TERMS

2. Elsevier hereby grants you permission to reproduce the aforementioned material subject to the terms and conditions indicated.

3. Acknowledgement: If any part of the material to be used (for example, figures) has appeared in our publication with credit or acknowledgement to another source, permission must also be sought from that source. If such permission is not obtained then that material may not be included in your publication/copies. Suitable acknowledgement to the source must be made, either as a footnote or in a reference list at the end of your publication, as follows:

“Reprinted from Publication title, Vol /edition number, Author(s), Title of article / title of chapter, Pages No., Copyright (Year), with permission from Elsevier [OR APPLICABLE SOCIETY COPYRIGHT OWNER].” Also Lancet special credit - “Reprinted from The Lancet, Vol. number, Author(s), Title of article, Pages No., Copyright (Year), with permission from Elsevier.”

4. Reproduction of this material is confined to the purpose and/or media for which permission is hereby given.

5. Altering/Modifying Material: Not Permitted. However figures and illustrations may be altered/adapted minimally to serve your work. Any other abbreviations, additions, deletions and/or any other alterations shall be made only with prior written authorization of Elsevier Ltd. (Please contact Elsevier at permissions@elsevier.com)

6. If the permission fee for the requested use of our material is waived in this instance, please be advised that your future requests for Elsevier materials may attract a fee.

7. Reservation of Rights: Publisher reserves all rights not specifically granted in the combination of (i) the license details provided by you and accepted in the course of this licensing transaction, (ii) these terms and conditions and (iii) CCC's Billing and Payment terms and conditions.

TH-964_05615301

8. License Contingent Upon Payment: While you may exercise the rights licensed immediately upon issuance of the license at the end of the licensing process for the transaction, provided that you have disclosed complete and accurate details of your proposed use, no license is finally effective unless and until full payment is received from you (either by publisher or by CCC) as provided in CCC's Billing and Payment terms and conditions. If full payment is not received on a timely basis, then any license preliminarily granted shall be deemed automatically revoked and shall be void as if never granted. Further, in the event that you breach any of these terms and conditions or any of CCC's Billing and Payment terms and conditions, the license is automatically revoked and shall be void as if never granted. Use of materials as described in a revoked license, as well as any use of the materials beyond the scope of an unrevoked license, may constitute copyright infringement and publisher reserves the right to take any and all action to protect its copyright in the materials.

9. Warranties: Publisher makes no representations or warranties with respect to the licensed material.

10. Indemnity: You hereby indemnify and agree to hold harmless publisher and CCC, and their respective officers, directors, employees and agents, from and against any and all claims arising out of your use of the licensed material other than as specifically authorized pursuant to this license.

11. No Transfer of License: This license is personal to you and may not be sublicensed, assigned, or transferred by you to any other person without publisher's written permission.

12. No Amendment Except in Writing: This license may not be amended except in a writing signed by both parties (or, in the case of publisher, by CCC on publisher's behalf).

13. Objection to Contrary Terms: Publisher hereby objects to any terms contained in any purchase order, acknowledgment, check endorsement or other writing prepared by you, which terms are inconsistent with these terms and conditions or CCC's Billing and Payment terms and conditions. These terms and conditions, together with CCC's Billing and Payment terms and conditions (which are incorporated herein), comprise the entire agreement between you and publisher (and CCC) concerning this licensing transaction. In the event of any conflict between your obligations established by these terms and conditions and those established by CCC's Billing and Payment terms and conditions, these terms and conditions shall control.

14. Revocation: Elsevier or Copyright Clearance Center may deny the permissions described in this License at their sole discretion, for any reason or no reason, with a full refund payable to you. Notice of such denial will be made using the contact information provided by you. Failure to receive such notice will not alter or invalidate the denial. In no event will Elsevier or Copyright Clearance Center be responsible or liable for any costs, expenses or damage incurred by you as a result of a denial of your permission request, other than a refund of the amount(s) paid by you to Elsevier and/or Copyright Clearance Center for denied permissions.

LIMITED LICENSE

The following terms and conditions apply only to specific license types:

TH-964_05615301

15. **Translation**: This permission is granted for non-exclusive world **English** rights only unless your license was granted for translation rights. If you licensed translation rights you may only translate this content into the languages you requested. A professional translator must perform all translations and reproduce the content word for word preserving the integrity of the article. If this license is to re-use 1 or 2 figures then permission is granted for non-exclusive world rights in all languages.

16. **Website**: The following terms and conditions apply to electronic reserve and author websites:
Electronic reserve: If licensed material is to be posted to website, the web site is to be password-protected and made available only to bona fide students registered on a relevant course if:
This license was made in connection with a course,
This permission is granted for 1 year only. You may obtain a license for future website posting,
All content posted to the web site must maintain the copyright information line on the bottom of each image,
A hyper-text must be included to the Homepage of the journal from which you are licensing at http://www.sciencedirect.com/science/journal/xxxxx or the Elsevier homepage for books at http://www.elsevier.com , and
Central Storage: This license does not include permission for a scanned version of the material to be stored in a central repository such as that provided by Heron/XanEdu.

17. **Author website** for journals with the following additional clauses:

All content posted to the web site must maintain the copyright information line on the bottom of each image, and
he permission granted is limited to the personal version of your paper. You are not allowed to download and post the published electronic version of your article (whether PDF or HTML, proof or final version), nor may you scan the printed edition to create an electronic version,
A hyper-text must be included to the Homepage of the journal from which you are licensing at http://www.sciencedirect.com/science/journal/xxxxx , As part of our normal production process, you will receive an e-mail notice when your article appears on Elsevier's online service ScienceDirect (www.sciencedirect.com). That e-mail will include the article's Digital Object Identifier (DOI). This number provides the electronic link to the published article and should be included in the posting of your personal version. We ask that you wait until you receive this e-mail and have the DOI to do any posting.
Central Storage: This license does not include permission for a scanned version of the material to be stored in a central repository such as that provided by Heron/XanEdu.

18. **Author website** for books with the following additional clauses:
Authors are permitted to place a brief summary of their work online only.
A hyper-text must be included to the Elsevier homepage at http://www.elsevier.com

All content posted to the web site must maintain the copyright information line on the bottom of each image
You are not allowed to download and post the published electronic version of your chapter, nor may you scan the printed edition to create an electronic version.
Central Storage: This license does not include permission for a scanned version of the

material to be stored in a central repository such as that provided by Heron/XanEdu.

19. **Website** (regular and for author): A hyper-text must be included to the Homepage of the journal from which you are licensing at http://www.sciencedirect.com/science/journal/xxxxx. or for books to the Elsevier homepage at http://www.elsevier.com

20. **Thesis/Dissertation**: If your license is for use in a thesis/dissertation your thesis may be submitted to your institution in either print or electronic form. Should your thesis be published commercially, please reapply for permission. These requirements include permission for the Library and Archives of Canada to supply single copies, on demand, of the complete thesis and include permission for UMI to supply single copies, on demand, of the complete thesis. Should your thesis be published commercially, please reapply for permission.

21. **Other Conditions**:

v1.6

Gratis licenses (referencing $0 in the Total field) are free. Please retain this printable license for your reference. No payment is required.

If you would like to pay for this license now, please remit this license along with your payment made payable to "COPYRIGHT CLEARANCE CENTER" otherwise you will be invoiced within 48 hours of the license date. Payment should be in the form of a check or money order referencing your account number and this invoice number RLNK10894976.
Once you receive your invoice for this order, you may pay your invoice by credit card. Please follow instructions provided at that time.

Make Payment To:
Copyright Clearance Center
Dept 001
P.O. Box 843006
Boston, MA 02284-3006

If you find copyrighted material related to this license will not be used and wish to cancel, please contact us referencing this license number 2563050872588 and noting the reason for cancellation.

Questions? customercare@copyright.com or +1-877-622-5543 (toll free in the US) or +1-978-646-2777.